The pathophysiology of Spinal Bulbar Muscular Atrophy: a longitudinal analysis of mouse muscle and spinal cord

By Leonette Victoria Naakuma Delali Annan

University College London, Institute of Neurology

PhD Supervisors: Professor Linda Greensmith and Professor Gyorgy Szabadkai

A Thesis submitted for the degree of

Doctor of Philosophy (PhD)

October 2017

Declaration

I, Leonette Victoria Naakuma Delali Annan, confirm that the work presented in this Thesis is my own. Where information has been derived from other sources, I confirm that this has been indicated in the Thesis.

Acknowledgements

I would like to express my huge gratitude to Professor Linda Greensmith who has provided immense guidance, support and mentoring throughout my time in her lab. I would like to thank Jim Dick, the Graham Watts Lab Manager, who is simply phenomenal in his assistance to all members of the lab. I would also like to thank the Greensmith lab Post-Docs: Dr Bilal Malik, Dr Mhoriam Ahmed, Dr Barney Bryson, Dr Ching-Hua Lu and Dr Bernadett Kalmar for their day-to-day laboratory guidance and stimulating discussions. Lastly, I would like to thank my fellow students for their company and support.

This Thesis was funded by a Wellcome Trust 4-year PhD in Neuroscience Studentship.

This Thesis is dedicated to my beloved sisters, Anouska and Suzette Annan.

All Glory and Honour be to God.

Abstract

Spinal Bulbar Muscular Atrophy (SBMA), also known as Kennedy's disease, is an X-linked, late-onset progressive neurodegenerative disease. SBMA is characterised by the selective loss of spinal and bulbar motor neurons and progressive muscle weakness. The disease is caused by an expansion in the CAG repeat in the androgen receptor (AR) gene which encodes a polyglutamine tract in the protein. The underlying pathophysiology of the disease is thought to be related to abnormal accumulation of the pathogenic AR protein within the nucleus.

The AR100 transgenic mouse model of SBMA has a progressive neuromuscular phenotype accompanied by motor neuron degeneration, thereby mirroring the human disease. Since ER stress has been suggested to play a role in motor neuron death in SBMA, I investigated the underlying mechanism by which ER stress may result in cell death. In particular, I tested whether the motor neuron-specific Fas/NO cell death pathway plays a role in SBMA. In addition, I examined whether the ER chaperone, Calreticulin forms a link between the Fas/NO MN-specific death pathway and ER stress. I found that Fas/NO induced cell death is not observed in AR100 MNs. However, an increase in Calreticulin is observed in the spinal cord of AR100 mice, suggesting it may contribute to SBMA pathology.

Although SBMA is considered to be a neurodegenerative disease affecting motor neurons, emerging evidence suggests that SBMA may also involve a primary muscle deficit. I examined this possibility by characterising muscle histopathology longitudinally, at different stages of disease progression, in AR100 mice. My results show that muscle atrophy is evident during early stages of disease, prior to any loss of motor neurons. Physiological deficits were accompanied by a change in the properties of the muscle fibres such as increase in oxidative capacity and signs of myogenic and neurogenic induced muscle atrophy. Furthermore, RNA-sequencing and pathway enrichment analysis of hindlimb muscles of AR100 mice identified some of the molecular signalling pathways which may underlie the changes within the muscle. These findings indicate that muscle deficits are an early and primary manifestation of disease in SBMA.

Contents

List of Figures

Chapter 1

Chapter 2

Chapter 3

Chapter 4

List of Tables

Abbreviations

ALS = Amyotrophic Lateral Sclerosis
AR = Androgen Receptor
ATF4 = Activating Transcription Factor
BAC = Bacterial Artificial Chromosome
BDNF = Brain-Derived Neurotrophic Factor
BiP = Binding Immunoglobulin Protein
BSA = Bovine Serum Albumin
CHOP = CCAAT/enhancer-binding protein homologous protein
CNB= Complete Neurobasal Medium
CNTF= Ciliary Neurotrophic Factor
CRT = Calreticulin
CytoC = Cytochrome C
DAVID = Database for Annotation, Visualization and Integrated Discovery
DBD = DNA-Binding Domain
DHT = Dihydrotestosterone
DIV = Days in Vitro
EDL = Extensor Digitorum Longus
eIF2a = Eukaryotic Initiating Factor 2 a
ER = Endoplasmic Reticulum
ERAD = ER-associated degradation
ETC = Electron Transport Chain
Fox01 = Forkhead box protein O1
GDNF= Glial cell line-derived Neurotrophic Factor
HD = Huntington's Disease
HRE = Hormone Response Element
HSP = Heat Shock Protein
IGF = Insulin like Growth Factor
IRE1 = Inositol Requiring Enzyme 1
KD = Kennedy's Disease
KEGG = Kyoto Encyclopaedia of Genes and Genomes
LBD = Ligand-Binding Domain
LDH = Lactate Dehydrogenase
MAPK = Mitogen Activated Protein Kinase
MND = Motor Neuron Disease
mt SOD1 = Mutant SOD1
MyoD = Myogenic Differentiation factor 1
NI = Nuclear Inclusion
NTD = Amino (N) – Terminal Domain
PERK = Pancreatic ER Kinase–like Kinase
PGC1α = Peroxisome Proliferator-activated receptor Co-activator-1α
PINK = PTEN-induced putative kinase 1
PKB = AKT, Protein kinase B
PolyQ = Polyglutamine
SBMA = Spinal Bulbar Muscular Atrophy

SDH = Succinate dehydrogenase
SERCA= Sarco/Endoplasmic Reticulum ATPase
SOD1= Superoxide Dismutase 1
Sol = Soleus
T= Testosterone
TA = Tibialis Anterior
TG = Thapsigargin
VCL = Vinculin
WEB GESTALT = Web-based Gene Set Analysis Toolkit
WT = Wild-Type
XBP1 = X box-binding protein 1
YAC = Yeast Artificial Chromosome

Chapter 1 General Introduction

Introduction

In this Thesis, I undertook a longitudinal analysis of muscle and spinal cord pathology in a transgenic mouse model of the progressive, adult onset neurodegenerative disease, Spinal Bulbar Muscular Atrophy (SBMA).

1.1 Patient Symptoms

Spinal Bulbar Muscular Atrophy (SBMA) was first described by Kennedy et al. (1968), from which it gets its alternative name 'Kennedy's Disease'. SBMA is an X-linked, slow onset motor neuron disease which characteristically only manifests in males, typically between 30 to 50 years of age (Harding et al., 1982). However, earlier onset cases have been reported (Grunseich et al., 2014a), and there is a marked variability in patient reports for age of onset (Finsterer and Soraru, 2015). SBMA is estimated to affect 1-2 per 100,000 males (Truant et al., 2006). The prevalence of SBMA may be underestimated due to misdiagnosis of SBMA as other motor neuron diseases (Parboosingh et al., 1997), and in some cases patients do not get diagnosed at all (Katsuno et al., 2006b, Finsterer and Soraru, 2015).

SBMA manifests as progressive proximal muscle weakness which eventually results in an inability to perform routine motor tasks such as walking. Difficulty in writing and hand tremor can occur as early as 15 years of age, 10 years prior to muscle weakness (Tsukagoshi et al., 1970). In addition, bulbar muscle dysfunction causes difficulty with swallowing and enunciation, due to atrophy of bulbar muscles. Electromyography shows evidence of denervation (Polo et al., 1996), and muscle histology shows both atrophy and hypertrophy of muscle fibres which varies greatly between patients (Soraru et al., 2008). There is a small incidence of necrotic fibres but biopsies do show clustering of pyknotic nuclei. Although there is no decrease in lifespan of SBMA patients, as disease progresses, hospitalisation with aspiration pneumonia does occur (Ringel et al., 1978). Heterozygous females have subclinical symptoms (Soraru et al., 2008). Even in the very rare case of homozygous expression in females symptoms are relatively mild (Schmidt et al., 2002).

1.2 Genetic cause of SBMA

In 1991, the underlying genetic cause of SBMA was identified as a mutation in exon 1 of the Androgen Receptor (AR) gene (La Spada et al., 1991). Normally, the AR gene has between 9 and 36 CAG repeats encoding for the polyglutamine stretch in the AR protein N-Terminal. Although the functional role of these repeats is still unclear (Parodi & Pennuto, 2011), more than 38 repeats is known to result in a toxic gain of function as well as some loss of androgenic function. Furthermore, there is a correlation between repeat length and the severity of the disease and an inverse correlation with the age of disease onset (Fratta et al., 2014b).

1.3 Polyglutamine Disorders

SBMA is classified as a lower motor neuron disease, yet it is also one of nine poly glutamine repeat disorders (See Table 1), a group of diseases that include Huntington's disease, Dentatorubral-pallidoluysian atrophy and six types of Spinocerebellar ataxia. SBMA was the first of the polyglutamine diseases for the pathogenic cause to be identified, and unlike the other causative mutant proteins of the other 8 polyQ diseases, the function of the AR protein was already well studied (La Spada, et al., 1991). Insoluble polyQ aggregates are the hallmark of all polyQ disorders (La Spada and Taylor, 2010). In all 9 types of polyQ diseases it appears that neuronal cells are particularly vulnerable to the polyQ repeat expansion, and disease severity is typically correlated with length of the mutated polyQ tract (Cortes and La Spada, 2015). However, recent developments in Huntington's disease as well as SBMA research have shown that, the muscle may be a site of primary pathogenesis (Mielcarek et al., 2015, Zielonka et al., 2014, Rinaldi et al., 2014).

1.3.1 Toxicity of the expanded polyglutamine tract

In all polyQ diseases, the repeat expansion is within the coding region of the protein, normally towards the N-terminal. For each specific disease, a different repeat length is considered to be pathogenic (see Table 1), but in almost all of

Table 1 Characteristics of the Polyglutamine diseases

Disease	Prevalence	Symptoms	Genetic Cause	Pathogenic repeat length
Huntington's Disease	3 -7 per 100,000 people of European ancestry	Dementia, chorea, and dystonia	Huntingtin- transcription factor, autophagy factor and signalling scaffold	36-121
Spinocerebellar ataxia type 1	1-2 per 100,000 world wide	Bulbar signs, ataxia, cognitive impairment	Ataxin 1- Transcriptional co-repressor	39-91
Spinocerebellar ataxia type 2	Rare, (More prevalent in Cuba- 40 per 100,00)	Parkinsonism, slow eye movements	Ataxin 2- RNA processing	32-200
Spinocerebellar ataxia type 3	Most common type of spinocerebellar ataxia	Spasticity, polyneuropathy, dystonia, diplopia	Ataxin 3- De-ubiquitinating enzyme	52-86
Spinocerebellar ataxia type 6	less than 1 in 100,000	Dysarthria, involuntary eye movement	CACNA1A- Voltage Gated Calcium Channel	18-30
Spinocerebellar ataxia type 7	less than 1 in 100,000	Retinal degeneration	Ataxin 7- Part of a Histone acetyl transferase complex	34-300
Spinocerebellar ataxia type 17	less than 1 in 100,000	Psychosis, seizures	TATA Binding Protein- Transcription factor	43-66
Dentatorubral-pallidoluysian atrophy	2 to 7 per 1,000,000 Japanese people	Ataxia, dementia, Epilepsy, emotional problems	Dystrophin 1- Transcriptional co-repressor	49-88

Information compiled from : Cortes and La Spada (2015), Takahashi et al. (2010) and The US National library of Medicine: [http://ghr.nlm.nih.gov/]

these polyQ diseases, a CAG repeat of greater than ~35 results in disease, suggesting there may be a pathogenic threshold within polyglutamine expanded proteins (Michalik and Van Broeckhoven, 2003). PolyQ diseases also display 'anticipation', where milder symptoms are evident in earlier generations (La Spada and Taylor, 2010). In all polyQ disorders, the presence of the polyQ tract leads to the formation of β pleated sheets within the protein structure, rendering the protein more prone to aggregation (Parodi and Pennuto, 2011, Perutz et al., 1994). The specific form that the β pleated sheets take has not yet been determined, although it has been proposed that the formation of a hairpin loop or cylindrical structures may occur (Takahashi et al., 2010).

In Huntington's disease, aggregate formation is considered pathogenic, as inclusions can be found prior to disease manifestation in post mortem brains (Zielonka et al., 2014). However in SBMA, the role of aggregate formation is less clear, as there is marked variation in aggregate localisation, as well as the presence of micro-aggregates (Adachi et al., 2005, Michalik and Van Broeckhoven, 2003). Whether the toxic form of polyQ is the inclusion bodies or the presence of soluble oligomers has been investigated. In cell lines, it has been shown that cells with inclusion bodies live longer than those with soluble oligomers (Takahashi et al., 2008). Furthermore, the presence of oligomers has been observed prior to disease onset in a mouse model of SBMA and ceases upon castration, which reverses disease (Li et al., 2007).

Poly Q inclusion formation typically forms in the nucleus of the affected neuronal population in the nine polyQ diseases, although the mechanism of protein degradation in the nucleus is not yet well understood. In all the polyQ diseases, toxicity takes the form of a variety of features, including transcriptional dysregulation, disruption of the Unfolded protein response (UPR), deficits in axonal transport, mitochondrial dysregulation and changes in calcium homeostasis (Takahashi et al., 2010).

The specific function of the polyQ repeats in humans is largely unknown. PolyQ expansion is not found normally in mice, yet mouse models can be generated to

artificially induce polyQ expansion to model such diseases (Perutz et al., 1994). In the androgen receptor, the polyglutamine tract has been shown to bind the C-terminal of the protein, bind co-activators, and trap ubiquitin thus its length is inversely correlated to the stability of the protein (Palazzolo et al., 2008).

1.4 The androgen receptor structure and function

The androgen receptor (AR) gene is located in the long arm of the X chromosome. There are approximately 20 splice variants of the protein (Lu et al., 2015a). It is a ligand dependent transcription factor of 110 kDa, with 8 exons and 917 amino acids and contains three main domains, the Ligand binding domain (LBD), the N-terminal transactivation domain (NTD) and the Zinc Finger DNA binding domain (DBD), with a connecting hinge region (Duff et al., 2006). The AR is activated by one of two steroid ligands, Testosterone (T), or its more potent metabolite Dihydrotestosterone (DHT), produced by 5 α-reductase (See Figure 1). The AR is responsible for controlling transcription of androgen responsive genes. It is found as a monomer in the cytoplasm with heat shock proteins (HSPs). Once T or DHT bind the LBD, an AR dimer is formed by N-terminal /C-terminal interaction, which is translocated into the nucleus, where the AR dimer binds the Androgen Response Element (ARE) upstream of the promoter of target androgen responsive gene, via its DBD. Here, it recruits various co-activators such as AR Associated protein 70 (ARA70) and transcriptional machinery (Centenera et al., 2008).

The AR protein is also regulated by a number of post-translational modifications, including phosphorylation, acetylation, and sumoylation. Many of the proteins that are responsible for the post-translational modifications of the AR can become dysregulated in disease, for example, increased repeat length has been associated with increased phosphorylation (Coffey and Robson, 2012).

The CAG repeats transcribing the polyglutamine tract are located in the NTD. There is an inverse correlation between polyQ length and protein stability, with an increase in the formation of β pleated sheets and toxic oligomers as repeat number increases. An

increase in the polyQ length also aids C/N interactions, causing an increase in nuclear location. (Michalik and Van Broeckhoven, 2003).

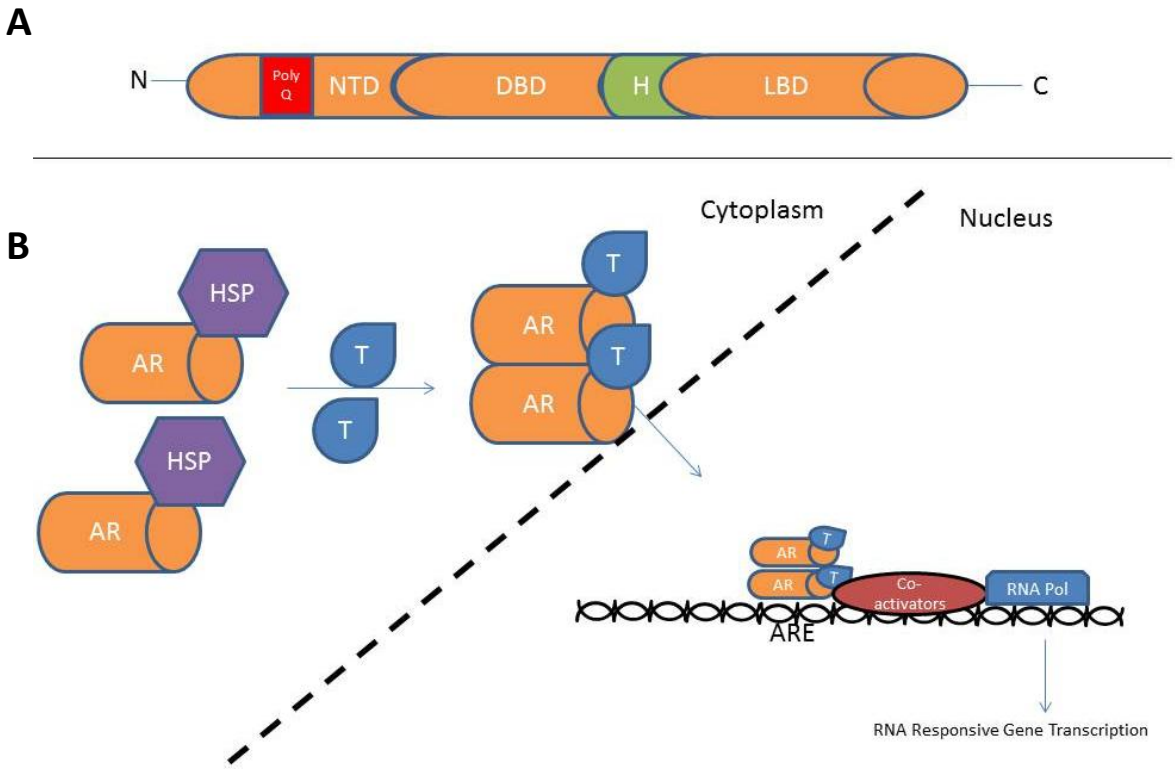

Figure 1 Structure and function of the androgen receptor (AR)

A) The AR protein is composed of the Polyglutamine region (PolyQ), the N-terminal domain (NTD), the DNA binding domain (DBD), a Hinge region (H) and a Ligand Binding domain (LBD). **B**) In the presence of testosterone (T), Heat shock proteins (HSPs) dissociate from the androgen receptor (AR) in the cytoplasm. The AR then dimerises and translocates into the nucleus and binds androgen response elements (ARE) on the DNA, recruiting co-activators and initiating gene transcription.

1.4.1 Non-genomic roles of the Androgens

Although the roles of the androgens are largely a result of transcriptional regulation, T and DHT also have 'non-genomic' roles which are mediated either by second messengers, such as the intracellular tyrosine kinases, or even by the presence of membrane bound androgen receptors (Heinlein and Chang, 2002). The non- genomic effects of androgens act to increase intracellular calcium levels in a number of cell types. To date the only study investigating whether the non-genomic roles of androgens have a role in SBMA pathogenesis was carried out by Schindler et al. (2012). This study showed that both the normal and mutated AR could be localised to the plasma membrane and lipid rafts. These authors suggested that SBMA phenotypes such as reduced neurite length and cell viability may, at least in part, be due to non-genomic signalling.

1.5 Pathogenic mechanisms of SBMA

There are a number of pathogenic mechanisms for SBMA that have been proposed using various models of the disease. These include impaired protein homeostasis, disrupted axonal transport, reduced neurotrophic support and altered gene transcription.

1.5.1 Impaired protein homeostasis

Impaired protein homeostasis is a pathogenic feature seen in a number of neurodegenerative diseases (Hetz and Mollereau, 2014). In SBMA, the generation of the polyQ AR requires protein quality control systems to remove or re-fold the pathogenic protein (Rusmini et al., 2015a). Focused on in detail in Chapter 2 of this Thesis is Endoplasmic Reticulum (ER) stress. 'ER stress' is a state where the protein load within the cell is too high. Therefore ER stress sensing proteins become activated in order to initiate a signalling cascade which results in either a pause in protein translation or, if the stressed state cannot be reversed, apoptosis (For a review of ER stress signalling see Hetz (2012)). An increase in ER stress sensing proteins have been observed in the muscle of AR97Q SBMA model mice (Yang et al., 2013), as well as in

the Greensmith lab in AR100 model mice primary motor neurons and spinal cord (Montague et al., 2014).

Another cellular process required for the proper handling of cellular proteins is autophagy (Menzies et al., 2015). Autophagy is a process that clears the build-up of mutant proteins such as the polyQ AR. However, in disease this process can become either overloaded or disrupted, enhancing vulnerability to cell death. Disrupted autophagy has been observed in MNs that model SBMA as well as in the spinal cord of AR100 mice (Cortes et al., 2014b). The study showed that a block occurs in the autophagy pathway progression as a result of polyQ AR. Furthermore, in the muscle of the knock-in model of SBMA, an upregulation of autophagic markers has been observed (Rusmini et al., 2015b).

The ubiquitin-proteasome system (UPS) is another method by which cells degrade mutant protein. There is evidence that in the muscle of knock-in mice, autophagy is preferential to the UPS (Rusmini et al., 2015b). Additionally, in AR97Q mice an over-active proteasome has been observed in mouse muscle, and in the spinal cord proteasome function is similar to that of wild-type mice (Tokui et al., 2009).

1.5.2 Disrupted axonal transport

A pathogenic feature often seen in motor neuron diseases is disrupted axonal transport owing to the fact that motor neuron (MN) axons are considerably long. It has been observed in the severe motor neuron disease Amyotrophic Lateral Sclerosis (Kieran et al., 2005), and is considered by some to also have a role in SBMA (Katsuno et al., 2006a, Kemp et al., 2011). Initially using the AR97Q mouse model of SBMA, it was observed that neurofilaments and synaptophysin accumulated in MN axons, and mRNA levels of retrograde transport motor, dynactin 1, were significantly reduced (Katsuno et al., 2006a). Additionally, using the knock-in and WT over-expressor models of SBMA, it was shown that retrograde labelling of spinal cord MNs after muscular injections was significantly reduced (Kemp et al., 2011). In contrast, deficits in axonal transport are not seen in all mouse models of SBMA. The AR100 mouse model does not show altered axonal transport (Malik et al., 2011), no alteration in

microtubule associated proteins was observed. Furthermore, *in vivo* analysis of axonal transport rates within the AR100 mouse sciatic nerve revealed no difference in comparison to wild-type.

1.5.3 Reduced neurotrophic support

Reduced neurotrophic support is an additional contributing factor to pathology in SBMA. It has been demonstrated that an increase in growth factor expression can reverse SBMA-like symptoms. It was observed in the AR97Q mouse model that constituent expression in the muscle, or systemic treatment of Insulin like Growth Factor- 1 could ameliorate disease symptoms (Palazzolo et al., 2009, Rinaldi et al., 2012). Additionally, in the WT over-expressor model and the AR97Q mice a reduction in Brain derived neurotrophic factor (BDNF) mRNA has been observed within the muscle, prior to the onset of symptoms (Halievski et al., 2015a). Furthermore, it has been shown that Hepatocyte growth factor overexpression too has beneficial effects in AR97Q mice (Ding et al., 2015). Work from the Greensmith lab has shown that there are altered mRNA levels of key trophic molecules such as VEGF in the spinal cord of AR100 mice (Malik et al., 2013).

1.5.4 Transcriptional dysregulation

The AR's role as a transcription factor leads to an important pathogenic mechanism in SBMA of distorted transcription. It has been suggested that altered transcription in SBMA is also mediated by inclusions disrupting histone acetyl transferase activity (Minamiyama et al., 2004). Furthermore, recent research has shown that there is altered Transcription factor EB (TFEB) interaction with polyQ AR resulting in impaired autophagic flux in AR100 mice (Cortes et al., 2014b). Additionally Yu et al. (2009) have reported altered RNA splicing in the muscle of SBMA knock-in model mice.

To date two studies have undertaken microarray analysis on muscle of mouse models of SBMA to determine the large number of genes disrupted in SBMA. The first study, conducted by Mo and colleagues, performed RNA sequencing analysis on three mouse models of SBMA (Mo et al., 2010). In total approximately 100 genes were up

regulated and 70 genes down regulated in each model. Surprisingly, despite the different genetic make-up of these mouse models, there was overlap in the genes dysregulated. The second micro-array study used female WT over-expressor mice treated with testosterone in order to determine genes that were altered specifically as a result of AR activation (Halievski et al., 2015b). Authors found approximately 400 genes dysregulated in transgenic mice depending on the length of testosterone treatment.

1.6 Cellular models of SBMA

A number of cellular models have been used to examine the effects of the mutant AR on different cell types. In this section I outline the different cellular models that have been developed and why in this Thesis I opted for the use of primary cells from the ventral spinal cord or hindlimb muscles for my *in vitro* analysis.

The first cell line model to be developed for SBMA was established in the Fischbeck laboratory, who found little evidence of the mutation causing any cell viability defects. Mis-localisation and aggregation of the AR was observed in this MN hybrid cell line containing the truncated form of the androgen receptor. There was no effect on the mutated AR's ability to bind ligand, AR transactivation, cell viability, or vulnerability to oxidative stress induced by hydrogen peroxide or Menadione treatment (Brooks et al., 1997).

Another model of SBMA that has been developed is the mouse neuroblastoma cell lines with cDNA for full length human AR protein with either 19 (control) or 52 (mutant) CAG repeats sub-cloned into the cell line. As seen in patients, this cell line model shows reduced levels of AR transactivation (Butler et al., 1998). However, Mibolerone treatment (a potent anabolic steroid), resulted in only weak AR immuno-reactivity in the nucleus of neuroblastoma cells carrying the mutant AR. Furthermore, this study also showed cytoplasmic inclusions that were C and N terminal AR positive, in some cases nuclear aggregates were seen although the frequency of the different expression patterns was not quantified (Butler et al., 1998).

In 1998 an additional cell line was developed in the Fischbeck laboratory. This was the first model to demonstrate that polyQ AR can infer toxicity on cells in a repeat length dependant manner (Merry et al., 1998). Only repeats length of 65 and 112 CAG produced both cytoplasmic and nuclear inclusion in neuronal like cell lines (MN-1 cells). Prior to this study, all reports had found insignificant effects of polyQ AR on cell viability.

An additional neuronal model was developed by Kobayashi et al. (2000). Using Neuro2a cells transiently transfected with truncated AR with either 97 or 24 CAG repeats, they found more nuclear AR aggregation and cytotoxicity in the AR97 cells, particularly if cells were transfected for longer. Interestingly, they also demonstrated that the aggregates co-localised with Hsp40 and Hsp70, and co-transfection with DNA for these two chaperone proteins reduced the number of cells with inclusions and decreased in cell death.

The effect of testosterone was first evaluated using an immortalised MN like cell line that does not express endogenous mouse AR (Simeoni et al., 2000). NSC34 cells were transfected with both control and pathogenic CAG repeat lengths in the AR. When the cells were not plated densely, there was dystrophic neurite development in cells expressing the mutant AR, but when the cells began to proliferate (a feature not possible in MNs), the “short dumpy neurites” began to develop into normal structure. Furthermore, this study showed that in cultures treated with Hydro-urea, to inhibit the proliferative feature of NSC34 cells, cell viability was reduced in cells transfected with GFP-AR-46Q in comparison with GFP-AR-24Q and GFP-AR-0Q. Testosterone treatment reversed the dystrophic neurite phenotype and interestingly, in contrast to what is now widely accepted in SBMA research, resulted in a global increase in cell viability (Simeoni et al., 2000).

1.6.1 Induced pluripotent stem cell models of SBMA

The development of human Induced pluripotent stem cells (iPSC) has now enabled modelling of neurodegenerative diseases in human neurons *in vitro*. A limited number of reports of iPSC use in SBMA research have been published.

The first report of iPSC from SBMA patients, derived 2 clone neuronal lines from a single patient and compared these cells to Parkinson's disease controls (Nihei et al., 2013). Interestingly, differentiated neurons from the SBMA patient showed features of SBMA previously observed using more traditional models. There was a higher expression level of AR in neurons in comparison to fibroblasts and DHT- dependent aggregate formation was present in IPSC neurons which was reversed by treatment with the HSP 90 inhibitor 17 AAG (Nihei et al., 2013). An additional study comparing IPSC motor neurons from 6 SBMA patients with healthy control MNs found that there was a reduction in the AR protein in patient lines after they had been differentiated into neurons (Grunseich et al., 2014b). However, the CAG repeat length was unstable throughout the differentiation process, and they did not find a difference in the cell survival of SBMA patient derived motor neurons.

In this Thesis I focus on the use of primary cells from a mouse model of SBMA to examine pathogenic mechanisms of SBMA *in vitro*. Primary neuronal models have the advantage of not being immortalised cells, which is particularly important for the study of motor neuron cell death. Using iPSC derived MNs would also be advantageous. However, at the start of this project there were still many issues with their development and reproducibility of results.

1.7 Chronological review of mouse models of SBMA

Since the molecular cause of SBMA was identified as a repeat expansion in the Androgen Receptor (La Spada et al., 1991), a number of animal models have been developed.

1.7.1 Early mouse models of SBMA

The first model of the disease was developed in the Fischbeck Laboratory (Bingham et al., 1995), using what would now be considered a modest repeat expansion of 46 CAGs as the pathogenic repeat, and 24 CAGs as the control. The mutant protein was expressed at lower levels than the endogenous mouse AR protein. There was no significant difference in the mouse model to that of a WT mouse. The lack of a

phenotype in these mice lead the authors to propose that a longer repeat expansion may be required in order to detect a phenotype within the life span of a mouse (Bingham et al., 1995).

Attempts to develop a mouse model then turned towards using Yeast Artificial chromosomes (YAC) rather than cDNA. The first YAC mouse model of SBMA contained 45 CAG repeats and demonstrated sex and age dependant intergenerational repeat transmission instability (La Spada et al., 1998). However, due to AR fragmentation, mRNA or AR protein could not be detected in the tissues of these mice, and so the effect on the motor phenotype was not evaluated.

Another mouse model of SBMA was developed by Adachi et al. (2001), which was the first to show that MN dysfunction can occur as a result of poly glutamine expansion without necessarily causing MN death. This mouse expressed 239 CAG repeats under the transcriptional control of the human AR promoter, although the repeat length is substantially higher than any pathogenic mutation found in humans (Fratta et al., 2014a). Nuclear inclusion formation was widespread, occurring in cell types not affected in humans (Adachi et al., 2001).

An additional mouse model with 112 glutamines using the neurofilament (NF) light chain promoter and only the 5' portion of the gene, was developed by Abel et al. (2001). Analysis showed that 8 month old mice showed signs of hindlimb clasping and reduced rotarod performance by 11 months. These authors hypothesised that AR truncation may increase the toxicity of poly Q AR. These mice become infertile at approximately 3 months. They also developed a strain under the prion promoter in which the pathogenic AR was ubiquitously expressed. These mice died by 10 weeks. They considered that the limited expression of the polyQ AR, under the control of the NF promoter, was better able to recapitulate an SBMA phenotype (Abel et al., 2001). However, more recent work has determined that the full length mutated AR protein is required for SBMA pathogenesis and AR fragmentation, which is a late event in disease progression, is what the mouse by Abel and colleagues models (Heine et al., 2015).

1.7.2 The AR97Q mouse model of SBMA

The majority of SBMA mouse model studies have been carried out on the AR97Q mice developed by Katsuno et al. (2002).This mouse model expresses the AR with 97 CAG repeats under the control of a cytomegalovirus enhancer and a chicken beta actin promoter. These mice show progressive muscle atrophy and weakness, small body size and, atypical of SBMA pathology in humans, a reduced life span. This model shows gender specific differences, with females only showing symptoms later in life or following administration of testosterone. However, an important drawback of the AR97Q mouse model is that males do not have significant spinal motor neuron loss despite developing a relatively severe pathology.

The AR97Q model has been used in studies showing that pharmacological induction of the Heat Shock response has beneficial effects (Katsuno et al., 2005). Furthermore, there is impaired axonal transport in diseased motor neurons of this mouse has been reported (Katsuno et al., 2006a). It has also been used to demonstrate that Insulin like Growth factor (IGF) can rescue SBMA like symptoms (Rinaldi et al., 2012, Palazzolo et al., 2009). ER stress has been identified in the muscle of AR97Q mice with AR co-localising with the ER stress sensor Binding immunoglobulin (Yang et al., 2013). More recently it has also been shown that there is a loss in important growth factors such as brain derived neurotrophic factor (BDNF) following testosterone treatment (Halievski et al., 2015a). Furthermore the AR97Q model has been used to determine the intrinsic strength of muscle as a result of mutant AR expression (Oki et al., 2015). In summary, the AR97Q mouse model has been undoubtedly useful in the study of SBMA, but critically, this mouse model has a serve phenotype resulting in premature death, not seen in SBMA patients.

1.7.3 The AR112Q mouse model of SBMA

The next model of SBMA to be developed was the AR112Q model by Chevalier-Larsen et al. (2004). Although a mouse model with identical repeat lengths had been developed previously (Abel et al., 2001), the Chevalier-Larson model encapsulated the full length human AR under the control of the prion promoter. Mice show a

progressive loss of motor function that is more severe in males as well as nuclear inclusions in the spinal cord. Castration rescues the phenotype. These mice have been used to show that the AR's ability to form N-terminal /C-terminal interaction is required for the full development of symptoms (Zboray et al., 2015).

1.7.4 The AR100 mouse model of SBMA

The AR100 model, used in the experiments described in this Thesis, was the next mouse model to be developed. It recapitulates many of the disease features seen in humans (Sopher et al., 2004). The AR100 mouse contains a YAC with the human AR containing 100 CAG repeats. The human AR is under the control of its endogenous regulatory elements. Initially the AR100 mouse model was characterised as showing a late onset, slowly progressive neuromuscular degenerative phenotype. The first sign of pathology, slight growth retardation, was reported at 8 months. Footprint analysis showed hindlimb weakness at 14 months. However, there is no reduction in the lifespan of these mice (Sopher et al., 2004).

It has been shown in the Greensmith lab that primary motor neurons from AR100 mice display pathology in the form of disrupted calcium signalling and ER stress (Montague et al., 2014). Additionally, signs of defective autophagy have been observed in the spinal cord of AR100 mice (Cortes et al., 2014b). Interestingly in this mouse model, there are no signs of defective axonal transport (Malik et al., 2011), despite this being seen in other models of SBMA (Katsuno et al., 2006a).

One of the drawbacks of the AR100 mouse model is it still contains the mouse AR, which could have compensatory effects, and it has been shown that crossing AR100 mice with Testicular feminisation mice, negative for the AR, exacerbates symptoms (Thomas et al., 2006b).

1.7.5 The knock-in model of SBMA

The most genetically relevant model of SBMA developed to date is the AR113 Knock – in model (Yu et al., 2006). The advantage of this model of SBMA is that there is no

mouse AR present that may confound results. The knock-in model of SBMA has primarily a muscular degenerative phenotype including reduced body weight, denervation and altered muscle membrane excitability. Interestingly, in this model testosterone treatment of females does not exacerbate symptoms, contrary to what has been observed in other models of disease.

The AR113 knock-in model has been used to show that there are mitochondrial abnormalities in the muscle, with decreased mRNA levels of mitochondrial biogenesis regulator Peroxisome proliferator-activated receptor gamma co-activator β (PGC1β) and Superoxide dismutase 2 (Ranganathan et al., 2009). Neuronal dysfunction is only observed very late in this disease model, but MNs do show signs of disrupted axonal transport, as measured by a reduction in retrogradely labelled MNs (Kemp et al., 2011). The unfolded protein response (UPR) is also triggered in the muscle of knock-in mice (Yu et al., 2011). Most recently, this mouse model has been used to demonstrate that an aberrant autophagic response is present in the muscle (Rusmini et al., 2015b).

1.7.6 The WT over-expressor model of SBMA

The WT over-expressor model of SBMA overexpresses the WT AR only in skeletal muscle (Monks et al., 2007). Interestingly, this model demonstrates that WT overexpression of the WT AR within skeletal muscle fibres is sufficient to induce SBMA-like symptoms. However, the WT AR is not responsible for pathogenesis in patient SBMA. WT over-expressor mice have been used to show that symptoms caused by aberrant AR function are dependent on serum testosterone levels (Johansen et al., 2009). Furthermore there are axonal transport deficits present in MNs in this mouse model (Kemp et al., 2011). The intrinsic muscle contractile properties are impaired (Oki et al., 2015), and BDNF expression reduces upon testosterone treatment (Halievski et al., 2015a). Most recently it has also been shown that in this model, as well as the Knock-in and the AR97Q models, the synaptic transmission between the muscle and motor neuron impaired (Xu et al., 2016).

1.7.7 The AR121mouse model of SBMA

A relatively new model of SBMA is the AR121 model developed in the La Spada laboratory (Cortes et al., 2014a). These mice contain a Bacterial Artificial Chromosome (BAC) containing the human AR with 121 CAG repeats. These mice develop a neuromuscular phenotype that has a progressive degenerative phenotype.

The floxed first exon in the AR121 allows tissue specific excision. When these mice are crossed with CMV- Cre mice the first exon of AR is removed from all tissues reversing the phenotype. Perhaps more interestingly, when AR121 mice were crossed with Human Skeletal Actin promoter (HSA)-Cre mice, removing its expression from skeletal muscle, this too abolished symptoms and the mouse phenotype returned to that of WT littermates. Furthermore, it has been shown using this mouse model as well as the knock-in model of SBMA, that anti- sense oligonucleotides targeting the mutant AR in periphery, are sufficient to reverse SBMA symptoms (Lieberman et al., 2014). This treatment was able to extend the lifespan of AR121 mice, which usually die by 8 months of age (Cortes et al., 2014a).

1.7.8 The AR113 mouse model of SBMA

The most recent mouse model of SBMA to be developed was made by Ramzan et al. (2015). This model does not fully model SBMA, as the mutant AR is expressed either solely in the muscle or spinal cord of mice. Furthermore, in this model the transgene is only expressed in adulthood using a tet-On and Cre-loxP system. However, this mouse model has enabled the examination of whether the muscle or the spinal cord is the primary site of pathology in SBMA (for a review see Rinaldi et al. (2014)). Adult mice that had the transgene expressed in adulthood exclusively in the muscle for 4 weeks prior to examination, had a normal motor phenotype, despite a shift in muscle fibre type and the presence of inclusions. Mice that had the mutant AR gene expressed exclusively in the spinal cord showed a mild motor deficit and oxidative stress within the muscle, despite the total lack of inclusions. These results have led to the conclusion that for the full SBMA phenotype to be seen polyQ AR must be expressed both in the muscle and spinal cord from birth.

Owing to the vast number of models of SBMA, increasingly research into the pathogenic causes of the disease often uses multiple genetically distinct models in order to get a better understanding of both the muscular and neuronal pathogenic mechanisms. A summary of the available mouse models of SBMA is presented in Table 2.

Table 2 Mouse models of SBMA

Developed by	Age of onset of symptoms	Affected lifespan?	Nuclear Inclusions (NIs) in affected areas?	NIs in unaffected areas	MN Loss?	Castration Reduction of symptoms	Anti-androgen treatment
Bingham et al. (1995)	NA	No	No	No	No	NA	NA
La Spada et al. (1998)	NA	NA	NA	NA	NA	NA	NA
Adachi et al. (2001)	NA	No	Yes	Yes	No	NA	NA
Abel et al. (2001)	8 months	Death at 14 months	Yes	Yes	Unknown	NA	NA
Katsuno et al. (2002) The AR97Q model	9 weeks	Yes	Yes	Yes	Only MN dysfunction	Yes- Katsuno et al. (2002)	Katsuno et al. (2003), Renier et al. (2014)
Chevalier-Larsen et al. (2004) The AR112Q model	3 Months	No	Yes	Yes	Only MN dysfunction	Yes- Chevalier-Larsen et al. (2004)	NA
Sopher et al. (2004) The AR100 YAC	6 Months	No	No	No	Yes	Unknown	NA
Yu et al. (2006) Knock-in model	2 months	Death by 6 months	Yes	Unknown	Very late	Yes- Yu et al. (2006)	Renier et al. (2014)
Monks et al. (2007) The WT over-expressor	Unclear	Prenatal death without anti- androgen treatment	Unknown	Unknown	No	Yes-Monks et al. (2007)	Renier et al. (2014)
Cortes et al. (2014a) The AR121 BAC	12 weeks	Death by 8 Months	Yes	Unknown	No	Unknown	Lieberman et al. (2014)
Ramzan et al. (2015) The AR113 model	By 4 weeks post expression	Unknown	No	Yes	Unknown	NA	NA

1.8 Therapeutic approaches in SBMA

There have been a number of attempts to develop therapeutic strategies for SBMA. These include: targeting the AR by reducing levels of its activating ligand, disrupting the AR structure directly and focussing on AR co-regulators such as the heat shock proteins (HSPs).

1.8.1 Androgen deprivation

Importantly, SBMA pathology is dependent on levels of serum testosterone rather than the level of mutant AR. Females carrying the mutation have only subclinical symptoms, possibly in part due to X inactivation, but primarily due to lower serum testosterone levels in females. Symptoms can be exacerbated in female mice that model SBMA by administering testosterone (Katsuno, et al., 2003 b). Translocation of the AR bound to testosterone into the nucleus is a critical feature for the pathology of SBMA. This has led to the most extensive treatment research for SBMA- Androgen deprivation.

1.8.1.1 Androgen deprivation pre-clinical trials

Early trials in multiple SBMA mouse models used castration as a method of androgen deprivation, and in all mouse models analysed, castration significantly reversed the neuromuscular degenerative phenotype (Katsuno et al., 2002, Chevalier-Larsen et al., 2004, Monks et al., 2007, Johansen et al., 2009, Yu et al., 2006). Chemical impairment of AR activation has also been used in a number of pre-clinical trials. Most recently, the non- steroidal AR antagonist Flutamide has been trialled on three models of SBMA. In one of the models, the AR97Q model the effects of Flutamide were limited to a mild increase in hang wire time (Renier et al., 2014). Previous studies using Flutamide on this mouse model have concluded that it had no beneficial effect (Katsuno et al., 2003). For Flutamide to have a marked effect AR97Q mice had to be castrated and testosterone artificially administered in a monitored fashion. Using the knock-in model of SBMA, AR113Q (Yu et al., 2006), which largely recapitulate the muscular phenotype of the disease, Flutamide was shown to increase life-span and ameliorate disease symptoms. Lastly in the WT over expressor model of SBMA

(Monks et al., 2007), Flutamide significantly improved motor function, even in mice that were fully symptomatic when treatment began (Renier et al., 2014).

Another compound that decreases androgen levels has been shown to have beneficial effects in a mouse model of SBMA. Katsuno et al. (2003) showed that treatment with Leuprorelin, a Luteinising Hormone releasing hormone agonist which leads to the eventual decline of testosterone levels, rescued the SBMA phenotype. In summary, it appears that either Testosterone deprivation through the use of Leuprorelin, or AR antagonism through the use of Flutamide can exert beneficial effects in mouse models of SBMA. It is likely that the synergistic effect of these two compounds could be beneficial in SBMA.

1.8.1.2 Androgen deprivation in the clinic

For many years, because of its anabolic effects and the mild androgen insensitivity seen in patients testosterone was used as a potential treatment of SBMA (Goldenberg and Bradley, 1996). However, it has been shown that administration of Testosterone is likely not to seriously exacerbate symptoms in male patients (Chevalier-Larsen and Merry, 2012), as the toxic effects of the AR are maximised at normal serum Testosterone levels. Furthermore it has been shown that any deterioration of symptoms seen in patients given testosterone were reversible (Kinirons and Rouleau, 2008).

Clinical trials have now been carried out to find the effect of androgen deprivation in patients. In 2013, a long term Testosterone suppression trial was conducted in Japan on 16 patients. There were no beneficial effects of Leuprorelin in these patients and the study concluded that treatment should be given earlier in disease pathogenesis (Yamamoto et al., 2013). However, a larger phase 2 clinical trial was conducted previously by Banno and colleagues, where beneficial effects of Leuprorelin were seen as measured by AR accumulation in scrotal skin and swallowing function (Banno et al., 2009).

An alternative method of androgen deprivation that has been trialled in the clinic is Dutasteride treatment. Dutasteride is a 5α reductase inhibitor, which stops the conversion of testosterone to its more potent analogue Dihydrotestosterone (DHT). The results of this trial were largely positive, although it was suggested that a longer treatment period was needed to fully elicit the effects of Dutasteride treatment on disease progression (Fernandez-Rhodes et al., 2011).

1.8.2 Targeting the AR structure as a therapeutic strategy

Androgen deprivation has the unavoidable, unwanted side effect of sexual dysfunction. This has therefore led to the use of other aspects of AR signalling to develop therapeutics for SBMA. For example, most recently Zboray and colleagues have inhibited AR protein C- terminal / N- terminal interaction, fundamental for mis-folding of the polyQ AR as well as transactivation. Beneficial effects were seen in both MN and muscle pathology in a mouse model of SBMA (Zboray et al., 2015).

1.8.3 Targeting the Heat Shock Response as a therapeutic strategy

Disruption of the AR and its co-regulators has also been shown to have beneficial effects. Treatment with the Heat Shock 90 inhibitor 17-(Allylamino)-17-demethoxygeldanamycin (17-AAG), a derivative of Geldanmycin, which stops Hsp90 forming a stabilising complex with client proteins, such as the AR, and instead preferentially forms a proteasome targeting complex, and increases HSP40 and HSP70 expression has been trialled. The effects of 17-AAG and Geldanmycin were largely positive in a cell line and a mouse model of SBMA, significantly stopping protein aggregation and delaying the onset of motor symptoms (Thomas et al., 2006a, Waza et al., 2005). An additional HSP90 inhibitor 17-Dimethylaminoethylamino-17-demethoxygeldanamycin (17-DMAG), a more potent derivative of 17-AAG, has shown similar effects, ameliorating AR97Q mouse model symptoms by preferentially targeting the mutant AR for degradation by the Ubiquitin proteasome system (Tokui et al., 2009).

Overexpression of the Heat shock protein 70 (Hsp70) stops AR cofactor dissociation and translocation of the AR into the nucleus. This method has been used to treat a mouse model of SBMA (Katsuno et al., 2006b). Hsp70 over-expression prevents the toxic structure formation of β pleats in the polyglutamine stretch. This leads to a reduction of toxic accumulation of mutant protein and can facilitate protein degradation. Overexpression of Hsp70 can reduce levels of nuclear AR, as well as monomeric AR in the cytoplasm, as shown in SBMA mice crossed with a transgenic mouse overexpressing human Hsp70 (Adachi et al., 2003). In a neuron like cell line, Hsp70 has been shown to be beneficial in reducing aggregation of truncated mutant AR (Kobayashi et al., 2000). In addition, Hsp70 over expression can increase solubility of aggregated protein and enhance degradation by the proteasome in a cell culture model of SBMA (Bailey et al., 2002).

The Heat Shock Factor 1 (HSF-1) inducer Geranylgeranylacetone (GGA), has been shown to be beneficial in both neuronal cell lines and a mouse model of SBMA (Katsuno et al., 2005). Specifically GGA was found to increase the levels of Hsp105, Hsp90 and Hsp70, although high doses of this compound had to be administered. This study showed that GGA reduced cell death *in vitro*, even though there was no change in the percentage of cells with nuclear inclusions. *In vivo* analysis revealed that oral doses of this compound ameliorated muscle atrophy and increased the lifespan of SBMA mice (Katsuno et al., 2005). Furthermore, lentiviral delivery of HSF-1 into the CNS has been shown to stop the accumulation of mutant AR protein (Kondo et al., 2013).

Although mice used to trial cofactor intervention approaches were free from observable side effects, targeting the heat shock response can have some unwanted effects. For example 17-AAG is known to cause adverse effects on the digestive system, due to it having a global effect on all nuclear receptors as well as Extracellular regulated kinases (Erk 1/2). Treatment with the more AR-specific therapeutic agent ASC-J9, which disrupts AR interaction with its co-factor ARA70, has been shown to increase survival and reverse muscle atrophy in a mouse model of SBMA, with fewer unwanted effects than 17 AAG (Yang et al., 2007). Furthermore in the Greensmith

lab, using the HSP co-inducer Arimoclomol, which only enhances the heat shock response (HSR) in stressed cells where the HSR has been activated, has been shown to have beneficial effects in the AR100 mouse model (Malik et al., 2013).

Whether HSP over expression reduces aggregate formation (Kobayashi et al., 2000), stops AR translocation into the nucleus (Adachi et al., 2003), or enhances degradation by the proteasome (Bailey et al., 2002, Tokui et al., 2009), it is indeed beneficial in models of SBMA (Malik et al., 2013).

1.9 Summary of Thesis Aims

In this PhD project, I aim to investigate the pathogenesis of SBMA through the use of a transgenic mouse model of SMBA. The AR100 mouse model was developed by La Spada's group by introducing a yeast artificial chromosome (YAC) containing human AR into mouse embryonic stem cells (Sopher et al., 2004). The mutant AR contains 100 CAG repeats and is expressed at close to normal levels under the control of endogenous regulatory elements. The mutant AR is ubiquitously expressed in the mice and they develop a progressive neuromuscular degenerative phenotype with motor neuron degeneration at approximately 8 months old. The onset of disease symptoms in these mice is similar to that in human patients, where onset occurs during midlife.

My first aim is to investigate the Fas/NO pathway of MN death, which has been proposed by Bernard-Marissal et al. (2012). Previous results from the Greensmith lab have shown that ER stress is an early pathogenic feature of MNs from AR100 mice (Montague et al., 2014). Thus I seek to investigate whether the Fas/NO pathway, which is proposed by Bernard-Marissal et al. (2012) to be specific to mutant superoxide dismutase Amyotrophic lateral sclerosis, can actually be extrapolated to SBMA.

A second aim of this project is examine whether the muscle is a primary site of pathology in SBMA. Although SBMA is widely considered to be a motor neuron disease, where primary pathology is in MNs, recent findings have suggested that

muscle may play a key role in SBMA pathogenesis (Rinaldi et al., 2014, Jordan and Lieberman, 2008).

The final aim of this Thesis is to investigate the molecular pathways that may play a role in muscle pathology in SBMA, to determine the molecular processes underpinning physiological and histological changes observed in the AR100 mouse model of SBMA.

Chapter 2 Mechanisms of MN degeneration in the AR100 Mouse model of SBMA

2.1 Introduction

In this Chapter, I undertook a series of experiments to determine whether a specific cell death pathway that has been implicated to play a role in Motor Neuron (MN) degeneration in the SOD1 mouse model of ALS, also played a role in SBMA. Specifically, ER stress, Calreticulin and the Fas/NO cell death pathway were examined.

2.1.1 ER stress, Calreticulin and the Fas/NO Cell death pathway: Do they play a role in SBMA?

In this Chapter, I investigated whether ER stress, an early pathogenic mechanism observed in a number of neurodegenerative diseases, including the AR100 mouse model of SBMA (Montague et al., 2014), resulted in a reduction of the ER calcium chaperone Calreticulin (CRT), leading to cell death via the Fas/NO cell death loop. This pathway has been proposed to play a role in MN death in SOD1- ALS (Bernard-Marissal et al., 2012). The unfolded protein response and ER stress are attractive candidates for investigation as therapeutic compounds which target these mechanisms, such as Salubrinal and GSK260614 have been used *in vivo* in other neurodegenerative diseases with a positive effect (Saxena et al., 2009, Moreno et al., 2012). Using both primary embryonic motor neuron cultures as well as spinal cord ventral horn tissue from AR100 mice at different stages of disease, I examined whether the Fas/NO and CRT pathway also play a role in MN death in the AR100 mouse model of SBMA. Furthermore, as the androgen receptor and Calreticulin bind directly, the nature of Calreticulin's possible involvement in SBMA pathogenesis was examined as it is known to play a role as an enhancer of nuclear export of nuclear receptors such as the androgen receptor.

2.1.2 The Unfolded Protein Response

ER stress is a result of the accumulation of misfolded proteins in the ER. The ER Unfolded Protein Response (UPR) is a highly conserved regulatory process in which the cell acts in order to either re-fold or degrade proteins that have been incorrectly synthesised. If this process is insufficient in comparison to the protein load, apoptosis is initiated (Hetz, 2012).

A state of ER stress is sensed in mammals by at least three sensors:

I) Binding Immunoglobulin Protein (BiP). BiP binds to misfolded proteins, such as the mutated androgen receptor (Yang et al., 2013) and in states of high misfolded protein load ('ER Stress') it remains bound to the protein, dissociates from IRE1, which releases it from suppression and by the process of autophosphorylation, it dimerises and forms clusters. This in-turn causes degradation of mRNA, thus halting translation as a pro-survival mechanism to reduce the protein load in the cell (Figure 2);

II) Activating transcription factor 6 (ATF6), another pro-survival ER stress sensor which is transferred to the Golgi where it is processed to release a cytosolic fragment (ATF6f) leading to the increased transcription of ER associated protein degradation (ERAD) associated genes.

III) Protein Kinase RNA-like ER kinase (PERK) initiates chronic ER stress -induced cell death. Upon high levels of protein load, PERK phosphorylates eukaryotic translation initiation factor 2 alpha (eIF2α), which allows translation of Activating Transcription Factor 4 (ATF4), which then allows transcription of genes which control apoptosis, such as C/EBP Homology Protein (CHOP), which down regulates the expression of the anti-apoptotic protein family B Cell Lymphoma 2 (BCL2), thus leading to apoptosis (Figure 3). There are of course cross links between these pathways, creating both a temporal activation of each of the pathways and an interlinked system. For example ATF6f, is thought to cause transcription of BiP, linking these two pathways and causing a cumulative response (Haze et al., 1999).

ER stress-induced apoptosis is mediated by caspase 12, which has been shown to be located in the ER membrane (Nakagawa and Yuan, 2000). Following aberrant Ca^{2+} signalling and unmanageable protein load, caspase 12 is cleaved by calpain and eventually caspase 3, activating proteolytic cleavage of cellular components (Martinez et al., 2010). Furthermore, it has been shown that knock out of caspase 12 is protective against ER stressors such as Tunicamycin (which blocks N glycosylation of

proteins in the ER), Thapsigargin (which depletes the ER of Ca^{2+} stores) and the Ca^{2+} ionophore A23187, both *in vivo* and *in vitro* (Nakagawa et al., 2000)

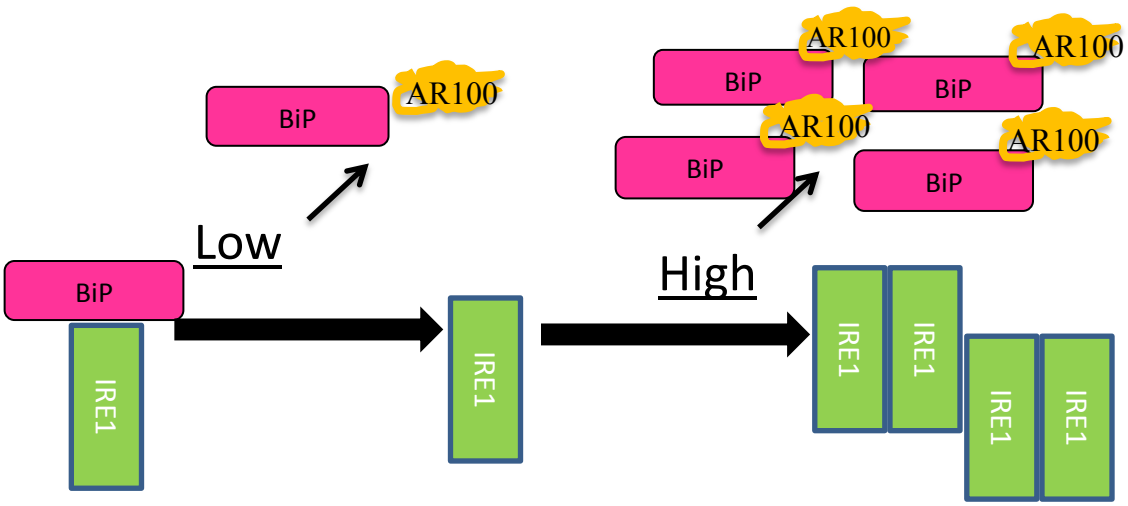

Figure 2 Binding Immunoglobulin Protein schematic

Binding Immunoglobulin Protein (BiP) is a marker of ER stress. In non-stressed cells BiP represses Inositol-requiring protein 1 (IRE1). However, in the presence of stress BiP dissociates from IRE1, and binds the misfolded protein such as AR100 allowing IRE1 to form dimers.

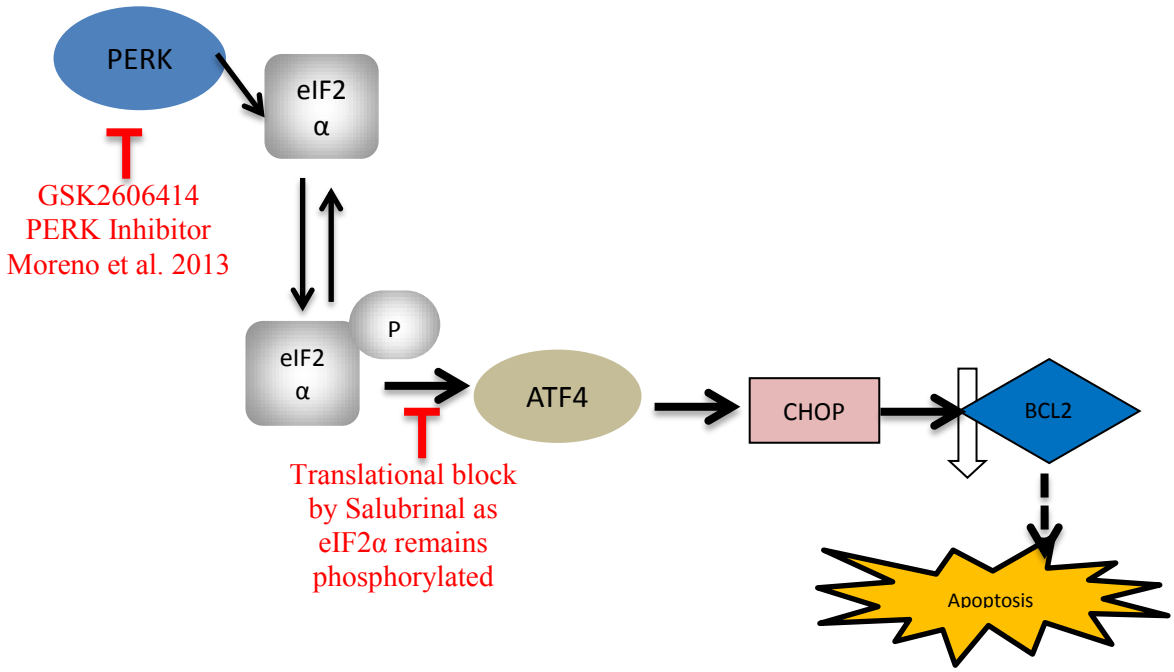

Figure 3 ER Stress response activation proteins

PERK pathway of ER stress mediated cell death when there is irreversible protein load in the cell. Two therapeutic agents, GSK2606414 and Salubrinal, target components of this pathway.

2.1.3 Calcium Homeostasis

Calcium plays a critical role in cells as a mandatory signalling molecule. Strict regulation of Ca^{2+} levels is particularly important in excitable cells such as neurons and muscle. Not only is it responsible for signalling at the neuromuscular junction, but it is also fundamental for excitation- relaxation coupling. The primary store of Ca^{2+} in the cell is the ER, or its muscular analogue the sarcoplasmic reticulum (SR). Calcium release from the ER is controlled by the inositol 1,4,5 triphosphate receptor, and the ryanodine receptor and levels are restored in using the Sarco/endoplasmic reticulum Ca^{2+}-ATPase (SERCA) (Tadic et al., 2014). Upon depletion of ER calcium transcriptional and translational cascades are initiated, termed the Unfolded Protein Response

(UPR). The ER chaperones discussed above, such as BiP and Calreticulin (discussed in section in 2.4.5 in greater depth), are responsible for maintaining ER Ca^{2+}levels.

2.1.4 Endoplasmic Reticulum stress in Poly Q Diseases and Motor Neuron Diseases

ER stress is a feature of a number of neurodegenerative diseases in which protein mis-folding is a pathological hallmark (Ciechanover and Kwon, 2015). In polyQ diseases, such as Huntington's disease (HD), ER stress and aberrant Ca^{2+} handling has been investigated. Fernandes et al. (2007) observed altered Ca^{2+} signalling in medium sized spiny neurones- as a result of NMDA receptor excitotoxicity. Furthermore, it has also been shown that the Huntington protein itself has an ER stress sensitive domain (Atwal and Truant, 2008). Braubach et al. (2014) found altered calcium signalling in skeletal muscle fibres in a mouse model of Huntington's disease. It has been shown that expanded polyglutamine alone, even when not just located in a misfolded protein, is sufficient to induce ER stress. Kouroku et al. (2002) have shown that transfection with polyQ72 is sufficient to cause the level of BiP protein to increase and caspase 12 to activate in cell lines. Further work from the same group showed that poly Q transfection- induced ER stress activates ER associated protein degradation (ERAD), including autophagy, which they suggest is initially protective, but becoming detrimental as the disease progresses. They also show that as polyQ aggregates become larger, the autophagy pathway is used to degrade them (Kouroku et al., 2007).

Interestingly, it has been shown that the ER stress response can be activated to protect cells from polyglutamine toxicity in preference to other cell defence processes. Duennwald and Lindquist (2008) have shown that mutant Huntington protein causes an ER stress response in both yeast cells and a neuron-like cell line, and that overexpression of ERAD proteins is protective. However in this study they also report that the Heat Shock Response (HSR), one of the most general cell defence mechanisms, was not activated. This is highly unusual and as the authors themselves state, in their own previous work as well as other models of polyglutamine toxicity, activation of the HSR usually occurs (Huen et al., 2007).

This finding highlights however, that ER stress is an important and early process in polyQ toxicity, even in the absence of other pathways normally responsible for regulating cell survival under stress. The ER stress pathway undoubtedly interacts with additional cell signalling pathways. Nishitoh et al. (2002) have shown that Apoptosis Signalling Kinase 1 (ASK1) is essential for mediating ER stress-induced cell death in neuronal cell lines. They found that treatment with the ER stressors Thapsigargin (which inhibits SERCA, and causes ER calcium depletion) and Tunicamycin (which inhibits N glycosylation), induced ASK1 expression, which then associated with IRE1. The different ER stress sensors are believed to activate different responses. Thomas et al. (2005) showed that in HeLA cells, IRE1 mutations did not alter levels of ER stress mediated cell death, however ATF6 mutations did, indicating that the ATF6 pathway is responsible for initiating apoptosis.

Altered Ca^{2+} processes are not limited to polyQ diseases. In fact, an increase in ER stress markers is one of the first pathogenic signs in mouse models of ALS, a usually rapidly progressive and fatal motor neuron disease (Saxena et al., 2009). Although the majority of ALS cases are sporadic, approximately 10% of cases are familial, and of these around 10-20% are due to mutations in the superoxide dismutase 1 (SOD1) gene (Bento-Abreu, et al., 2010). Saxena et al. (2009) reported that an increase in ER stress markers as early as postnatal day 5 (P5), although no data was presented at this time point to support this finding. They also identify a subtype of motor neurones, fast fatigable MNs, which are particularly vulnerable to this ER stress response. Moreover treatment of a small number of $SOD1^{G93A}$ mice, which model SOD1-ALS (n=5 per group), with a specific eIF2α dephosphorylation inhibitor, Salubrinal (Boyce et al., 2005), was found to improve disease phenotype. Continuous activation of eIF2α-P leaves the ER stress response activated in order to enhance the clearage of misfolded proteins. This treatment was well tolerated in $SOD1^{G93A}$ mice, and resulted in a delay of disease progression. These findings suggest that targeting of ER stress may be a potential therapeutic strategy for other neuromuscular diseases, including SBMA.

Salubrinal has also been used *in vivo* in the treatment of excitotoxic brain injury in rats (Sokka et al., 2007), where it reduced the number of degenerating hippocampal neurons. Conversely in a model of Prion disease, it has been shown that due to the translational repression activity of eIF2α in its phosphorylated form, Salubrinal treatment can actually exacerbate disease (Moreno et al., 2012). Further work by the same group targeted a different component of the ER stress response, PERK. Following treatment with the compound GSK2606414, which blocks the activation of PERK, there was an increase in the lifespan of a mouse model of prion disease. It should be noted that although GSK260614 is highly selective for PERK, treatment with this compound did have significant systemic affects leading to a cohort of mice being culled prematurely due to significant loss of body weight (Moreno et al., 2013).

Salubrinal has also been tested in cellular models of HD, where it was shown to decrease levels of ER stress markers (Reijonen et al., 2008). Since there is no effective, acceptable treatment for SBMA, and in view of reported beneficial effects of ER stress inhibitors in models of MND (Saxena et al., 2009) and polyglutamine diseases (Reijonen et al., 2008), it is possible that targeting of ER stress may be effective in SBMA.

2.1.5 ER Stress in SBMA mouse models

Work undertaken in the Greensmith lab (Montague et al., 2014), using the AR100 mouse model of SBMA (Sopher et al., 2004) has shown that AR100 motor neurons exhibit features of ER stress, both in cultured embryonic motor neurons as well as in the spinal cord of AR100 mice. Indeed ER stress was observed *in vivo* as early as the postnatal period, a similar time to the reported appearance of ER stress in the $SOD1^{G93A}$ model (Saxena et al., 2009). Interestingly, as observed in $SOD1^{G93A}$ mice, expression of ER stress markers peaked as early P5 in AR100 mice, leading authors to suggest that ER stress may be a trigger of motor neuron degeneration in SBMA. Using Calcium imaging techniques Montague et al. (2014) found that embryonic AR100 MNs *in vitro* had a higher level of basal cytosolic calcium and DHT treatment caused a significant reduction in ER calcium concentration. They also detected a higher level of

expression of cleaved caspase 12, an ER stress-specific caspase (Martinez et al., 2010), in AR100 primary MNs.

Furthermore, other authors have reported a higher incidence of BiP and AR co-localisation in the nucleus of AR97Q SBMA mice, in comparison to the non-pathogenic AR24Q mice (Yang et al., 2013). A key finding of this paper is the proposal that BiP can translocate from the ER to the nucleus bound to the AR, as BiP is classically reported to only be located in the ER. Interestingly, BiP binds the AR even when it is in its normal conformation and has been shown to regulate embryonic stem cell differentiation along with caspase 3 (the executioner caspase). In the absence of DHT, both BiP and AR were found dispersed in the cytoplasm, yet when DHT is added the proteins form inclusions in the nucleus of differentiating embryonic stem cells.

The ER stress response is thought to occur as a result of misfolded protein accumulation and aggregate formation in the ER. However, as BiP, an ER stress chaperone, can be found external to the ER, this raises the possibility that ER chaperone proteins may have roles in protein homeostasis outside the ER. This is particularly relevant to SBMA because aggregation occurs in the nucleus in the presence of DHT (Li et al., 1998a, Li et al., 1998b).

2.1.6 ER stress and the Fas/NO cell death pathway

In 2012, the ER stress response in ALS was linked to the tissue necrosis factor family member FasL and Nitric Oxide (NO) - induced cell death, by the work of Bernard-Marissal et al. (2012). The Fas pathway of programmed cell death was described as specific to MNs by Raoul et al. (1999), where they showed that in 50% of MNs, Fas Ligand is responsible for regulating programmed cell death. The activation of Fas was seen as a result of trophic factor deprivation and acted in the classical pathway causing clustering of the Fas - associated death domain (FADD), which activates the 'initiator caspase,' caspase 8, leading to mitochondrial release of Cytochrome c and apoptosis (See Figure 4). The authors proposed that this pathway was involved in MN development, since FasL expression coincides with the occurrence of programmed

cell death *in vivo* 4-6 days after MNs first make contact with target muscles in the mouse. Exogenous addition of FasL did not trigger cell death after 5 DiV, due to the expression of FADD-like interleukin-1 beta-converting enzyme-like inhibitory protein (FLIP), its long isoform is responsible for caspase 8 inhibition (Chang et al., 2002). FLIP expression was shown to increase after 5 DiV, thus demonstrating that Fas activation is a developmentally regulated pathway.

In MNs, a specific Fas induced cell death pathway can be activated that is slower than the classical Fas- Caspase 8 cell death pathway. The delay in completion of cell death is due to the requirement of translational up-regulation of neuronal Nitric Oxide Synthase (Raoul et al., 2002). Briefly, FasL activation causes activation of Death associated protein 6 (Daxx), Apoptosis signal-regulating kinase 1 (Ask1) and phosphorylated p38 mitogen-activated protein kinase (p-p38 Kinase). This leads to a transcriptional up-regulation of neuronal NOS (nNOS) causing NO production, ultimately generating perioxinitrite, leading to MN damage. Little evidence of this cell death pathway has been found in other Fas sensitive cell types, including fibroblasts and thymocytes, leading the authors to hypothesise that this pathway may be a mediator of MN death seen in ALS due to its cell type specificity (Raoul et al., 2002).

Increased vulnerability to Fas-induced cytotoxicity in purified embryonic day 12.5 (E12.5) MNs from three different SOD1 mutants has been reported (Raoul et al., 1999, Raoul et al., 2000). NO, which does not kill normal MNs (Estevez et al., 1999a, Estevez et al., 1999b), does induce mutant SOD (mtSOD) MN cell death. Interestingly, the increased vulnerability of mtSOD MNs to Fas and NO did not demonstrate a linearly proportional relationship. High doses of sFasL caused the same amount of death in WT and mtSOD MNs, and only at a concentration of 0.1ng/ml sFasL were mtSOD MNs more vulnerable (Raoul et al., 2002). It is well known that mtSOD MNs are no more vulnerable than WT MN to most cell stressors, and indeed in the study by Raoul et al. (2006), MNs trophic factor deprivation or glutamate excitotoxicity killed no more mtSOD than WT MNs. However the Fas/NO pathway has also been detected *in vivo,* where an increase in FasL in $SOD1^{G93A}$ spinal cord has been shown to act in a feedback loop, with NO actually causing the increase FasL (Raoul et al., 2006).

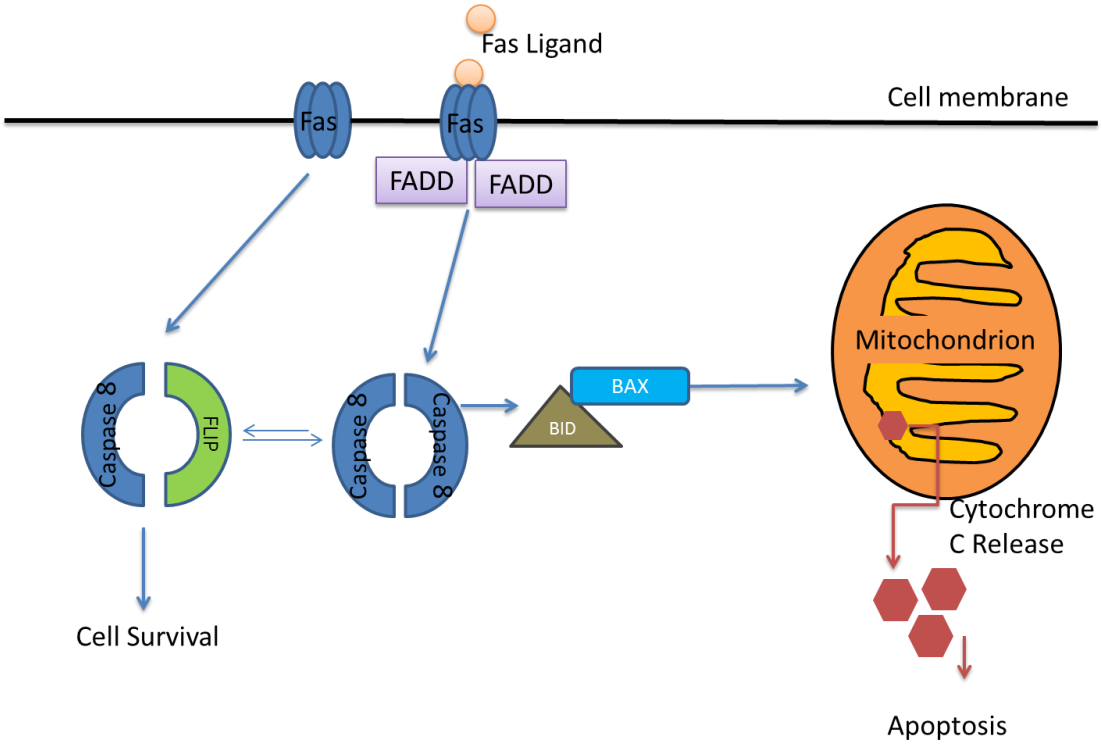

Figure 4 Schematic of Classical Fas activation leading to cell death

Upon activation Fas ligand binds to its receptor on the cell membrane. This leads to clustering of the Fas associated death domain (FADD) this leads to the activation of caspase 8 by dis-inhibition by its repressor protein FADD-like interleukin-1 beta-converting enzyme-like inhibitory protein (FLIP). This cases activation of BH3 Interacting domain (BID), allowing its association with Bax (a pro- apoptotic Bcl-2 like protein) and the formation of pores on the mitochondrial membrane allowing cytochrome C release and apoptosis.

The ER stress response was originally linked to the Fas/NO cell death loop by Duplan et al. (2010). Taking a proteomic approach to quantify proteins, they found that treatment of SOD^{G85R} MNs with the NO donor DetaNONOate, resulted in a decrease in the ER chaperone Calreticulin (CRT). Bernard-Marissal et al. (2012) examined the role of CRT in SOD1 MN death. They reported altered intracellular Ca^{2+} in primary motor neurons of $SOD1^{G93A}$ mice at 3 DiV, as well as increased expression of ER stress related markers such as BiP and ATF4, which was associated with a decrease in CRT levels. This reduction in CRT was also detected *in vivo,* in the ventral spinal cord of $SOD1^{G93A}$ mice, where CRT levels were reduced by 50% by P37 compared to WT levels. This lead Raoul and colleagues to propose a cell death pathway, that was specific to fast fatigable MNs in mtSOD mouse models (See Figure 5). The relatively slow time course of this cell death pathway, taking days rather than seconds (as in classical Fas activation), recapitulates the features of a progressive neurodegenerative disease such as ALS.

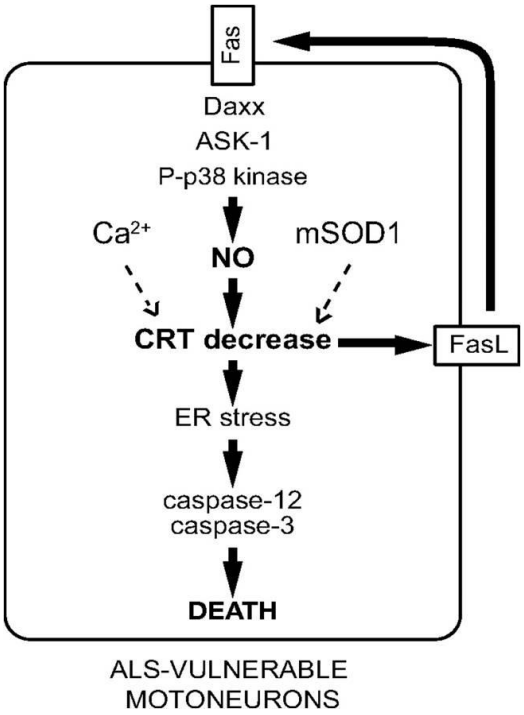

Figure 5 The Fas- NO Cell death loop

This diagram summarises the cell death pathway proposed to be specific to mutant SOD1- induced MN death (Taken from Bernard-Marissal et al. (2012))

2.1.7 Aims of this Chapter

In this Chapter I examined whether the Fas/NO cell death pathway that depends on changes in CRT levels, and which has been implicated to be specific to mtSOD1 MN death, also plays a role in the death of MNs in the AR100 mouse model of SBMA. This was examined in primary embryonic MN cultures from AR100 mice, which were exposed to a number of cell stressors. The response of WT and AR100 MNs was then examined by assessment of a number of parameters: including i) MN Survival, ii) Expression of Calreticulin and iii) Neurite outgrowth.

2.2 Materials and Methods

2.2.1 Maintenance and identification of AR100 and SOD1^{G93A} mice

All the experimental procedures carried out in mice in this study were performed in accordance with the Scientific Procedures Act (1986), under a licence from the UK Home Office following the approval from UCL IoN Animal Welfare and Ethical Review Board (AWERB).

2.2.1.1 AR100 Mice Genotyping

The generation of the AR100 mouse model has been previously described (Sopher et al., 2004) and the mice characterised (Malik et al., 2013, Sopher et al., 2004, Thomas et al., 2006b). AR100 mice were originally obtained from Albert R. La Spada's laboratory (UCSD, USA) and a colony established and maintained at UCL Biological Services. The genotype of the mice was confirmed by PCR. Tail snips were taken from each individual embryo or postnatal mouse, and the samples were digested in a Rapid digestion buffer (50mM Potassium Chloride, 10mM Tris-Hcl pH8.3, 0.1mg/ml Gelatine, 0.45% NP40 and 0.45% Tween-20). Tail snips were then incubated at 55°C for 10 minutes, vortex then put in a 95°C water bath for 5 minutes. Samples were then centrifuged at 14000g at 4°C for 5 minutes.

Eluted DNA was genotyped using PCR amplification prior to culturing using the forward primer 5'-CATCTGAGTCCAGGGAACAGC-3' and the reverse primer 5'-GCCCAGGCGTGCCGTAGTC-C3'. The PCR product was then digested with the Bgl1 restriction enzyme (Figure 8). Alternatively, some genotyping employed a shorter protocol, using the primers 5'-AG CCC GAG TTT GCA GAG A-3' and 5'- TCT CCG CGT GCA GCC TA -3' to detect the human androgen receptor and as an internal control to detect the mouse prion protein 5- AAA GGG CTG TTC TCA GAG GCA C -3' and 5'-CTG CAT GAC CTG AAG CAA AAT CA-3' (Figure 8B).

2.2.1.2 SOD1^{G93A} mice Genotyping

SOD1^{G93A} mice were originally purchased from Jacksons Labs (USA) and a colony subsequently bred and maintained at UCL Biological Services. This colony was

maintained on a BL6/SJL background, by cross mating SOD1^{G93A} mice with F1 progeny were genotyped using the following primers 5'- CTA GGC CAC AGA ATT GAA AGA TCT -3', 5'- GTA GGT GGA AAT TCT AGC ATC ATC -3', 5'- CAT CAG CCC TAA TCC ATC TGA -3', and 5'- CGC GAC TAA CAA TCA AAG TGA -3' (Figure 8C). PCR products were run in a 3% agarose gel for 25 minutes at 90v. Bands were visualised using Genesnap from syngene software (Figure 8).

2.2.2 Primary Motor Neuron Cultures

2.2.2.1 Mixed ventral horn cultures

AR100, SOD1^{G93A} and wild type (WT) E12-14 ventral spinal cords were dissociated in 0.025% trypsin and plated on laminin and poly-ornithine coated plates. Cells were grown in neurobasal medium supplemented with 2 % B27 Supplement, 0.5 mM glutamine, 0.05% mecaptoethanol , 2% horse serum (Invitrogen) 0.5ng/ml ciliary neurotropic factor (CNTF), 0.1ng/ml Brain derived neuroplasticity factor (BDNF), 0.1ng/ml glial derived neurotropic factor (GDNF) (Caltag, Silverstone), 50 U/ml penicillin and 50µg/ml streptomycin (Sigma-Aldrich).

2.2.2.2 Treatment of AR100 and SOD1^{G93A} MN cultures

AR100 cultures were grown for 7 DiV and were treated with Dihydrotestosterone 50 nM (DHT) on DIV 5 (Figure 6). Both AR100 and SOD1^{G93A} cultures were incubated in the presence of 5% CO_2 at 37°C for 6 DiV and then treated with a stressor: DetaNONOate (0-50µM), Thapsigargin (0-1 µM) or soluble Fas ligand (0-150 ng/ml), with enhancer for ligand at a constant concentration of 1µg/ml (Enzo-Life Sciences), for 24 hours prior to fixation with 4% paraformaldehyde.

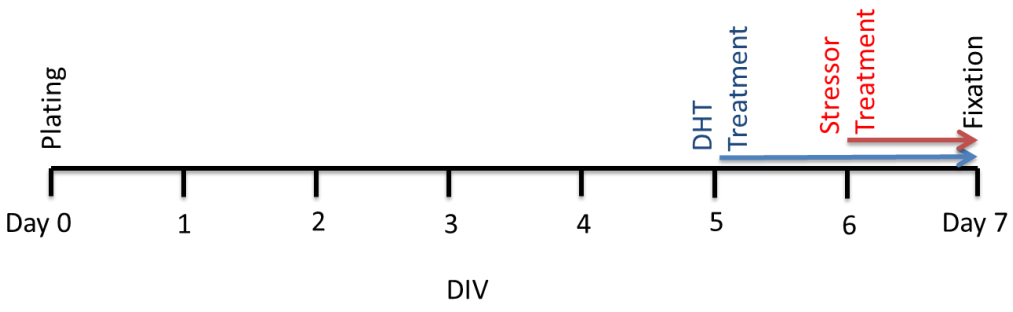

Figure 6 Treatment timeline for 7 DiV MNs

Table 3 Stressors mode of action

Stressor	Mode of action
Thapsigargin	An ER stressor that acts by inhibiting sarco/endoplasmic reticulum Ca^{2+}-ATPase (SERCA) therefore stopping ER calcium being replenished
DetaNONOate	A Nitric Oxide (NO) donor that spontaneously dissociates into NO molecules in a pH dependent manner
Soluble Fas Ligand with enhancer	Recombinant human Fas. Kills Fas sensitive cells with a cross linking enhancer. The enhancer increases the biological activity of Fas. Induces apoptosis. See Figure 4 for a description of the cell death pathway.

2.2.2.3 Purified motor neuron cultures

AR100, $SOD1^{G93A}$ and WT ventral horn cells were dissociated and grown as described above, but a maximum of 5 embryos were pooled according to genotype before dissociation. Cells then underwent an additional purification step, which involved spinning at 760g for 20 minutes through Optiprep (Axis-Shield), at 10.5 % v/v in HBSS. Cells were alternatively maintained for a total of 3 DiV (Figure 7). In these experiments, AR100 cells were treated with DHT 24 hours after plating. Stressor treatment of both AR100 and $SOD1^{G93A}$ with cell stressors occurred at 2DiV and maintained for 24 hours before fixation at 3DiV. The concentration of stressors were 10µM DetaNONOate, 100ng/ml sFasL with enhancer for ligand or 100nM Thapsigargin. However analysis of these cultures revealed that the purity of cultures was not enhanced by this method, and fibroblasts and glial cells remained in the culture.

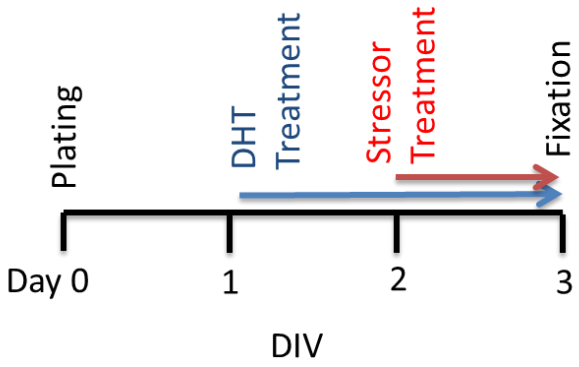

Figure 7 Treatment timeline for 3 DiV MNs

2.2.3 Spinal Cord Dissection and storage for Western Blotting

Lumbar spinal cord samples were collected from 5 day old (P5), 3, 12 and 18 month old WT and AR100 mice. Spinal cord samples were collected from $SOD1^{G93A}$ mice at 5 days, 30 days (pre-symptomatic) and 120 days (end stage). The mice were terminally anesthetised with phenobarbitone and perfused with transcardially 0.9% saline. The lumbar section of the spinal cord was identified and the spinal cord was cut above L2 and below L6 and removed. The cords were snap frozen in liquid nitrogen and stored at -80°C until ready for further processing for western blotting.

2.2.4 Mouse Perfusion, Spinal Cord dissection and sectioning for immunohistochemistry

For immunohistochemistry, mice were transcardially perfused with fixative (4% PFA in PBS), and the lumbar spinal cord removed and post fixed overnight at 4°C. The lumbar region was defined by identification of the lumbar nerves, and L2 to L6 region was isolated. The cords were then cryo-protected in 30% Sucrose in PBS with 0.001% Sodium Azide at 4°C, until sectioned using a cryostat. Cross sections of spinal cord were cut at 12µm, and collected serially onto polylysine coated slides. Lumbar sections were stained overnight with the neuronal marker β III Tubulin (1 in 1000; Covance), Calreticulin (1 in 500; Santa Cruz) and DAPI (5 minutes, 1 in 1000; Sigma), to identify nuclei.

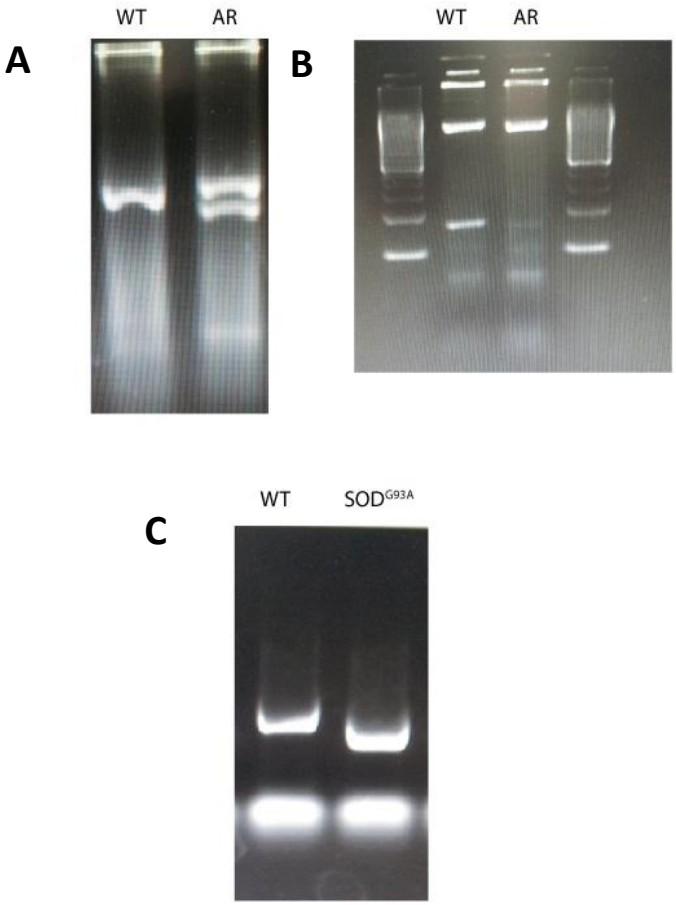

Figure 8 Genotyping of AR100 and SOD1^{G93A} Mice

PCR Products for A) the androgen receptor protein with Bgl1 restriction digest, B) the AR PrP genotyping protocol C) the SOD1^{G93A} mutation. PCR Products were run on a 3% agarose gel, in TBE, for 25 minutes at 90v.

2.2.5 Western Blotting

P5 and adult spinal cord tissue were homogenised on ice in 50mM Tris pH 7.5, 150mM, Sodium Chloride, 1% NP40, 0.5% Sodium Deoxychloride, 0.1% Sodium dodecyl sulphate, 1mM EDTA, 1mM EGTA , 1mM PMSF and Sigma Protease inhibitor cocktail. Samples were spun at 14000 rpm at 4 °C for 20 minutes. The supernatant containing soluble proteins was decanted. Bio-Rad DC protein assay was used according to the manufacturer's protocol. Proteins were separated according to SDS-PAGE and transferred onto nitrocellulose membrane. The membrane was incubated with primary antibodies (CRT 1:1000 Pierce Antibodies; β Actin 1:5000 abcam) in 5% milk protein for 12 hours at 4°C. The membranes were incubated with HRP-conjugated secondary antibodies (Dako 1:1000) for 2 hours at room temperature. The blot was visualised using SuperSignal West Pico Chemiluminescent Substrate (Thermo Scientific).

2.2.6 Immunocytochemistry on cell cultures

Cell cultures were immuno-stained with antibodies for the neuronal marker β III Tubulin (1:1000 Covance), and for Calreticulin (1:500; Pierce antibodies). For Androgen receptor localisation, cells were stained with either the N20 or C19 primary antibody (1:200; Santa Cruz). A digram of where the AR antibodies bind to the AR protein can be found in Figure 9. Cultures were pre-blocked for 1 hour in 5% animal serum in PBS 0.1% Triton at room temperature, the cultures were then incubated for approximately 12 hours at 4°C with the primary antibody at the concentrations stated above. AlexaFlur secondary antibodies were then used at a concentration of 1:1000 in PBS Triton. Nuclei were stained with DAPI (Sigma, 1:2000 for 5 minutes).

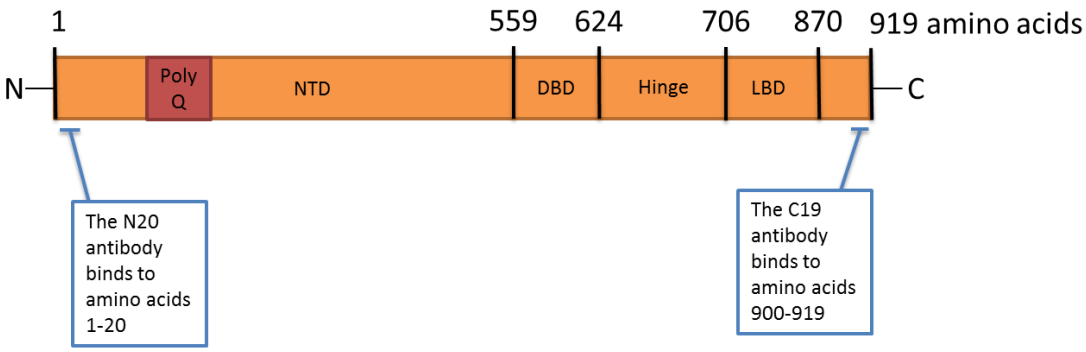

Figure 9 Diagram showing where AR antibodies bind to the protein

The N20 antibody binds in the N terminal Domain (NTD) at amino acids 1-20. There is also a DNA binding domain (DBD) a hinge region and a Ligand binding domain. The C19 antibody binds at amino acids 900-919 in the C terminal.

2.2.7 Motor Neuron Survival *in vitro*

The survival of primary MNs *in vitro* under the various experimental conditions was determined using cell counts and a biochemical assay as described below.

2.2.7.1 Motor Neuron Counts *in vitro*

The number of MNs present in cultures under various conditions was assessed morphologically, using the following criteria: immunostaining for the pan-neuronal marker, β III tubulin and the presence of more than 3 neurites. A minimum of 18 systematically chosen fields from at least 2 coverslips from each culture were examined and a minimum of 3 cultures per experimental condition was studied. Cells were defined as pyknotic when the nuclei had a fragmented appearance, the size of the nucleus was reduced by approximately 50% from normal, accompanied by an increase in the staining for nuclear marker DAPI. The total number of βIII Tubulin-positive, pyknotic nuclei was also determined.

2.2.7.2 Lactate Dehydrogenase assays

Lactate dehydrogenase (LDH) is an oxidoreductase enzyme that catalyses the interconversion of pyruvate and lactate. Upon lysis, cells release cytosolic LDH, which can be quantitatively measured. The Roche Cytotoxicity Detection Kit (LDH)

was used according to the manufacturer's protocol to determine cell survival. Briefly the supernatant from pure MN cell cultures was combined with the reaction mixture and samples were read using the FLUOStar Omega plate reader at 490nm. Levels of LDH activity were normalised to the Bio-rad DC protein assay for each individual well.

2.2.7.3 Automated Cell counts Using MetaXpress and Intensity Measurements

Cell counts were performed using MetaXpress analysis software. Cells were immuno-stained for the neuronal marker β III Tubulin, the nuclear marker DAPI and for CRT intensity analysis with and an anti CRT primary antibody. Cells were plated in Falcon® 96 Well Black plates with Clear Flat Bottom, coated with polyornitine and laminin. The number of viable cells was determined with the aid of Trypan blue (Sigma), and cells were plated at a density of 10,000 per well and were maintained for 3DiV. AR100 MNs were treated with 50nM DHT for 48 hours prior to fixing.

Images were acquired using the 20x lens, 9 fields per well were imaged with a minimum of 3 wells per condition in at least 3 independent cultures. MetaXpress Multi wavelength cell scoring application was used to count the number of all cells (DAPI positive), the number of neurons (β III Tubulin positive) and the average intensity of CRT staining for each individual cell. Using Excel, the CRT intensity for neurons only was calculated and differences in protein were analysed in reference to the relevant control for each individual experiment.

2.2.8 Neurite Outgrowth Analysis

Using MetaXpress's Neurite outgrowth application, the number of processes per neuron, the total outgrowth length per neuron, the maximum process length and the number of neurite branches per cell were determined. All analyses were undertaken on neurons after 3DiV, in cultures stained with β III Tubulin and DAPI. Analyses were undertaken in WT and AR100 cultures grown in the presence or absence of 50nM DHT.

2.2.9 Statistical analysis

All data was analysed using SPSS statistics version 21. Data is depicted as mean ± standard error. Data was deemed significant when $P<0.05$. Cell counts and densitometry data was analysed using one way ANOVA and Tukey post hoc tests, with data normalised to the relevant control.

2.3 Results

ER stress has been implicated in a number of MN diseases including ALS (Doyle et al., 2011). Previous results from our lab have shown that ER stress may also play a role in the death of MNs in the AR100 mouse model of SBMA. In the SOD1 mouse model of ALS, it has been suggested that a reduced expression of the ER chaperone, Calreticulin (CRT) resulted in ER stress initiated by the mSOD1 specific cell death pathway (Bernard-Marissal et al., 2012). In view of the finding of ER stress in AR100 MNs, in this Chapter I examined whether decreased CRT- induced MN ER stress and degenerating was restricted to the SOD1- specific Fas/NO cell death pathway, as suggested by Bernard-Marissal et al. (2012).

In the first instance, primary MN cultures from AR100 mice were characterised and compared to WT and $SOD1^{G93A}$ MN cultures. Ventral horn cultures were cultured for either 3 or 7 days and a number of parameters assessed including cell death and neurite outgrowth, as well as the response to stimulation of the Fas/NO cell death pathway. I also examined changes in CRT protein expression in AR100 and $SOD1^{G93A}$ MN cultures. In addition, I undertook an *in vivo* analysis of CRT protein levels in the lumbar spinal cord in AR100 and $SOD1^{G93A}$ mice at various stages of disease progression.

2.3.1 Characterisation of 3 DiV and 7 DiV Primary MN Cultures

Primary MN cultures were established from E12-14 WT, $SOD1^{G93A}$ and AR100 mouse embryos. There was no morphological difference in MNs in these cultures at 3 DIV or at 7 DIV, as shown in Figure 10 and Figure 11, respectively. Within 24 hours of plating, neurons had attached to laminin- polyornithine coated plates, and by 72 hours, the cell had the characteristic MN morphology, with a large cell body with a pyramidal shape and diameter greater than 15µm, with at least 2 or more processes (Figure 10, arrow). The MN purity of these cultures at 3 DIV was found to be 64.0% ± 16.7 % (Mean ± SD), as assessed with the main contaminating cell being fibroblasts and a small number of glial cells. By 7 DIV, due to fibroblast proliferation and MN

death, 35% of cells were classified as MNs, which is similar to the MN population previously reported in mixed ventral horn cultures (Kalmar and Greensmith, 2009).

2.3.2 Effect of cell stressors on AR100 MN survival

WT and AR100 MNs were exposed to a variety of cell stressors and the effect on MN survival was assessed using a number of approaches.

2.3.2.1 Manual Cell counts

2.3.2.1.1 The response of MNs to cell stressors at 3 DiV

WT and AR100 MNs were examined at an early stage in development, at 3 DiV, prior to the expression of glutamate receptors and FADD-like interleukin-1 beta-converting enzyme-like inhibitory protein (FLIP) expression (Van Den Bosch et al., 2000, Raoul et al., 1999). However, as shown in Figure 12, there was a large variability in the response of AR100 MNs to each stressor, so that no significant difference between WT and AR100 MNs could be established. Although following treatment to Thapsigargin, the effect on AR100 MNs was relatively reproducible, with 87.8 ± 8.6% of MNs surviving, the following treatment with Fas and DetaNONOate, 61.0 ± 42.8% and 91.7± 37.0% of MNs survived respectively. It is possible that this large variability in the response of MNs to these stressors is due to their relative immaturity at 3 DiV. However, WT MNs appeared to have a more consistent response, in particular to Fas and DetaNONOate.

2.3.2.1.2 The response of MNs to cell stressors at 7 DiV

I next went on to analyse the response of AR100 MNs to cell stressors at 7 DiV, when primary MN in culture express glutamate receptors (Van Den Bosch et al., 2000) and after the developmental regulation of cell death mediated by FLIP and Fas has ceased (Raoul et al., 1999). Primary WT and AR100 MN cultures maintained *in vitro* for 7 days were exposed to Thapsigargin in a dose dependant manner at concentrations ranging from 0 to 1µM to determine whether there was a difference in the response of WT and AR100 MNs to this ER stressor (Figure 13 A). I found no significant difference in cell survival between WT and AR100 MNs at any concentration tested.

Furthermore, there was no significant difference in the extent of cell death induced by Thapsigargin at different concentrations between 30nM and 1 µM treatment, with ~40% cell death detected in MNs of both WT and AR100 genotype. This may have been due to the lack of sensitivity in the manual cell count technique. DetaNONOate had no significant effect on MN survival in cells of either genotype (Figure 13 B). Even 24 hour treatment with 50 µM DetaNONOate, 5 times the dose used to treat 3DiV MN, resulted in 87 % ± 15.3% survival (which was not significant). However, it has previously been shown that DetaNONOate exposure is not toxic to WT MNs (Estevez et al., 1999a, Estevez et al., 1999b). The results presented Figure 13B therefore suggest DetaNONOate is also not toxic to SBMA MNs.

2.3.2.2 Biochemical analysis of MN Survival

As an alternative to manual cell counts, Lactate dehydrogenase assays (LDH) were carried out as a potentially more sensitive read out of cell cytotoxicity than manual cell counts. LDH assays were performed on WT and AR100 primary ventral horn cultures treated with 50nM DHT to determine if there was an increased vulnerability of AR100 MNs in the presence of the AR ligand. In three out of four independent experiments there appeared to be a trend of increased LDH in media isolated from AR100 cultures. However, this was not statistically significant over the four experiments average. Furthermore, I went on to analyse the effect of 100nM Thapsigargin on WT and AR100 cultures in the presence and absence of 50nM DHT. On average there was no significant difference in survival of MNs of either genotype in these conditions, with a result of 64 % ± 7.0 % of total LDH release in media isolated from WT cultures and 67.1 ± 9.9% LDH release in AR100 media (Figure 14). These results suggest that at 7 DIV, AR100 MNs do not show an increased vulnerability to the ER stressor, Thapsigargin, in the presence or absence of the AR ligand DHT.

2.3.2.3 High throughput analysis of MN Survival

To determine whether a high throughput cell counting analysis would be more sensitive to changes in cell survival than the LDH assay or manual cell counts, I next performed automated cell counts in 96 well plates analysing approximately 80,000

cells per experiment, with the aid of MetaXpress software. However, using this method, I again found no significant difference between WT and AR100 MN viability in the presence of absence of DHT (Figure 15).

However, the automated analysis of a large number of cells per experiment did enable me to undertake an automated assessment of other neuronal features that may reflect cell stress, such as neurite outgrowth. Since DHT has a regulatory role in neurite development (see Section 2.4.8), I next went on to establish if there was a difference in the neurite architecture in AR100 MNs. Using MetaXpress neurite outgrowth analysis, I analysed 3 independent ventral horn cultures for four measurements of neurite architecture: I) Mean number of processes per cell; II) maximum process length; III) total outgrowth per cell; and IV) mean number of branches per cell. However, as shown in Figure 15 and Figure 16 for all measures there was no significant difference between genotype or in the presence or absence of 50nM DHT. A possible explanation for the lack of an effect of DHT, at a relatively high concentration, as shown in Figures 17 and 18. DHT treatment did not appear to cause a change in the pattern of staining for either the C terminal or N terminal of the AR. Figure 17 shows that staining with the C19 antibody showed staining in the cell body and some neurite staining, whereas staining with the N20 AR antibody (Figure 18) produced an exclusively nuclear signal. This may be a contributing factor to why there was no significant difference in neurite architecture as the AR appears to be located in the nucleus even in the absence of DHT. This finding suggests that these cells may be under stress in culture, even in the absence of DHT.

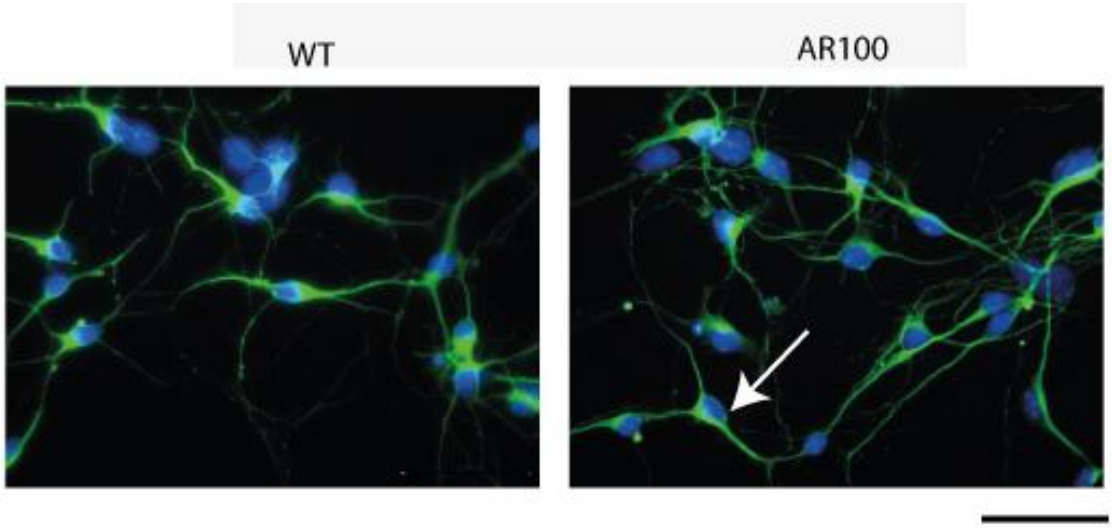

Figure 10 WT and AR100 MN Cultures at 3DiV

Primary ventral horn cultures from WT and AR100 E13 mouse embryos at 3 DIV. The cultures were treated with 50nM DHT for 48 hours, stained with the neuronal marker β III Tubulin (Green) and the nuclear marker DAPI (Blue). The arrow indicates the typical morphology used to identify a cell as a MN for manual cell counts. Scale bar = 50 µm.

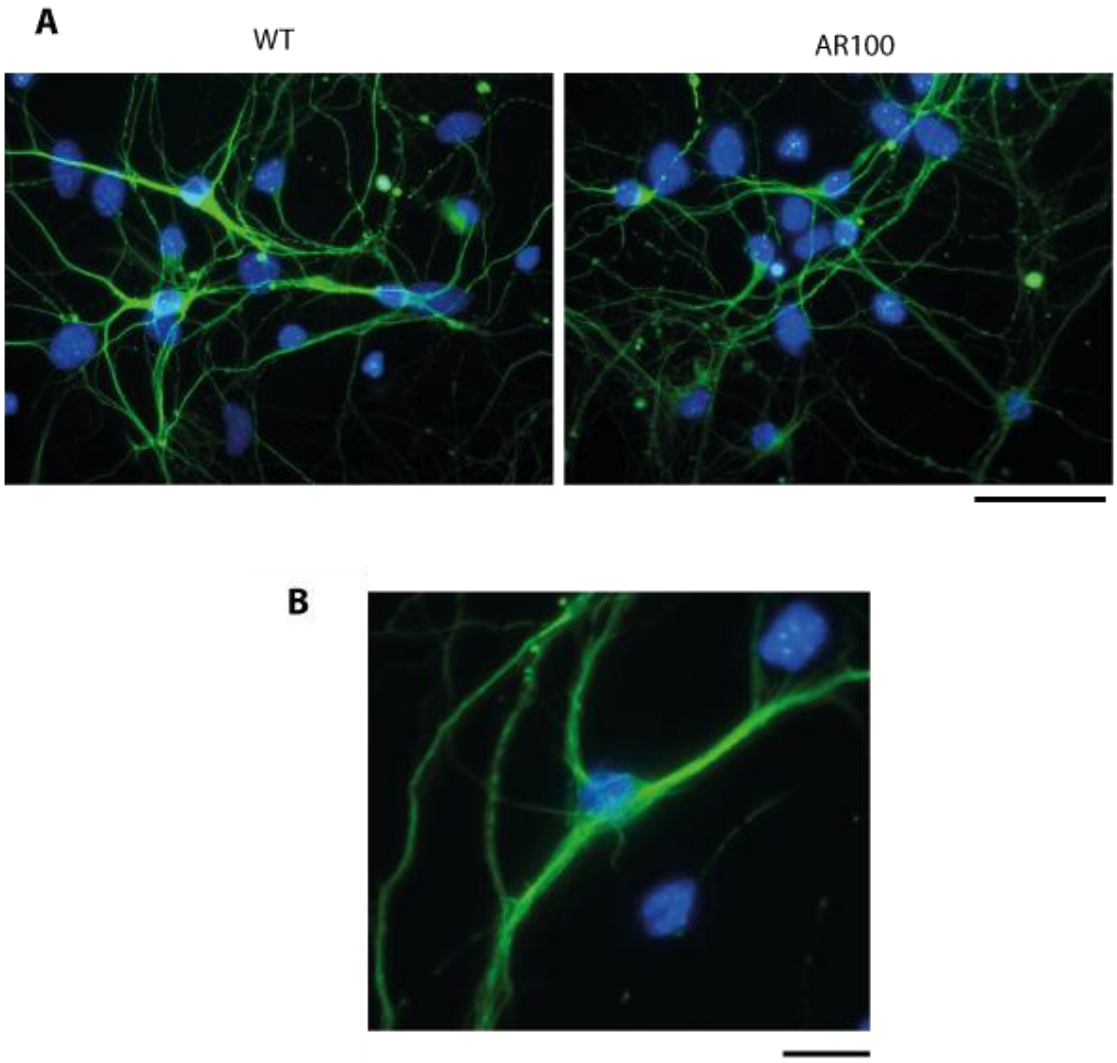

Figure 11 WT and AR100 MN Cultures at 7DiV

A) Primary ventral horn cultures from WT and AR100 E13 embryos cultured for 7 DiV. The cultures were treated with 50nM DHT for 72 hours, stained with the neuronal marker β III Tubulin (Green) and the nuclear marker DAPI (Blue). Scale bar = 50 µm. **B)** An example of a MN displaying the characteristic morphology used for manual cell counts at this stage in development. Scale bar=15µm

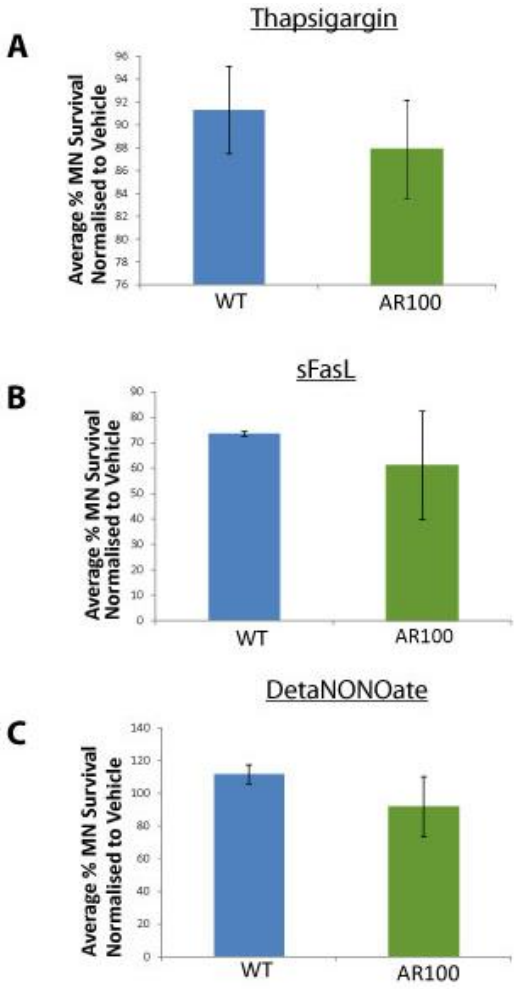

Figure 12 The effect of cell stressors on AR100 MN survival at 3 DiV: Manual cell counts

Primary ventral horn cultures from WT and AR100 E12-14 embryos were maintained for 3 DIV and then stained with the neuronal marker β III Tubulin and the nuclear marker DAPI for in order to assess MN survival using manual cell counts. Eighteen 20 x fields over two coverslips were counted using Image J software. The effect of treatment with **A**) 100nM Thapsigargin, **B**) 100ng/ml sFasL or **C**) 10µM DetaNONOate on MN survival was determined. The average effect of stressors over two consecutive experiments showed that there was no significant difference in the vulnerability of AR100 MNs to any of the stressors. Error bars= SEM

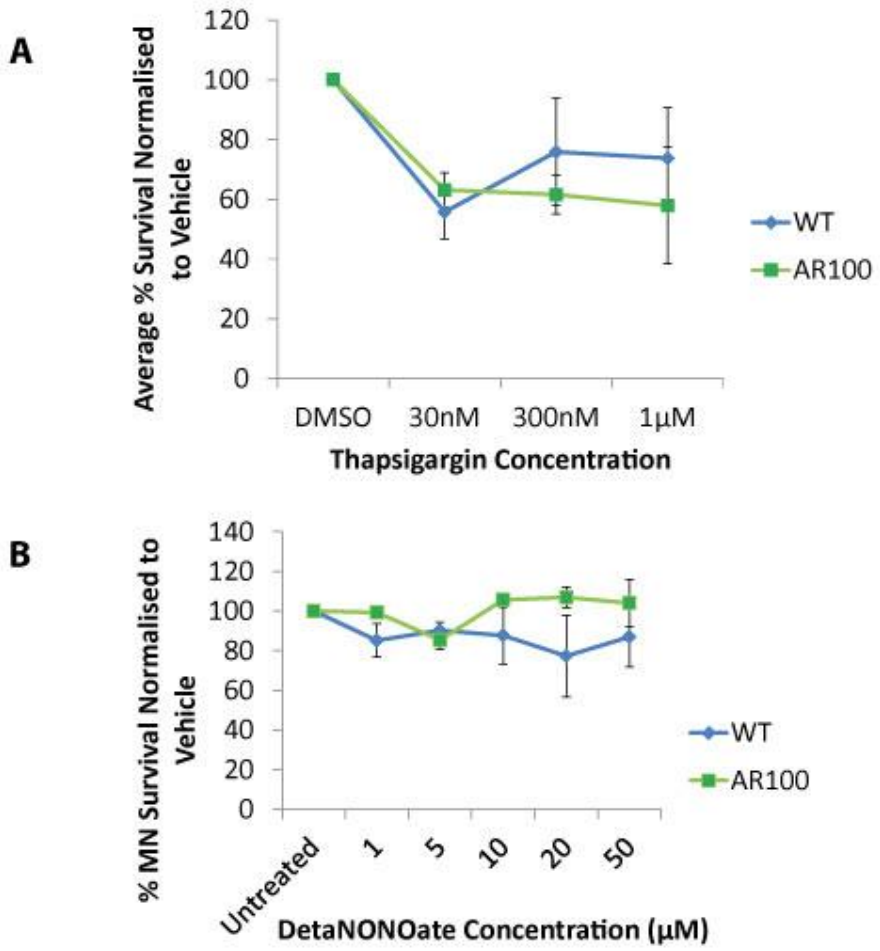

Figure 13 The effect of cell stressors on AR100 MN survival at 7 DiV: Manual cell counts

Primary ventral horn cultures from WT and AR100 E12-14 embryos were cultured for 7 DiV. The effect of treatment with **A**) Thapsigargin and **B**) DetaNONOate at various concentrations on MN survival was assessed. Treatment with Thapsigargin had a significant effect on both WT and AR100 MN Survival at all concentrations tested (30nM- 1µM). Treatment with DetaNONOate had no significant effect on MN survival in either AR100 or WT MN cultures. Error bars = SEM.

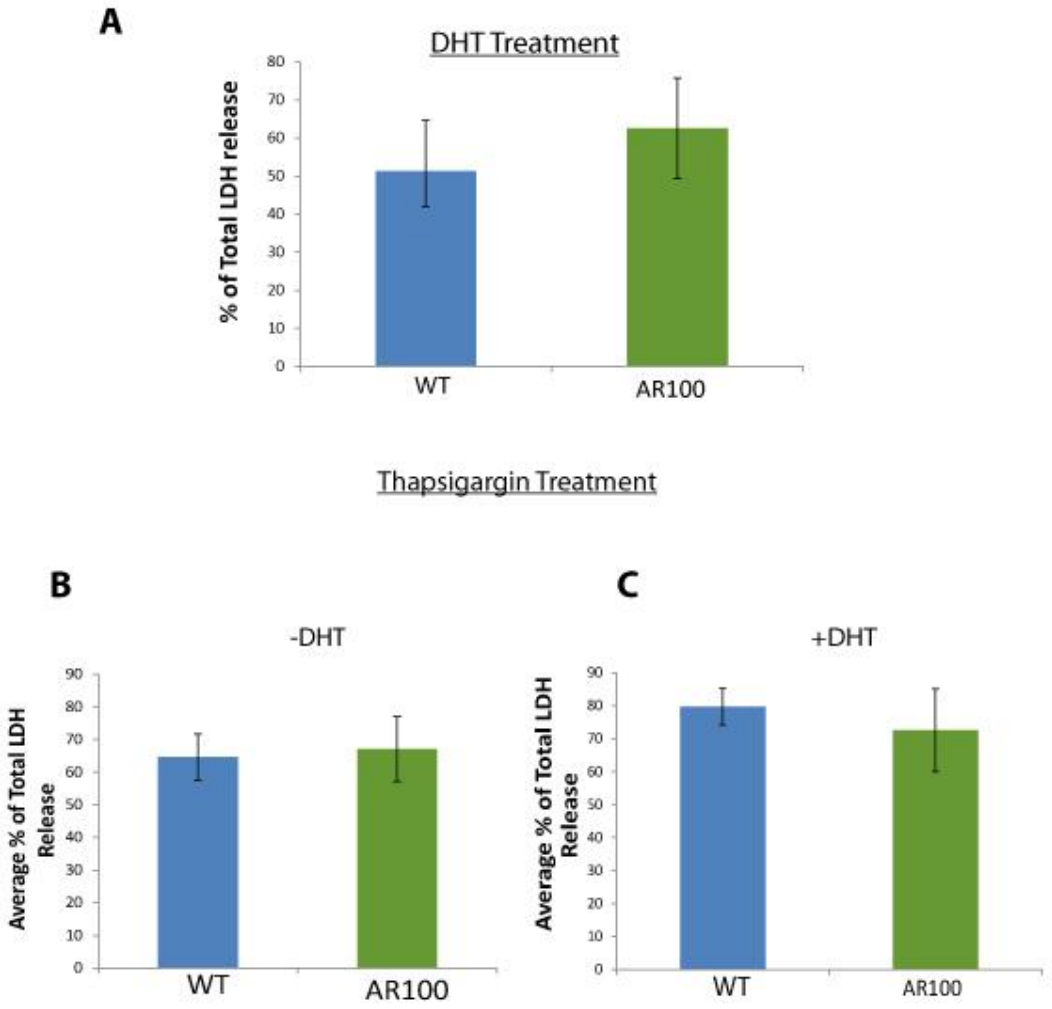

Figure 14 The effect of cell stressors on AR100 MN Survival at 7DiV : LDH Assays

The effect of **A**) 72 hour 50nM DHT treatment on 7 DiV MNs as assessed by LDH assay. There was a trend of increased LDH levels in the media of AR100 cultures indicative of an increase in cell death; however this did not reach significance. In the **B**) absence or **C**) presence of DHT there was no significant difference between WT and AR100 MNs after 100nM Thapsigargin Treatment. Error bars= SEM

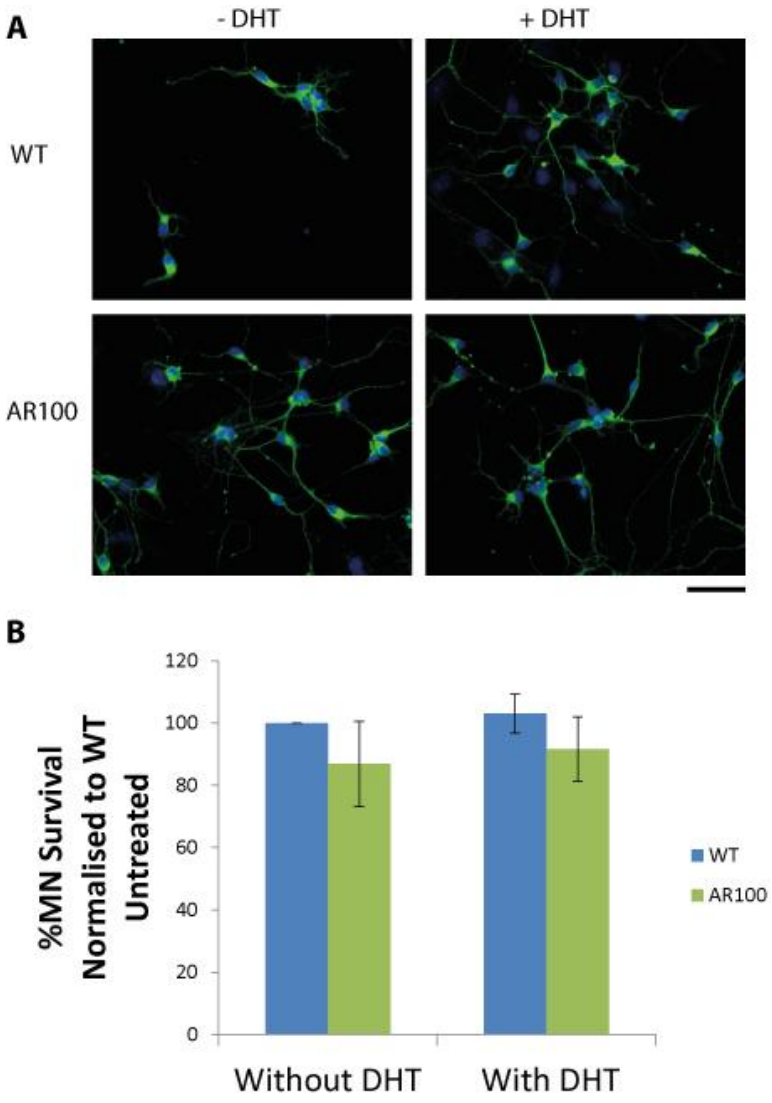

Figure 15 The effect of DHT on AR100 MN Survival at 3 DiV: MetaXpress analysis

Primary MN cultures from WT and AR100 E12-E14 embryos were maintained for 3DiV in the presence or absence of 50nM DHT for 48 hours. **A**) WT and AR100 MNs cultured for 3 DiV in the presence or absence of 50nM DHT were indistinguishable morphologically. Cells were stained with the neuronal marker β III Tubulin (Green) and the nuclear marker DAPI (Blue) Scale bar= 50µm **B**) The percentage of MNs surviving in three independent experiments was analysed using MetaXpress imaging and analysis software. Data was normalised to WT untreated cultures for each experiment. No significant effect of DHT treatment was observed and although there was a trend of a lower number of AR100 MN surviving, this was not significant. Error Bars= SEM

Figure 16

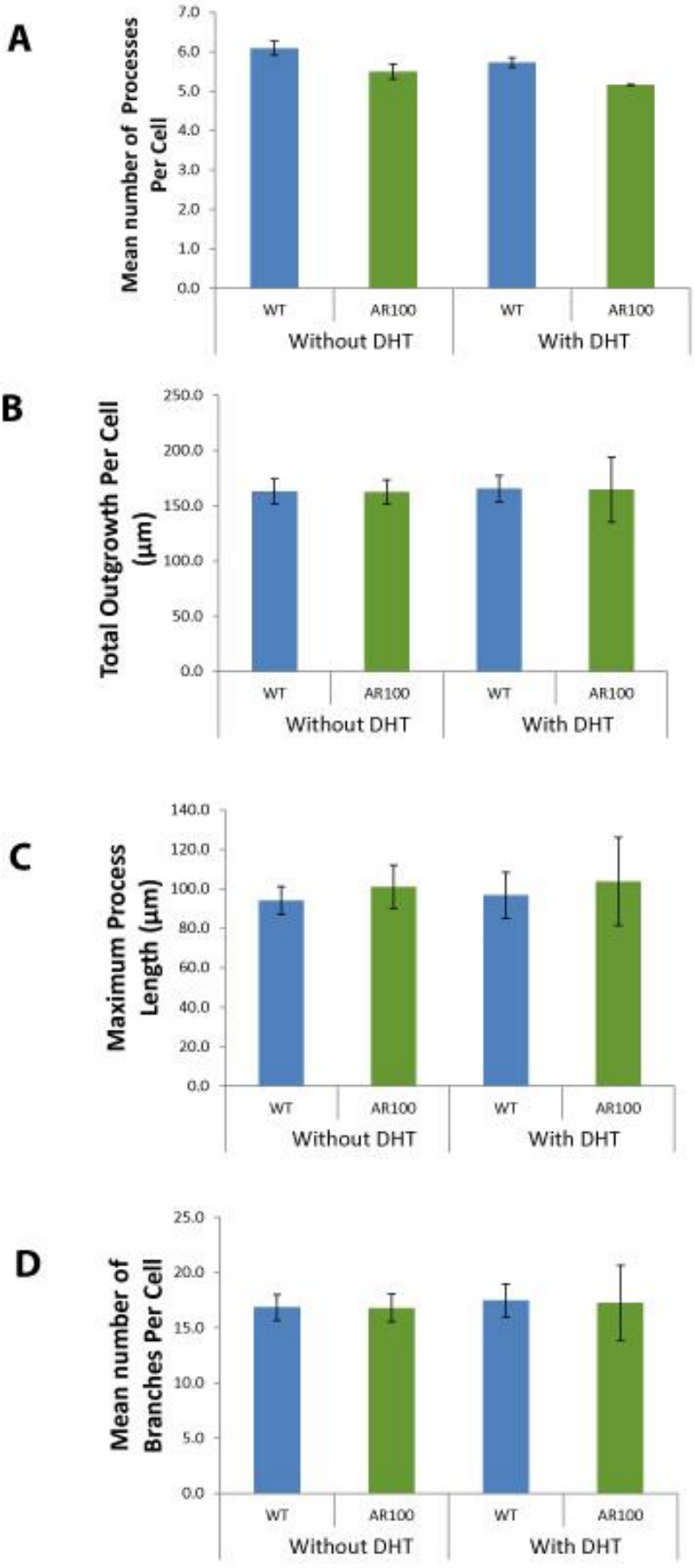
A
Mean number of Processes Per Cell
7.0
6.0
5.0
4.0
3.0
2.0
1.0
0.0
WT
AR100
WT
AR100
Without DHT
With DHT
B
Total Outgrowth Per Cell (µm)
250.0
200.0
150.0
100.0
50.0
0.0
WT
AR100
WT
AR100
Without DHT
With DHT
C
Maximum Process Length (µm)
140.0
120.0
100.0
80.0
60.0
40.0
20.0
0.0
WT
AR100
WT
AR100
Without DHT
With DHT
D
Mean number of Branches Per Cell
25.0
20.0
15.0
10.0
5.0
0.0
WT
AR100
WT
AR100
Without DHT
With DHT

Figure 16 Effect of DHT on neurite outgrowth of AR100 MNs at 3 DiV

WT and AR100 MNs at 3 DiV show no significant difference in neurite architecture in the presence or absence of 50nM DHT. Experiments were performed using the Neurite Outgrowth Module from MetaXpress software to analyse 80,000 cells per culture in 3 independent experiments. Four measurements of neurite architecture: **A**) Mean number of processes per cell, **B**) Maximum process length, **C**) Total outgrowth per cell and **D**) Mean number of branches per cell were assessed. Error Bars= SEM.

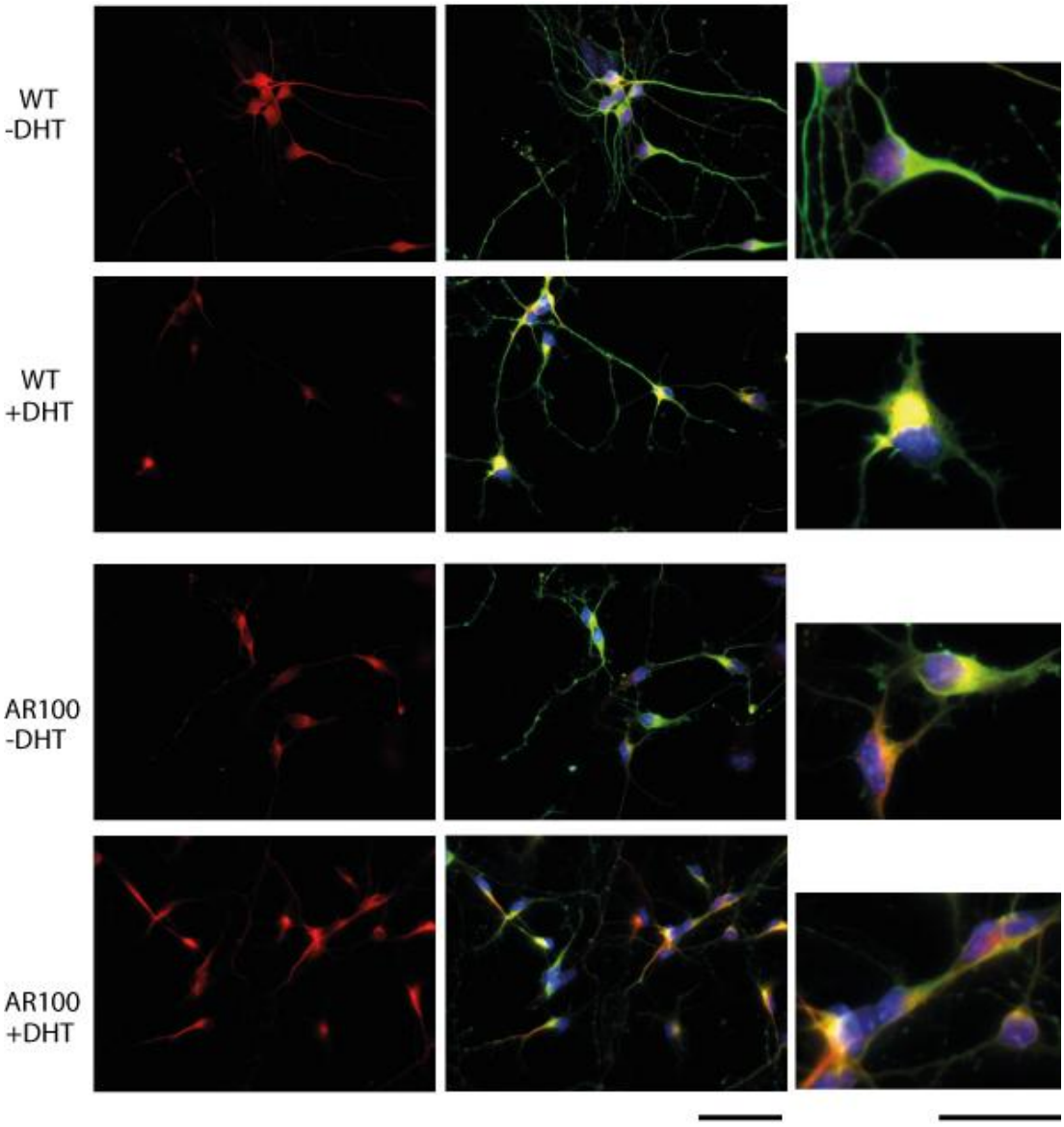

Figure 17 Effect of DHT on AR C- Terminal Localisation in AR100 MNs

WT and AR100 MNs at 3DiV stained with an androgen receptor C Terminal antibody, C19 (red), β III Tubulin (green) and DAPI (blue), in the presence or absence of 50nM DHT. There is no difference in the pattern of staining or AR localisation in either genotype or as a result of DHT treatment. Scale bar= 50µm

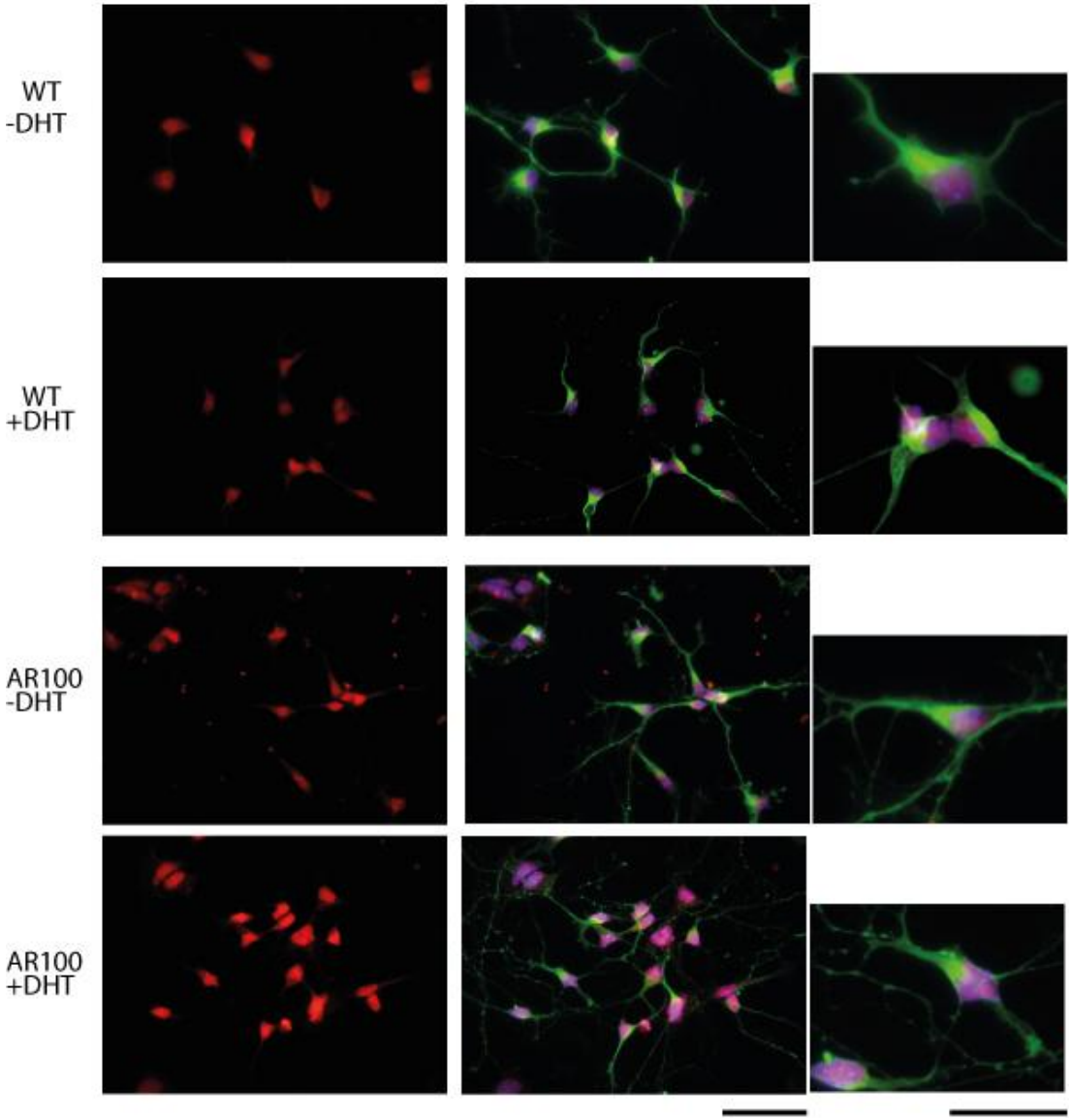

Figure 18 Effect of DHT on AR- N Terminal localisation in AR100 MNs

WT and AR100 MNs at 3 DiV stained with an androgen receptor N- Terminal antibody, N20 (red), β III Tubulin (green) and DAPI (blue), in the presence or absence of 50nM DHT. There is no difference in the pattern of staining or AR localisation in either genotype or as a result of treatment. Scale bar= 50µm or 25µm in high power images.

2.3.3 Effect of cell stressors on SOD1^{G93A} MN survival

In order to determine whether there was an inherent difference in cell viability in cultures established from SOD1^{G93A} mice compared to AR100 MNs, I next examined MN survival in cultures established from SOD1^{G93A} mice that model ALS,.

2.3.3.1 Survival of SOD1^{G93A} MNs *in vitro*

Since the results from WT and AR100 primary MN culture were highly variable, and thus largely inconclusive, I next proceeded to analyse primary MN cultures from the SOD1^{G93A} model, with a more severe phenotype and marked MN loss *in vivo*. This was an attempt to establish whether the methodology used to examine cell viability *in vitro* was too insensitive to detect a possible mild, defect in the AR100 primary cultures, but sensitive enough to detect a more severe phenotype in SOD1^{G93A} MNs.

SOD1^{G93A} MN survival was assessed by both the manual counting method and by automated cell counts, under basal, unstressed conditions as well as following exposure to the cell stressors Thapsigargin, sFasL and DetaNONOate. As can be seen in Figure 19 A, at 3 DiV, SOD1^{G93A} MNs were morphologically indistinguishable from WT MNs. Furthermore, assessment of SOD1^{G93A} MN survival using either the manual cell count method (data not shown) or automated cell counts (Figure 19 B). In which at least nine 20 times objective fields in 3 wells per condition were examined, found that there was no significant difference in SOD1^{G93A} MN survival compared to WT MNs at 3 DIV.

The effects of cell stressors on SOD1^{G93A} MN survival were also examined. As can be seen in Figure 20, using manual cell counts, no significant difference in SOD1^{G93A} survival, as observed following treatment with either Thapsigargin, sFasL or DetaNONOate, compared to vehicle treated cultures at 3 DIV. Thus treatment of primary MNs to 100nM Thapsigargin resulted in a significant loss of both WT and SOD1^{G93A} (Figure 20 A). Treatment with 100ng/ml sFasL, also reduced MN survival, but to a lesser extent (Figure 20B). In contrast, treatment with 10 µM DetaNONOate, caused no loss of either WT or SOD1^{G93A} (Figure 20C). Similarly, high throughput analysis of SOD1^{G93A} MN survival following exposure to Thapsigargin,

sFasL or DetaNONOate also showed that there was no difference in the extent of SOD1^{G93A} MN survival compared to vehicle (See Figure 21).

2.3.4 Expression of Calreticulin in AR100 and SOD1^{G93A} MNs

It has previously been reported that decreased expression of Calreticulin (CRT) plays a role in a Fas/NO cell death pathway that is specific to fast fatigable mutant SOD1 positive MNs. In the next set of experiments, I examined I) whether changes in CRT expression could be detected in AR100 MNs and II) whether the changes in CRT expression previously described for SOD1^{G93A} MNs at 3 DIV (Bernard-Marissal et al., 2012) were also present in more mature SOD1^{G93A} MNs at 7DIV

2.3.4.1 CRT levels in AR100 MNs

WT and AR100 MNs were stained at 3DIV and 7DIV for CRT (Figure 22). In all cells, including both neurons and fibroblasts, CRT was expressed throughout the cell body with slightly lower staining intensity in the nucleus. CRT had a diffuse staining pattern, uncharacteristic of a protein elusively located in the ER, thus supporting resent research showing that CRT also has non-ER related functions. No difference in staining intensity was detected between WT and AR100 MNs at either 3DIV or 7DIV.

2.3.4.2 SOD1^{G93A} MNs show reduced CRT intensity levels

Since previous reports have suggested that CRT Levels were altered in SOD1^{G93A} MNs, the pattern of expression was also examined in SOD1^{G93A} MN cultures at 3DiV, a time when mSOD1- dependent changes have been observed (Bernard-Marissal et al., 2012).

As shown in Figure 23, no obvious difference in the pattern or intensity of CRT expression was observed in SOD1^{G93A} MNs at 3 DiV compared to WT controls. I therefore examined the effect of cell stressors on the CRT expression by treatment of 3DiV SOD1^{G93A} and WT cultures with SFasL, DetaNONOate or Thapsigargin. However, there was no clear change in the pattern of CRT expression in either WT or SOD1^{G93A} MNs at 3DiV (Images not presented for all treatments).

I next examined whether changes in CRT protein expression could be detected using a high throughput approach as well as well as Western blotting. In the first instance, I examined whether exposure of $SOD1^{G93A}$ MNs to cell stressors altered CRT protein expression, as has been previously reported in Bernard-Marissal et al. (2012), using the $SOD1^{G93A}$ model as a positive control for changes in CRT levels.

Using MetaXpress Image analysis software, CRT staining intensity was examined in WT and $SOD1^{G93A}$ MNs at 3DiV. Surprisingly even in untreated cultures, CRT protein levels are lower in $SOD1^{G93A}$ MNs, which express 90 ± 8.6 % (Figure 24; p=0.045) of WT MN CRT protein levels. Inducing ER stress by treatment with Thapsigargin caused CRT levels to decrease by ~40% but in both WT and $SOD1^{G93A}$ MNs, compared to vehicle treatment. However, there was a trend for a greater decline in $SOD1^{G93A}$ MNs, although this did not reach significance (Figure 25A). Following exposure to 100ng/ml sFasL treatment, there was also a significant reduction in CRT protein levels in $SOD1^{G93A}$ MNs, which was not observed in WT MNs (Figure 25 B; 90.2±11.4, p=0.003). DetaNONOate treatment had no significant effect on CRT levels in either WT or $SOD1^{G93A}$ cultures (Figure 25C).

2.3.4.3 $SOD1^{G93A}$ and AR100 mutations cause different responses in CRT protein levels in the spinal cord.

The expression level of CRT in spinal cord homogenates of P5, P30 and P120 $SOD1^{G93A}$ mice were determined using western blotting (Figure 26). At P5, there was no significant difference in CRT expression between $SOD1^{G93A}$ and WT controls. Similarly at P30, a pre-symptomatic stage of disease in $SOD1^{G93A}$ mice, there was no change in CRT expression in $SOD1^{G93A}$ spinal cord. However, by 120 days, a late stage of disease, there was a clear significant decrease in CRT expression in $SOD1^{G93A}$ mice. These findings confirm the results of Bernard-Marissal et al. (2012), which also reported a decrease in CRT expression in $SOD1^{G93A}$ spinal cord from 38 days.

In contrast, in the spinal cord of AR100 mice, at 5 days of age, a very early, pre-symptomatic stage of disease, there was a clear and significant increase in CRT

expression in the spinal cord of AR100 mice compared to WT (Figure 27A). However, as disease progressed, this increase in CRT levels was no longer observed, and at 3 and 12 months of age, CRT levels were not significantly different from WT (Figure 27B, C). By disease end stage, at 18 months, there was a slight, but not significant increase in CRT levels in the AR100 spinal cord (Figure 27D). Immunostaining of spinal cord sections showed that there was a clear increase in CRT staining intensity in the AR100 spinal cord at P5 (Figure 28), but at all other ages examined (3, 12 and 18 months), no detectable difference in CRT expression was observed (Figure 29). Furthermore, at all ages, there was no difference in the localisation of CRT expression between AR100 and WT spinal cord, which remained largely cytoplasmic (Figure 28 and Figure 29).

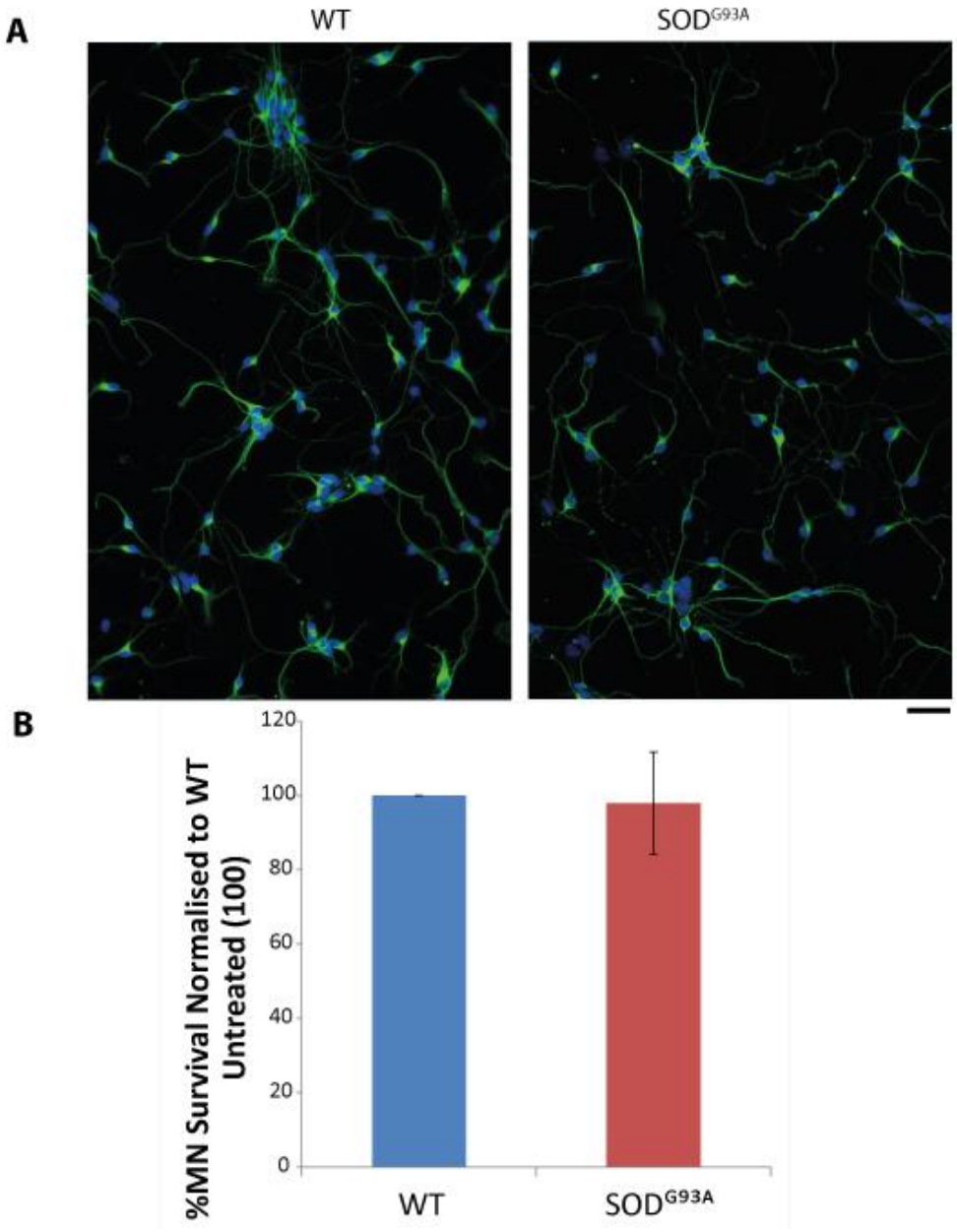

Figure 19 Survival of SOD1^{G93A} MNs at 3 DiV under basal culture conditions: MetaXpress analysis

WT and SOD1^{G93A} primary MNs are indistinguishable at 3 DIV in culture morphologically. **A**) Cultures were stained for β III Tubulin (Green) and DAPI (Blue). Scale bar = 50µm. **B**) Automated cell counts performed using MetaXpress software on three independent cultures showed no significant difference in survival at 3DiV. Error bars= SEM

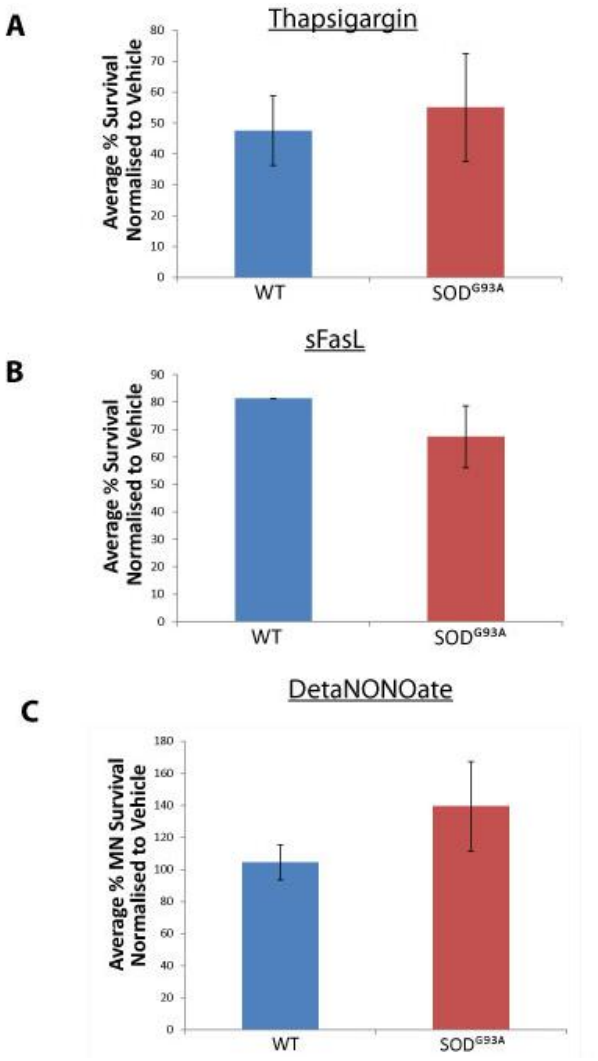

Figure 20 The effect of Cell stressors on SOD1^{G93A} MN Survival at 3 DiV: Manual Cell counts

Primary ventral horn cultures from WT and SOD1^{G93A} E12-E14 embryos cultured for 3 DIV were stained with the neuronal marker β III Tubulin and the nuclear marker DAPI. Number of MNs in eighteen 20 x fields over two coverslips for each condition were counted manually with the aid of Image J. Cultures were treated with **A**) 100nM Thapsigargin, **B**) 100ng/ml sFasL or **C**) 10µM DetaNONOate. Average results over two independent experiments showed there was no significant difference between WT and SOD1^{G93A} MNs in terms of vulnerability to cell stressors. Error bars= SEM

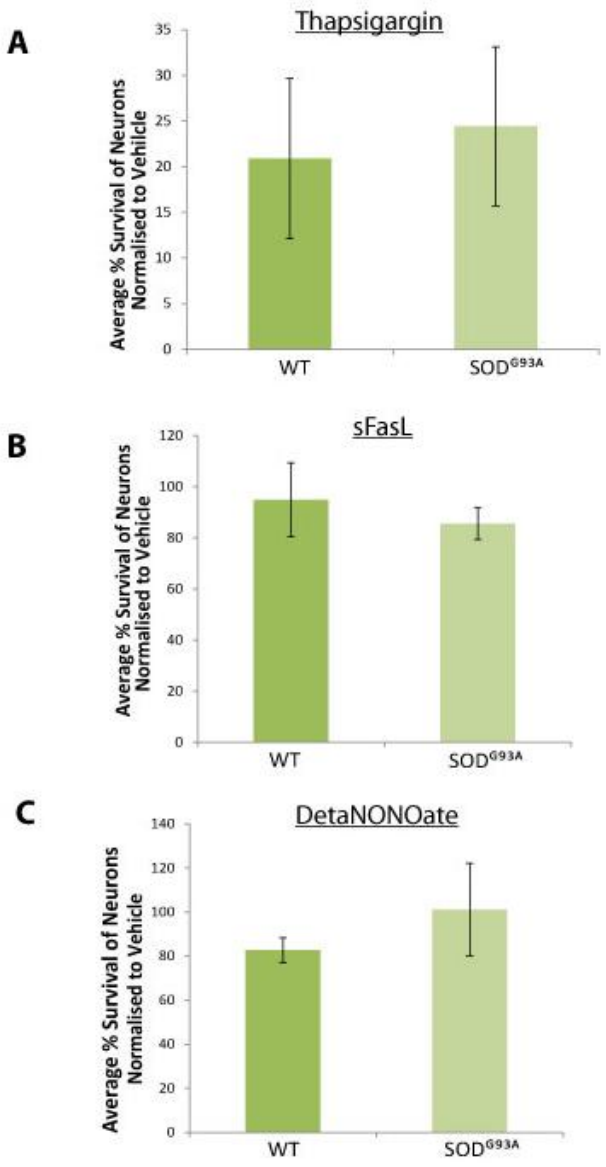

Figure 21 Effect of cell stressors on SOD1^{G93A} MN survival at 3 DiV: MetaXpress analysis

WT and SOD1^{G93A} MNs cultured for 3 DiV were treated with **A**) 100nM Thapsigargin, **B**) 100ng/ml sFasL or **C**) 10µM DetaNONOate for 24 hours prior to fixation and counted using MetaXpress multi-wavelength cell sorting module. The average of four independent experiments showed no significant difference in cell survival between WT and SOD1^{G93A}. Error bars= SEM

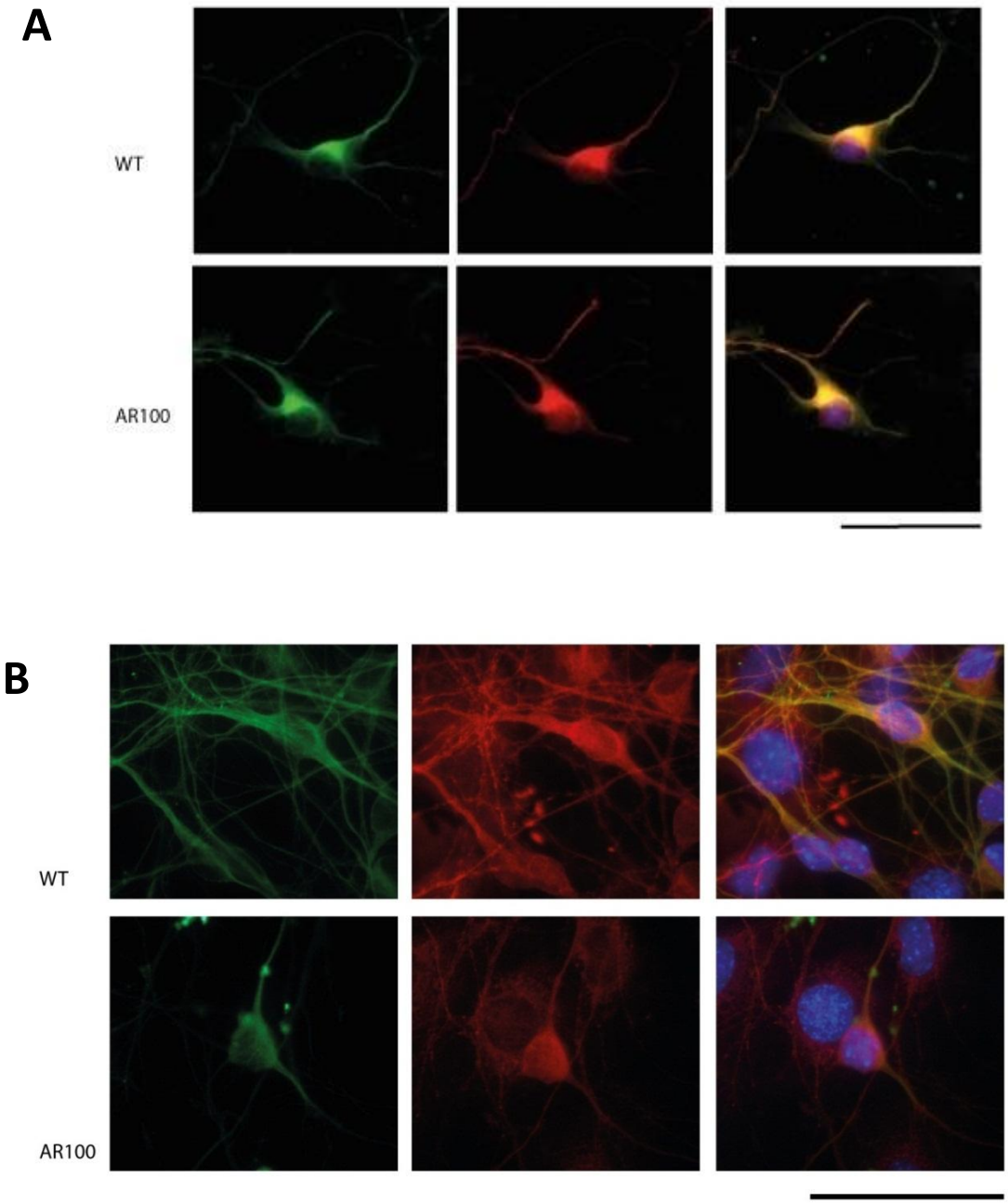

Figure 22 Pattern of CRT expression in AR100 MNs at 3 and 7 DiV

Immunostaining of **A)** 3 DIV and **B)** 7 DIV Primary and AR100 MN cultures for β III Tubulin (Green) CRT (Red) and DAPI (Blue). CRT expression is nuclear as well as cytoplasmic. WT and AR100 MNs do not appear to differ in intensity or pattern of staining. Scale bars= 50 µm

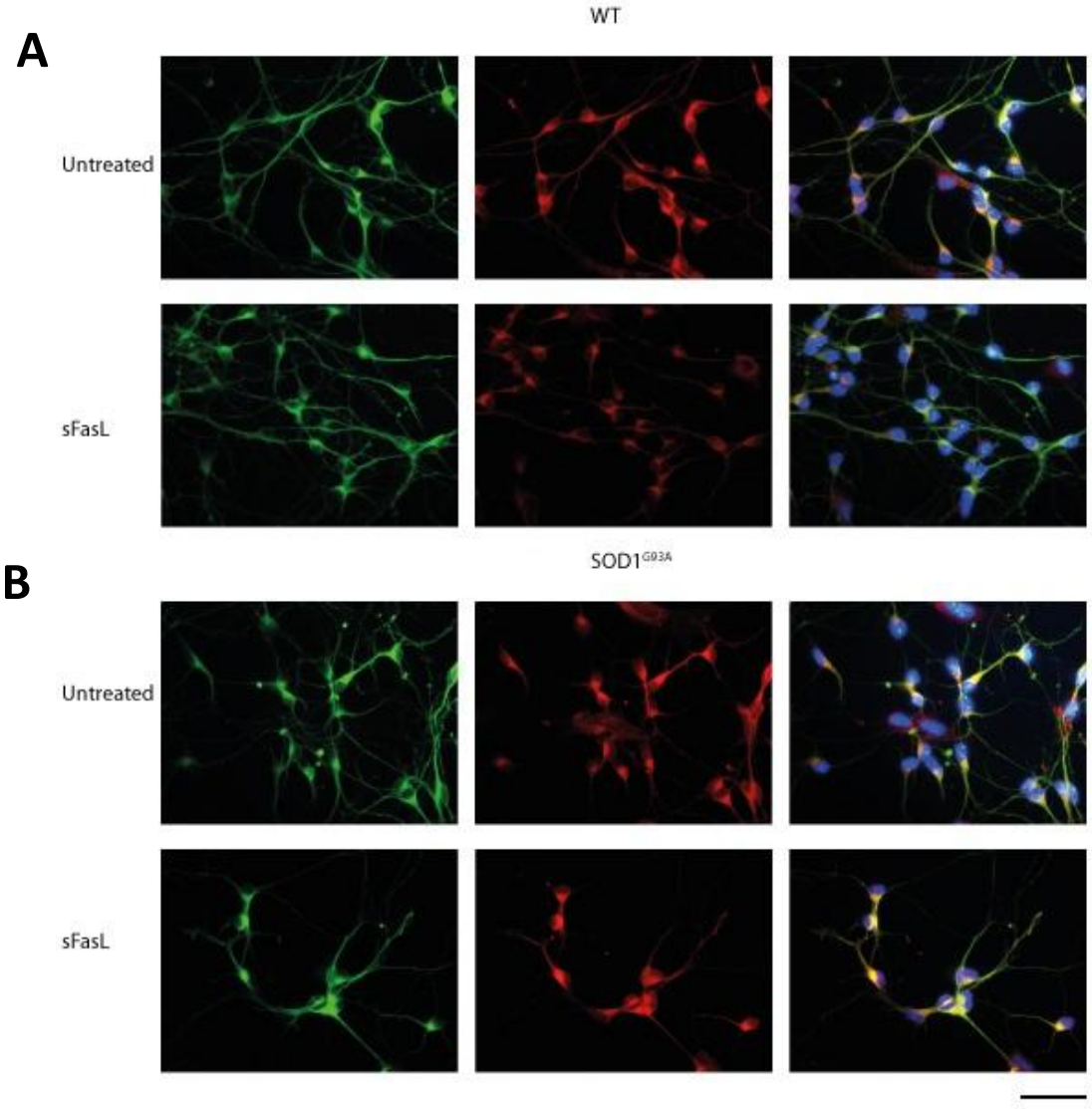

Figure 23 The effect of cell stressors on CRT expression pattern in SOD1^{G93A} MNs at 3DiV

Staining of **A**) 3 DIV Primary WT and **B**) SOD1^{G93A} MN cultures for β III Tubulin (Green) CRT (Red) and DAPI (Blue). Cultures were either left untreated or treated with 100ng/ml sFasL, 10µM DetaNONOate, DMSO, or 300nM Thapsigargin (Images for all treatments not shown). Consistent and noticeable changes in levels of CRT were not detected. Scale bar= 50 µm

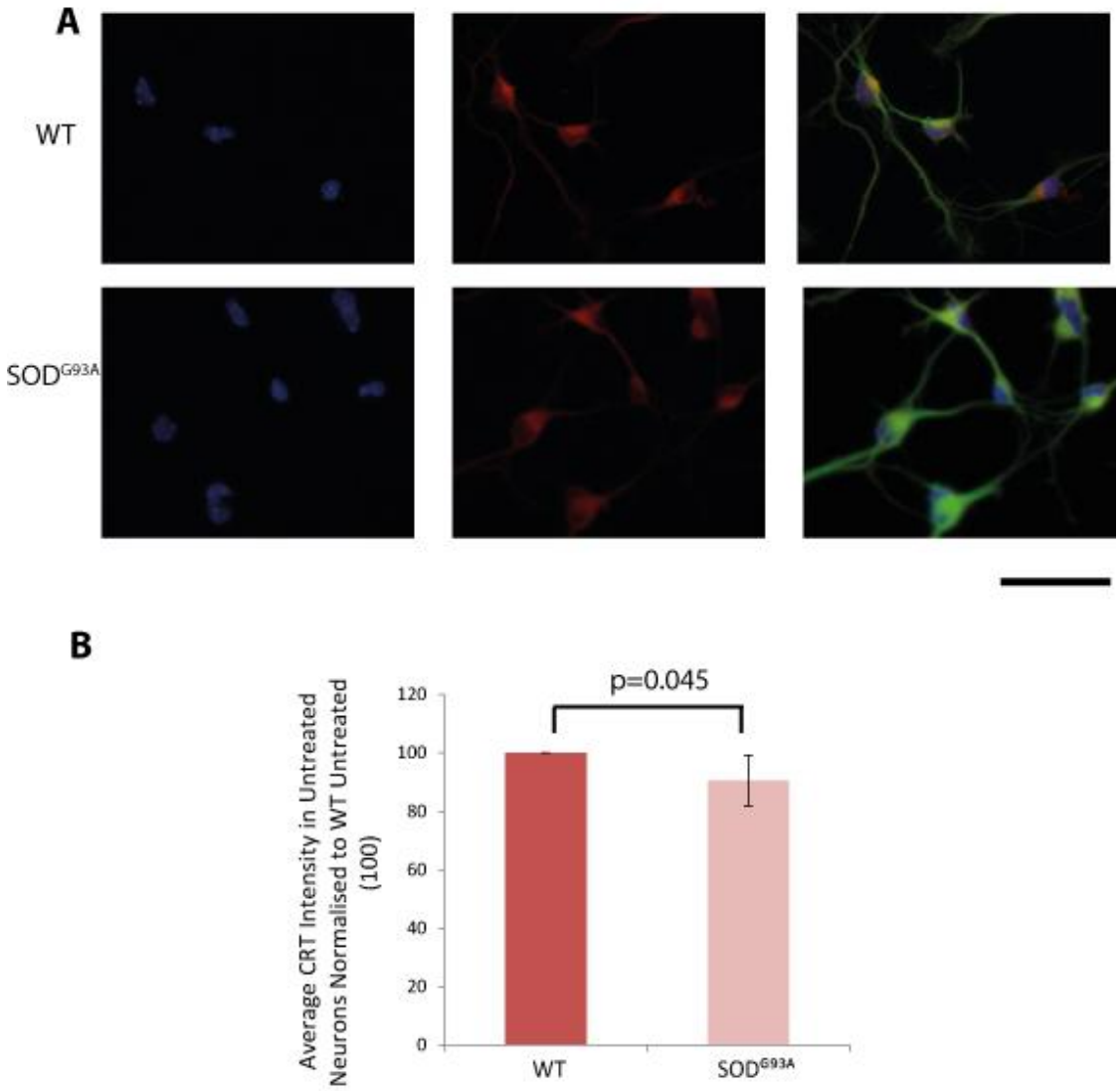

Figure 24 CRT staining intensity in SOD1^{G93A} MN cultures at 3 DiV under basal conditions: MetaXpress analysis

A) WT and SOD ^{G93A} MN cultures at 3 DiV were immuno-stained for CRT (Red) and neuronal marker β III Tubulin (Green), and the level of CRT fluorescence intensity was analysed with MetaXpress and normalised to CRT levels in WT MNs. Scale bar = 50µm. **B**) There was a significant reduction in SOD1 MNs. Error bars= SEM.

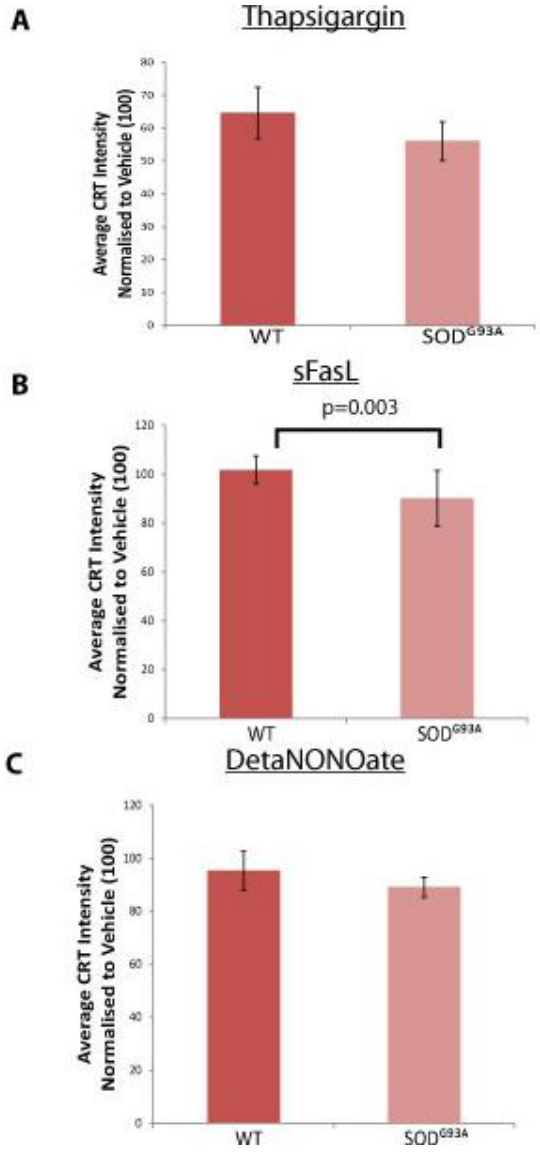

Figure 25 The effect of cell stressors on CRT expression in SOD1^{G93A} MNs at 3 DiV: MetaXpress analysis

WT and SOD1^{G93A} MNs were treated with **A)** Thapsigargin, **B)** sFasL or **C)** DetaNONOate at 3DiV, and immuno-stained for CRT and the neuronal marker β III Tubulin. The level of CRT immunofluorescence was assessed using MetaXpress. The staining intensity was expressed as a percentage of that of untreated MNs. The results show that there was a significant decrease in CRT expression in SOD1^{G93A} MNs following treatment to sFasL, but although Thapsigargin and DetaNONOate. Error bars=SEM

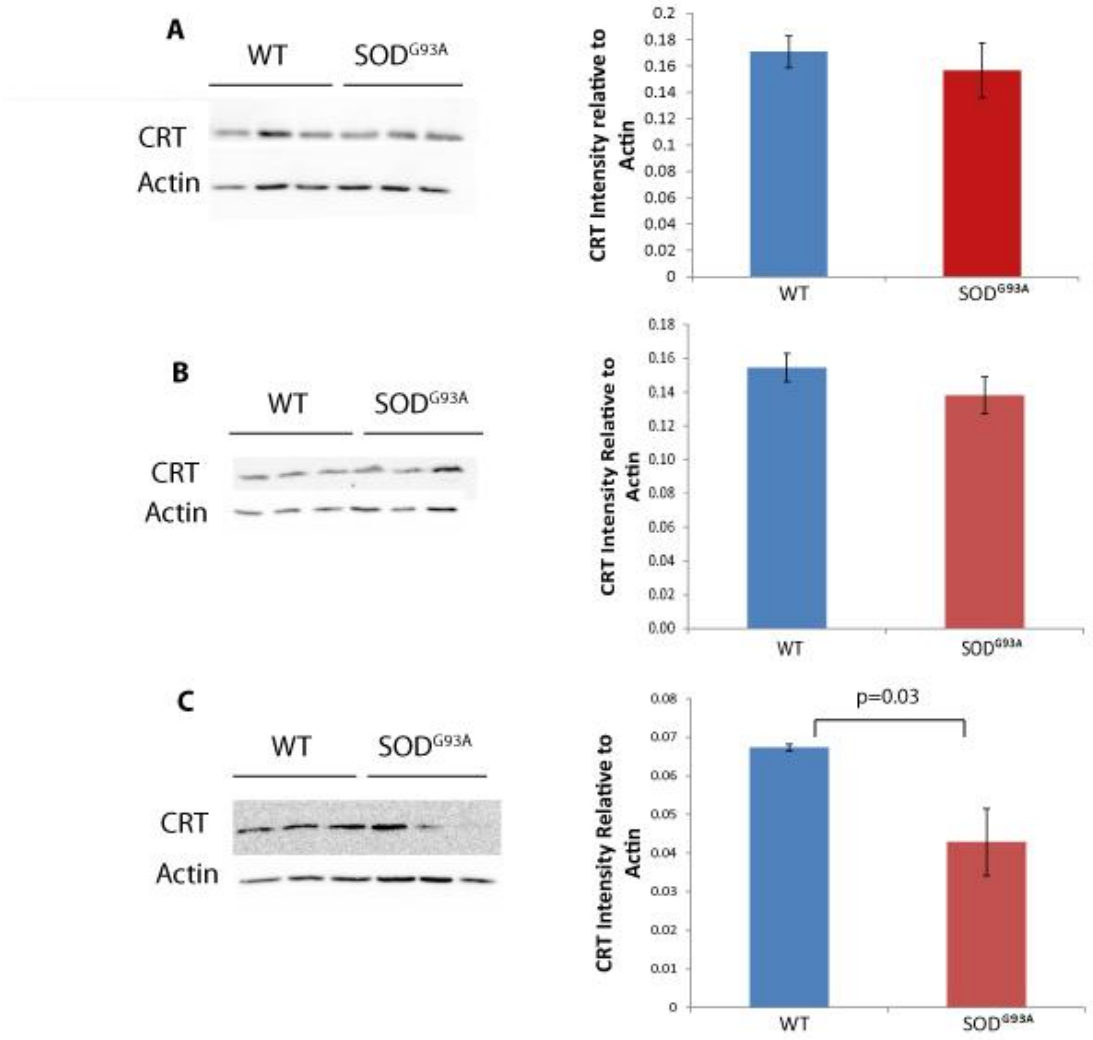

Figure 26 Expression of CRT in SOD1^{G93A} mouse spinal cord at different stages of disease

Western Blot and densitometry analysis of **A**) 5 days, **B**) 30 day **C**) and 120 day ventral spinal cord from WT and SOD1^{G93A} mice blotted for Calreticulin (CRT). The densitometry results are expressed relative to actin loading controls. Error bars= SEM

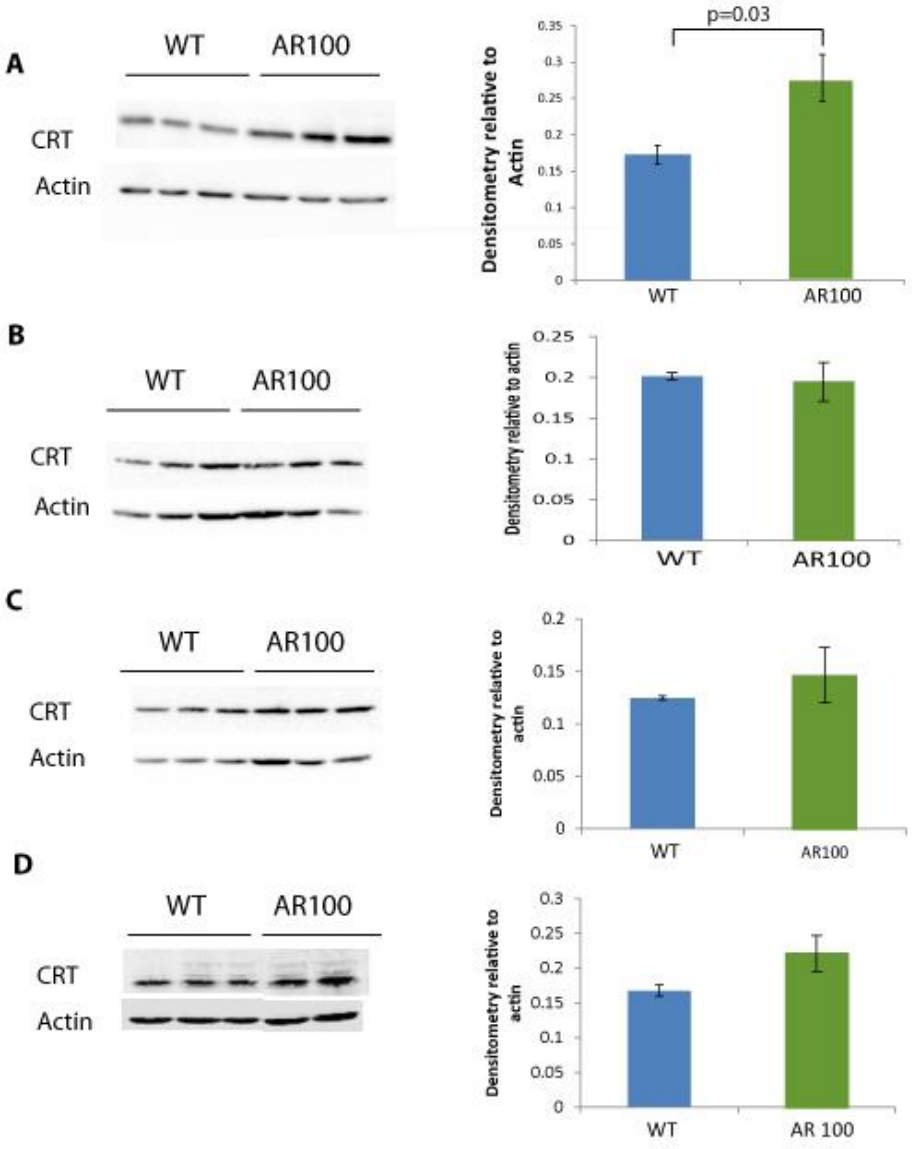

Figure 27 Expression of CRT in AR100 mouse spinal cord at different stages of disease

Western blot and densitometry analysis of whole spinal cord from pre-symptomatic stages, **A)** 5 days and **B)** 3 Months, **C)** after disease onset 12 months, and **D)** at disease end stage of 18 Months AR100. P5 mouse spinal cords have higher protein levels of CRT than WT controls. CRT levels in AR100 mice are not significantly different to WT at all adult stages. Error bars= SEM.

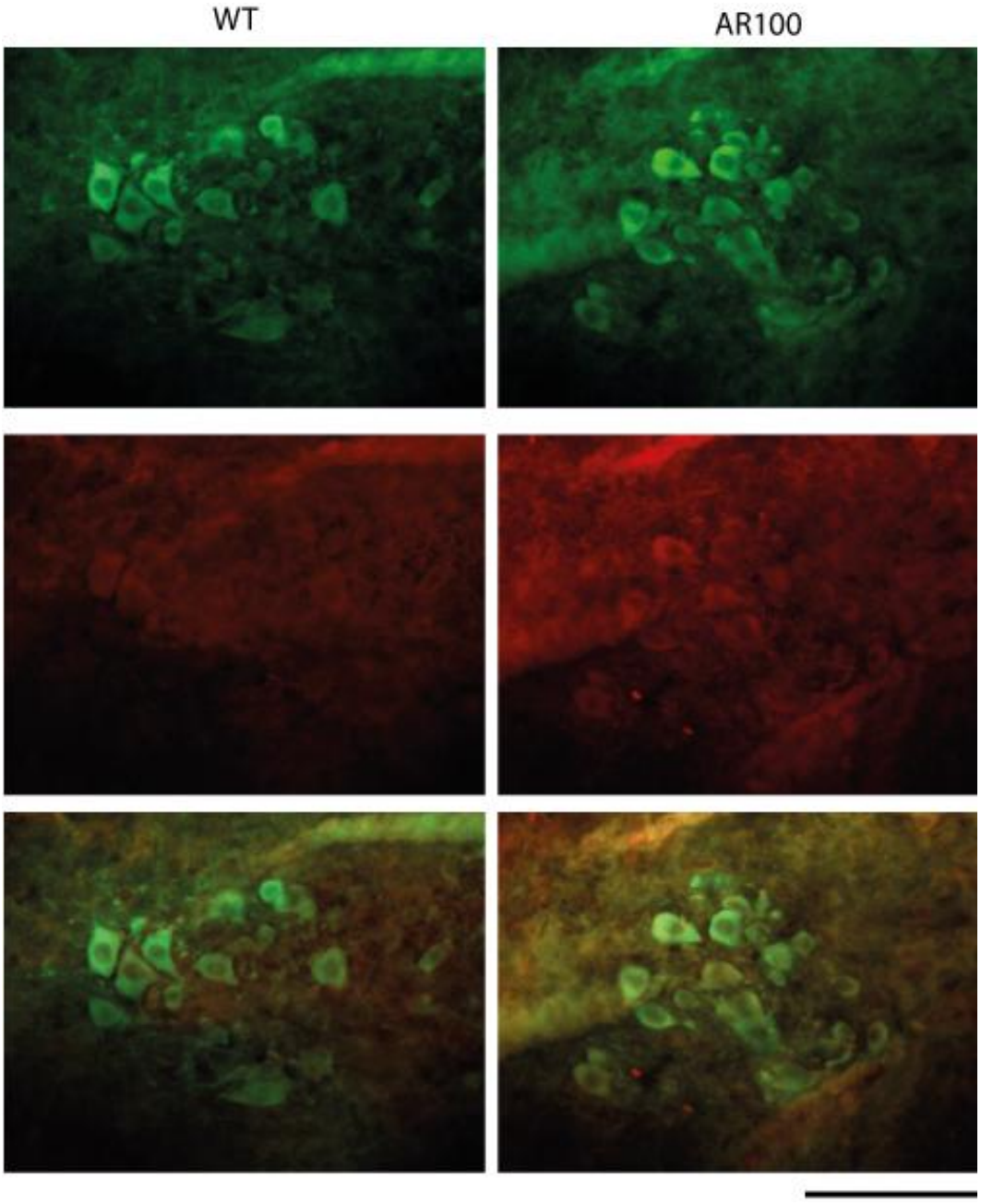

Figure 28 Calreticulin staining of the spinal cord in AR100 mice at P5

12µm sections were stained for Choline Acetyl Transferase (Green), and Calreticulin (Red). There is a higher level of CRT immunoreactivity in AR100 spinal cord than WT spinal cord at this stage of development. Scale bar= 50 µm

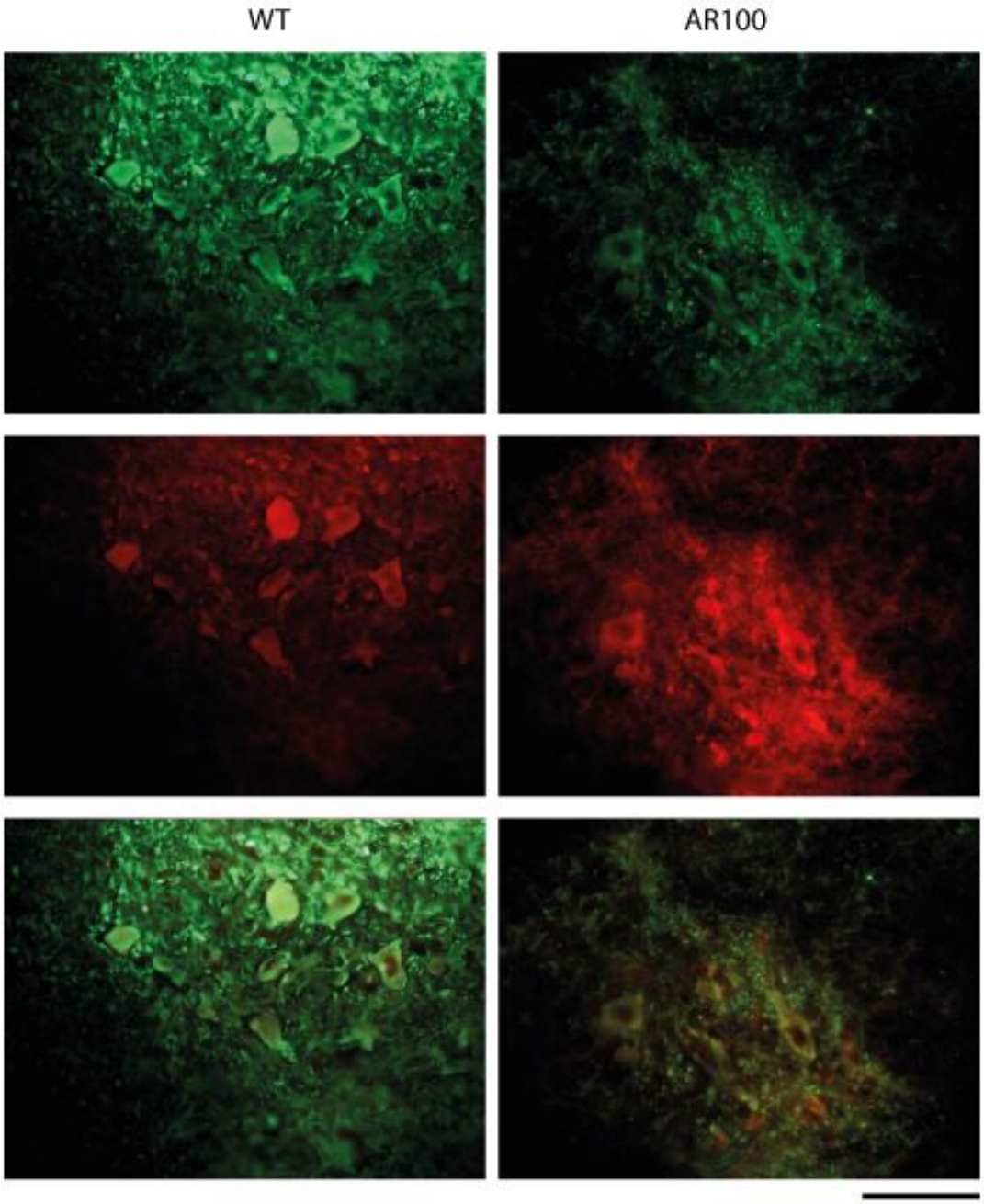

Figure 29 Calreticulin staining of the lumbar spinal cord at disease end stage

Immunohistochemical analysis of WT and AR100 spinal cord at 18 months. 12µm sections were stained for Beta III Tubulin (Green), and Calreticulin (Red). Images show an increase in in Calreticulin immuno-reactivity. Scale bar= 50 µm

2.4 Discussion

In this Chapter I undertook a series of experiments designed to examine the mediators that play a role in MN death in SBMA. In particular I was interested in examining the role of CRT in the death of SBMA MNs. Previous results have shown that CRT plays a role in the Fas/NO specific cell death pathway in mutant SOD1 (mSOD1) MNs (Bernard-Marissal et al., 2012). These authors suggested that changes in CRT expression in mSOD1 MNs was critical for Fas-mediated mSOD1 MN death a pathway they propose is specific to mSOD1 MNs. These authors demonstrated a pathway in which exposure to NO or sFasL resulted in a decline in CRT protein expression, leading to ER stress and apoptosis. The Greensmith lab has previously shown that SBMA MNs, from AR100 mice, are also vulnerable to ER stress (Montague et al., 2014). Therefore we hypothesised that CRT may also play a role in MN death in SBMA. However, the results presented in this Chapter suggest that AR100 SBMA MNs do not show the same pattern of expression as mSOD1 MNs.

2.4.1 SBMA MNs do not show an increased vulnerability to cell stressors

In vitro, at both a developmentally immature stage of 3 DiV, and a more mature stage of 7 DiV, when MNs are known to express glutamate receptors (Van Den Bosch et al., 2000), AR100 MNs showed no significant increase in vulnerability to any of the stressors tested, Thapsigargin, sFasL or DetaNONOate (See Figures 12 to Figure 14). Although there was a trend for a reduction in AR100 MN survival at 3 DiV using manual cell counts (Figure 12), this reduction did not reach significance. Furthermore, this decrease in survival was not observed at 7 DiV (Figure 13), or by using less variable assays such as LDH (Figure 14) or the more reliable MetaXpress automated analysis (Figure 15). In addition treatment of AR100 MNs with DHT had no detectable effect on AR100 neurite architecture (Figure 16). Despite the high variability in the response of both WT and AR100 MNs to cell stressors in culture, these findings suggest that AR100 MNs are not more susceptible to any of the cell stressors tested in comparison to WT MNs. However, it is possible that AR100 MNs did not show any alterations in cell viability because SBMA is a ligand dependent disorder, in which the AR binds to androgens and translocates to the nucleus, and

this may have not occurred in vitro, even in DHT treated cultures. I therefore examined the localisation of AR in MNs in vitro by immunostaining (Figure 17 & Figure 18). There was no difference in the localisation of the AR in either WT or AR100 MNs in response to DHT treatment. This lack of ligand dependant changes in AR localisation may explain the absence of any increased vulnerability of SBMA MNs to stressors due to the presence of hormones in the media.

Alternatively, it is also possible that the results reported by Bernard-Marissal et al. (2012) in mutant SOD1 MNs were not be reproducible. I therefore next examined the effect of cell stressors on $SOD1^{G93A}$ MN using the same methodology as AR100 experiments. $SOD1^{G93A}$ MNs were treated with either Thapsigargin DetaNONOate or sFasL at 3 DIV and the effects on MN survival assessed by manual cell counts, LDH assays and MetaXpress.

As shown in Figure 19 to 25 the survival of $SOD1^{G93A}$ MNs was also highly variable. Using the most robust the methods tested, MetaXpress analysis, I found that under basal conditions there was no significant difference between WT and $SOD1^{G93A}$ MNs and that neurones of either genotype could not be distinguished morphologically (Figure 19). Furthermore, as shown in Figure 20, manual cell counts of MN survival following exposure to cell stressors at 3DIV, there was no significant difference between WT and $SOD1^{G93A}$ MNs, although there was a trend of increased vulnerability to sFasL. MetaXpress analysis of 3DiV $SOD1^{G93A}$ MNs showed no significant difference in vulnerability to any cell stressor (Figure 21).

2.4.2 CRT expression in AR100 and $SOD1^{G93A}$ MNs

The pattern and level of CRT expression was examined in AR100 and $SOD1^{G93A}$ MNs following exposure to cell stressors. There was no obvious difference in the pattern of CRT expression in either $SOD1^{G93A}$ or AR100 MNs under stress (Figures 22 to Figure 23).

However, high throughput analysis, revealed a mild reduction in CRT expression in $SOD1^{G93A}$ MNs under basal conditions, which was not the result of stressor

treatment (Figure 24). As a result of Thapsigargin and DetaNONOate treatment, there was a trend of reduced CRT levels, as determined by MetaXpress intensity analysis. A significant decline in CRT levels in SOD1^{G93A} was observed following sFasL treatment (Figure 25). The fact that lower CRT levels can be detected in SOD1^{G93A} MNs compared to WT under basal, unstressed conditions contradicts the results of Bernard-Marissal et al. (2012), in which authors suggest that the decline in CRT expression SOD1^{G93A} MNs is due to Fas/NO activation. The data presented here suggests that CRT levels are reduced in mutant SOD1 MNs consistently. Furthermore, *in vivo*, there was a trend of lower CRT levels in SOD1 ^{G93A} spinal cord, as early as 30 days (Figure 26), a pre-symptomatic stage in the SOD1^{G93A} mice. Bernard-Marissal and colleagues hypothesise that there may be a direct effect of mutant SOD1 on CRT expression that results in ER stress. My results show that there are lower levels of CRT in motor neurons, in the absence of cell stressors, and at pre-symptomatic stages of disease, which does support the overall findings of reduced CRT in SOD1^{G93A} MNs reported by Bernard-Marissal et al. (2012).

2.4.3 Do changes in CRT expression play a role in MN death in Models of MND?

Surprisingly, a recent follow-up paper from the same research group found that CRT may not actually have a role in SOD1^{G93A} MN cell death *in vivo*, but may instead contribute to muscle denervation (Bernard-Marissal et al., 2014). CRT heterozygous knock out mice crossed with SOD1^{G93A} only show a mild difference in pathology, coinciding with a peak in ER stress originally described in the SOD1^{G93A} model. The authors note that there are some discrepancies between their *in vitro* and *in vivo* findings. They suggest that there is increased vulnerability to low levels of CRT *in vitro* because primary culture may induce some cell stress, particularly as their methods include purification of MNs which creates what could be considered a non-physiological environment. Alternatively, they suggest that there could be compensatory mechanism *in vivo* and/or that there must be a more drastic CRT decrease in MNs *in vivo* in order for it to have a pathological effect. However, an alternative possibility is that the Fas/NO CRT cell death pathway may only present at a particular point in development and in non-physiological settings. Nevertheless

mutant SOD1 may have a direct effect on CRT as I observe lower levels of CRT in the ventral spinal cord of $SOD1^{G93A}$ mice even during early, non-symptomatic stages of disease.

Furthermore, I went on to evaluate the level of CRT expression in AR100 spinal cord at different stages of disease development (Figure 27). Surprisingly I found that there was an increase in CRT levels at postnatal day 5, synonymous to when Montague et al. (2014) first observes elevation in ER stress markers. There is also a non-significant trend of increased CRT levels in the AR100 spinal cord throughout disease progression. These results suggest that CRT is not acting in the same way in AR100 and mutant SOD1 MNs in relation to ER stress. In mutant SOD1 MNs there is a decrease in CRT expression which may induce ER stress, whereas in AR100 spinal cord there is an increase in CRT expression, which may or may not result in activation of other stress pathways.

2.4.4 Calreticulin may have alternative functions in SBMA MNs than $SOD1^{G93A}$ MNs

CRT may be involved in either pathogenesis in the AR100 mouse model or potentially could have compensatory roles. Montague et al. (2014) reported an increase in ER stress markers such as BiP in AR100 mice at P5, synonymous to when ER stress is first claimed to be present in $SOD1^{G93A}$ mice (Saxena et al., 2009). In Montague et al. (2014) the authors propose that ER stress may play a role in initiating pathogenesis in the AR100 mouse model. However it is possible that the increase in ER stress markers may be compensatory, as there are two components to the ER stress response. In the first instance the ER stress response attempts to remove or resynthesize misfolded protein, and it is only when the process is overloaded does apoptosis occur (Hetz, 2012, Hetz and Mollereau, 2014). The results presented in this chapter showed that there was an increase in CRT expression in the spinal cords of SBMA mice at P5. This finding is opposite to the change observed in mutant SOD1 mice, where a reduced CRT expression was reported (Bernard-Marissal et al., 2012). However, the increased levels of CRT observed in AR100 spinal cords at P5 are not maintained throughout disease

progression. In adult AR100 mice at pre-symptomatic, symptomatic or end-stage disease there is only a non-significant trend of increased CRT expression. Therefore CRT does not appear to play the same role in SBMA as it does in mutant SOD1 ALS, although ER stress appears to be involved in MN degeneration in both SOD1-ALS (Saxena et al., 2009) and AR100 SBMA (Montague et al., 2014). Despite this common pathology, CRT is unlikely to play the same role in MN death in SOD1 ALS and SBMA.

2.4.5 Calreticulin- a multifunctional protein

Calreticulin (CRT) is a multifunctional protein which was originally thought to be localised exclusively to the ER. It was first discovered in the SR of rabbit skeletal muscle (Ostwald and MacLennan, 1974). CRT contains an ER localisation signal. It has an acidic C terminal with many low affinity Ca^{2+} binding sites and its high affinity (Jiang et al., 2014). Ca^{2+} binding site is located in its N terminal (See Figure 30) yet this protein is not only localised to the ER and it remains unclear how the protein is transported to the cell membrane or the cytoplasm (Michalak et al., 2009). Calreticulin's primary role was originally described as a Ca^{2+} binding chaperone responsible for keeping Ca^{2+} localised in the ER or SR. (Waisman et al., 1985, Fliegel et al., 1989). It is also responsible for the addition of glycan groups to proteins in glycoprotein synthesis in conjunction with its homologue calnexin, forming the Calreticulin/calnexin cycle. These two highly homogylous proteins remain attached to the protein being synthesised whilst glycosidase enzymes cleave glucose residues from the oligosaccharide Glc3Man9GlcNAc2. If the glycosylation process is not completed correctly the nascent protein remains attached to Calreticulin and Calnexin whilst the protein UGGT (UDP-glucose: glycoprotein glucosyltransferase) reactivates the glycosylation process (Molinari et al., 2004). Interestingly, ATF6 protein expression is also regulated by the Calreticulin/ calnexin cycle, allowing the glycosylation status of proteins in the ER to act as a trigger for the UPR (Hong et al., 2004).

As mentioned in Section 2.1.3, SERCA is responsible for restoring ER Ca^{2+} stores, and upon its inhibition ER Ca^{2+} becomes depleted and this results, if not reversed, in

apoptosis. Interestingly, CRT and SERCA-2b bind directly and CRT is thought to modulate SERCA-2b's structure. CRT overexpression can cause Inositol trisphosphate (IP_3) mediated Ca^{2+} mediated release, contributing to Ca^{2+} waves seen in a number of cell types (John et al., 1998). Although it should be stressed that studies investigating CRT and SERCA-2b interactions were carried out in oocytes and not motor neurons.

In recent years, research has revealed that CRT function is not limited to the ER. CRT has a role in wound healing, activation of the complement immune response, cardiac development and neural tube closure. CRT has also been shown to be a potential candidate for a biomarker for patients with Alzheimer's disease (Lin et al., 2014). CRT is down regulated in cortical neurons in patients suffering from Alzheimer's disease as these neurons too exhibit an ER stress response (Endres and Reinhardt, 2013). CRT is indeed a multifunctional protein, and its functions discovered to date are summarised in Table 4 (Michalak et al., 1999, Michalak et al., 2009, Wang et al., 2012, Gold et al., 2010).

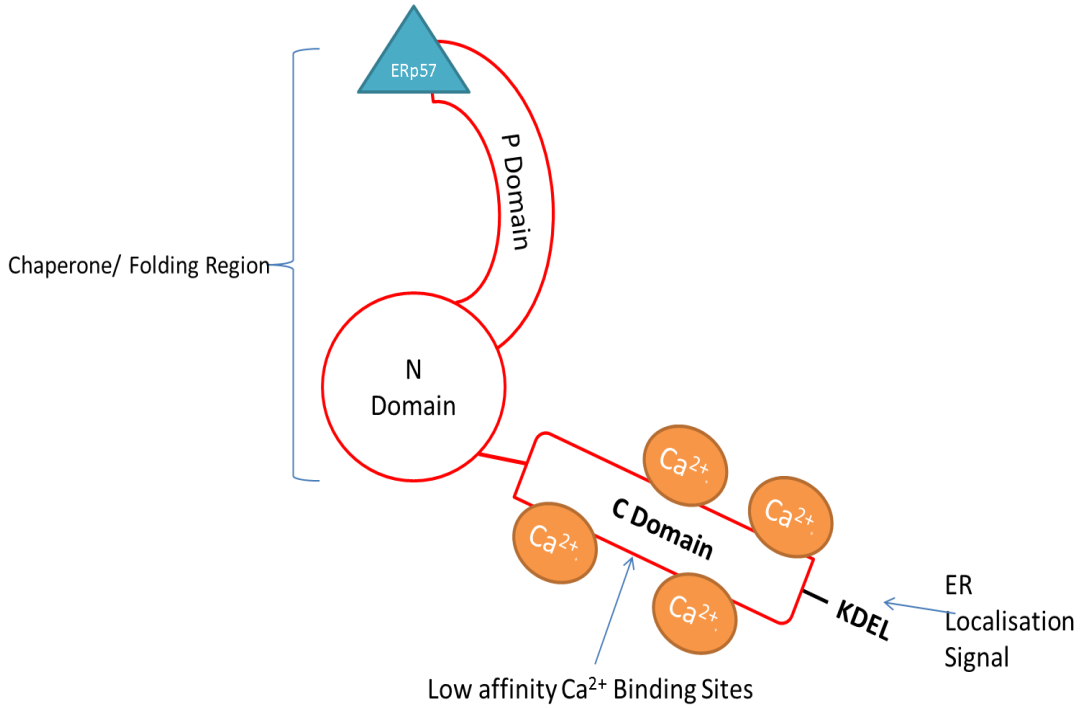

Figure 30 Structure of Calreticulin

Calreticulin (CRT) is a 400 amino acid protein with a molecular weight of 46.6 kDa, responsible for Ca^{2+} homeostasis and N glycosylation of proteins in the ER. CRT also has several non-endoplasmic reticulum functions.

Table 4 Summary of Calreticulin's Functions

Functions of Calreticulin	References
Adipogenesis	Szabo et al. (2008)
Cancer Biology; angiogenesis, immunity, neuroblastoma	Lu et al. (2015b),de Bruyn et al. (2015), Weng et al. (2014)
Cardiac Muscle development	Lynch et al. (2006)
Cell adhesion and Migration	Villagomez et al. (2009)
Cell Surface Protein Expression and signal transduction	Jiang et al. (2014)
Neural tube defects	Rauch et al. (2000)
Rheumatoid arthritis	Ding et al. (2014)
Wound Healing	Gold et al. (2006)

2.4.6 Calreticulin and the Androgen receptor

Particularly relevant to SBMA is the ability of CRT to bind the AR. CRT binds the AR in its DNA binding region at the CRT binding motif KXFFKR (Parodi & Pennuto, 2011). It has interestingly been shown to inhibit DNA binding and transactivation (Dedhar, et al., 1994). CRT possesses a nuclear receptor binding region and it has been suggested that it may contribute to export of nuclear receptors such as the glucocorticoid receptor and the AR (Walther et al., 2003, Holaska et al., 2001, Holaska et al., 2002). However, more recent research has shown that nuclear receptors can be exported independently to CRT and that methods in original studies may have been flawed, as cell fusion techniques cause perforation of the ER membrane leading to CRT leakage (Nguyen et al., 2009). Nguyen et al. (2009) do not dispute however that CRT may act as an enhancer for CRT export. Mutating CRT androgen binding site does not perturb nuclear receptor translocation out of the nucleus showing nuclear export thus it is not completely reliant on it.

Furthermore it has been shown that depletion of ER Ca^{2+} can cause translocation of CRT to the cell surface membrane (Tufi et al., 2008). As reported in Montague et al. (2014), primary AR100 MNs have increased cellular Ca^{2+} levels upon DHT application. Additionally, as CRT can modulate SERCA isoforms following Ca^{2+} concentration oscillation (John et al., 1998), and since there are reduced SERCA-2b levels in AR100 MNs (Montague et al., 2014), this further supports the hypothesis that CRT may play a role in AR100 pathology.

Although CRT is widely agreed to play a role in apoptosis, its precise role is unclear as increases and decreases in CRT have been found to have different effects in different cell types. Nakamura et al. (2000) showed that increased CRT levels in HeLa cells can be protective against apoptosis, due to lower ER Ca^{2+} stores available to activate apoptosis. Conversely, in the study by Bernard-Marissal et al. (2012), the only one to evaluate the role of CRT in MNs, showed that *in vitro,* decreased CRT results in ER stress leading to apoptotic cell death.

Interestingly, in addition to being able to bind AR and have a subsidiary role in its export, CRT has been shown to play a role in the suppression of androgen-mediated prostate cancer (Alur et al., 2009), further linking CRT and androgen regulated processes. There is also limited evidence that CRT co-localises with polyQ expansion in the mutated ataxin II protein in a model of Spinocerebellar ataxia type 2 (van de Loo et al., 2009). CRT has also been shown to co-localise with polyQ in a Huntington disease model (Ueda et al., 2014).

In summary, there are a number of reasons why CRT may be of particular interest to SBMA pathology. Although the Bernard-Marrisal et al., (2012) pathway linking Fas/NO mediated cell death with CRT levels and ER stress in mutant SOD1 MNs may not be relevant to its role in SBMA, CRT does have a role in mediating SERCA-2b expression, and as CRT and SERCA-2b have been shown to co-localise in the axon terminal (Johnson et al., 1993). Lastly and perhaps most importantly CRT can act as an enhancer of nuclear receptor export. As AR inclusion formation is a characteristic and feature of SBMA (Li et al., 1998a, Li et al., 1998b).

Due to the multifunctional role of CRT (Wang et al., 2012) and its ability to bind the AR (Dedhar et al., 1994), it is perhaps not surprising that CRT mediates stress in a different way as in SBMA than it does in $SOD1^{G93A}$ MNs. The increase in CRT I observed in spinal cord of P5 AR100 mice, may in fact be having a protective response that aims to enhance the cytoplasmic location of the AR and control nuclear export (Holaska et al., 2001, Holaska et al., 2002). This would reduce, which is believed to be a pathogenic cause of SBMA, irrespective of whether this is in the form of nuclear inclusions or diffuse staining (Adachi et al., 2005).

In contrast, it also has been shown, in non-neuronal cells that an increase in CRT can increase a cell's vulnerability to apoptosis (Nakamura et al., 2000), and a decrease in ER Ca^{2+} increases the membrane distribution of CRT (Tufi et al., 2008). I could not detect a difference in the localisation of CRT immuno-staining in AR100 MNs, although it is possible that the use of triton in the staining protocol may have confounded our ability to detect any changes in membrane localisation of CRT. To

date the role of CRT in MNs has only been explored in Bernard-Marissal et al. (2012). Further research that could be done based on the work in this chapter should include the analysis of how/ whether polyQ AR and CRT bind in the same way as normal AR and CRT. This could be investigated using co- immuno-precipitation assays and co-localisation immuno-staining using confocal imaging.

2.4.7 Motor Neuron Markers and Development *in vitro*

It is important when using *in vitro* cellular models of disease to determine the precise stage in development to analyse particular cell pathways. As already mentioned FLIP expression in development can confer MN sensitivity to cell death (Raoul et al., 1999). However this is by no means the only protein that is regulated in expression levels as MNs develop. Fundamental to *in vitro* classification of MN's is glutamate receptor signalling. As AMPA receptor signalling is responsible for communication between the brain stem and higher MNs to the lower MNs, it is important that the cells examined in the study of MN degeneration are in fact functional MNs. Two time points were chosen to investigate in this study, 3 DiV (prior to FLIP protein expression) and 7 DiV, when Glutamate receptors are expressed (Van Den Bosch et al., 2000). No differences were seen in the examination of AR100 MNs to the cell death pathway of interest, but even morphologically it is clear that between 3 DiV and 7DiV a vast amount of development occurs.

It was also of particular importance to assess the correct cells in mixed ventral horn culture. To do this prior work in the Greensmith lab has defined MNs by their morphological criteria once stained with the neuronal marker β III Tubulin (Bilsland et al., 2010, Montague et al., 2014). I have also attempted the use of other MN markers such as the transcription factor Homobox 9 (Hb9) expressed in post mitotic MNs until postnatal development (Arber et al., 1999). Yet 7 DiV MNs, as cultured using the methods of Kalmar and Greensmith (2009) did not did not stain positively for Hb9. The Greensmith lab has also attempted use SMI32 staining, a motor neuron neuro-filament marker to identify MNs in culture. However, lab members have found that not all MNs were SMI32 positive. Furthermore there is evidence

that there are varying levels of SMI32 in another model of SBMA (Chevalier-Larsen et al., 2004). Particularly attractive were the Islet proteins (Islet 1 and 2), although not specific to MNs and are also expressed in inter neurons, the nuclear nature of the staining would perhaps allow more precise automated identification of MNs using image analysis software. Again, thus far all attempts at using islet staining to identify MNs cultured have yet to produce positive results in the Greensmith lab. Lastly Delta like kinase 1 (Dlk1) staining was also examined. Recently this transcription actor was shown to be preferentially expressed in MNs sensitive to degeneration (Muller et al., 2014). Alpha MNs, which innovate fast, twitch muscle fibres, the first to degenerate in the mutant SOD1 model of ALS, express Dlk1 (See Chapter 3 for detailed discussion on muscle fibre type and its features in neuromuscular disease). However I found that this protein was expressed in β III Tubulin negative non-neuronal cells, with a nucleus smaller than that of a fibroblast.

2.4.8 The function of the AR in neurite outgrowth

In my experiments I also evaluated the neurite architecture of the primary ventral horn cultures. Although DHT is thought to control development of neurite architecture (Fargo et al., 2008). I found that neurite length was not significantly different in either WT or AR100 MNs in the presence or absence of DHT. This was somewhat surprising as research to this date has shown that DHT has a direct role in the modulation of neurite outgrowth. Overexpression of the AR in rats has been shown to generate larger dendrites in motor neurites that innervate the quadriceps (Huguenard et al., 2011). Work by Marron et al. (2005) showed that depriving an immortalised MN like cell line of androgens caused a decrease in both cell body size and the length of dendrites. Additionally Simeoni et al. (2000) have shown that expression of the AR containing pathogenic polyQ repeats results in the formation of short dumpy neurites initially *in vitro*, however this difference disappears as the neurons mature. This process is thought to be due to neuritin, which the synthesis of β Tubulin and β actin, fundamental for MN development (Marron et al., 2005). As the polyQ AR mutation is thought to cause a combination of a toxic gain of function and loss of function, as demonstrated by the mild androgen insensitivity

observed in patients (Beitel et al., 2013), I hypothesised that the loss of function in the AR100 mice might also lead to a disrupted MN morphology. I treated primary cultures from WT and AR100 mice with high concentrations of DHT and found no difference in neurite architecture. However, I followed this experiment up by staining for the AR and found that DHT treatment did not in fact alter the localisation of AR staining. This is possibly due to the presence of hormones within horse serum contained in my culture medium which would result in some nuclear staining, even under basal conditions. Subsequent experiments should opt for the use of charcoal stripped media.

2.4.9 Summary

In this Chapter I evaluated whether the altered Ca^{2+} homeostasis in SBMA MNs reported in Montague et al. (2014) lead to an increased vulnerability to the ER stressor Thapsigargin. The presence of ER stress in AR100 MNs suggests that AR100 MNs may be selectively vulnerable to sFasL and DetaNONOate treatment. The Fas/NO cell death loop has been reported in fast fatigable MNs of the $SOD1^{G93A}$ model (Bernard-Marissal et al., 2012). However, I examined the possibility that this pathway could also contribute to AR100 MN death. I used a combination of techniques, including manual cell counts, high through-put automated cell counting and intensity analysis, lactate dehydrogenase (LDH) assays and western blotting for ER stress markers. I also attempted to validate my methods using primary MNs from the $SOD1^{G93A}$ mice in which the Fas/NO dependant MN specific pathway was first reported (Bernard-Marissal et al., 2012).

My results indicated that this pathway is not highly reproducible, and difficult to detect using the methods listed. I also found that this pathway may not only be limited to mutant SOD1 MNs, but it may be a general feature of MN death early in *in vitro* development. Difficulties with primary MN culture variability and purity made it challenging to come to a definitive conclusion over whether this pathway is important in the pathogenesis of MNDs. I also analysed protein levels of CRT *in vivo* and found that in the spinal cord of $SOD1^{G93A}$ mice there was a lower level of CRT protein expression at end stage, replicating results already published (Bernard-

Marissal et al., 2012). However, this was highly variable with one out of three samples expressing levels of CRT comparable to WT. More recent work from Bernard-Marissal et al. (2014) has shown that CRT may not be as important for MN survival *in vivo* as the suggested in their original paper, with minimal effects on the SOD1 phenotype occurring by crossing these mice with CRT knockouts.

Unexpectedly, I found that in AR100 mouse spinal cord there was a higher level of CRT protein expression at pre-symptomatic stages of disease. More variable CRT protein expression levels at were detected adult stages, with a trend of higher levels of CRT protein, although this did not reach significance. The higher levels of CRT in AR100 mouse spinal cord could perhaps indicate that this protein indeed has a function, either compensatory or in pathogenesis of SBMA independent to the Fas/NO pathway.

Chapter 3 Analysis of the AR100 mouse model muscle

3.1 Introduction

Over the past few years, several mouse models have been developed to model the pathological and physiological characteristics of SBMA (Pennuto and Basso, 2016). In our group, we have focused on the AR100 model generated by La Spada and colleagues (Sopher et al., 2004). In the original description of these mice, the authors showed a progressive muscular deficit with growth retardation occurring at approximately 8 months, and an obvious kyphotic appearance by 10 months. Marked hind limb atrophy was reported by 14 months of age. Ultimately AR100 mice developed hind limb paralysis and died of unknown causes or required euthanasia by 15-24 months of age.

Research from our group was the first to undertake a full physiological characterisation of the neuromuscular phenotype of these mice (Malik et al., 2013). *In vivo* physiology recordings of muscle force showed that by 18 months of age in male AR100 mice there was a significant decrease in hind limb muscle force, a decrease in the number of surviving motor units, and histopathological analysis of the spinal cord confirmed that this was associated with loss of ~40% MNs in the sciatic pool. This data therefore confirmed the SBMA phenotype of AR100 mice.

However, these studies did not reveal the age at which these disease features manifested. Therefore, in a recent study in our group Anna Gray undertook a full behavioural and physiological analysis of the neuromuscular phenotype of male AR100 mice, from 3 months to 18 months of age. Her unpublished data showed for the first time that there was a clear onset of disease deficits at 6 months of age, with a significant decline in hind limb muscle force detected at 6 months (See Figure 31). This was prior to any clear behavioural signs of muscle weakness, and long before any MN death. These findings are important as they suggest that the muscle may be a primary target of disease in SBMA and that the muscle weakness observed at 18 months of age (Malik et al., 2013) may not simply be the result of loss of MNs and subsequent denervation. However, this study was based on a comparison of male AR100 mice with WT littermates and it is therefore possible, that the muscle phenotype observed in AR100 mice may be due to the expression of the AR

transgene per-se. It is therefore important to undertake a full study of an appropriate control strain, such as the AR20 mice, which have a non- pathogenic expansion of the AR. This was the first aim of the present study. In addition no histopathological characterisation of the hind limb muscles of AR100 or AR20 mice at different stages of disease has been undertaken to date. Therefore, in this study I examined the TA and EDL muscles of male AR100 and AR20 and control WT mice at different stages of disease, from 3 months to 18 months of age.

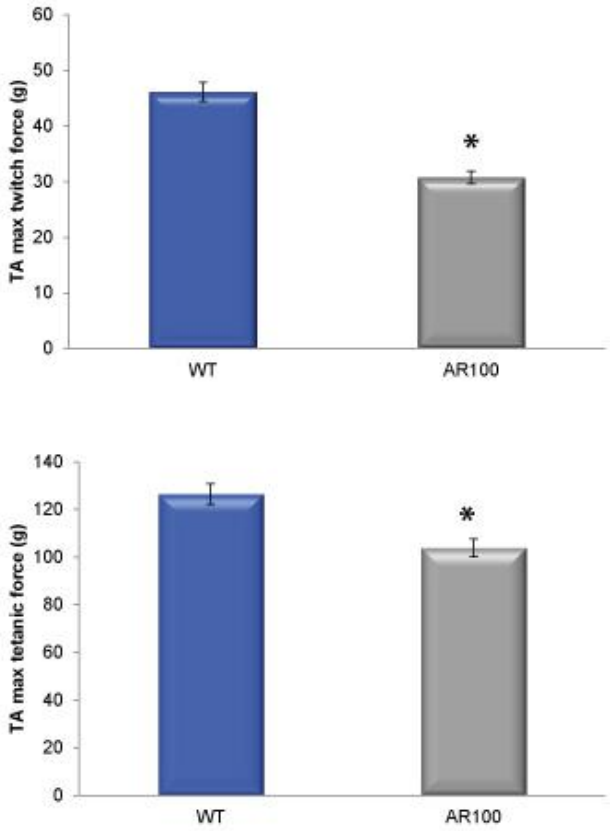

Figure 31 Summary of AR100 6 months muscle physiology by Anna Gray

Muscle physiology analysis of WT and AR100 muscle at 6 months shows a decline in TA muscle force early in disease progression. Error bars =SEM. Figure taken from A. Gray, PhD Thesis.

3.1.1 Is SBMA a multisystem disease?

Traditionally SBMA has been viewed as a cell-autonomous disease, with almost all of the early research following discovery of its genetic cause (La Spada et al., 1991), focussing on MNs. In line with this view, the clear pathology observed in muscles was viewed as the consequence of dysfunction and deterioration of MNs. In more recent years the possibility that muscle may play an important primary role in SBMA has begun to emerge (Rinaldi et al., 2014). However, the question of whether SBMA is a muscle or MN disease is by no means a new one (Jordan and Lieberman, 2008). The generation of a number of mouse models for SBMA (discussed in Section 1.7), with different phenotypes, has contributed to the ongoing un-certainty of whether SBMA pathogenesis initiates in the muscle or in the spinal cord.

Using one of the newest mouse models of SBMA, the Bacterial Artificial Chromosome (BAC) AR121, developed by Cortes et al. (2014a), it has been shown that treatment of AR121 or AR113 mice using antisense oligonucleotides strictly in the periphery, can ameliorate disease (Lieberman et al., 2014). In contrast, RNA knockdown of the mutant AR in the CNS had no effect on mouse phenotype. Cortes et al. (2014a) have also shown that either ubiquitous or muscle specific knock down of the human AR121 transgene can also rescue symptoms. However the AR121 mouse model has been viewed as a model of primary myopathy, whereas patients do show symptoms that a neurogenic in origin such as muscle fasciculation (Hashizume et al., 2015). Conversely, Sahashi et al. (2015) have shown using the AR97Q mouse model that antisense oligonucleotides which knock down the AR in the CNS, can ameliorate symptoms. However it is therefore possible that the two preclinical trials of antisense oligonucleotides (Lieberman et al., 2014, Sahashi et al., 2015) may have had contrary effects due to differences in their treatment in terms of timing and concentrations of injections.

Recent work by Ramzan et al. (2015) attempted to clarify whether polyQ AR toxicity generates SBMA like symptoms in mice as a result of expression in MNs or myocytes. They transiently expressed polyQ AR in mice for 4 weeks, in either muscle or spinal cord and found that it was only mice with neuronal expression that

developed gross motor symptoms. Mice with specific expression of polyQ AR in myocytes had shrunken glycolytic fibres in the muscle. However, both mice developed a reduced oxidative capacity in the Extensor Digitorum Longus (EDL) muscle, and had no evidence of neurodegeneration. This suggests that in order to get a full spectrum of SBMA symptoms in mice the mutant androgen receptor must be expressed in both muscle and spinal cord. Nevertheless, the recent findings in the AR100 mice from the Greensmith lab; discussed above, which clearly show functional muscle deficits prior to any MN death, suggest that primary muscle deficits may indeed play a role in SBMA pathogenesis.

Taken together, recent developments show that SBMA has features of both muscle and MN pathology, and therefore both the CNS and the muscle should be considered as sites for therapeutic intervention. Analysis of the AR100 mouse model in our lab so far has largely focused on examination of pathology within the spinal cord. In this Chapter I undertake an in depth analysis of the hind limb muscles of AR100 mice throughout disease progression.

3.1.2 The AR100 mouse model of SBMA

The AR100 mouse model was developed in the La Spada laboratory (Sopher et al., 2004), primarily to investigate polyQ AR neurotoxicity. The transgenic AR100 pathogenic line expressing 100 CAG repeats and the control line expressing 20 non-pathogenic repeats (AR20) were generated by fusing yeast cells containing the full human androgen receptor (AR) with embryonic stem (ES) cells. These ES cell clones were then injected into blastocysts to yield chimeric mice. The AR100 mice demonstrate a late onset neuromuscular degenerative phenotype (Malik et al., 2013, Sopher et al., 2004). To date most of the research using these mice has focused on pathology in the spinal cord or primary embryonic MNs.

The original paper to describe AR100 and AR20 mice (Sopher et al., 2004) identified the first symptom of disease at 8 months as slight growth retardation, which became obvious by 10 months. Foot print analysis and rotarod testing showed that by 14 months of age mice had hind limb weakness and difficulty walking. In addition

AR100 mice have a reduced lifespan, with no survival beyond 22 months. The earliest reported sign of dysfunction in AR100 mice was at 6.5 months where a non-significant trend for decreased stride length was detected, which became significant by 11 months. Some histopathological analysis was performed on AR100 muscle at disease end stage, where fibre type grouping was observed. In the spinal cord there was no evidence of AR aggregation in AR100 mice. Punctate AR staining was found in AR100 astrocytes, and some degeneration of spinal MNs was noted although this was not quantified. No analysis of AR20 mice was presented in this paper.

The next study to utilise the AR100 mouse model was Thomas et al. (2006b), where AR100 mice were crossed with Testicular feminisation mice, negative for the mouse AR. In this cross the SBMA disease phenotype was exacerbated, with spinal MN loss evident from 10 months. However, functional analysis of underlying patho-mechanisms of disease in AR100 mice showed that axonal transport deficits did not play a role in MN death in the AR100 model of SBMA (Malik et al., 2011). In contrast to findings in other models of MN disease such as mutant SOD1 mice (Kieran et al., 2005), and other models of SBMA (Katsuno et al., 2006a). In 2013, further work from our lab, confirmed that by 18 months of age ~40% of lumber spinal cord MNs had degenerated, accompanied by a decrease in muscle function (Malik et al., 2013).

However, more recent work in the Greensmith lab both in primary MNs (Montague et al., 2014) as well as *in vivo* (A. Gray, PhD Thesis 2015) examined pathology in the AR100 model. Montague et al. (2014) detected ER stress *in vitro* in primary MNs in culture and in vivo in the AR100 spinal cord as early as postnatal day 5. Further functional analysis of muscle in AR100 mice by Anna Gray in our lab, identified a decline in hind limb muscle strength at 6 months of age. In the Tibialis anterior (TA) and Extensor Digitorum Longus (EDL) muscles maximum force and weight is reduced, and this is seen prior to any motor neuron loss or decline in motor unit survival (Anna Gray, PhD Thesis 2015).

3.1.3 Histopathological changes in neurogenic and myogenic muscle atrophy

One of the key diagnostic measures of myopathies is muscle histopathology. Muscle structure undergoes characteristic changes dependent on whether the causes of atrophy are neurogenic or myogenic (Seidman, 2013). For example in Inclusion Body Myositis (IBM), where pathology initiates in the muscle, fibre hypertrophy, lobulated fibres, and internalised nuclei are often observed and are used to diagnose the condition sometimes in conjunction with more ultra-structural tests (Machado et al., 2014). In contrast in ALS, in which the loss of muscle function is neurogenic in origin due to the loss of MNs, degenerating muscle fibres are found to be angulated and atrophied and muscle fibre grouping and splitting is observed (Simon et al., 2014). However, muscle biopsies from SBMA patients show a combination of these features (Soraru et al., 2008) possibly suggesting both a neurogenic and myogenic component. However, the marked variability in SBMA patients in terms of symptom onset and phenotype can make it difficult to ascertain whether the onset of symptoms are neurogenic or myogenic (Finsterer and Soraru, 2015).

3.1.4 The development of an i*n vitro* model of AR100 muscle pathology

Since the spinal cord has been widely considered the main site of SBMA pathology, there is limited research utilising muscle cells in culture to investigate pathogenesis in this disease. To date, the only study to develop a muscle culture method for SBMA muscle is Malena et al. (2013). Authors isolated satellite cells from SBMA patients and cultured the cells for up to 15 days into myoblasts or differentiated into myotubes. Even at this early stage of development, myotubes showed evidence of pathology. Authors found that SBMA patient cells lost androgen dependent hypertrophy and had disrupted myofibrillar organisation in culture. Importantly, in the absence of DHT, both control and SBMA patient samples grew similarly, illustrating the ligand dependency of SBMA.

3.1.5 Aims of this Chapter

In this Chapter, I first took the initial steps in characterising AR100 primary myotubes in culture and attempted to quantify any effect of treatment with DHT. I next characterised the control AR20 mice which express a non-pathogenic CAG repeat length, to confirm that these mice do not have a significant disease phenotype. In addition I examined muscle histopathology at various stages of disease progression in AR100 mice, to determine the onset of muscle atrophy, if there are signs of muscle denervation and to establish whether pathology is myogenic or neurogenic in origin.

3.2 Materials and Methods

3.2.1 SBMA Mouse colony

The experiments described in this Chapter were undertaken using AR100 mice that model SBMA. As controls, mice expressing non-pathogenic AR20 were examined as well as WT littermates. The original AR100 and AR20 mouse colonies were originally obtained from Albert R. La Spada's laboratory (UCSD, USA), and colonies established and maintained at UCL Biological Services. All procedures were performed in accordance with the Scientific Procedures act 1986, under licence from the UK Home office following approval from the UCL IoN Animal Welfare and Ethical Review Board. Genotyping was carried out as described in section 2.2.1.

3.2.2 Primary Neonate Satellite Cell Culture

3.2.2.1 Muscle culture preparation and maintenance

WT and AR100 mice aged P0 –P2 were decapitated and the hind limb muscles distal to the knee joint dissected. The muscles were then minced on ice in a sterile tissue culture hood. The samples were then pooled (maximum 5) according to genotype and incubated at 37°C in 3ml 0.1% Collagenase type II (Gibco, Life Technologies). Samples were triturated every 15 minutes then passed through a 100µm nylon mesh, followed by a 40µm mesh to remove pieces of undigested tissue. The samples were then centrifuged at 480g for 10 minutes, and suspended in 1 ml of 'Cell plating medium' (15% Foetal Calf Serum, 2% Pen Strep, 0.5 % Chick Embryo extract in DMEM Glutamax). The number of cells in the suspension was determined using Trypan Blue (Sigma), and were plated at a density of 10,000 sells per 96 well plate well on 0.1% Gelatine coated plates. Satellite Cells were maintained for 3 DiV then medium was changed to 'Differentiating media' containing 10% Normal Horse Serum instead of Foetal Calf Serum. A subset of cells was then treated with 50nM DHT. Cells were fixed at 7 DiV with 1:1 Acetone Methanol at 4°C.

3.2.2.2 Automated image analysis

Primary myotubes from WT and AR100 mice were immuno-stained with the muscle specific intermediate filament marker Desmin (Dako, 1:100) and DAPI for analysis

with MetaXpress software. The percentage of myogenic nuclei as well as the area of each myotube was assessed. Due to the software limitations of not being able to identify multinucleate cells, measurements for myotube area are calculated in reference to each nucleus.

3.2.3 In vivo analysis of muscle function in AR20 mice

3.2.3.1 In vivo assessment of isometric muscle force

AR20 Mice were anaesthetised with 3 % Isoflurane in oxygen, using a Fortec vaporizer (Vet Tech Solutions Ltd). Once reflexes had ceased, they were transferred over to a mouth piece and Isoflurane concentrations were adjusted throughout the experiment to maintain anaesthesia. The hind limbs were shaved and the distal tendons of the Tibialis Anterior (TA) and the Extensor Digitorum Longus (EDL) muscles were cut and attached to an isometric force transducer (Dynamometer UFI Devices) using silk thread. The length of the muscles was adjusted in order to produce maximum force. The sciatic nerve was exposed in the mid-thigh region and cut, then placed on a stimulating electrode, and kept moist with saline throughout the experiment. By stimulating the sciatic nerve with square-wave pulses of 0.02 ms in duration, isometric contractions were generated in the TA and EDL muscles and the maximum twitch and tetanic force recorded. Trains of stimuli with frequencies of 40, 80 and 100Hz were used to elicit tetanic tension and with the aid of force transducers, the amount of weight the force of contraction could carry was calculated using a Picoscope 3423 oscilloscope and Picoscope software (version 6). Typical examples of twitch and tetanic contractions for the EDL of WT mice are shown in Figure 32 to Figure 34.

3.2.3.2 Muscle Contractile characteristics

Muscle contractile characteristics were calculated from the muscle twitch traces. The time taken for the muscle to reach maximum force (time to peak contraction; TTP) as well as the half relaxation rate (the time taken for muscle to relax to half its maximum contraction; ½ RT). See Figure 32.

3.2.3.3 Muscle Fatigue

The fatigue characteristics of the EDL were examined by repeatedly stimulating the muscles at 40 Hz for 250mV/s for 3 minutes. The tension at the end of the stimulation was calculated as the ratio of that at the start of the stimulation to give a Fatigue Index (FI). A value approaching 1 indicates that the muscle was highly resistant to fatigue. An example trace is shown in Figure 34.

3.2.3.4 Estimation of Motor Unit Survival

The number of motor units innervating the EDL was estimated by stimulating the sciatic nerve with stimuli of increasing intensity, causing stepwise changes in twitch force, as a result of recruitment of motor axons with increasing stimulus thresholds. A typical example of motor unit recordings from an EDL muscle of WT mice is shown in Figure 35.

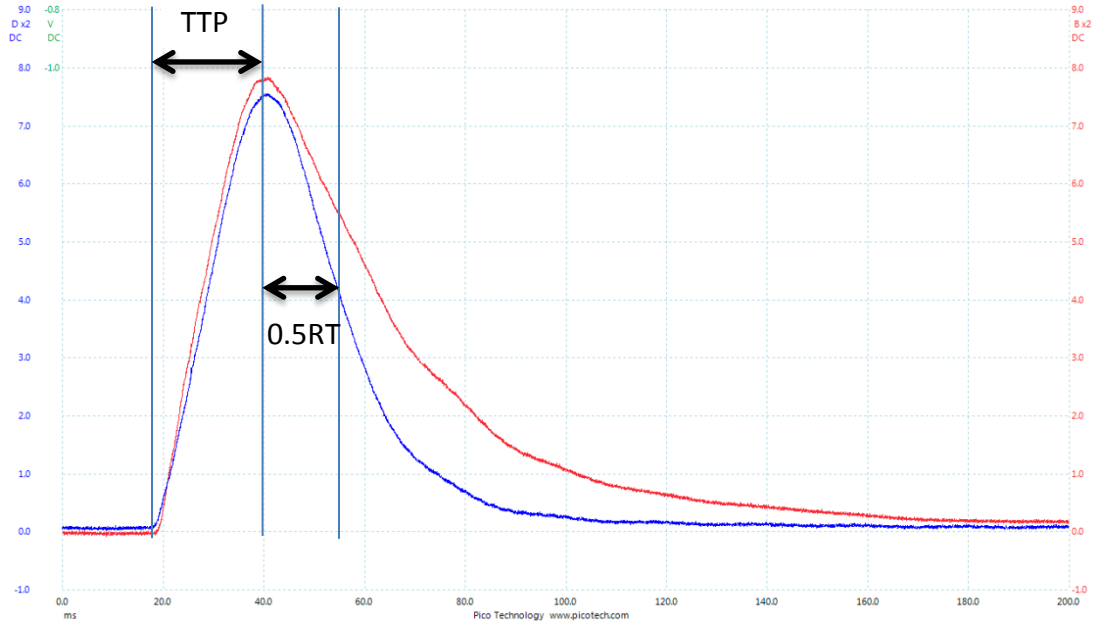

Figure 32 Recording of a mouse EDL muscle twitch

A characteristic recording of a WT mouse EDL muscle twitch after stimulation of the exposed sciatic nerve, recorded by Picoscope version 6. The time to peak (TTP) and the half relaxation time (0.5 RT) were calculated from twitch traces. The blue line denotes muscles of the right leg and the red line denotes the left leg.

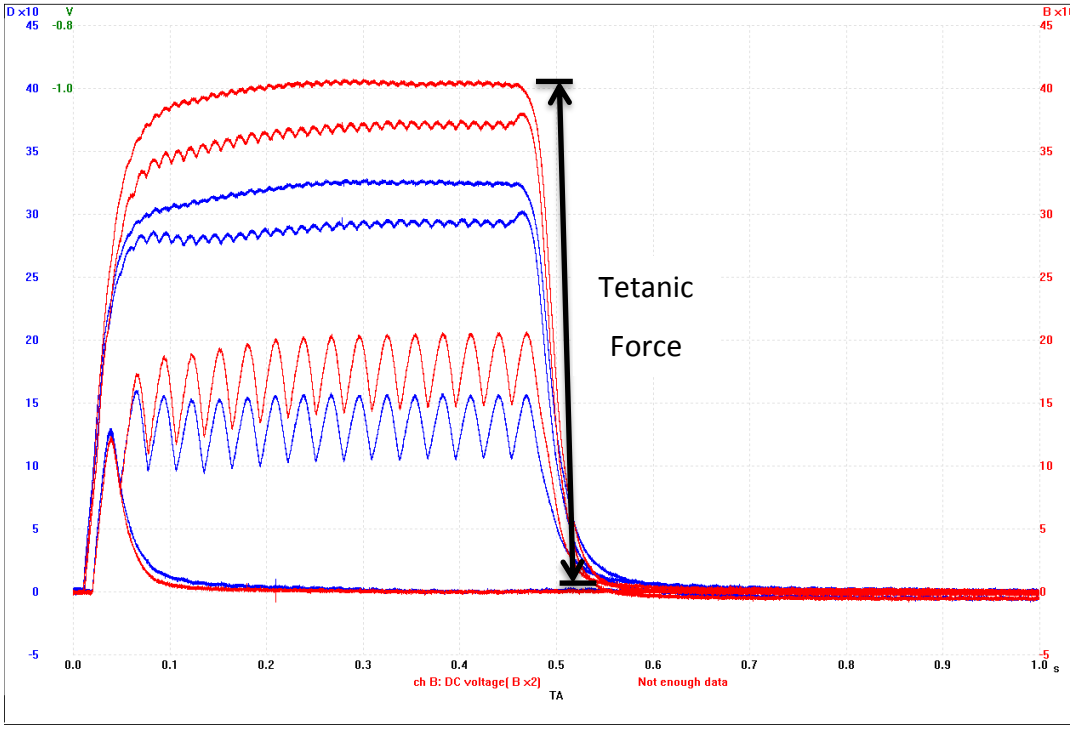

Figure 33 EDL muscle Tetanus

A characteristic trace of an EDL muscle tetanus experiment as recorded by Picoscope version 6. The exposed sciatic nerve was stimulated for 250v for 40Hz, 80 Hz and 100 Hz in succession. The maximum amplitude is recorded for analysis of tetanic force. The blue line denotes muscles of the right leg and the red line denotes the left leg.

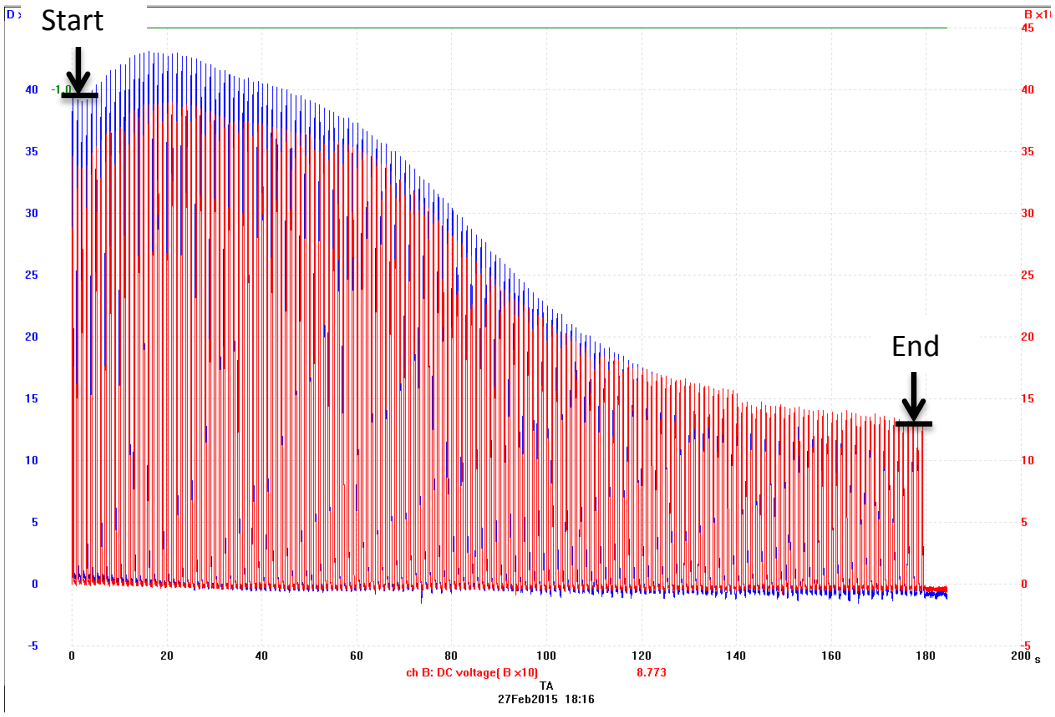

Figure 34 EDL Fatigue trace

Characteristic recording of a WT mouse EDL muscle fatigue trace as recorded by Picoscope version 6, using 250mV stimulations every second for 3 minutes. The fatigue index was calculated as a ratio of the force at the end of the stimulation period to that at start of stimulation.

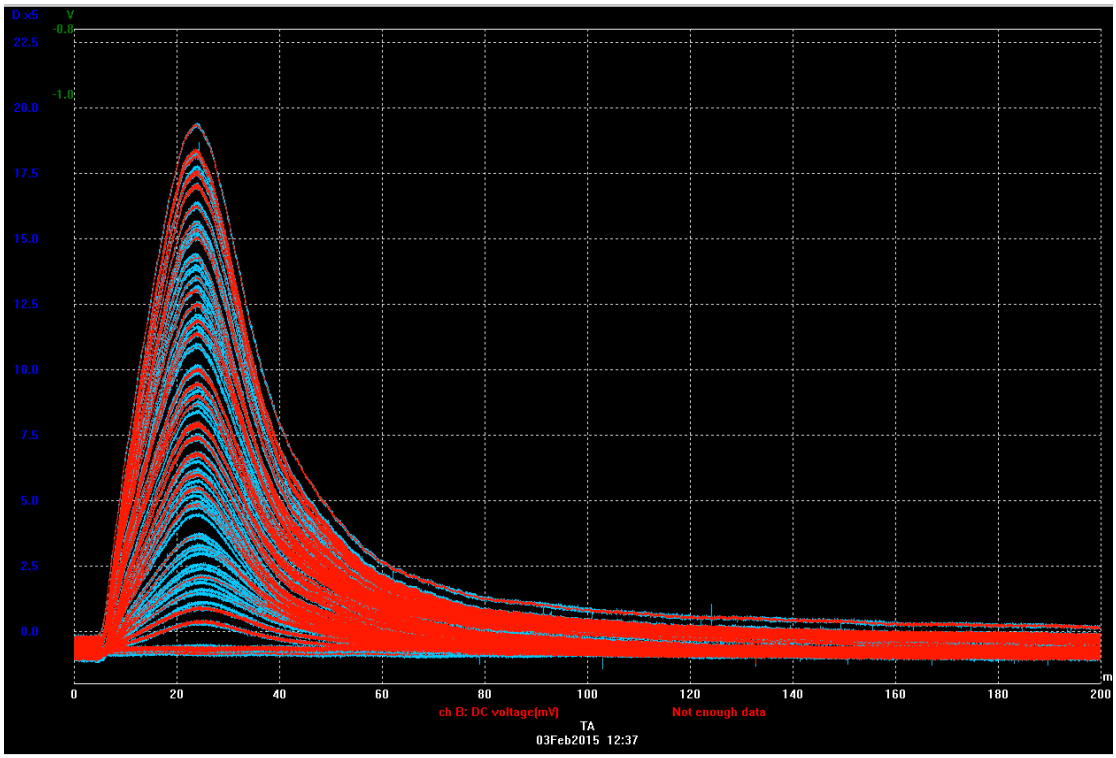

Figure 35 Motor Unit Estimation

Characteristic recording of an EDL Motor Unit estimation experiment using Picoscope version 6. The sciatic nerve was stimulated for using varying stimulus magnitudes to recruit motor units with increasing stimulus thresholds. Each motor unit was isolated at least twice. This example shows approximately 34 motor units.

3.2.4 Muscle and spinal cord dissection

Following the acute *in vivo* muscle physiology experiments, mice were terminally anesthetised with 4.5% Chlorohydrate (i.p: 100µl per 10g body mass). The TA, EDL and soleus muscles were then rapidly dissected, mounted in O.C.T, frozen in melting isopentane, then flash frozen in liquid nitrogen. Muscles were then stored at -80°C until processing. The mice were then transcardially perfused with 0.2% saline, and upon blood clearance from the liver, 4% Paraformaldehyde (PFA) in PBS. The lumbar spinal cord was removed and dissected out of the spinal column. The spinal cord was then post fixed in PFA overnight at 4 °C, and then cryoprotected in 30% sucrose in water at 4 °C until cryo-sectioning. In some cases, muscles (TA, EDL and soleus) and spinal cord were removed for Western Blot analysis. In this case, the mice were terminally anesthetised and the tissues collected as above; spinal cords were removed following 0.2% saline perfusion; muscles were dissected prior to perfusion. These fresh tissue samples were flash frozen in liquid nitrogen and stored at -80°C prior to homogenisation.

3.2.5 Muscle Histopathology

Muscles mounted in O.C.T. were transferred from storage in a -80°C freezer in liquid nitrogen then allowed to equilibrate in a cryostat at -16°C for 5 minutes prior to sectioning in order to minimise the occurrence of freezing artefacts. Muscles were sectioned at 12.5 µm prior to processing as described below:

3.2.5.1 Haematoxylin-Eosin staining

Sections were submerged in Weigert's Iron Haematoxylin (1% Solution in absolute alcohol combined with 30% aqueous solution of ferric chloride in 1% Hydrochloric acid in distilled water) for one minute then washed under running tap water for one minute. Sections were then submerged in Eosin for one minute and then placed under running tap water for a further minute. Sections were washed two times in Histoclear for a minute each and then mounted with DPX before visualisation.

3.2.5.2 Van Gieson Staining

Sections were fixed in 90% ethanol for 20 minutes, then rinsed in 70% ethanol and placed in Weigert's iron Haematoxylin for 20 minutes. Slides were rinsed in tap water for 1 minute, and then differentiated in in 1% acid alcohol. Slides were washed in running tap water for 10 minutes, then submerged in Van Gieson (10ml 0.1% acid Fuchsin was added into 100ml saturated aqueous solution of picric acid). Slides were washed briefly in tap water, 90% alcohol, 100% alcohol twice and were lastly placed in histoclear twice for 3 minutes each. Slides were mounted with DPX.

3.2.5.3 Succinate dehydrogenase (SDH) staining

The SDH stain was prepared as follows: 32.8ml of 0.1M Phosphate buffer pH 7.6 was added to 2ml of 1M Sodium Succinate, 4ml 15mM nitroblue-tetrazolium, 0.4ml of 0.1M Potassium Cyanide and 0.8ml of 10mM Phenazine methosulphate. The working solution was kept in a dark bottle at 4°C. TA Muscle 12.5 µm sections were removed from -20°C storage and place into a 37°C oven for 10 minutes. The working SDH solution was also warmed to 37°C for 10 minutes prior to use. A few drops of the working solution were placed over the slides then they were place back into 37°C equilibration for 3-5 minutes. After sufficient colour development, slides were passed through 0.9% saline, 70, acetone and 90% alcohol, each for a total of 1 minute. Slides were then passed through Histoclear for 2 minutes twice and coverslips mounted with DPX.

3.2.6 Muscle Immunohistochemistry

Tibialis anterior (TA) muscle cross sections (12.5µm) were ringed with a Pap pen, and placed in a humidified chamber. Sections were washed 3 times for 5 minutes in TBS triton to remove O.C.T. They were then blocked in 5% animal serum, corresponding to the host animal of the secondary antibody, in TBS 0.1% Triton for 1 hour at room temperature. The primary antibodies used (see Table 5), were incubated on slides overnight at room temperature. Sections were then washed 3 times for 5 Minutes in TBS Triton and appropriate secondary antibodies were placed on the samples for 2 hours, in 5% animal serum in TBS triton in a darkened humidified chamber for 2 hours. Secondary antibodies were then washed off with

TBS 3 times for 5 minutes. Amplification kits such as the ABC kit (Vector labs, PK 6100) or Tyramide Signal Amplification (Perkin Elmer, NEL741001KT) were used as required. Sections were lastly stained with the nuclear marker DAPI (Sigma) 1 in 100 for 10 minutes in TBS, washed and mounted with Dako Florescent mounting medium.

Table 5 Primary Antibodies used for Muscle Immunohistochemistry

Primary Antibody	Supplier and Product Code	Concentration
Choline acetyltransferase (ChAT)	Millipore, AB144	1:100
α- Bungarotoxin	Sigma, T0195	1:500
TDP-43 – C Terminal	Protein tech, 12892-1-AP	1:100
Androgen receptor (AR) – C Terminal	Santa Cruz, SC-815	1:200
Desmin	Dako, M0760	1:100
Nogo-A	R&D Systems, AF3515-SP	1:20
Myosin heavy chain subtypes identifying all fibre types except type 2X	Developmental Studies Hybridoma Bank, BF-F3-s	1:10
Myosin heavy chain subtypes identifying type 2A fibres	Developmental Studies Hybridoma Bank, SC- 71-s	1:10
Myosin heavy chain subtypes type 2A or type 1 fibres	Developmental Studies Hybridoma Bank, BF-35-s	1:10

3.2.7 Muscle Innervation

The extent of muscle fibre innervation in the EDL muscles was determined by labelling the post synaptic acetyl choline receptor with florescent α-Bungarotoxin and immunolabelling the motor nerve terminus with the MN marker Choline Acetyl transferase (ChAT; see table 4). The EDL muscle was mounted in a block of O.C.T. in

dry ice, and then cut longitudinally. Alternate sections were analysed and the number of end plates that were I) fully innervated, where there was total co-localisation of ChAT and α-Bungarotoxin; II) partially innervated, where there was some co-localisation of α-Bungarotoxin and ChAT; or III) denervated, where there was no ChAT staining in the presence of an α- Bungarotoxin endplate, was determined.

3.2.8 Muscle fibre typing

Cross sections (12.5 μm) of the TA muscle from WT and AR100 mice were stained with antibodies for Myosin heavy chain subtypes to identify the combination of muscle fibre type. Sections were stained with an antibody for all myosin heavy chain subtypes identifying all fibre types except type 2X (Developmental hybridoma bank product code BF-F3-s), in combination with either an antibody specific for type 2A fibres (Developmental studies hybridoma bank product code SC- 71-s) or an antibody specific to either type 2A or type 1 muscle fibres (Developmental Studies Hybridoma bank product code BF-35-s) in serial sections. As Type 1 fibres are not normally found in the TA this permits the examination of 2A, 2B and 2X muscle fibres. Sections were blocked in 5% goat serum in PBS+ 0.1% Triton for 30 minutes at room temperature. All primary antibodies were used at a concentration of 1:10 in 5% Normal goat serum in PBS + 0.1% Triton. Primaries were incubated at room temperature for two hours in a humidified chamber. Alexa Fluor Secondary antibodies specific to the antibody subclass, e.g. for BF-F3-s, Goat anti Mouse IgM secondary antibody was used. All were used at a concentration of 1:500 in 2% goat serum in PBS+ 0.1% Triton. Stained sections were visualised at 40 X magnification on a Leica light microscope to obtain high resolution images of the muscle. Multiple images for each section were then optimised using image J and used to create a montage of the whole muscle. Below is a summary of muscle fibre types and their characteristics (Table 6).

Table 6 Summary of Muscle fibre type and characteristics

	Type I	**Type IIa**	**Type IIx**	**Type IIb**
Contraction time	Slow	Moderately fast	Fast	Fastest
Fatigue Resistance	High	Fairly High	Moderate	Lowest
Oxidative Capacity	High	High	Moderate	Low
SDH Staining	Intense	Intense	Medium	Pale
Mitochondrial density	Very High	High	Moderate	Lowest
Glycolytic capacity	Low	High	High	High
Myosin ATPase activity	Low	High	Highest	Highest

3.2.9 Analysis of Muscle fibre size and number

SDH stained muscle sections were visualised under a Leica light microscope and muscle fibre size was analysed with the aid of Image J for three TA muscles per Genotype (WT or AR100), at each age: 3 Months (pre-symptomatic), 6 Months,(symptom onset) and 18 Months, (disease end stage). Results of muscle fibre size were plotted into a frequency distribution in order to analyse the

distribution of fibre size. The average number of muscle fibres and the average fibre size were also determined.

3.2.10 Statistical analysis

Quantitative data was analysed using SPSS statistics version 21. Data is expressed as Mean ± SEM. Muscle fibre number and size were analysed using Student's T Tests. Primary myotube percentage of myogenic nuclei and myotube area were analysed with one way ANOVAs. Significance was set at $P<0.05$.

3.3 Results

In view of the findings that suggest that muscle may be a primary site of pathology in SBMA (Cortes et al., 2014a), in this chapter I undertook an *in vivo* and *in vitro* analysis of the hind limb muscle of WT, AR20 and AR100 mice.

3.3.1 Longitudinal physiological assessment of muscle function in AR20 mice

The AR20 mouse contains a Yeast artificial chromosome (YAC) containing the Human androgen receptor, with 20 CAG repeats, a number considered non-pathogenic (Fratta et al., 2014b). However, as these mice are taken to be a control for AR100 mice, it was important to first establish whether the presence of a human AR transgene, albeit at non-pathogenic length, had deleterious effects on muscle function.

AR20 mice were examined at time points comparable to the investigation of AR100 physiology previously undertaken: 3 months (pre-symptomatic), 6 months (symptom onset in AR100 mice), 12 months (when AR100 mice are fully symptomatic) and 18 months (disease end stage in AR100 mice). *In vivo* muscle physiology of the TA and EDL muscles revealed that muscle force and contractile characteristics in AR20 mice were similar to those of WT mice (Figure 36 and Figure 37). AR20 mouse physiology data was compared to that previously obtained in the lab for WT and AR100 (A. Gray, PhD Thesis). As can be seen in Figure 36 and Figure 37 AR20 TA and EDL force and contractile characteristics are no different from WT. Twitch force, tetanic force, half relaxation time and time to peak force did not change significantly as the mice aged, and were not different from comparable data from WT. In addition, the number of functional motor units innervating the EDL muscle of AR20 mice was determined and the results compared to data from WT and AR100 mice. As shown in Figure 38, there was no loss of motor units in AR20 mice even at 18 months of age, and an average of 34 ± 2.6 (n=5 mice) motor units innervated which is not significantly different to WT mice. Furthermore, both body weight and muscle weight increased steadily with age in AR20 mice, in contrast to

the marked decline in weight observed in AR100 mice as they age (Figure 39). All further analysis prioritised the evaluation of age matched WT and AR100 mice.

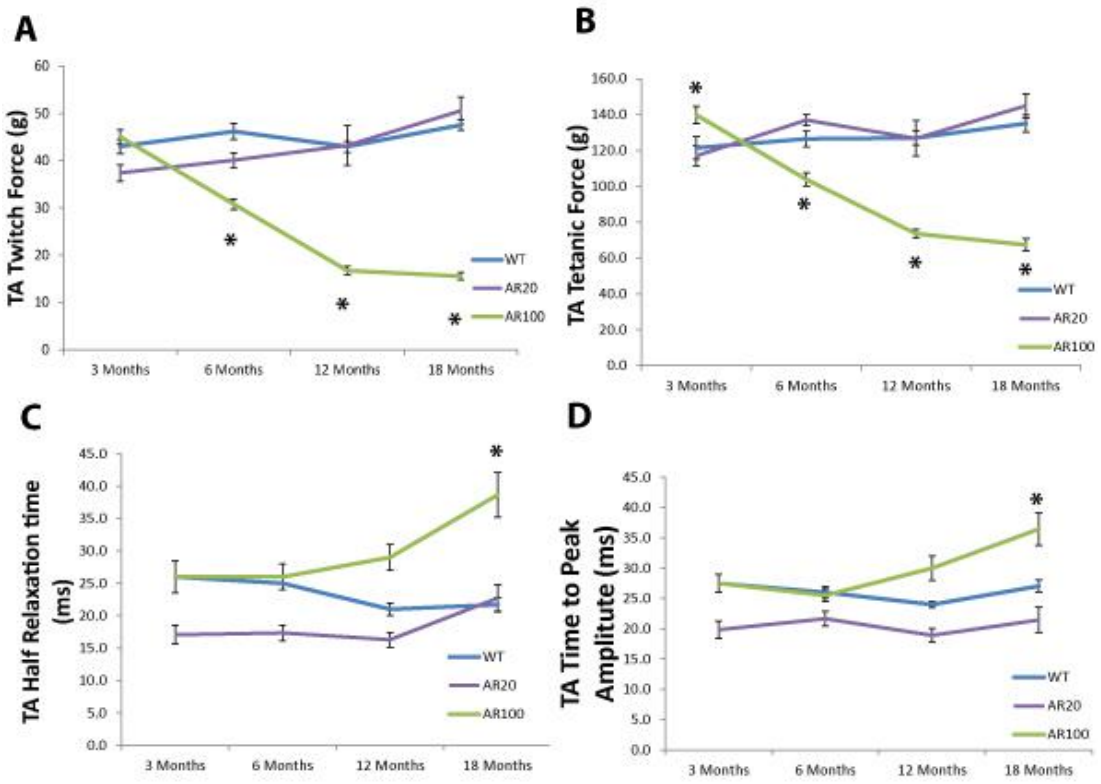

Figure 36 Longitudinal analysis of TA force and contractile characteristics in AR20 mice: comparison with WT and AR100 mice

AR20 mice do not develop a disease phenotype in the TA muscle as analysed by *in vivo* muscle physiology. **A**) Maximum twitch force, **B**) Tetanic force, **C**) half relaxation time and **D**) time to reach peak force did not significantly change between 3 and 18 months of age. n= minimum 5 animals per group. Error bars = SEM. WT and AR100 data was taken from A. Gray's PhD thesis for comparison. Significance asterisk ($P<0.05$) denotes differences between WT and AR100.

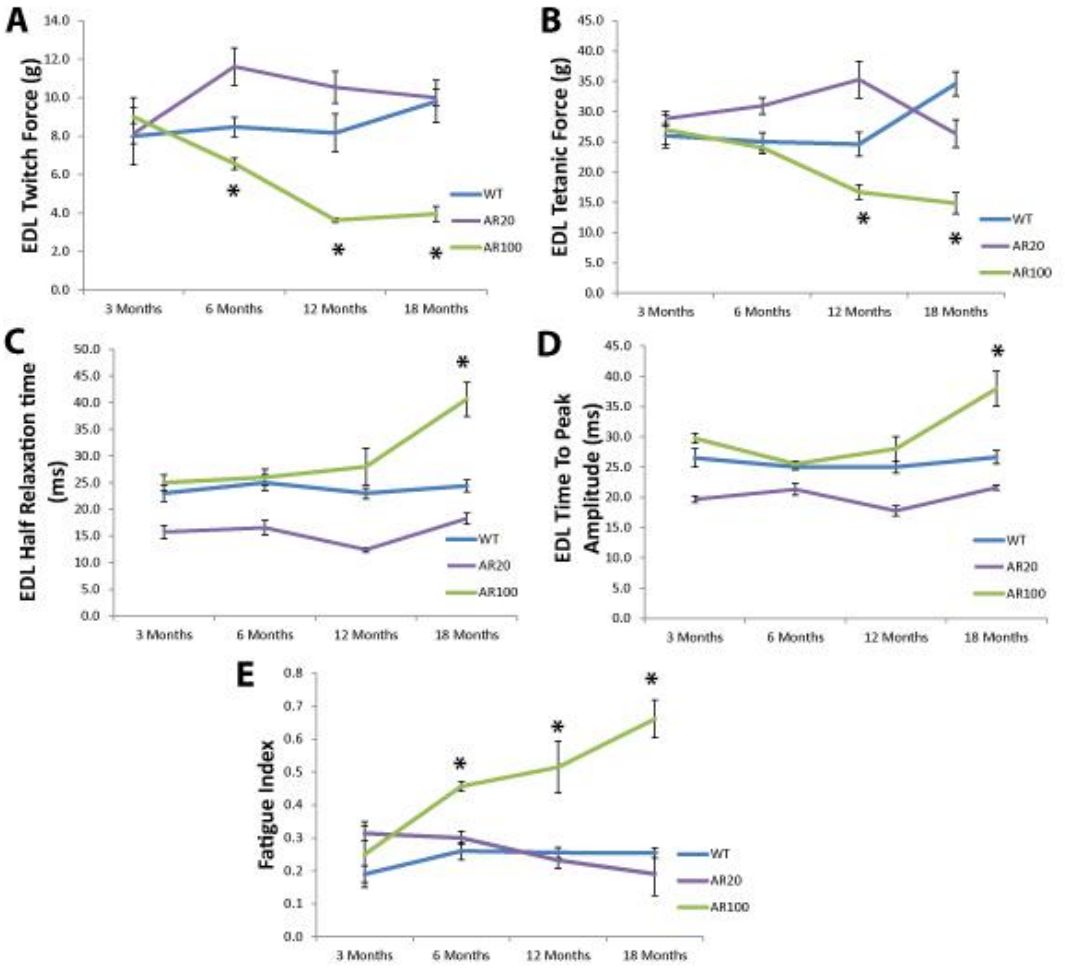

Figure 37 Longitudinal analysis of AR20 mouse EDL contractile characteristics

AR20 mice do not develop a disease phenotype in the EDL muscle as analysed by *in vivo* muscle physiology. **A**) Maximum twitch force, **B**) Tetanic force, **C**) half relaxation time, **D**) time to reach peak force and **E**) Fatigue Index did not significantly change between 3 and 18 months of age. n= minimum 5 animals per group. Error bars = SEM. WT and AR100 data was taken from A. Gray's PhD thesis for comparison. Significance asterisk ($P<0.05$) denotes differences between WT and AR100.

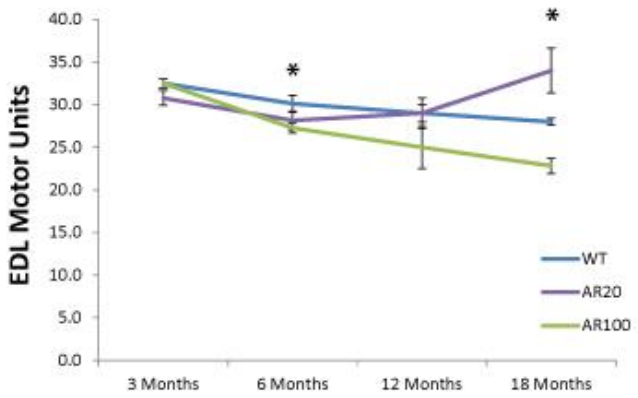

Figure 38 Longitudinal analysis of Motor Unit survival in EDL muscles of AR20 mice: comparison with WT and AR100 mice

Analysis of the number of motor units innervating the EDL muscle of AR20 showed that there was no significant decline in motor unit survival between 3 and 18 months of age, and no significant difference in motor unit survival in AR20 mice compared to WT mice at any age. In contrast there was a significant difference in motor unit survival at 6 and 18 months of age. N= minimum 5 per group. Error bars = SEM. WT and AR100 data was taken from A. Gray's PhD thesis for comparison. Significance asterisks ($P<0.05$) denote differences between WT and AR100.

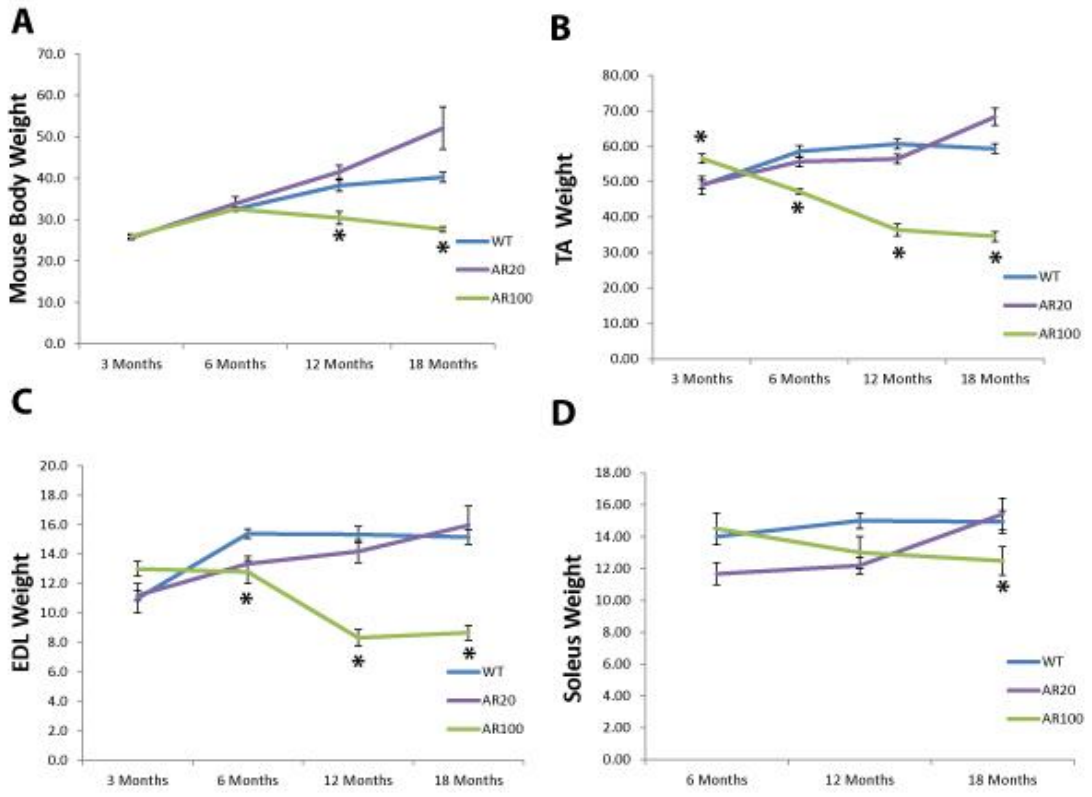

Figure 39 Longitudinal anlysis body and muscle weight in AR20 mice: comparison with WT and AR100 mice

A) Body weight **B**) TA **C**) EDL and **D**) Soleus muscle weights were recorded between 3 and 18 months of age in AR20 mice and the results compared to data from WT and AR100 mice. AR20 mice do not show a decline in body weight or muscle weight as they age, demonstrating that they do not show a degenerating neuromuscular phenotype. In contrast, there is a clear decrease in body and muscle weight in AR100 mice. n= minimum of 5 animals per group. Error bars = SEM. WT and AR100 data was taken from A. Gray's PhD thesis for comparison. Significance asterisks ($P<0.05$) denote differences between WT and AR100.

3.3.2 AR100 myotubes show no significant pathology *in vitro*

WT and AR100 primary muscle cultures were maintained for 7DiV in the absence or presence of 50nM DHT. Cultures were immuno-stained for Desmin and DAPI (Figure 40). Visually AR100 myotubes appeared thinner and slightly underdeveloped (Figure 40).However, using MetaXpress analysis the percentage of myogenic nuclei and the myofibre area was analysed in 4 independent cultures. There was no significant difference between WT and AR100 cultures in terms of percentage of myogenic nuclei (Figure 41), Furthermore, treatment with DHT had no significant effect on myotube number or area (Figure 41).

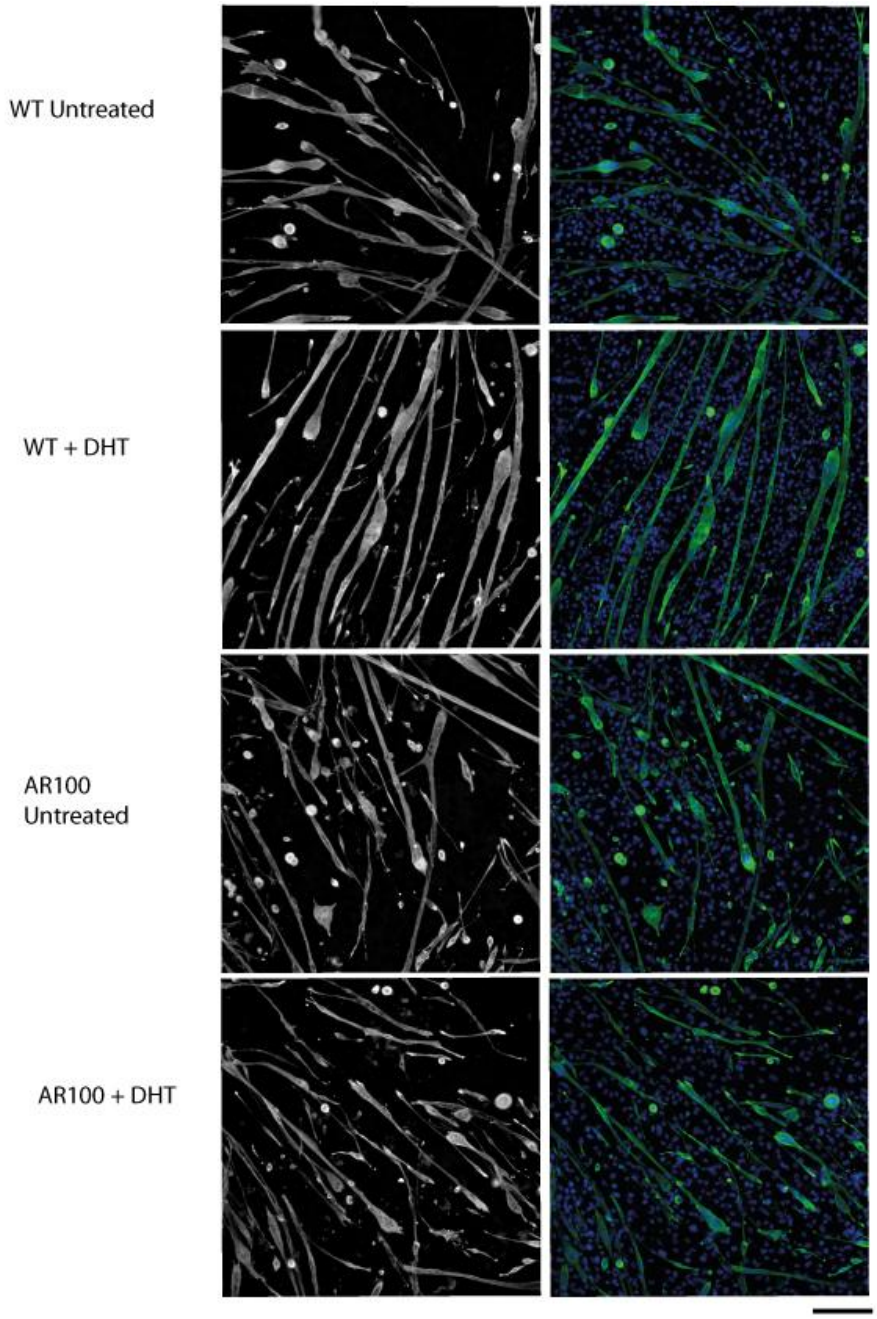

Figure 40 Primary myotube cultures from WT and AR100 mice

Primary satellite cells from WT and AR100 mice were maintained in culture for 7 DiV and differentiated into myotubes. Cultures were either left untreated or treated with 50nM DHT in the differentiating media from 3 DiV. Cultures were fixed and stained with the nuclear marker DAPI (Blue) and myotube filament marker Desmin (White, Green). AR100 cultures appeared thinner and slightly underdeveloped. Scale bar= 50μm

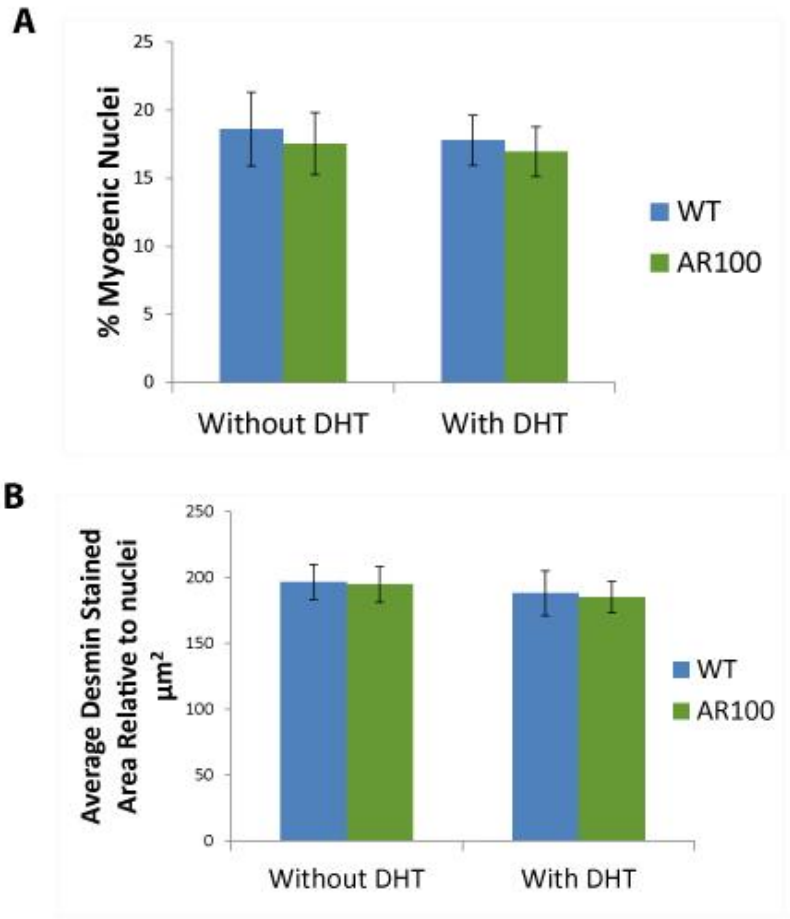

Figure 41 Percentage of myogenic nuclei and myotube area in AR100 cultures

WT and AR100 mouse primary myotubes maintained in culture for 7 DiV with or without the addition of 50nM DHT were fixed and stained with DAPI and the myotube filament marker Desmin. Using MetaXpress software **A**) the percentage of myogenic nuclei and **B**) the average area of Desmin staining were determined. There was no significant difference between WT and AR100 cultures. Treatment with DHT also had no significant effect. N= 4 independent experiments. Error bars= SEM

3.3.3 Histopathology

3.3.3.1 Muscle Fibre Size

Sections of TA muscle were stained for SDH and muscle fibre number and size determined in AR100 mice at 3, 6 and 18 months of age and the results compared to TA muscles from age- matched WT mice (n=3 muscles per age per genotype). Examples of SDH images can be found in Figure 44 -Figure 46.

The mean number of muscle fibres in TA muscles of AR100 mice compared to age matched WT control mice is shown in Figure 42. It can be seen that at 3 months of age, there was an average of 2817 (±23.4, n=3) fibres in WT TA muscles compared to 2661 (±60.1, n=3) in AR100 TA. Although there were fewer fibres in the AR100 TA, this did not reach significance (Student T test, P= 0.12). Similarly at 6 and 18 months of age, there was no significant difference in muscle fibre number in TA muscles of AR100 mice compared to WT. At 6 months a mean of 2782 (±134.0, n=3) WT fibres and 2690 (±190.3, n=3) AR100 fibres were found. At 18 months of age, a mean of 2547 (±234.1, n=3) WT fibres and 2132 (±190.3, n=3) AR100 fibres were found.

In addition, mean muscle fibre area as well as the distribution of fibre area was determined in TA muscles of AR100 and WT mice at 3, 6 and 18 months of age. As can be seen in Figure 43A, at 3 months of age there was slight increase in the mean fibre area in the TA of AR100 mice, from 2303.6 μm^2 (±107.8, n=3) in WT to 2669.0 μm^2 (±90.5, n=3) in AR100 mice. Although, this was not significant (Student T test, P=0.10). However, by 6 months of age, mean fibre area in the TA of AR100 mice (2052.4 μm^2 ± 215.5, n=3) was reduced compared to WT mice (2511.9 μm^2 ± 198.7, n=3, p=0.13), although this did not reach statistical significance. By 18 months of age, the mean fibre area in TA of AR100 (2166.4 μm^2 ± 69.8, n=3) was significantly less than age matched WT mice (3023.2 μm^2 ± 123.1, n=3, p=0.004).

Analysis of the distribution of fibre areas in TA muscle fibres of WT and AR100 mice (Figure 43B) revealed that as early as 3 months of age, there was a change in fibre size distribution, with a greater proportion of larger size fibres than in WT TA. This

pattern of fibre size distribution changed as the disease progressed, and by 18 months, there was a clear reduction in larger size fibres in AR100 TA, and an increase in the number of smaller fibres (See Figure 43B).

3.3.3.2 Oxidative Capacity- Succinate Dehydrogenase (SDH) staining

The oxidative capacity of muscle fibres in AR100 mice TA muscle was determined. Using the SDH staining method (Suvarna et al., 2013), muscle fibres with a high oxidative capacity, typically slow twitch muscle fibres stain intensely blue, whereas fast twitch, largely glycolytic muscle fibres, stain pale. This technique to some extent also identifies intermediate muscle fibres, as they stain with an intermediate intensity (See WT muscle sections in Figure 44). The distribution of fibres normally varies throughout the WT TA muscle, with highly oxidative fibres clustering within the centre of the muscle. However, in other models of neuromuscular disease such as ALS, there is a shift in the oxidative capacity of muscle fibres in fast twitch muscle, from primarily glycolytic to oxidative fibres.

As can be seen in the low power images of TA muscle from WT and AR100 mice in Figure 44, there was no obvious change in the pattern of SDH staining in AR100 TA muscle until late stage of disease. At 18 months the fibres in the outer region became more uniformly stained and stained darker for SDH, (See high power images in Figure 45). Figure 44 also illustrates the significant atrophy of AR100 TA muscles from 6 months of age that becomes significant at 18 months described above. The most obvious difference in SDH staining was seen at 18 months, where there were areas of apparent muscle fibre loss, identified by areas of negative staining in the AR100 TA (Figure 46).

3.3.3.3 Van Gieson Staining

To investigate whether the areas of negative SDH staining reflected a loss of fibres Van Gieson staining was carried out on WT and AR100 TA sections to determine if the 'empty' areas within the TA were in fact areas of connective tissue infiltration (Figure 47). At 3 months there was no obvious difference in the connective tissue in WT and AR100 TA muscle sections. By 6 and 18 months of age, Van Gieson staining

too showed areas of negative staining indicative of fibre loss within the TA muscle, rather than connective tissue that would stain red in this technique (Figure 47). Furthermore, the connective tissue within the AR100 muscle had a slightly disorganised appearance, most prominent at 6 months of age.

3.3.3.4 Haematoxylin & Eosin Staining

Haematoxylin & Eosin (H&E) staining was carried out on TA muscles from WT and AR100 mice in order to assess whether AR100 muscle exhibited myogenic or neurogenic changes. Evidence of myogenic muscle changes were observed at 12 months in AR100 TA muscle (Figure 48). Fibre splitting, lobulated fibres and clear fibre loss was present. In a very low number of muscle fibres, there was evidence of necrosis. Muscle atrophy as a result of neurogenic changes is usually inferred by the presence of angulated muscle fibres, which were not seen in these preparations. Surprisingly there was a lack of internalised nuclei in AR100 muscle at 12 months of age, characteristically seen in SBMA patient muscle (Figure 49). However, at 18 months internalised nuclei were observed more frequently (Figure 50).

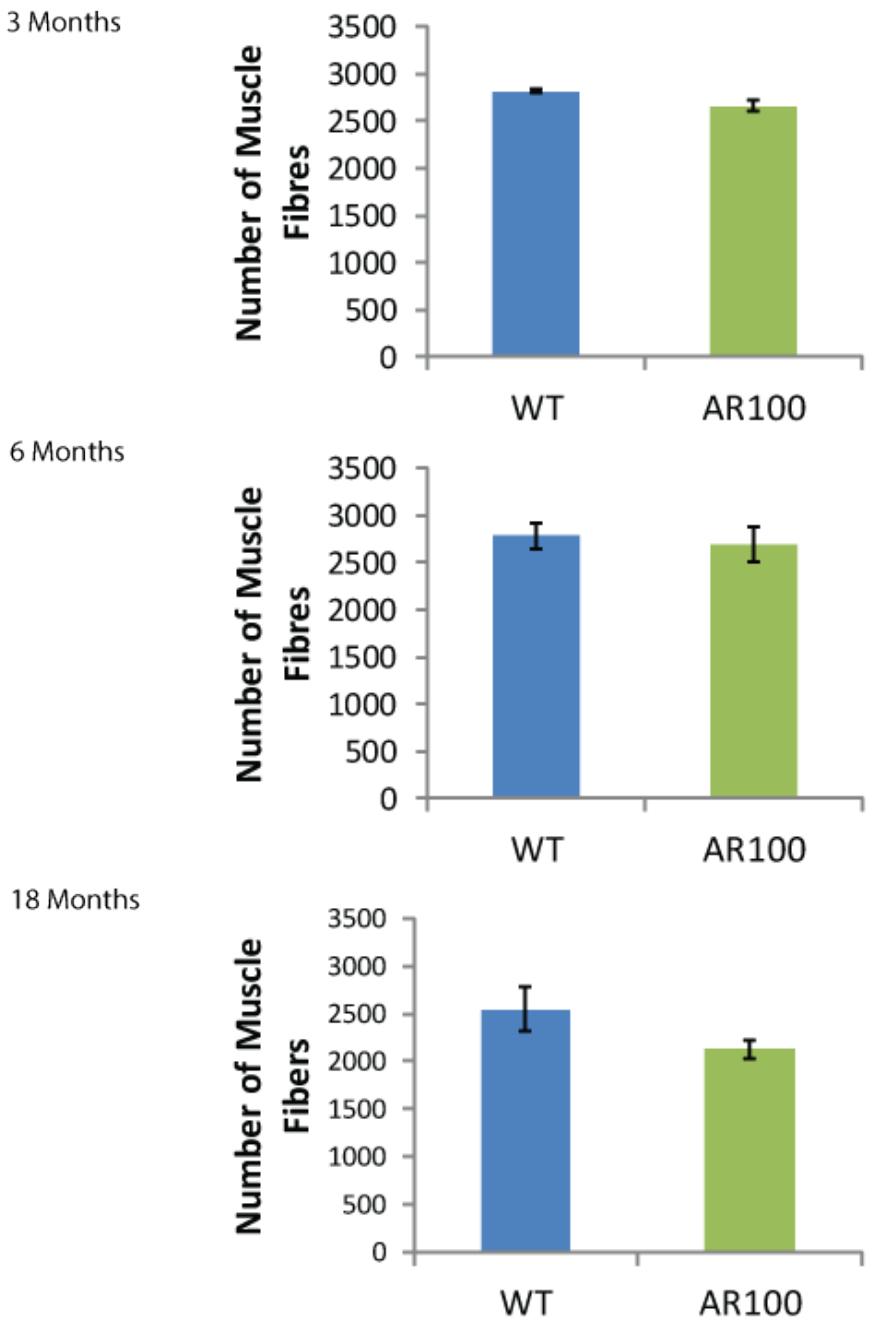

Figure 42 The number of muscle fibres in the TA of WT and AR100 mice

The numbers of WT and AR100 muscle fibres in the TA were counted in SDH stained images with the aid of image J. There was no significant difference in the number of muscle fibres within the AR100 TA muscle in comparison to WT at **A**) 3 months, **B**) 6 months, or **C**) 18 months of age (Student T-test $P<0.05$, $n=3$). Error bars= SEM.

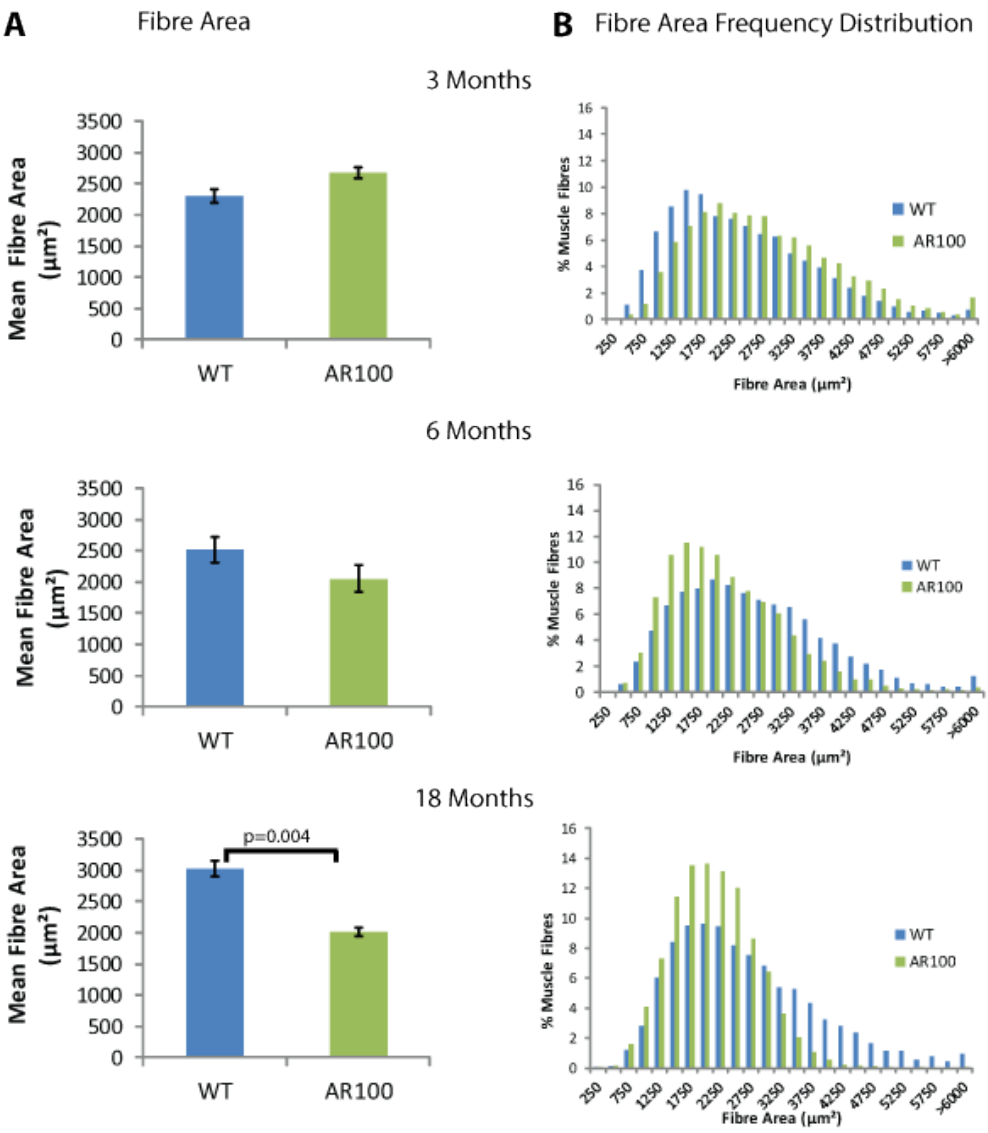

Figure 43 TA Muscle Fibre Area in WT and AR100 mice

The area of SDH stained muscle fibres within the TA of WT and AR100 mice were measured using Image J software. **A**) Mean muscle fibre area in AR100 mice was not significantly different to WT at 3 and 6 months of age. However, at 18 months of age there was significantly less muscle fibres in AR100 mouse TA (Student T test, P=0.004, n=3). The distribution of muscle fibre size was also analysed. **B**) At 3 months of age there was a trend of increased percentage of muscle fibres in the AR100 TA having a larger fibre area. At 6 months of age, AR100 muscle fibre distribution shows an increase in the percentage of intermediate size fibres and at 18 months of age there are a higher percentage of smaller muscle fibres.

Figure 44

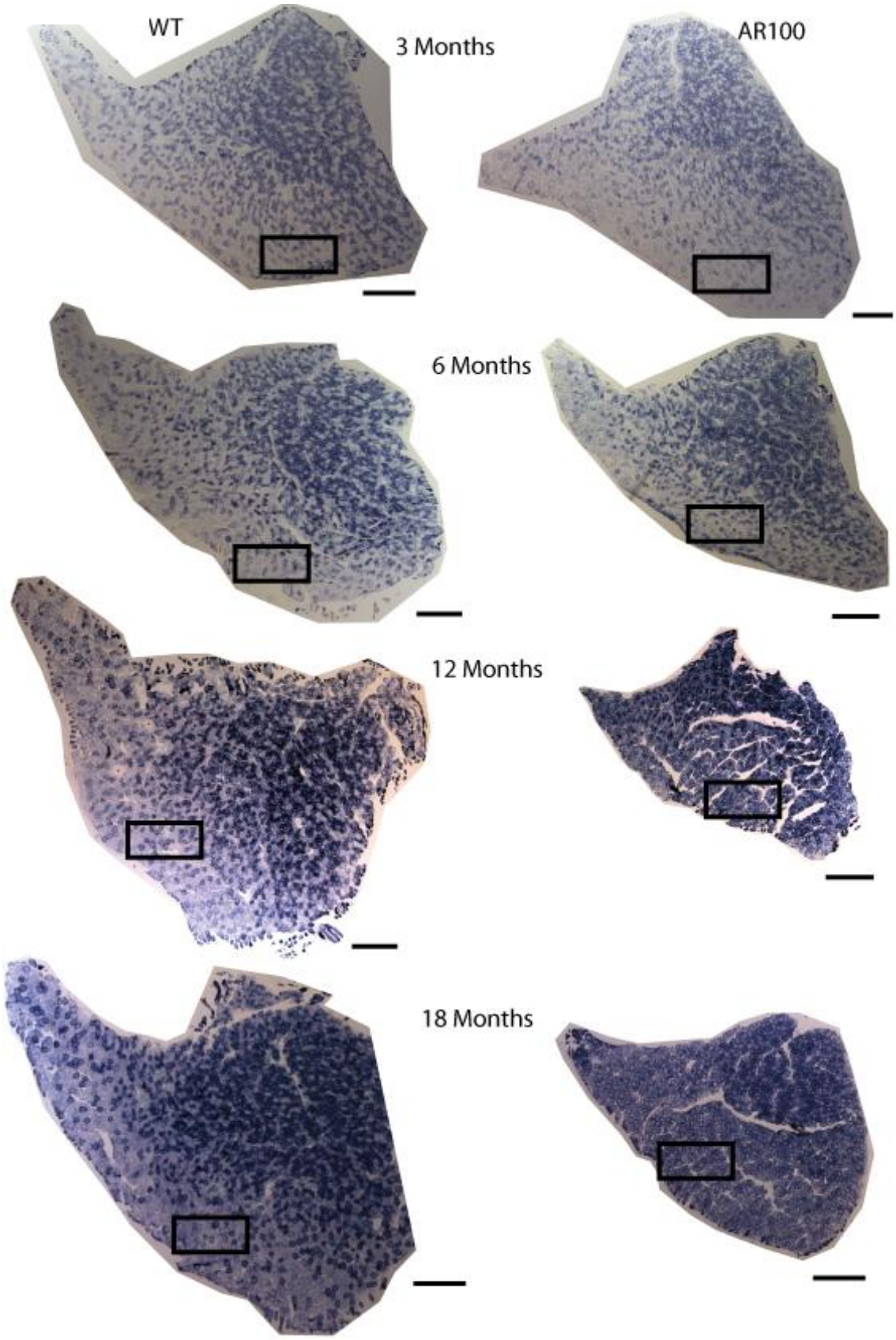

Figure 44 SDH staining of WT and AR100 TA muscle cross sections

SDH staining of WT and AR100 TA muscle at 3, 6, 12 and 18 months of age. Muscle fibres with a high oxidative capacity, typical of slow twitch muscle fibres, stain more intensely. No significant difference between WT and AR100 muscle oxidative capacity was detectable at 3 and 6 months. Slight muscle atrophy is evident from 6 Months. By 18 months there was an apparent decrease in pale stained fibres around the periphery of the muscle as well as clear muscle atrophy. Scale bars= 500µm.

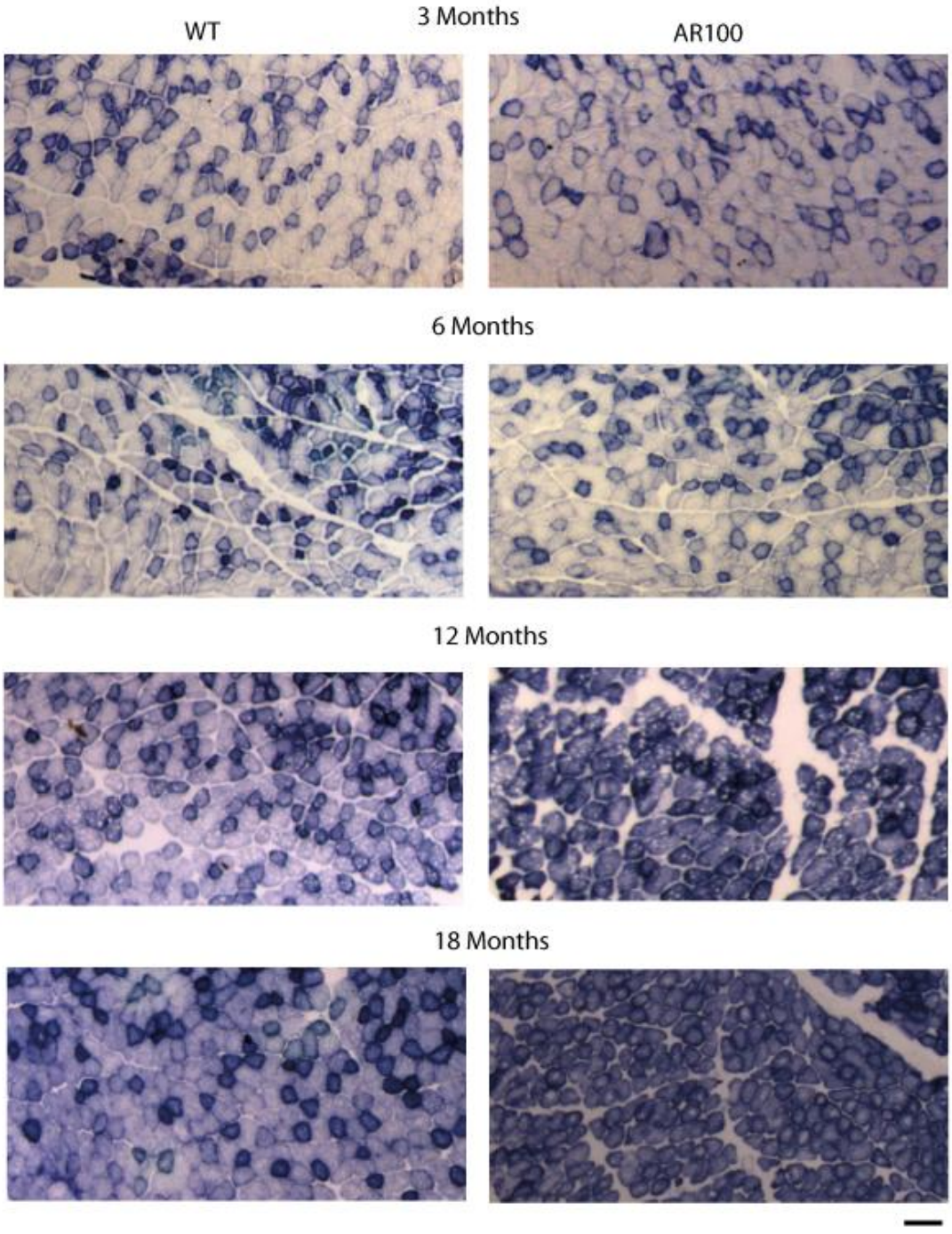

Figure 45 SDH Staining of WT and AR100 mice TA muscle: High power images

SDH staining of WT and AR100 TA muscle sectioned to 12.5 µm. High power images exemplify dark stained areas indicate fibres with a high oxidative capacity, typical of slow twitch fibres. At 18 months there is a reduced variation in the oxidative capacity of muscle fibres and more intense staining. Scale bars = 100µm.

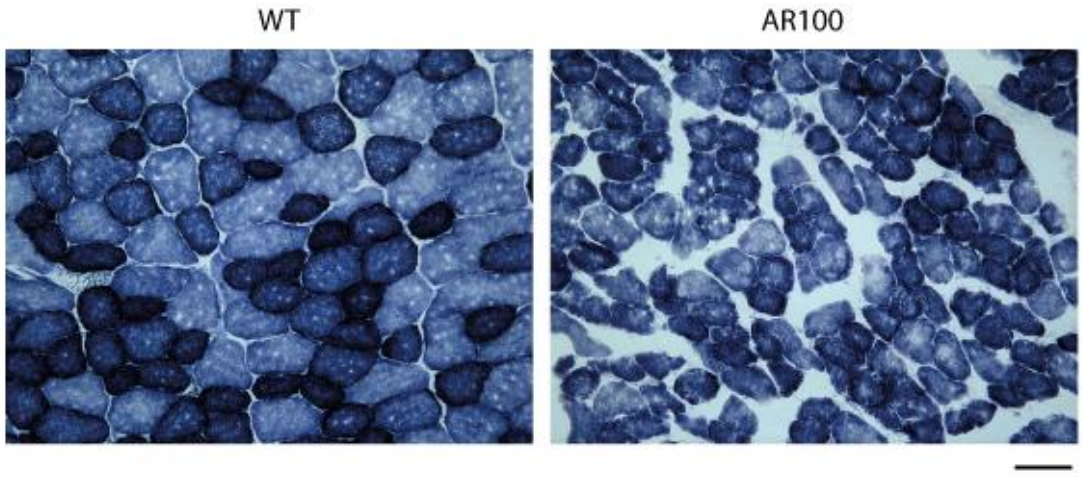

Figure 46 SDH Staining of 18 Month WT and AR100 mice TA Muscle

SDH staining of WT and AR100 TA muscle cryo-sectioned to 12.5 µm. Dark stained areas indicate fibres with a high oxidative capacity, typical of slow twitch fibres. AR100 muscle shows evidence of fibre loss (white 'empty' areas) and muscle atrophy. Scale bars = 50µm.

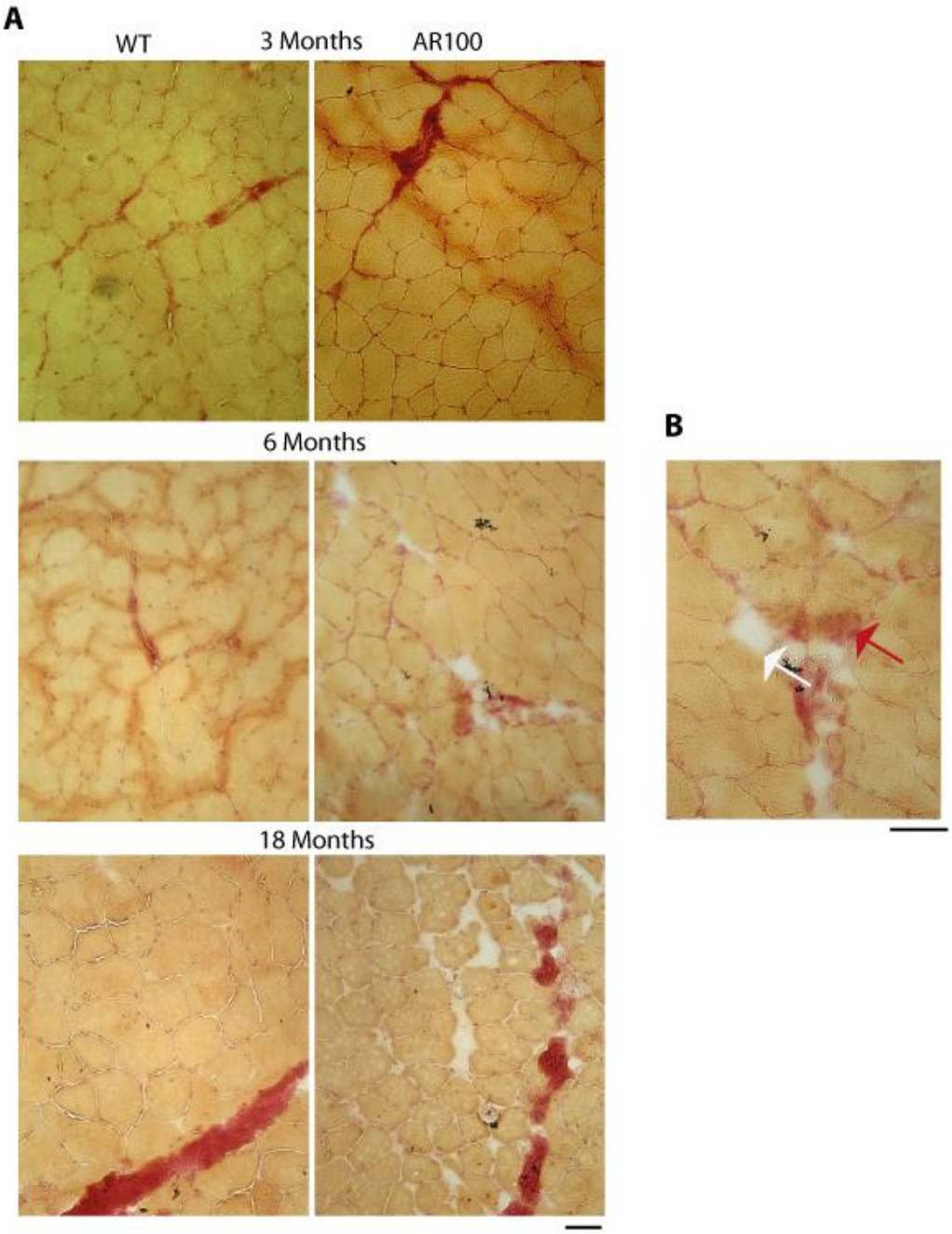

Figure 47 Van Gieson staining of WT and AR100 TA muscle

A) TA muscle 12.5 µm sections from WT and AR100 mice at 3, 6 and 18 Months of age were Van Gieson stained. No obvious infiltration of connective tissue was detected (red staining) at any age in WT or AR100 muscle. **B**) At 6 Months of age, connective tissue seemed dispersed between muscle fibres in the TA of AR100 muscle (Red arrow). White arrow shows possible sites of muscle fibre loss. Scale bars = 50 µm.

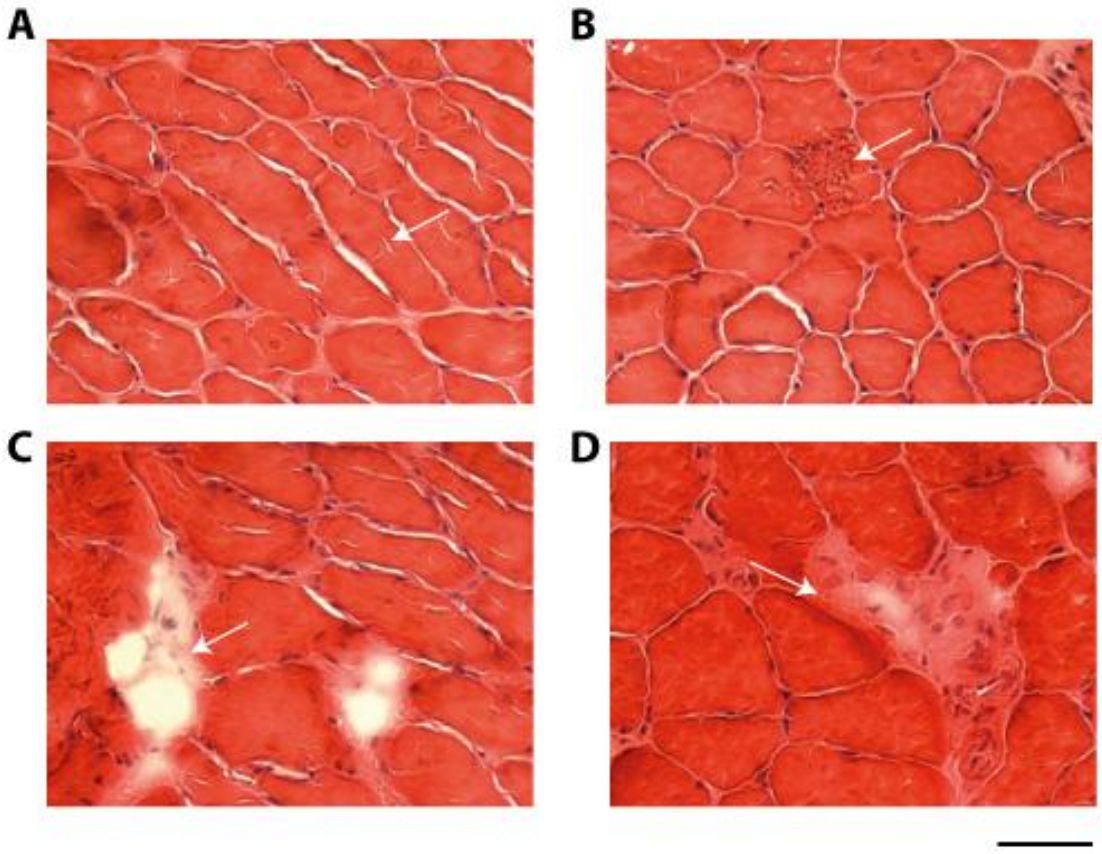

Figure 48 Characteristic H&E Staining of AR100 12 month mouse TA muscle

Haematoxylin and Eosin staining of 12 month AR100 TA muscle revealed characteristics of mostly myogenic changes of muscle fibre morphology. There is evidence of **A**) fibre splitting (arrow) and lobulated fibres characterised by the tubular appearance in cross section, **B**) features of necrosis (arrow) were also observed in a small number of muscle fibres, **C**) considerable fibre loss (arrow) was present as well as **D**) areas of inflammatory infiltration (arrow). Scale Bar= 50 µm.

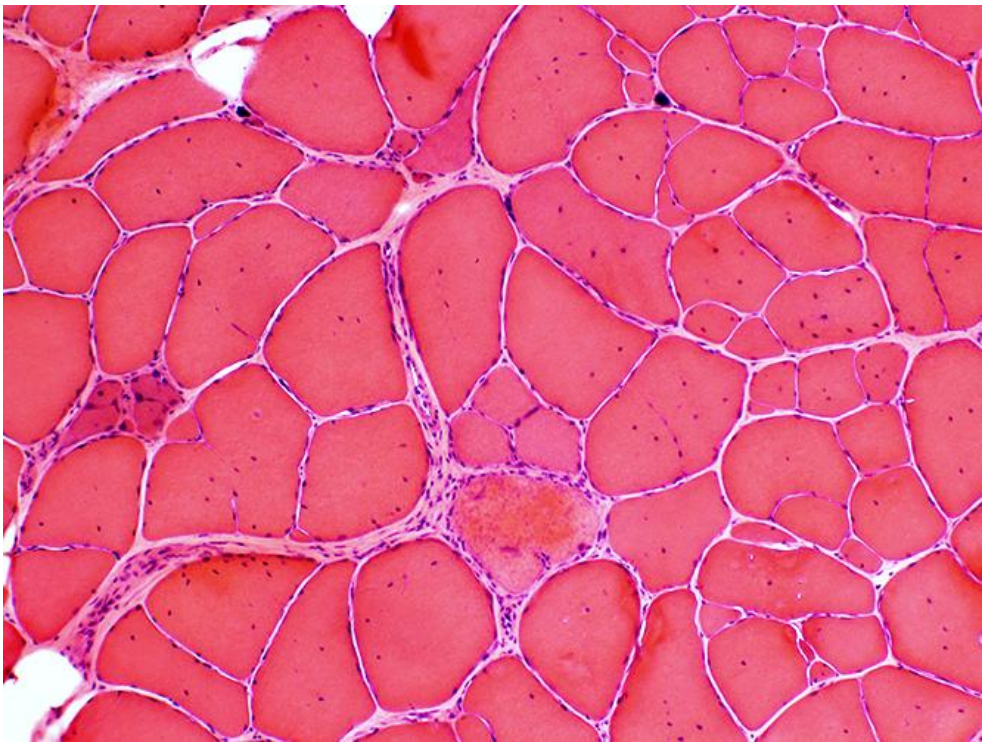

Figure 49 H &E staining of SBMA patient muscle

H&E staining of patient SBMA muscle. Affected muscle shows evidence of internalised nuclei, muscle atrophy, angular atrophic muscle fibres and scattered large fibres. This image exemplifies both neurogenic and myogenic features. Figure taken from Washington University Neuromuscular diseases website http://neuromuscular.wustl.edu/pathol/bsma.htm

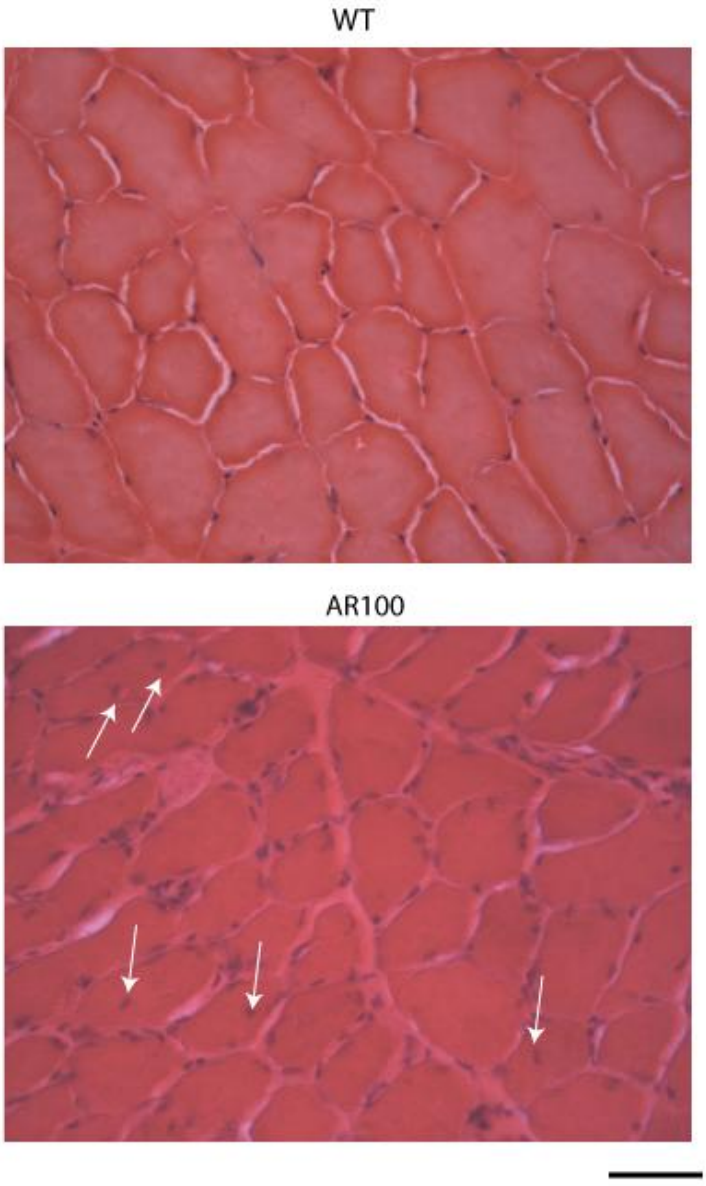

Figure 50 H&E Staining of 18 Month WT and AR100 TA muscle

WT and AR100 18 month mouse TA muscle. H&E staining shows more frequent internalised nuclei (arrows) in AR100 muscle at this stage but this is not present in all areas of the tissue. Scale bar= 50 µm

3.3.3.5 Androgen receptor positive inclusions are present in AR100 muscle

TA muscles of WT and AR100 mice were stained for the C-terminal portion of the AR. Nuclear inclusions were not detected in hind limb muscles at 3 or 6 months of age, but were present in AR100 muscle by 12 months of age (Figure 51). It should be noted that nuclear aggregates were not present in all 12 month muscle samples analysed. Additionally by 18 months, disease end stage, no inclusions were observed in TA muscle sections examined.

3.3.3.6 TDP-43 expression in AR100 muscles

WT and AR100 TA muscles were immuno- stained for TDP-43 (Figure 52 and Figure 53). TDP-43 is a nuclear protein, which has been found to translocate from the nucleus in a number of other neuromuscular disorders including Inclusion Body Myositis (IBM) and ALS (Machado et al., 2014, Arai, 2014). At 12 months of age, there was no apparent difference in the localisation of TDP-43 in WT and AR100 muscle fibres (Figure 52). However, by 18 months, disease end stage in the AR100 mouse, there was a clear increase in the number of muscle fibres in which TDP-43 was mis-localised to the cytoplasm (Figure 53).

3.3.3.7 IGF-1 expression in AR100 muscles

WT and AR100 TA muscle sections were immuno-stained for IGF-1. At 3 months, prior to symptom onset and 6 months, the start of detectable symptoms, no significant difference in IGF-1 expression was observed between genotypes (images not shown). However, by 12 months of age, WT muscle had a higher number of intensely stained IGF-1 positive muscle fibres than AR100 muscle sections, in which there was diffuse cytoplasmic staining (Figure 54). By 18 months, WT and AR100 TA were indistinguishable for IGF-1 immuno-reactivity.

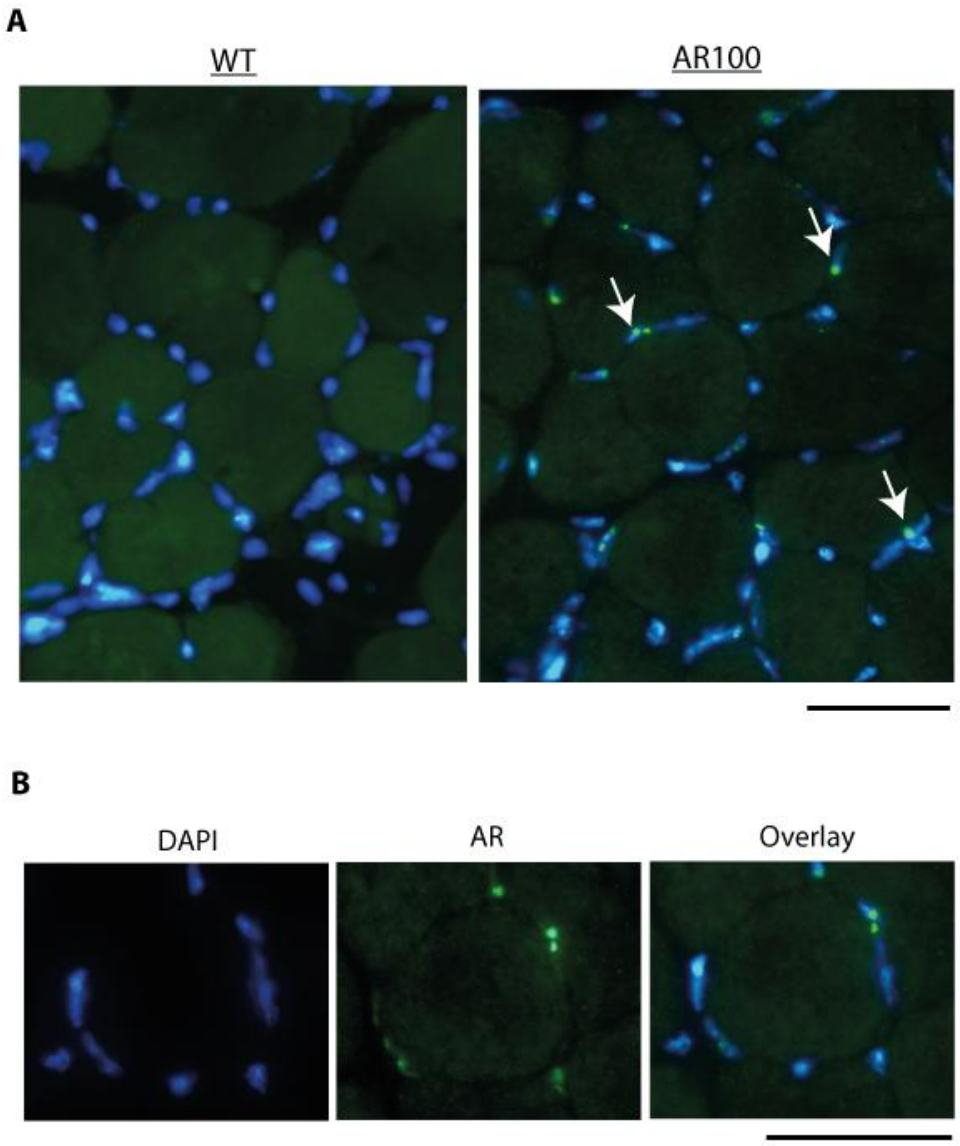

Figure 51 AR Protein aggregation in AR100 Muscle

A) Twelve month WT and AR100 mouse TA muscle sections were stained for the nuclear marker DAPI (Blue) and the androgen receptor C terminal (Green). White arrows indicate AR positive inclusions which appear to be present in nuclei. **B**) A single muscle fibre from a 12 month old AR100 mouse showing AR positive nuclear inclusions. Scale bars= 50 µm

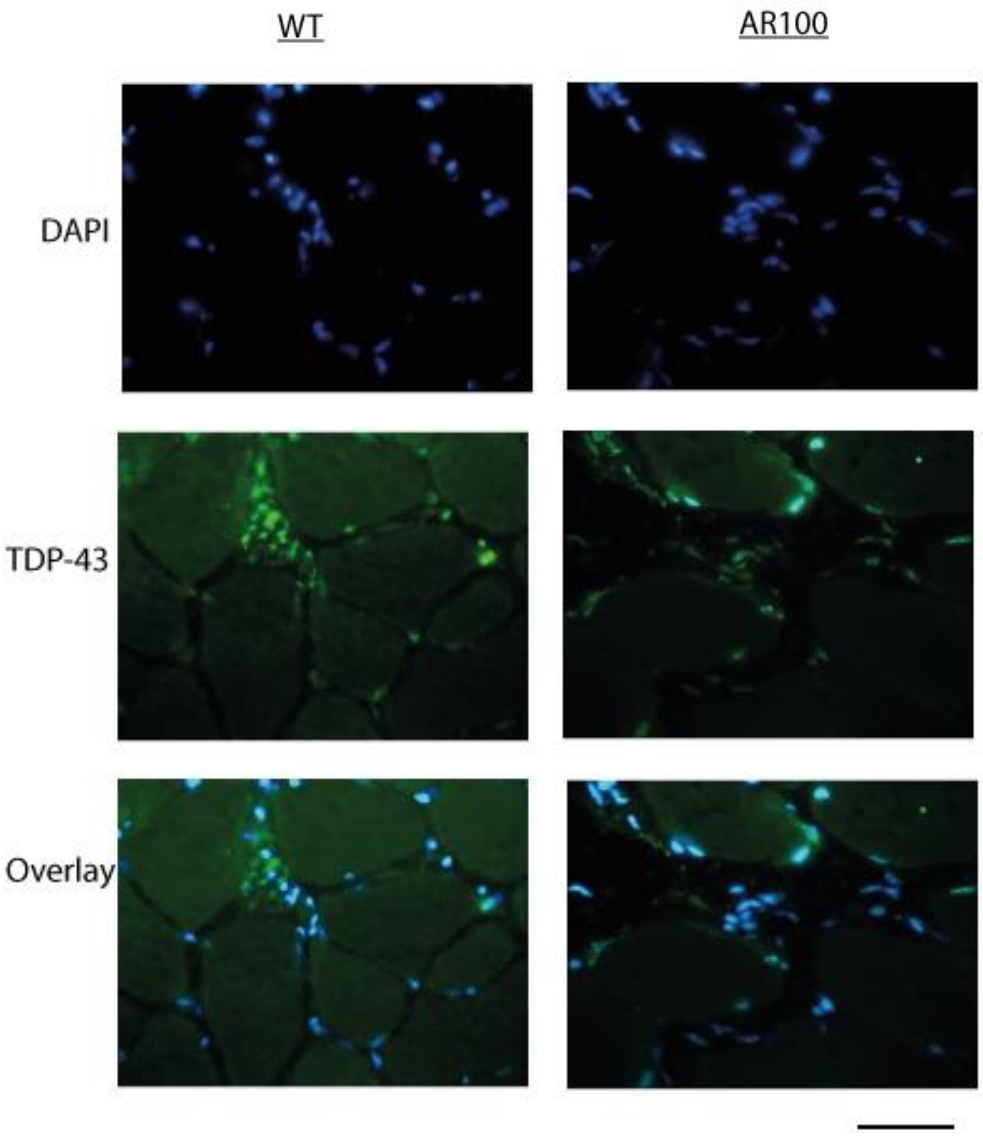

Figure 52 TDP-43 expression in WT and AR100 mouse TA muscle at 12 Months

TA muscles from 12 month old WT and AR100 mice were stained for the neuronal marker DAPI (Blue) and TDP-43 (Green). No difference was seen in the localisation of TDP-43 expression, which was largely nuclear in both WT and AR100 muscle. Scale bar= 50µm

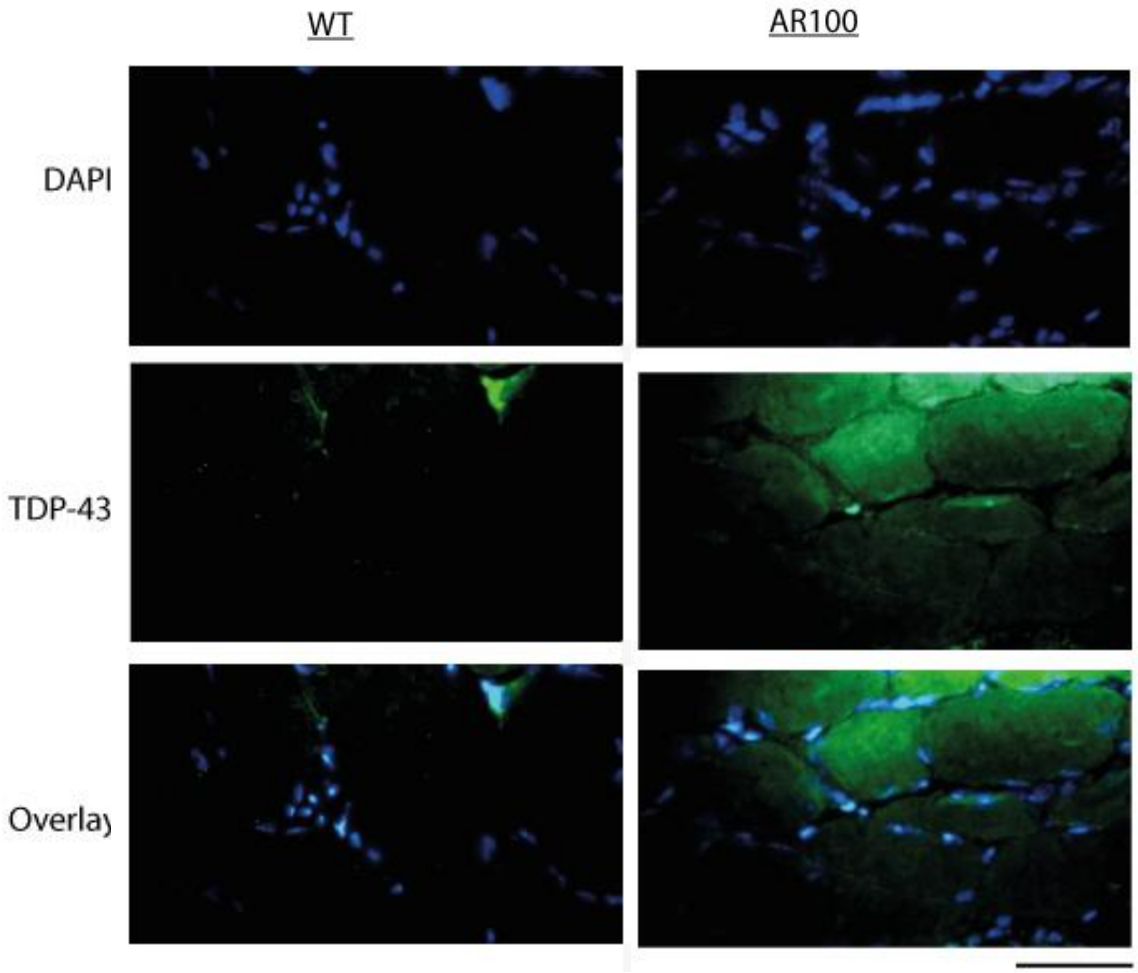

Figure 53 TDP-43 Expression in WT and AR100 TA muscle at 18 months

WT and AR100 TA muscles stained for nuclear marker DAPI (Blue) and TDP-43 (Green). AR100 muscle shows an increase in cytoplasmic mis-localisation of TDP-43. Scale bar =50µm

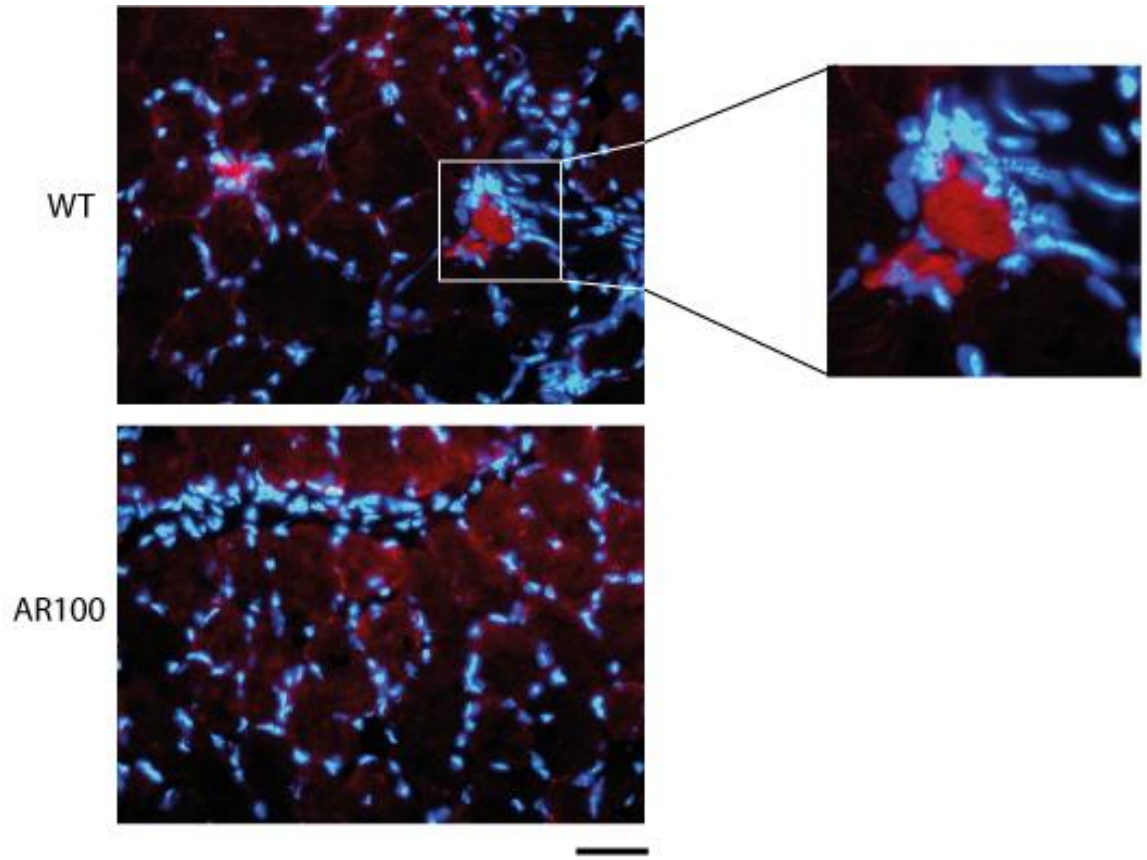

Figure 54 IGF-1 expression in TA muscles of WT and AR100 mice at 12 months

TA muscles of 12 month WT and AR100 mice were stained for Insulin-like Growth Factor one (IGF- 1; red), and the nuclear marker DAPI. IGF-1 positive fibres, typically smaller than surrounding muscle fibres were observed in WT TA muscles, but were absent in AR100 muscle. In AR100 muscle diffuse and less intense immunoreactivity was observed. Scale bar= 50 µm

3.3.4 Muscle denervation occurs late in disease in hind limb muscles of AR100 mice

3.3.4.1 EDL Muscle denervation in the AR100 mouse model

EDL muscles of WT, AR20 and AR100 mice were analysed for evidence of denervation, at different stages of disease progression. Longitudinal sections of EDL were stained with α-Bungarotoxin which labels the post synaptic acetyl choline receptor, and immuno-stained for choline acetyl transferase (ChAT) a marker of motor axons (Figure 55). The following analysis of innervation was undertaken: I) percentage of end plates fully innervated; II) percentage of end plates partially innervated; III) percentage of end plates completely denervated. Examples of each of these parameters are shown in Figure 55. At 3 months of age, there was no significant difference in any of these parameters (Figure 56). By 6 months of age however, there was an increase in the number of denervated fibres (Figure 57); so that in WT EDL 12.3 % (±2.9; n=5) were denervated, 11.0 % (±3.2; n=5) were denervated in AR20 mice, compared to 18.5 % (±4.2; n=7) in AR100 mice. Thus there were more fibres denervated in AR100 compared to AR20 mice at 6 months of age, although this failed to reach statistical significance (One-way ANOVA, p= 0.321). A high level of denervation was observed even in WT muscle, pehaps owing to the technique used to stain such complex structures.

3.3.4.2 Changes in Muscle Fibre Type in TA muscle of AR100 mice

TA muscles of WT and AR100 mice were stained for myosin heavy chain subtypes in order to determine the composition of muscle fibre types in the TA muscle at 6, 12 and 18 months of age. The TA is normally a fast twitch muscle, composed largely of fast twitch, type 2B fibres (See Figure 58A). In AR100 mice TA at 6 months of age, a slight increase in type 2A immunoreactivity was observed (Figure 58). In AR100 mice, by 12 months of age there was clear increase in the number of type 2A fibres and evidence grouping of type 2X fibres (Figure 59). These changes in muscle fibre type became more pronounced by 18 months of age (Figure 60). The clear increase in the number of type 2A fibres indicates that a change in the muscle phenotype has occurred, with an increase in the propagation of slow twitch. The appearance of 2X fibre grouping is synonymous with muscle denervation.

3.3.4.3 Changes in Nogo-A expression in AR100 TA muscle

The expression of Nogo-A, a marker of muscle denervation was assessed in the TA muscle of AR100 mice. At 3 and 6 months of age there was no difference between WT and AR100 muscle Nogo-A expression. By 12 months of age there was an increase in Nogo-A immunoreactivity in AR100 TA muscle which was maintained in the muscles of 18 month old mice (Figure 61).

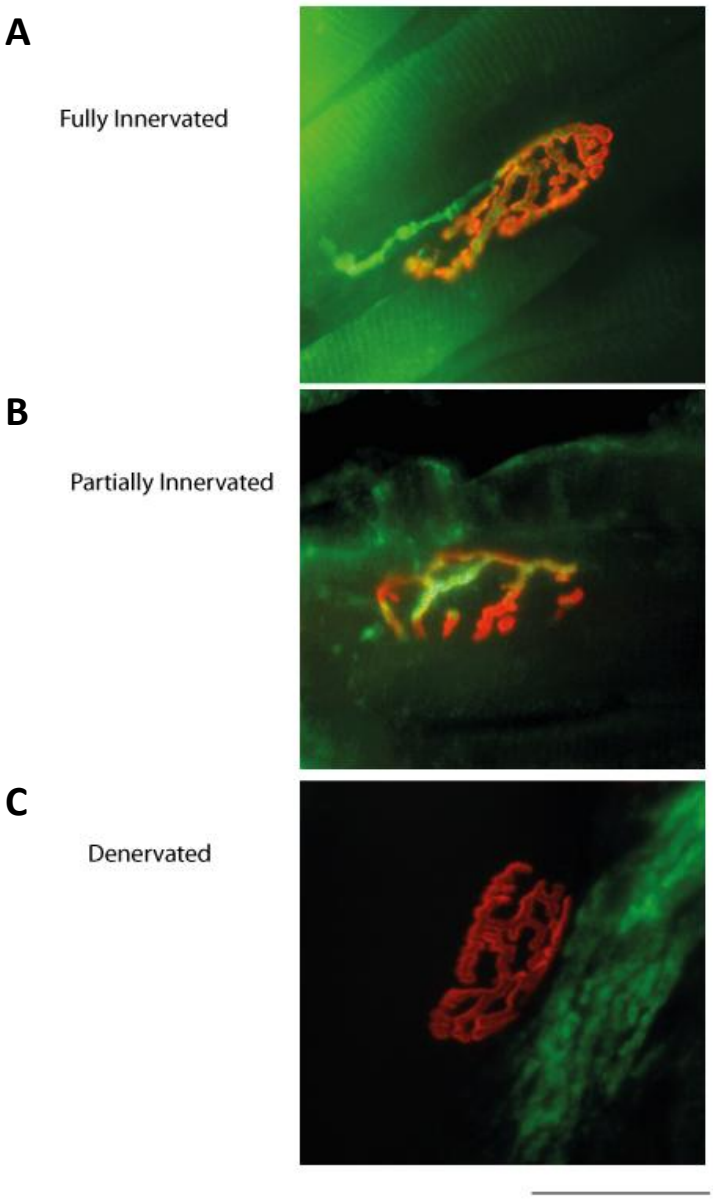

Figure 55 Example images of muscle denervation analysis of WT, AR20 and AR100 EDL muscle

Longitudinal WT EDL sections were stained with α-Bungarotoxin (red) and immuno-stained for the motor neurone marker ChAT (green). **A**) Shows an example of a fully innervated neuromuscular junction, where green and red staining overlay completely; **B**) shows a partially innervated NMJ with partial green and red overlap; and **C**) shows a denervated NMJ with α- Bungarotoxin positive end plates in the absence of ChAT staining. Scale bars= 50 µm

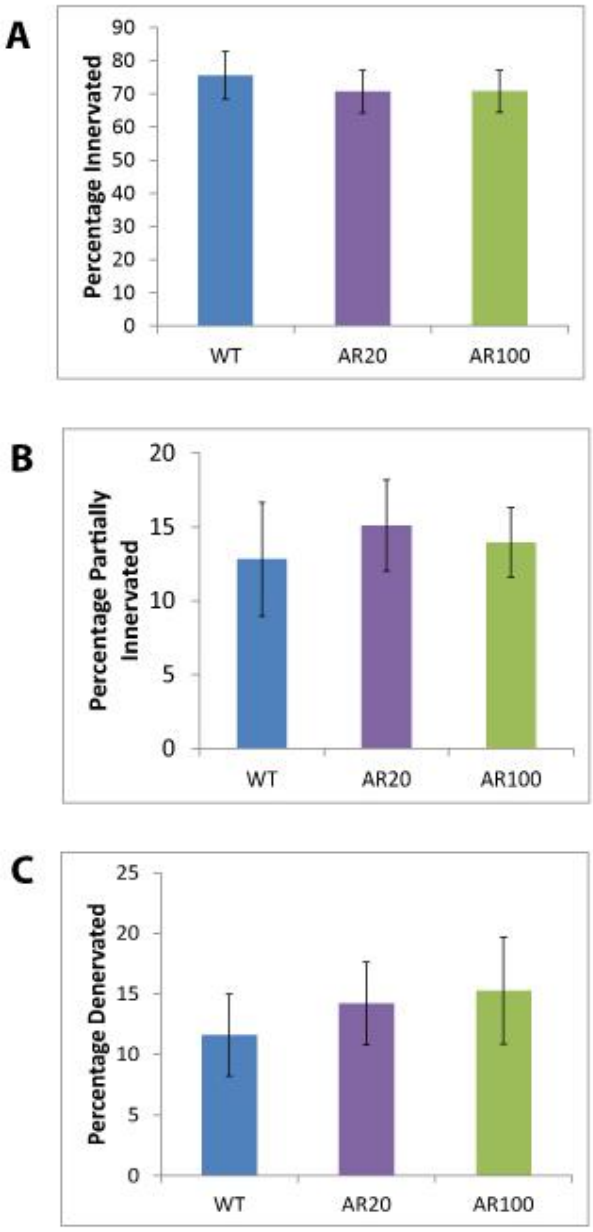

Figure 56 Innervation of EDL muscles of WT, AR20 and AR100 mice at 3 months

The numbers of **A**) fully innervated; **B**) partially innervated and; **C**) denervated end plates were counted in serial sections of EDL muscles. Data is presented as mean percentage ± SEM. Statistical analysis was performed using One Way Analysis of Variance, n=6 per genotype. No significant differences were seen.

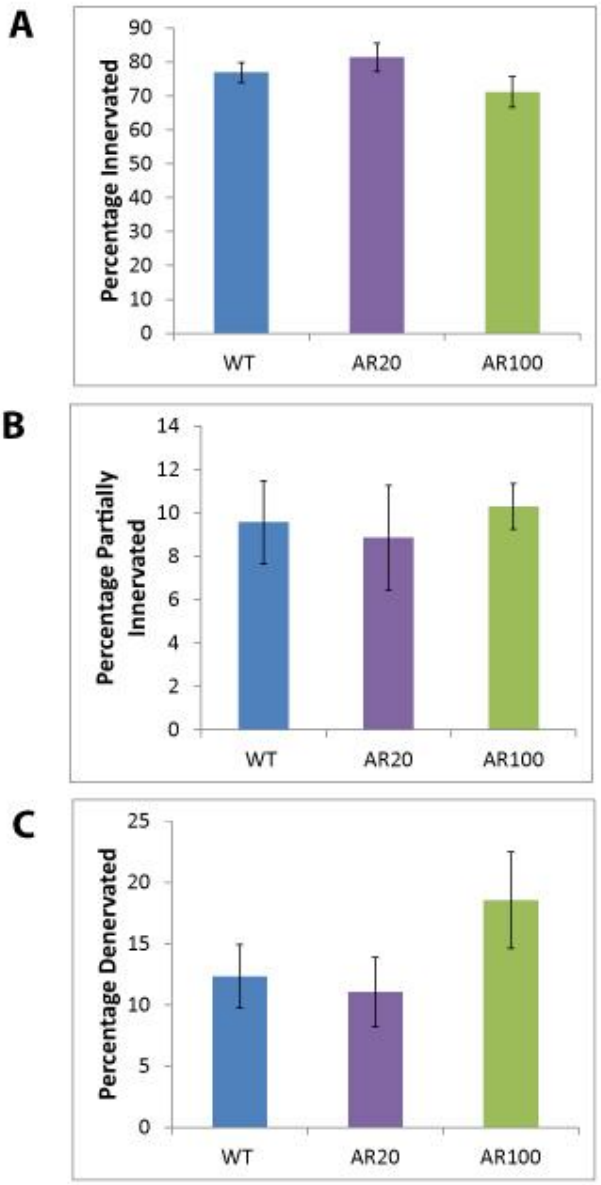

Figure 57 Innervation of EDL muscles of WT, AR20 and AR100 mice at 6 months.

The numbers of **A**) fully innervated; **B**) partially innervated and; **C**) denervated end plates were counted in serial sections of EDL muscles of each genotype. Data is presented as mean percentage ± SEM. Statistical analysis was performed using One Way Analysis of Variance, n=6 per genotype. No significant differences were seen.

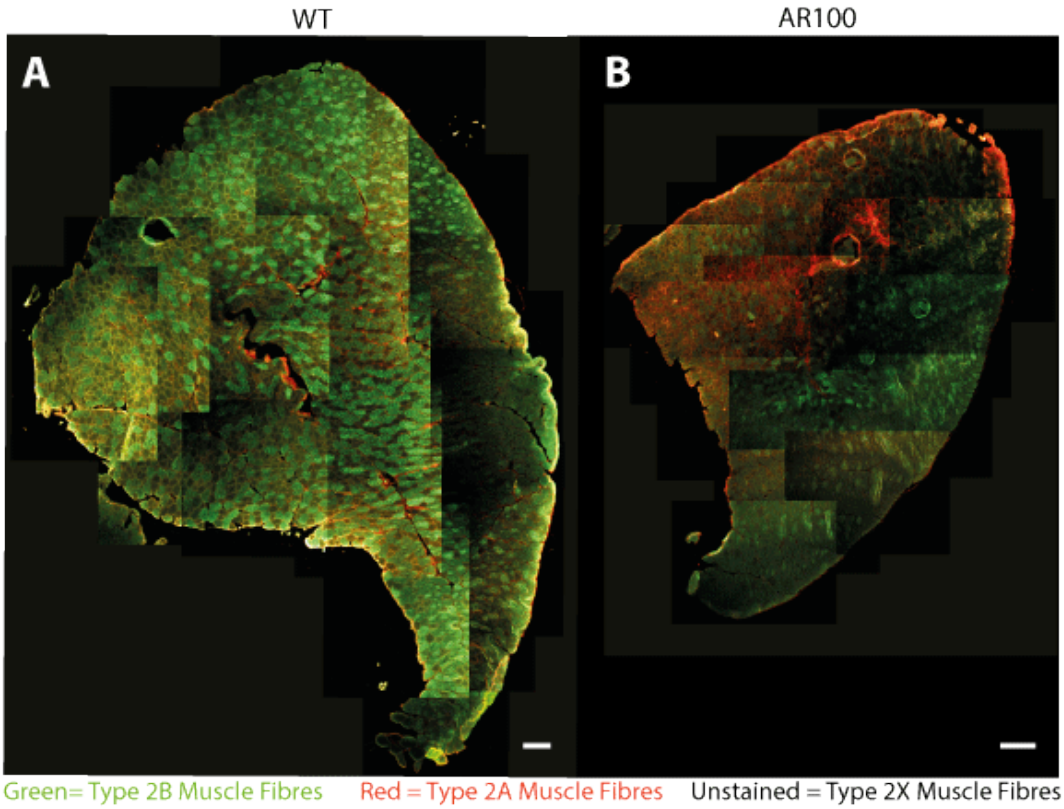

Figure 58 Muscle fibre type analysis of WT and AR100 TA muscle at 6 Months

TA muscles were stained for Myosin heavy chain subclasses to identify the composition of muscle fibre types at 6 months. **A)** WT TA muscle is mainly composed of type 2B muscle fibres (Green). In contrast, **B)** TA muscles of AR100 mice showed increased immunoreactivity for type 2A antibodies (Red), suggesting a switch in fibre type. Type 2X fibres remain unstained (Black). Scale bars =100µm.

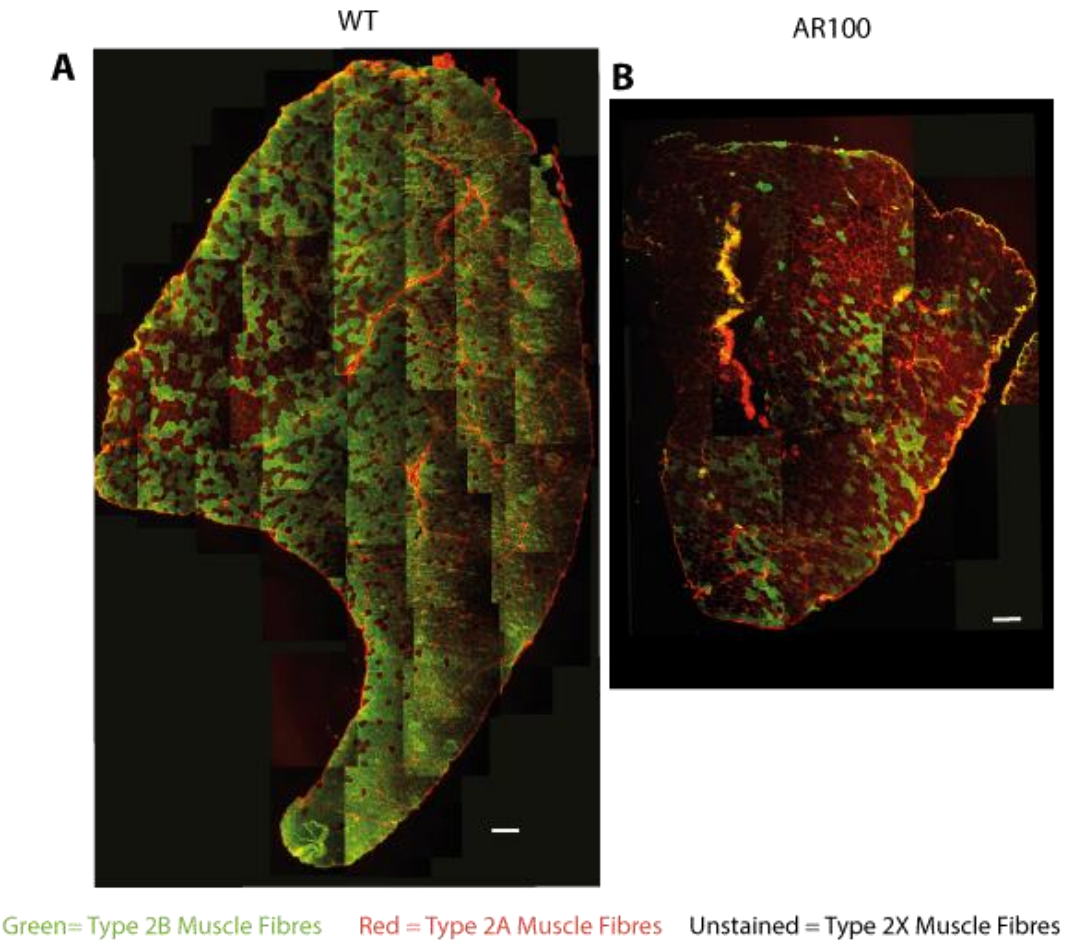

Figure 59 Muscle fibre type analysis of WT and AR100 TA muscle at 12 Months.

TA muscles stained for Myosin heavy chain subclasses to identify muscle fibre type composition at 12 months. **A)** WT muscles are mainly composed of Type 2B muscle fibres (Green). In contrast, TA muscles of AR100 mice are largely composed of Type 2A fibres (Red). Type 2X fibres are unstained (Black). Scale bars =100µm.

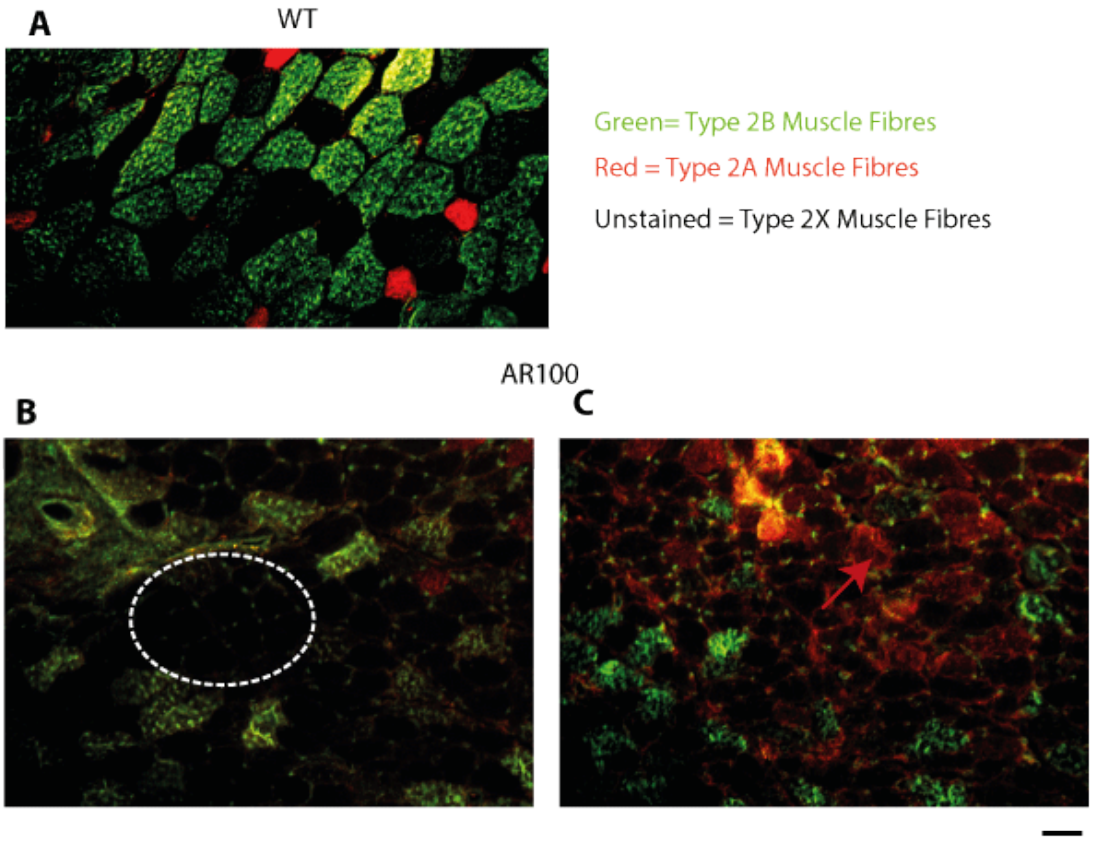

Figure 60 Muscle Fibre typing of WT and AR100 TA at 18 months of age.

TA muscles were stained for Myosin heavy chain subclasses to identify muscle fibre type composition in at 18 months. **A)** In WT TA muscles the majority of fibres were Type 2B (Green), although a small proportion of Type 2A fibres (Red), and Type 2X fibres Black; unstained) were also present. **B)** In AR100 TA muscle evidence of grouping of type 2X fibres (white circle) was observed yet, in **C)** the majority of fibres were type 2A (Red arrow). Scale bar = 50µm.

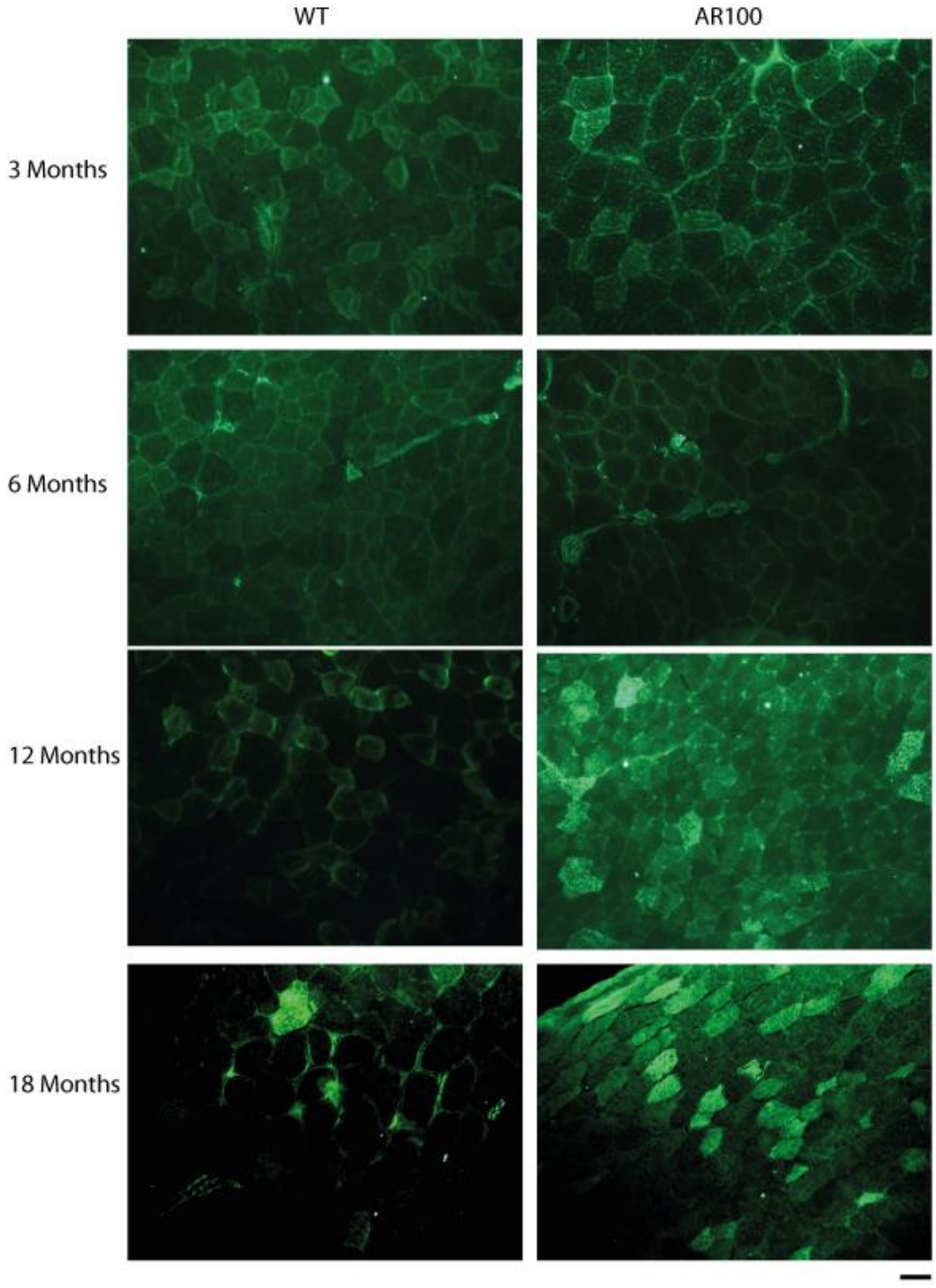

Figure 61 Nogo-A staining in the TA muscle

Sections of WT and AR100 TA muscle from 3, 6 , 12 and 18 month old mice were immuno-stained for Nogo-A. In AR100 muscle there was a clear increase in the intensity of staining and the proportion of individual muscle fibres positive for Nogo- A by 12 months. Scale bar= 50 µm

3.4 Discussion

In this Chapter I undertook a detailed histopathological analysis of hind limb muscle of AR100 mice at various stages of disease progression. In addition I confirmed that AR20 mice which carry a non-pathological 20 CAG repeats showed no sign of muscle pathology.

3.4.1 AR20 Longitudinal muscle physiology shows no sign of degeneration

Longitudinal analysis of AR20 mice showed that AR20 control mice do not show a degenerative phenotype, as assessed by *in vivo* physiology experiments (Figure 36 to Figure 38). Furthermore, there was no decline in muscle or body weight between 3 and 18 months of age (Figure 39). These findings indicate that the degenerative phenotype observed in the AR100 mouse model (Malik et al., 2013, Sopher et al., 2004) is the result of a pathogenic repeat length i.e. 100 CAG repeats rather than the presence of the yeast artificial chromosome.

3.4.2 Analysis of WT and AR100 muscle

Muscle has been suggested to be a primary site of pathology in SBMA (Rinaldi et al., 2014, Cortes et al., 2014a) and treatment targeted at the muscle has been shown to be sufficient to reverse symptoms in several mouse models of SBMA (Lieberman et al., 2014). Indeed, the question of whether SBMA is a Motor Neuron Disease or a muscle disease is by no means a new one (Jordan and Lieberman, 2008). Muscle biopsies from SBMA patients show a variable pathological picture, due to age of onset, repeat length and time of diagnosis (Soraru et al., 2008), preventing a definitive conclusion of whether the pathology is myogenic or neurogenic. However, data from our lab in which muscle physiology experiments were undertaken in AR100 mice at different stages of disease, suggest that muscle deficits manifest long before any indication of MN degeneration (A. Gray, PhD Thesis 2015).

3.4.2.1 Primary Myotubes from AR100 mice show signs of atrophy

Examination of SBMA muscle during the early stages of development in AR100 mouse myotubes showed that there was a clear difference in the morphology of these cultures, with AR100 myotubes appearing thinner and less developed than WT myotubes (Figure 40). However, attempts to quantify this difference using MetaXpress proved difficult, most likely because the software was unable to recognise multinucleate cells (Figure 41).

3.4.2.2 Muscular atrophy is present in the AR100 mouse model from 6 months of age

Results show that there was no significant difference in the number of muscle fibres in the TA of WT and AR100 mice until 18 months of age where the was a trend less fibres, indicative of fibre loss (Figure 42). Analysis of the TA muscle of WT and AR100 muscle revealed that there was a shift in the distribution of muscle fibre size from 3 months of age, a pre-symptomatic stage of disease in the AR100 mouse model (Figure 43). Surprisingly, there was an increase in the percentage of muscle fibres with a larger area in 3 month AR100 mouse muscle. This suggests an early compensatory hypertrophy, which is characteristic of myopathies (Machado et al., 2014). By 6 months, there was a shift in muscle fibre size reflecting fibre atrophy in the AR100 mouse model. This decline in fibre size coincides with the first time where a loss in hind limb force can be detected (A. Gray, PhD Thesis 2015). By 18 months, there was significant fibre atrophy in AR100 TA muscles, shown by a significant reduction in average fibre size as well as a shift in the frequency distribution of muscle fibres (Figure 43).

3.4.2.3 Histopathological analysis of AR100 muscle suggests muscle deficits contribute to SBMA

Succinate Dehydrogenase (SDH) staining of TA muscles showed that there was a clear change in the composition of high and low oxidative capacity fibres in AR100 mice. There was a decrease in the variation of staining intensity, with AR100 TA muscles staining darker and more uniformly by 18 months of age compared to WT TA muscle, (Figure 44 and Figure 45) suggesting a shift in oxidative capacity to a

more oxidative phenotype than normal although there was some variability between mice. In patients SDH or NADH analysis shows an increase in oxidative capacity in typically fast twitch muscles (Soraru et al., 2008).

A clear shift in the oxidative capacity of fast twitch muscle fibres such as the TA has been reported in a number of neuromuscular diseases (Simon et al., 2014, Bryson et al., 2012, Machado et al., 2014, Atkin et al., 2005). However, different animal models of SBMA show different changes in the oxidative capacity of muscles with disease progression. One model of SBMA over expressing WT AR exclusively in muscle, has shown that the slow twitch muscle, the soleus, degenerates rather than fast twitch muscles like the TA and the EDL (Oki et al., 2013, Oki et al., 2015). Thus authors observed a decrease in oxidative capacity in the soleus muscle a normally oxidative muscle. However, this model may not be an accurate model of SBMA since it is the WT AR that is over expressed and this expression is restricted to muscle alone- clearly controversial for a disease considered to be a MN disorder. Additionally, the WT AR over expressor model of SBMA, shows an increase in oxidative capacity, determined by increased NADH staining, in the EDL muscle (Monks et al., 2007). Other groups have found that as a result of transient expression of polyQ AR in both EDL and soleus muscle fibres, a decrease in oxidative capacity occurs (Ramzan et al., 2015). This led authors to suggest that in models of SBMA, like the AR100 model, perhaps a brief and transient compensatory shift to becoming less oxidative may be an early feature of SBMA (Ramzan et al., 2015). However, the longitudinal analysis of oxidative capacity presented in this Chapter has shown that at 3 months, pre-symptomatic in this mouse model no obvious differences in oxidative capacity were observed.

In the AR100 mouse model by 18 months, clear muscle atrophy was present as well as apparent ‘gaps’ in the muscle tissue (Figure 46). Van Gieson staining was carried out to inspect the connective tissue within the muscles, as there have been multiple transcriptomic studies that have identified the connective tissue as a site of pathogenesis (Mo et al., 2010, Halievski et al., 2015b). Van Gieson staining revealed that the apparent ‘gaps’ were not due to an infiltration of connective tissue but was

more likely to be fibre loss. The connective tissue did however take a more disorganised appearance in AR100 muscle early in disease (Figure 47).

H&E analysis of 12 month TA muscle revealed characteristics of myogenic muscle degeneration, such as lobulated fibres (Figure 48). Most marked was the apparent absence of internalised nuclei at this stage. As presented in Figure 49, human SBMA muscle shows a high proportion of internalised nuclei. In a normal muscle, around 3% of muscle fibres will have internalised nuclei (Dubowitz, 1985), but in diseased muscle, the fraction of muscle fibres with internalised nuclei can increase to up to 95%, depending on the specific disease (Vladutiu and Idiculla, 1997). Although the percentage of fibres with internalised nuclei in the TA of AR100 mice was not quantified, it is clear from Figure 48 that there is an absence, it is not until disease end stage, 18 months, that this feature is seen (Figure 50). A longitudinal quantification of the percentage of internalised nuclei within SBMA muscle would allow the analysis of whether there is a reduced regenerative capacity in SBMA muscle.

3.4.2.4 Androgen Receptor Inclusions are Present in 12 Month Muscle

The mutant AR aggregates within the nucleus in SBMA and this has long been considered a pathogenic cause of pathology. In a small number of AR100 muscle fibres there were AR positive inclusions present within the nucleus, although this was not seen in all muscle sections analysed (Figure 51). This could either be due to fibre loss, meaning the muscle fibres that had nuclear aggregation were no longer present, particularly as no inclusions were identified in 18 month muscle. Alternatively, it is possible that the lack of inclusions is actually a positive feature as there is controversy over whether inclusion formation is pathogenic or compensatory as inclusions have been detected in unaffected tissues of SBMA patients (Adachi et al., 2005).

3.4.2.5 TDP-43 Pathology in the AR100 Mouse Model of SBMA

Trans-activation response DNA protein 43 (TDP-43) has been linked to a number of degenerative diseases, now classed as TDP- 43 proteinopathies (Arai, 2014). Few, if

any reports exist about TDP-43 expression in SBMA. TDP-43 is an RNA binding protein that has been shown to translocate from the nucleus into the cytoplasm in affected cell types in ALS as well as Inclusion Body Myositis (IBM). TDP-43 inclusions are also ubiquitin positive. There is also evidence that TDP-43, although not localising with polyQ inclusions, can have patho-mechanistic involvement in polyglutamine diseases (Toyoshima and Takahashi, 2014). Furthermore, TDP-43 sequestered within polyQ repeats in the nucleus has been shown to disrupt TDP-43 mediated splicing (Fuentealba et al., 2010).

In the TA muscle of 12 month old AR100 mice there was no evidence of TDP-43 mislocalisation to the cytoplasm (Figure 52), but by disease end stage, 18 months, cytoplasmic mislocalisation of TDP-43 was observed (Figure 53). This is a surprising finding in a model of SBMA as polyQ expansion has previously been shown to sequester TDP-43 within the nucleus within aggregates, preventing it's degradation within the cytosol (Fuentealba et al., 2010). However, as TDP-43 mislocalisation did not occur until disease end stage, it is possible that this is not a causative feature of SBMA.

3.4.2.6 The AR100 Mouse Model Shows Signs of Reduced IGF-1 Signalling

Skeletal muscle contains satellite cells that have the ability to regenerate in damaged muscle. These resident stem cells are located along the basement membrane and are activated upon damage (Blau et al., 2015). IGF-1 signalling is responsible for the activation of satellite cells (Musaro et al., 2001). Insulin like growth factor (IGF-1) is a signalling molecule that features in many pathways responsible for muscle fibre homeostasis (Schiaffino and Mammucari, 2011). It has been shown to be reduced in the muscle of the AR97Q model of SBMA and its overexpression can attenuate disease (Palazzolo et al., 2009) Furthermore, systemic treatment with IGF-1 in AR97Q mice can also attenuate disease (Rinaldi et al., 2012). However, there are varying responses of IGF-1 to disease, with an increase in IGF-1 in the muscle of a Spinal Muscular Atrophy model (Biondi et al., 2015).

TA muscles of 12 month old AR100 mice, did not contain small IGF-1 positive muscle fibres seen in muscle of age matched WT mice (Figure 54), suggesting there may be a loss of the regenerative capacity normally a feature of healthy muscle. This is particularly interesting as there is an increasing viewpoint in SBMA research, that there may be defective satellite cell activation and repair within SBMA muscle (Soraru et al., 2008). Indeed, it has even been suggested that SBMA may be a form of myotonic dystrophy (Oki et al., 2013).

3.4.3 The AR100 Mouse Model Does Not Show Signs of Early Denervation.

Denervation is a primary cause of muscular atrophy (Cohen et al., 2015). There is evidence of denervation appearing early in pathogenesis of the mutant SOD1 models of ALS as well as in humans (Fischer et al., 2004, Jokic et al., 2006). Not only is there a retraction of axons, (Dadon-Nachum et al., 2011), there is evidence that the morphology of end plates can be greatly disrupted as disease progresses (Bruneteau et al., 2015). In SBMA, the AR97Q model has shown that denervation is present in this mouse model and it is reduced by intra cranial anti-sense oligonucleotide knock down of the mutant androgen receptor (Sahashi et al., 2015). Furthermore using the AR100 mouse model, it has been shown by Thomas et al. (2006b) that the marker of re-innervation, Neuronal cell adhesion molecule (NCAM), is up-regulated in the muscle of AR100 mice, crossed with Testicular feminisation Mice (Tfm), which express no endogenous mouse AR. Furthermore electro myo-cardiogram (EMG) analysis of patients has shown denervation is present in patients with SBMA (Araki et al., 2015).

Surprisingly H&E analysis of muscles of AR100 mice (Figure 48 to Figure 50) primarily showed myogenic changes. No angulated fibres were observed, a characteristic feature of neurogenic muscle degeneration (Seidman, 2013). Analysis of muscle innervation, in the EDL, showed that there was no significant change in the number of innervated end plates at 3 months (Figure 56) However, there was a trend of an increase in the number of denervated end plates in AR100 muscle from 6 months of age, although this did not reach significance (Figure 57). It is possible that denervation is only present very late in the AR100 mouse model of SBMA,

particularly as other experiments investigating this in the AR100 model involved exacerbating the AR100 phenotype by crossing with Tfm mice. Furthermore recently it has been shown that there is evidence of fragmented neuromuscular junctions in WT over-expressor and knock-in SBMA model mice in absence of signs of denervation (Poort et al., 2016).

3.4.3.1 Muscle Fibre Type Changes during Disease Progression in the AR100 Mouse Model of SBMA

Myosin Heavy Chain (MHC) isotopes in the TA muscle were examined as a marker of fibre types (Bloemberg and Quadrilatero, 2012). Characteristically during muscle denervation and re- innervation, type 2X fibres form clusters within the muscle, termed '2X grouping'. Furthermore, in ALS, a rapidly progressing motor neuron disease, fibre type switching occurs in fast twitch muscles, so that muscles such as the EDL and the TA become slow twitch muscles, as characterised by an increase in fatigue resistance and an increase in the proportion of type 2A fibres (Bryson et al., 2012).

Both 2X fibre grouping and 2A fibre expansion was observed in the TA muscle of AR100 mice. At 6 months of age the muscle fibre composition within the TA was largely similar to that of WT (Figure 58). By 12 months of age, an increase in the proportion of type 2A fibres was observed (Figure 59) and by disease end stage, 18 months, there was a clear increase in type 2A fibres and grouping of 2X fibres was clear (Figure 60). As these features are associated with muscle denervation and re-innervation it is likely that there is a neurogenic component to SBMA, which manifests later in disease progression.

3.4.3.2 Nogo-A Expression Increased in AR100 Muscle

To further evaluate the involvement of denervation in SBMA the protein Nogo- A, a molecular marker of denervation, was also examined. Expression of Nogo-A in skeletal muscle has been shown to correlate with disease progression in ALS (Bruneteau et al., 2015), and auto Nogo-A antibodies have been trialled in the $SOD1^{G93A}$ mouse model (Bros-Facer et al., 2014), with clinical trials in ALS patients

are already underway (Meininger et al., 2014). In TA muscles of 12 month old mice Nogo-A expression was increased (Figure 61). Targeting this upregulation of Nogo-A may therefore also be a potential therapeutic approach for SBMA.

3.4.4 Summary

In this Chapter I performed a longitudinal histopathological analysis of AR100 muscle as well as confirming that the AR20 control mouse does not show any signs of degeneration. Taken together, the results confirm that muscle is a primary site of pathogenesis in the AR100 muscle, with both myogenic and neurogenic changes. These finding suggest therefore that targeting pathology in muscle may be an important approach in the development of therapy for ALS.

Chapter 4 Molecular Pathway Analysis of Fast Twitch Muscle in the AR100 Mouse Model of SBMA

4.1 Introduction

The results presented, in Chapter 3 showed that the AR100 mouse model of SBMA shows histopathological features of muscle degeneration, atrophy and possibly an impaired capability to regenerate. Therefore in this Chapter, I attempt to investigate these processes at a molecular level to determine pathways of interest that might be targets for therapeutic intervention. In the first instance, candidate pathways that have previously been shown to mediate muscle homeostasis such as Myogenin and Myogenic Differentiation factor 1 (MyoD) are examined. Next RNA sequencing data from WT, AR20 and AR100 muscle is examined in order to analyse changes in mRNA expression at a transcriptomic level. The gene lists generated can then be enriched using pathway analysis. Finally candidate proteins identified from RNA sequencing and pathway analysis are examined, to determine if changes at the mRNA level are mirrored at the functional protein level.

4.1.1 Myogenic Regulatory Factors in Muscle Atrophy

Two transcription factors that play a role in muscle differentiation are Myogenic Differentiation factor 1 (MyoD) and Myogenin. They belong to a group of proteins known as myogenic regulatory factors that are transcription factors responsible for mediating prenatal myogenesis and muscle atrophy signalling pathways. MyoD and Myogenin are most active during myogenesis and act to mediate the fusion of myoblasts into myotubes (Berkes and Tapscott, 2005). However, in neuromuscular diseases, such as ALS, these two genes have been shown to be upregulated in muscle of presymptomatic mSOD1 mice, perhaps depleting the muscles regenerative capacity (Galbiati et al., 2012). However, gene transfer of Myogenin has been shown to increase motor performance of mSOD1 mice, MyoD was shown to decrease survival of MNs and facilitate denervation (Park et al., 2013). Myogenin has also been shown to play a role in muscle denervation (Macpherson et al., 2011). This study showed that Myogenin was released in response to denervation. However, in Myogenin knock-out mice there was no muscle atrophy in response to denervation.

Taken together there is some uncertainty whether increasing myogenic regulatory factors, in particular Myogenin, is indeed beneficial or detrimental to muscle in MNDs. To date it has only been shown to be altered in the muscle of SBMA knock in model mice, where there is an increase mRNA expression of Myogenin and MyoD in the muscle (Yu et al., 2006). Interestingly, it has been shown in Huntington's disease, another polyQ disease, that Myogenin is a marker of muscle atrophy (Mielcarek et al., 2015). It is therefore important to investigate the potential changes in Myogenin and MyoD in SBMA, in an additional model at the functional protein, level to determine if these transcription factors may be mediating muscle atrophy.

4.1.2 Altered Transcriptional Regulation in SBMA

In this Chapter I also examine transcriptional regulation in the muscle of AR100 mice in an attempt to identify pathways that mediate pathogenesis. The AR's role as a transcription factor leads to an important pathogenic mechanism in SBMA of distorted transcription believed to be an early pathogenic event in polyQ diseases (Katsuno et al., 2006b). It has been suggested that altered transcription in SBMA is mediated by inclusions disrupting histone acetyl transferase activity (Minamiyama et al., 2004). Furthermore since the AR functions as a transcription factor and the polyQ tract is involved in transactivation; altered transcriptional regulation is thought to play a role in SBMA.

Work from the Greensmith lab has shown that there are altered mRNA levels of key trophic molecules such as VEGF in the spinal cord of AR100 mice (Malik et al., 2013). Furthermore recent research has shown that there is altered Transcription factor EB (TFEB) interaction with the AR results in alteration in autophagic flux in AR121 mice (Cortes et al., 2014b). Additionally Yu et al. (2009) have reported altered RNA splicing in the muscle of SBMA model mice.

To date two studies have undertaken microarray analysis on muscle of mouse models of SBMA to determine the effect of the polyQ repeat expansion on the transcriptome. The first study, conducted by Mo and colleagues, performed RNA

sequencing analysis on three mouse models of SBMA (Mo et al., 2010). Interestingly, there was a considerable overlap in gene expression changes in three genetically distinct models of SBMA. However, this study did not determine which gene expression changes were causative of disease or due to the maintenance of disease. Furthermore, this study did not determine which changes were androgen dependent and authors found limited the involvement of IGF-1 signalling specifically, Insulin-like growth factor binding protein 5 (*Igfbp5*) was down regulated (Mo et al., 2010). More recent research from the same group also involved microarray analysis, but these experiments were carried out on female mice carrying the mutated androgen receptor that had been treated with Testosterone to induce symptoms (Halievski et al., 2015b). They found dysregulated expression in genes responsible for muscle fibre integrity particularly genes responsible for myogenic differentiation and myoblast fusion.

4.1.3 Aims of this Chapter

In this Chapter I undertook an analysis of RNA sequencing data from the Tibialis anterior (TA) muscle of AR100 mice at various stages of disease progression, and compared the results to those from WT and AR20 mice. My aim was to identify novel genes that mediate AR100 muscle pathology. I also undertook pathway enrichment to determine which signalling pathways are disrupted in AR100 mouse muscle. Results from mice at pre-symptomatic stages were examined to determine which changes initiate disease. Thus muscles from mice at the following stages of disease were examined: presymptomatic, symptomatic and disease end stage. The pathways I focused on will include: I) Mitochondrial based II) Insulin like growth factor (IGF-1) signalling and III) ER stress. I aim to focus on these pathways, and validate their involvement in SBMA pathogenesis using western blot as previous micro array studies have identified changes in mitochondrial genes (Halievski et al., 2015b). Furthermore, IGF-1 signalling has been identified as having therapeutic potential in SBMA (Rinaldi et al., 2012). Lastly, I focus on ER stress as it has been previously shown in our lab that motor neurons from the AR100 mouse show early signs of ER stress (Montague et al., 2014).

4.2 Materials and Methods

4.2.1 Total RNA Extraction and RNA-sequencing

Total RNA was extracted from AR20 and AR100 TA muscle (n=4 per genotype for each time point) using the guanidine isothiocyanate-based method (Chomczynski and Sacchi, 1987), using TRIzol® solution (Invitrogen) according to the manufacturer's instructions and as described by Malik et al. (2013). Total RNA was re-suspended in nuclease-free water and RNA integrity and quality was assessed using an Agilent Bioanalyser. For RNA-sequencing, strand specific paired -end libraries were generated from total RNA using the Illumina TruSeq RNA kit v2 according to the manufacturer's directions. *Libraries were sequenced at the UCL Genomics facility on a HiSeq 2000. Data was analysed with the assistance of UCL genomics.* All FASTQ files containing raw count data were generated using HTseq, which counts how many reads map to each gene. FASTQ files were analysed using FastQC software, a quality control tool for RNA-sequencing data and were aligned to the reference genome using Tophat (v 2.0). DESeq2 was used to normalise data and determine differential gene expression.

4.2.2 Enrichment

To gain a better understanding of the differently expressed genes, significant genes ($p < 0.05$ and FDR < 0.05) were further grouped into biological and molecular pathways which allow biological interpretation of large gene expression data sets. The first pathway analysis used was WEB- based GEne SeT AnaLysis Toolkit (WEB GESTALT) version 2013 (Zhang et al., 2005, Wang et al., 2013). To get a broad classification of the biological processes altered between WT and AR100 muscle GO Slim classification was used, which can classify the differential genes identified based on Biological Processes, Molecular Classification and Cellular Component. For the identification of pathways significantly deregulated, the *m.musculus* genome was selected as a reference set, data was input in the form of a gene symbol, and the statistical method used was Hypergeometric. To compensate for multiple comparisons, and to reduce the false discovery rate, the Benjamini Hochberg test

was used with a p value of 0.05. Kyoto encyclopaedia of genes and genomes (KEGG) pathway analysis was carried out

The second Pathway analysis method used was The Database for Annotation, Visualization and Integrated Discovery (DAVID) version 6.7 (Huang da et al., 2009b, Huang da et al., 2009a). Separate lists for whether gene expression was either up or down regulated were created, and then KEGG pathway analysis was carried out on each list separately and in combination. A significant Benjamini Hochberg test was set at $P<0.05$.

The Final pathway analysis method used was the Search Tool for the Retrieval of Interacting Genes/Proteins (STRING) version 10 (Szklarczyk et al., 2015). The differentially expressed genes were used as an input to obtain direct and indirect protein-protein interactions using STRING 9.0 database. This database provides information on both experimental and predicted interactions of genes/protein from sources such as co-occurrence, co-expression experiments and literature mining. Here I identified the main clusters of interacting proteins translated from my gene lists visually as well as using the built in pathway analysis software.

4.2.3 Western Blotting

Western Blot analysis was carried out as described in Chapter 2 Methods (see Section 2.2.5). For Western blotting of phosphorylated proteins TBS was used in place of PBS, 5% BSA was used for blocking and in the RIPA buffer the Halt protease and Phosphatase inhibitor cocktail (Thermo Scientific 78440) was used. Results for densitometry were either normalised to alpha tubulin, Vinculin or GAPDH (Table 7). Primary antibodies and concentrations used for WB are listed in Table 8. Blots were imaged and densitometry readings were obtained using Bio-Rad's Image lab. Densitometry was analysed for significant changes using SPSS. Data was checked for significant evidence of non-normality using the Shapiro Wilk Test and Q-Q plots. Where data was normally distributed one-way ANOVAs and post hoc Tukey tests were used when there were three groups in the analysis, or Student T tests when comparing two groups directly. If there was enough evidence to assume a non-

normal distribution a Kruskall- Wallis test was used for groups of 3 and Mann-Whitney- Whitney you tests were used for post hoc analysis or for where comparing groups of two.

Table 7 Western Blot Loading controls

Loading control	Product Code	Size	Concentration
Tubulin	T9026 Sigma	55kDa	1 in 5000
GAPPDH (HRP)	ab9385 Abcam	38kDa	1 in 4000
Vinculin	ab129002 Abcam	124kDa	1 in 5000

Table 8 Primary Antibodies used for Western Blotting

Antigen	Code and Supplier	Size	Concentration	µg Protein
BiP	ab21685 Abcam	75kDa	1 in 1000	50
Caspase 9	ab47537 Abcam	45kDa	1 in 500	50
Cleaved Caspase 3	9664 Cell signalling	19kDa	1 in 1000	100
Cytochrome C	ab76237 Abcam	12kDa	1 in 500	50
FoxO1 (C29H4)	2880 Cell signalling	78to 82kDa	1 in 1000	50
Mitochondrial Complex II Cocktail	ab110410 Abcam	CIIa-70kDa	1 in 250	25
		CV- 50kDa	1 in 250	25
		CIIb-30kDa	1 in 250	25
Myogenin	ab124800 Abcam	34kDa	1 in 1000	50
Pan-AKT(C67E7)	4691 Cell signalling	60kDa	1 in 1000	50
PGC1	SC-13067 Santa Cruz	90kDa	1 in 200	50
PINK	ab23707 Abcam	66kDa	1 in 200	50
Phospho AKT (Thr308)	D25E6 Cell signalling	60kDa	1 in 1000	50

4.3 Results

4.3.1 Analysis of myogenic regulatory factors in TA muscles of AR100 mice.

Two regulatory components of muscle homeostasis are Myogenin and MyoD. I therefore began the molecular analysis of AR100 mouse muscle by western blotting for these two candidate proteins. The results showed that there was no significant difference in MyoD expression at 6 and 12 months of age, but by 18 months, Myo D expression had decreased, although this fell just short of statistical significance (Figure 62). Analysis of myogenin revealed that there was a significant decrease in myogenin expression in AR100 TA muscles by 18 months of age (Figure 63).

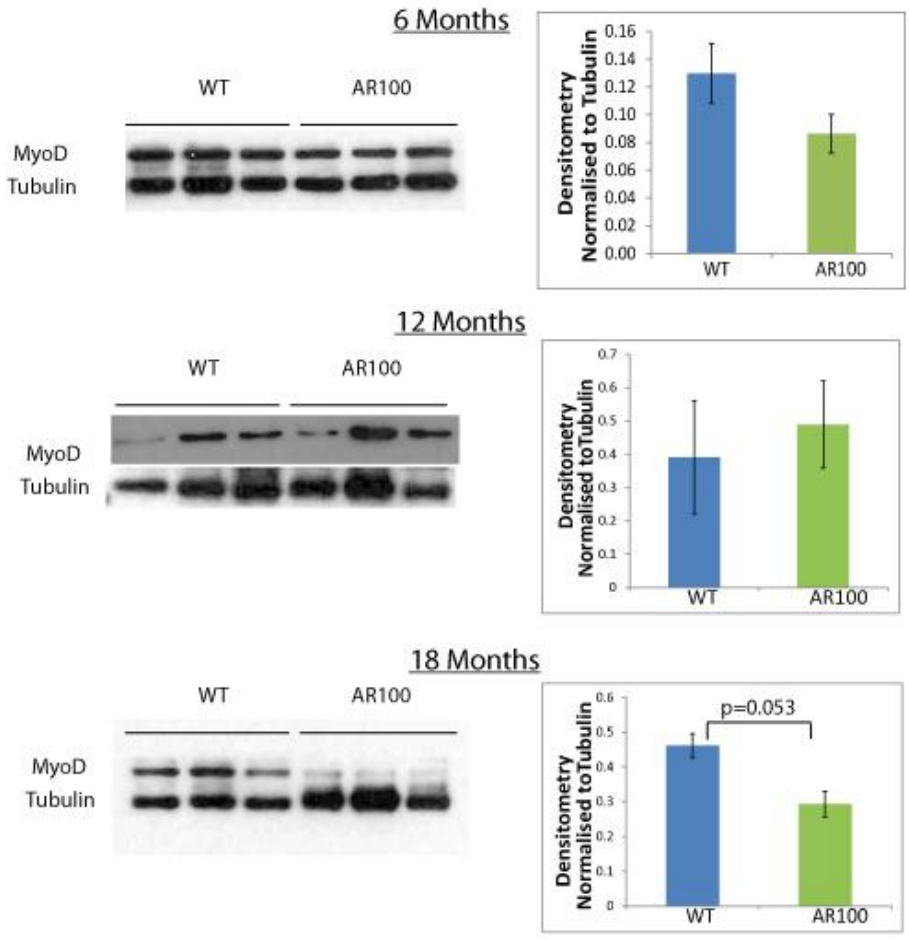

Figure 62 Western Blotting for MyoD in adult TA muscle

WB and densitometry analysis of adult TA muscle for MyoD protein levels in the TA muscle of WT and AR100 mice. Independent samples t- tests were used to analyse significance (n=3, $p<0.05$). There is a trend of reduced MyoD WB densitometry levels in 18 months AR100 muscle falling just short of significance. Error bars= SEM.

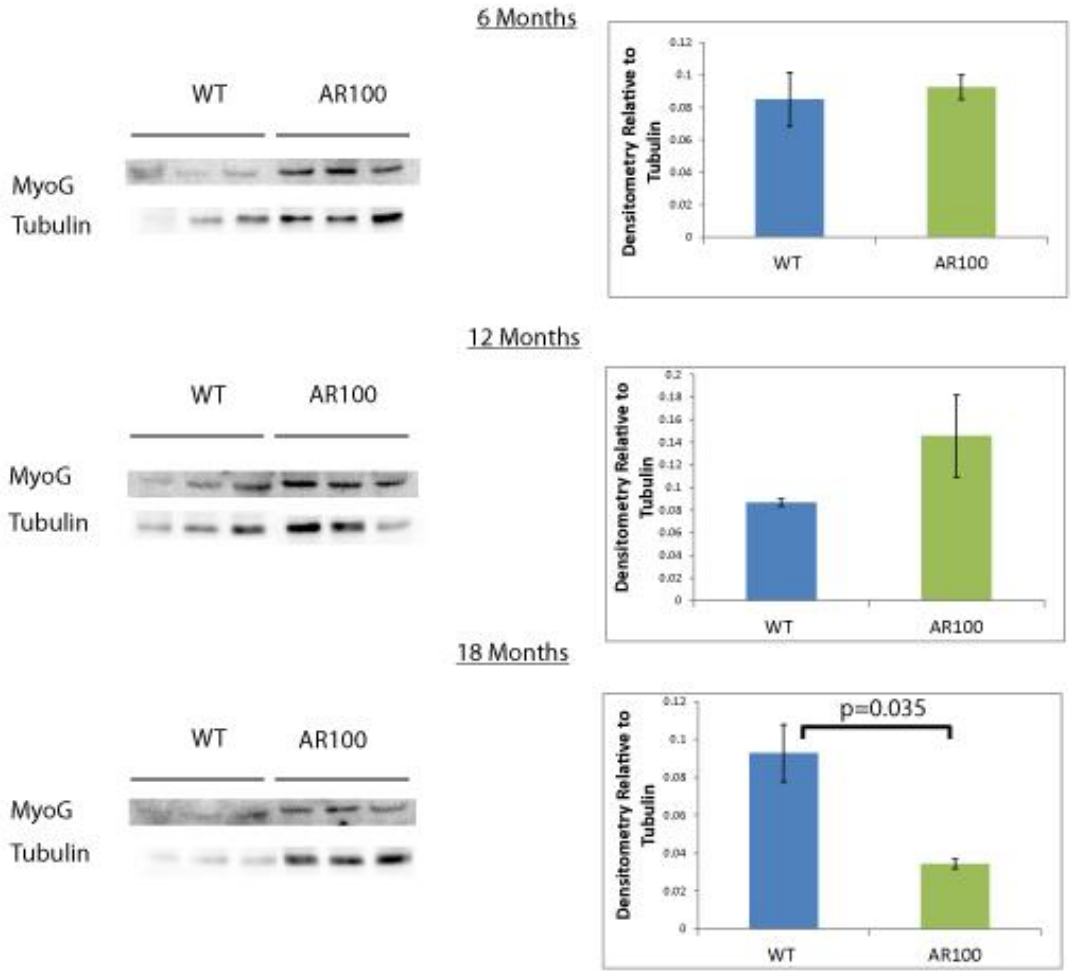

Figure 63 Western Blotting for Myogenin in adult TA muscle

WB and densitometry analysis of adult TA muscle for Myogenin protein levels in the TA muscle of WT and AR100 mice. By 18 months of age there is a significant reduction in AR100 TA myogenin protein expression in comparison to WT (Independent samples T-test, n=3 p=0.035). Error bars= SEM.

4.3.2 Non-Hypothesis mediated pathway analysis of SBMA Muscle prior to symptom onset

Using RNA sequencing analysis of 3, 12 and 18 month muscle, we identified candidate genes for investigation in AR100 muscle. The top 100 genes differentially expressed at each stage of disease is summarised in Appendix I.

As shown in Table 9, a large number of genes were differentially expressed in AR100 TA muscle comparison to AR20 muscle. One could speculate that the genes changed at 3 months may have more of a causative, early role in SBMA pathology. The highest level of gene dysregulation was observed at 12 months, when disease is in full progression. Interestingly, fewer genes were dysregulated at 18 months, disease end stage, in comparison to 12 months.

Table 9 Number of Gene changes in AR100 TA muscle in comparison to AR20

Age	Total Gene Changes	Number Increased	Number decreased
3 Months	514	302	212
12 Months	5962	3031	2931
18 Months	2499	1129	1370

Next, a three way comparison was carried out between WT, AR20 and AR100 to determine a list of genes altered between AR20 and AR100 mice (FDR<0.05), but not significantly different between WT and AR20 (P>0.05). Venn diagrams show the number of genes that satisfied these criteria (Figure 64 to Figure 66). See appendix II for a list of genes significantly changed via a 3- way comparison. Interestingly, there were only 26 genes identified at 3 months of age, pre-symptomatic in the AR100 mouse model of SBMA. At 12 months, when disease is in full progression, there were 2924 genes significantly different and at disease end stage, 18 months, the number of genes that were significantly dysregulated was reduced to 69 using these criteria. One could speculate that by 18 months most of the genetic changes in the already degenerated muscle have already happened.

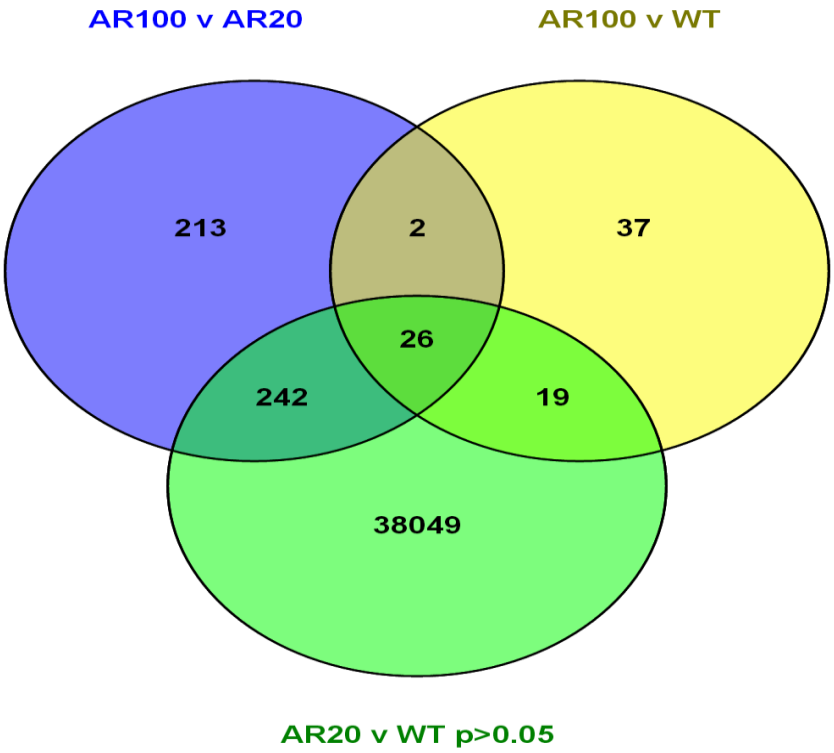

Figure 64 Three Month 3 way gene list comparison

Venn diagram showing the number of genes from RNA sequencing analysis significantly different between WT and AR100, AR20 and AR100 but not WT and AR20 at 3 months of age. Genes identified using the P values for the False discovery rate were for AR20 vs AR100 $P<0.05$ but also WT vs AR20 $P>0.05$.

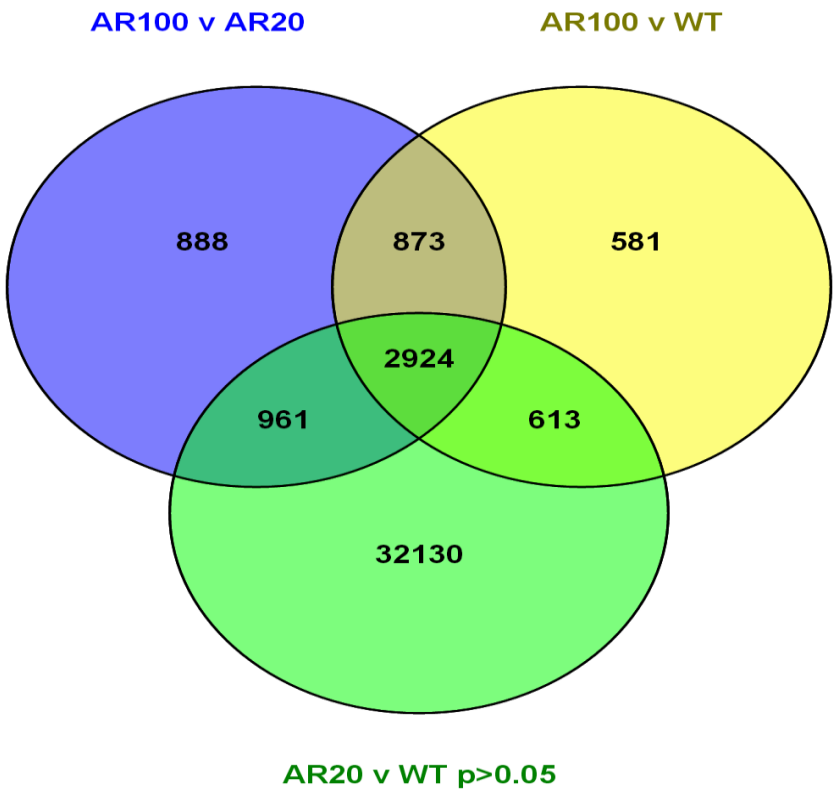

Figure 65 Twelve Month 3 Way gene list comparison

Venn diagram showing the number of genes from RNA sequencing analysis significantly different between WT and AR100, AR20 and AR100 but not WT and AR20 at 12 months of age. Genes identified using the P values for the False discovery rate were for AR20 vs AR100 $P<0.05$ but also WT vs AR20 $P>0.05$.

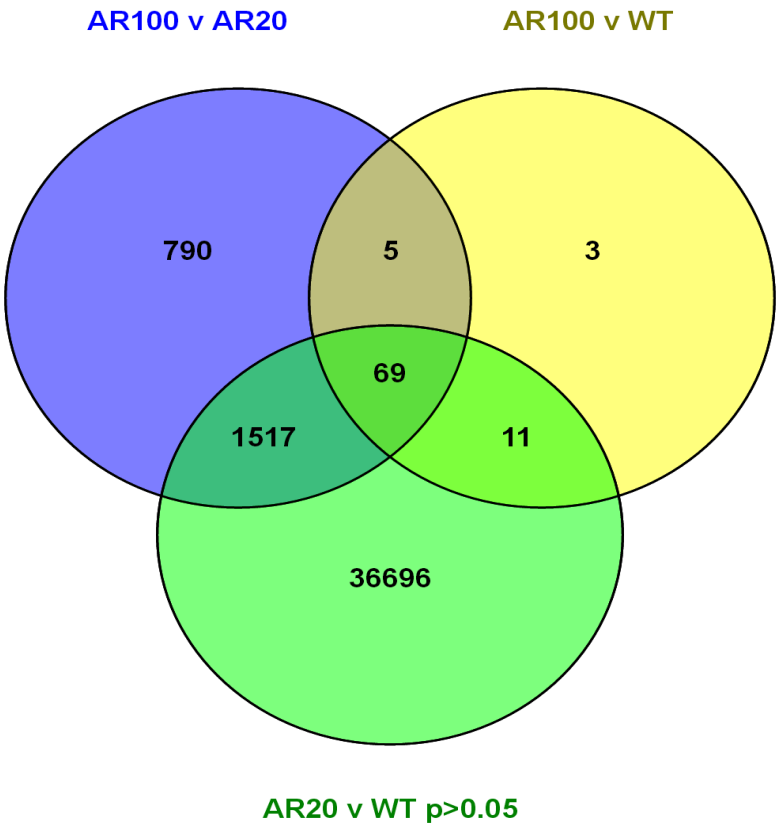

Figure 66 Eighteen Month Three Way gene list comparison

Venn diagram showing the number of genes from RNA sequencing analysis significantly different between WT and AR100, AR20 and AR100 but not WT and AR20 at 18 months of age. Genes identified using the P values for the False discovery rate were for AR20 vs AR100 $P<0.05$ but also WT vs AR20 $P>0.05$.

4.3.3 Three Month Pathway analysis

At 3 Months of age, a pre-symptomatic stage in the AR100 mouse model of SBMA, the biological classification of altered genes using GO SLIM analysis identified 'metabolic processes' as the largest altered biological process. The main molecular function of the altered genes at 3 months was 'protein binding' and the cellular component where most altered genes were classified under was the membrane (Figure 67).

Using KEGG pathway analysis, DAVID analysis and String analysis, these candidate gene lists were enriched to identify pathways of interest for further investigation at the functional- protein level. See Appendix III for a list of the Top 10 pathways dysregulated at 3, 12 and 18 months. The pathways with the greatest number of dysregulated genes were; the Alzheimer's disease pathway- 41 genes (Figure 68); oxidative phosphorylation pathway- 35 genes (Figure 69); Huntington's Disease and Parkinson's Disease pathways- 33 genes (Figure 70 and Figure 71 respectively). Although all these pathways were identified as being deregulated in AR100 muscle, central to all these pathways was the complexes of the electron transport chain (Figure 68 to Figure 71 highlighted in yellow).

One of the major components of Go slim analysis (Figure 67) identified protein binding as one of the top classifications of dysregulated genes. I therefore went on to perform STRING analysis (Figure 72) which identified 3 main clusters of protein-protein binding. The largest cluster being Collagens followed by ribosomal proteins and NADH dehydrogenases (Figure 68 to Figure 75).

As a result of this pathway analysis of muscles of 3 month old mice, I decided to follow up the electron transport chain and mitochondrial homeostasis at a protein level.

Figure 67

A

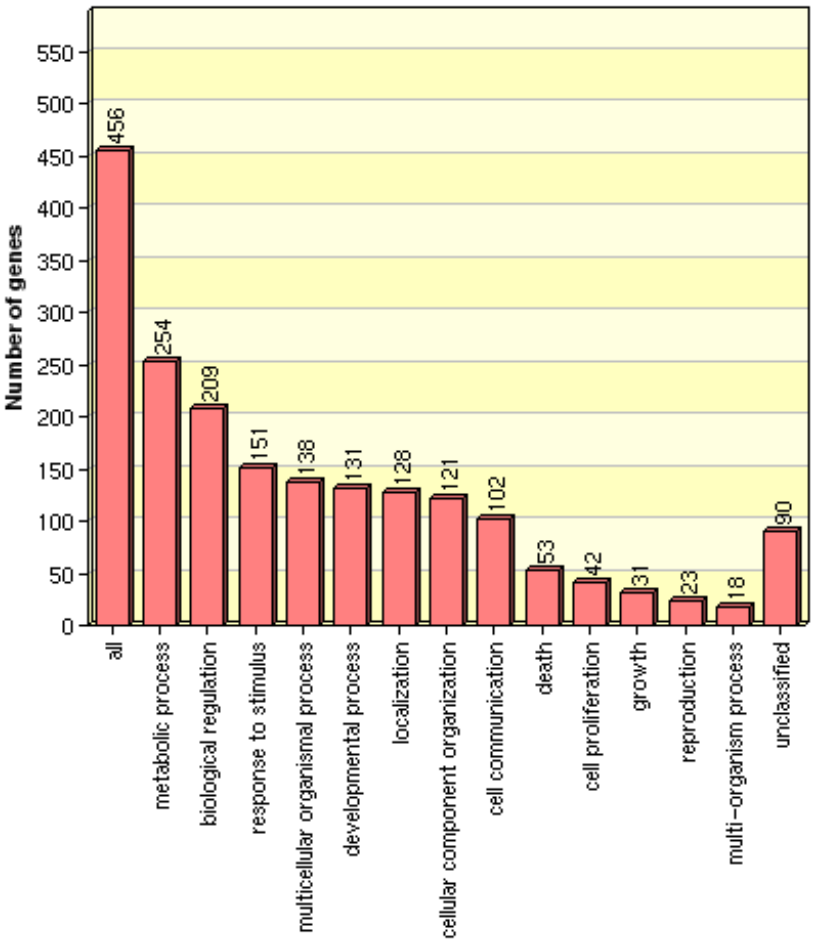
Number of genes
0
50
100
150
200
250
300
350
400
450
500
550
456
254
209
151
138
131
128
121
102
53
42
31
23
18
90
all
metabolic process
biological regulation
response to stimulus
multicellular organismal process
developmental process
localization
cellular component organization
cell communication
death
cell proliferation
growth
reproduction
multi-organism process
unclassified

B

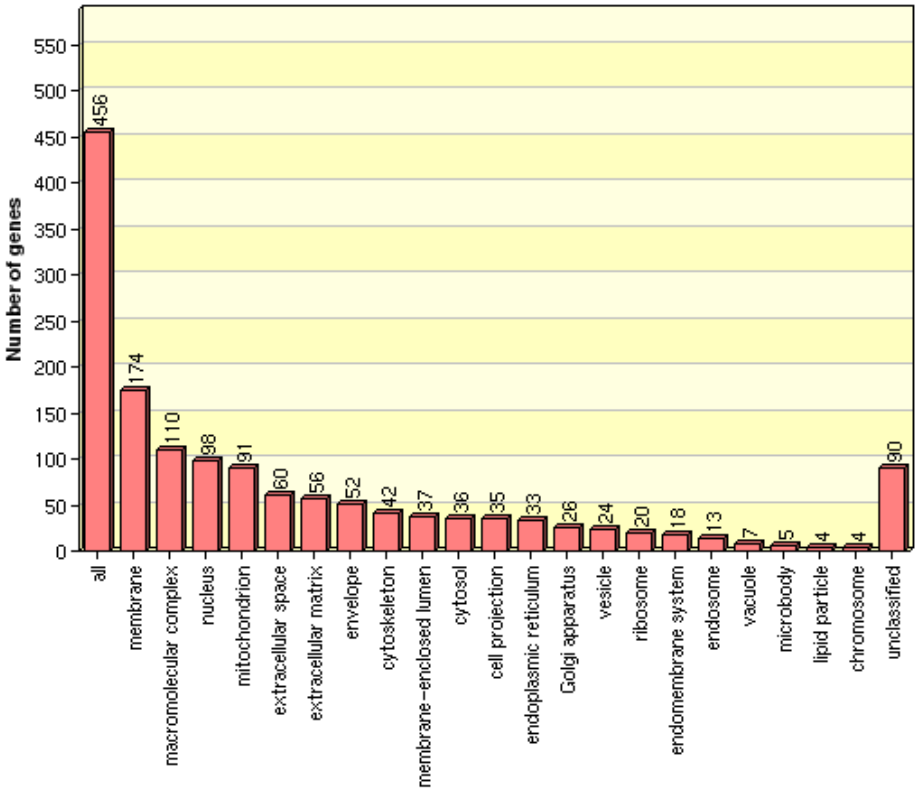
Number of genes
0
50
100
150
200
250
300
350
400
450
500
550
456
174
110
98
91
60
56
52
42
37
36
35
33
26
24
20
18
13
7
5
4
4
90
all
membrane
macromolecular complex
nucleus
mitochondrion
extracellular space
extracellular matrix
envelope
cytoskeleton
membrane-enclosed lumen
cytosol
cell projection
endoplasmic reticulum
Golgi apparatus
vesicle
ribosome
endomembrane system
endosome
vacuole
microbody
lipid particle
chromosome
unclassified

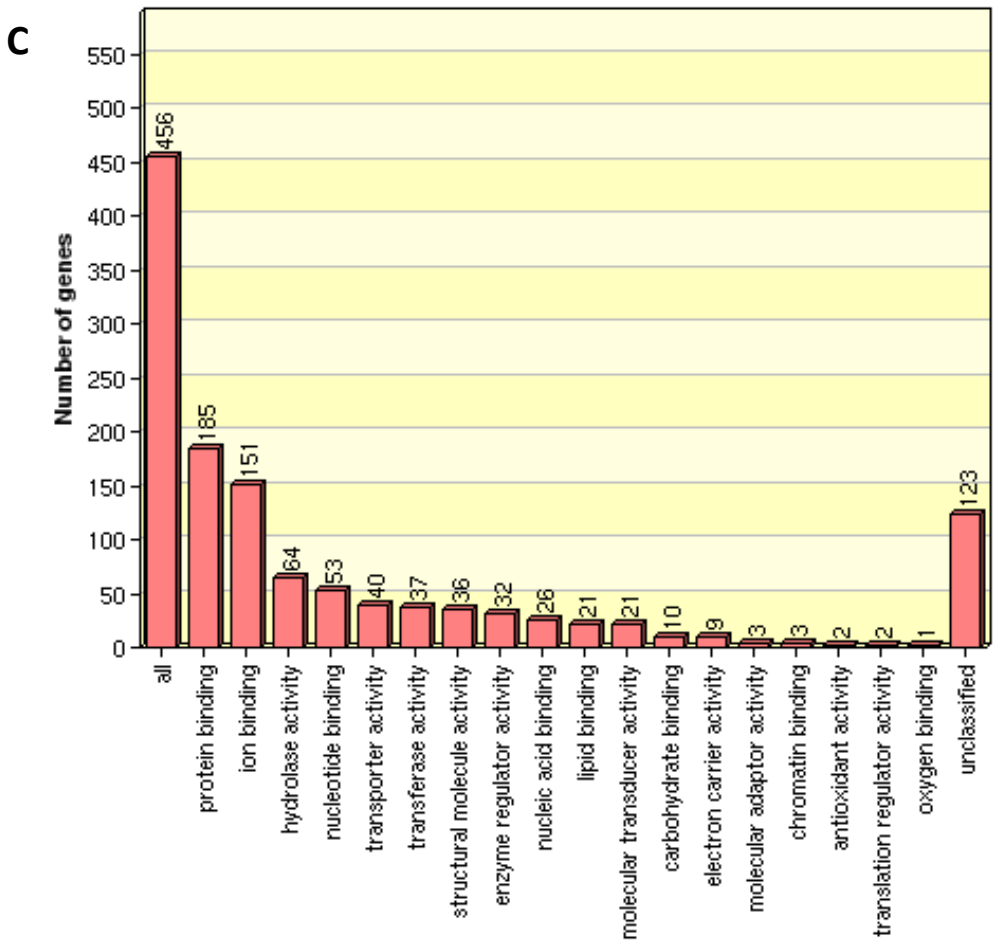

Figure 67 Classification of Altered Genes in 3 Month TA Muscle using Go Slim Analysis

A) Biological Process- identified metabolic processes to be the most altered category of genes **B**) Molecular function- Protein binding **C**) Cellular compartment- identified the cell membrane to be the site of most altered gene changes

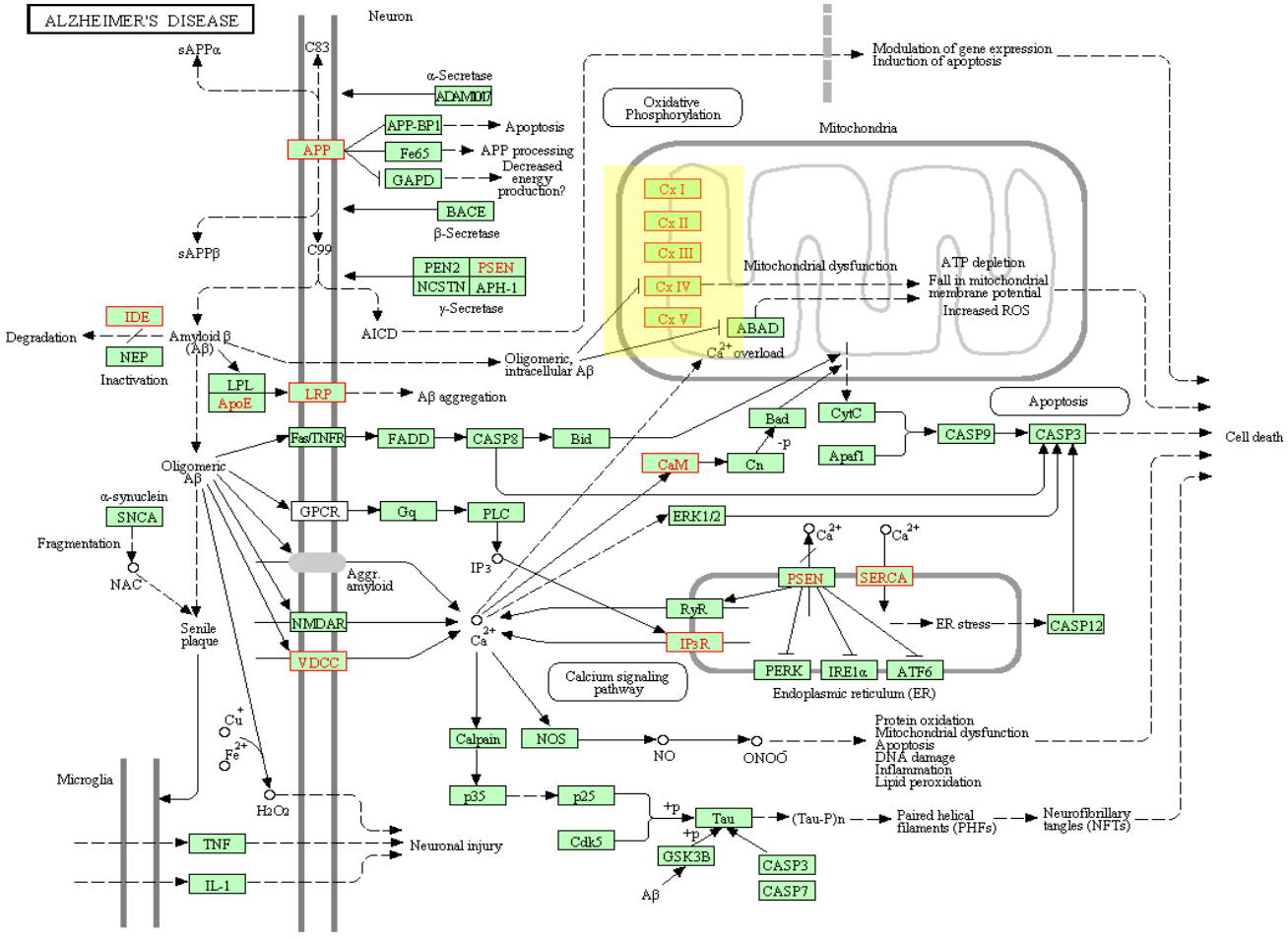

Figure 68 Dysregulated gene expression in TA muscles of AR100 mice at 3 months of age: analysis of the Alzheimer's disease Pathway

41 Genes were found to be dysregulated in TA muscles of 3 month old AR100 mice within the so called 'Alzheimer's disease pathway'. Central to this pathway is the electron transport chain, highlighted in yellow.

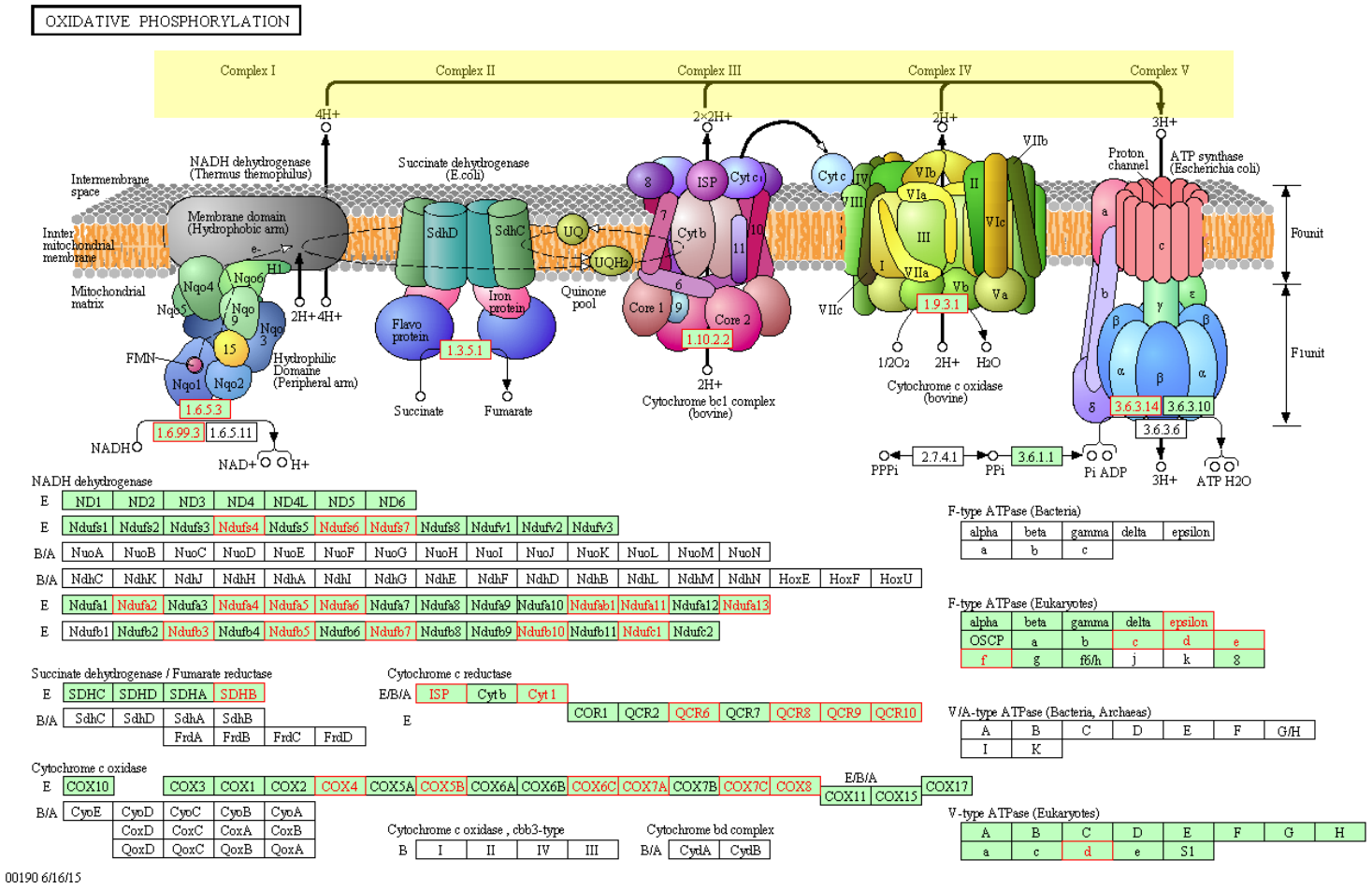

Figure 69 Dysregulated gene expression in TA muscles of AR100 mice at 3 months of age: analysis of the Oxidative phosphorylation pathway

35 Genes were found to be dysregulated in TA muscles of 3 month old AR100 mice within the Oxidative phosphorylation pathway. Central to this pathway is the electron transport chain, highlighted in yellow.

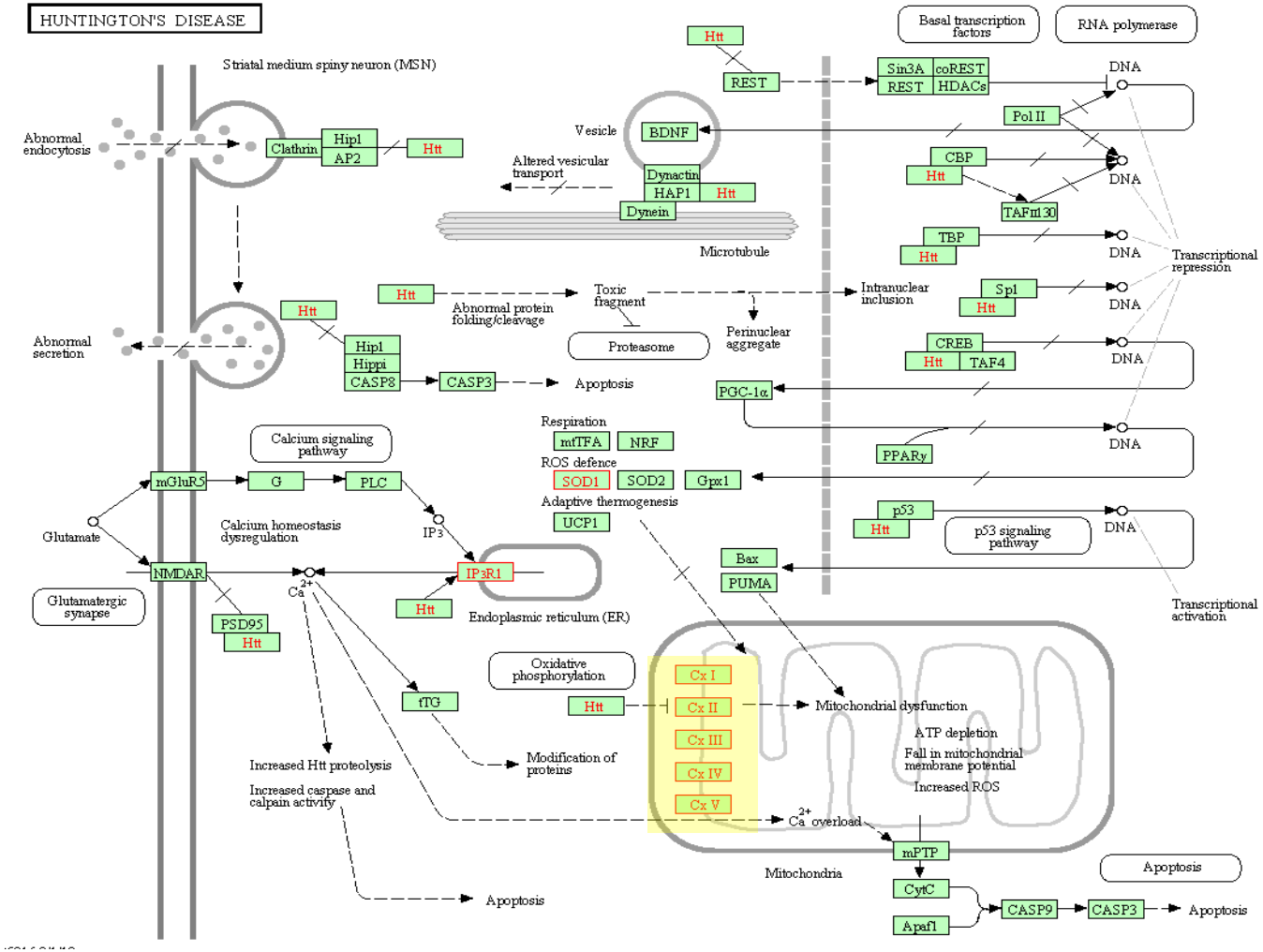

Figure 70 Dysregulated gene expression in TA muscles of AR100 mice at 3 months of age: analysis of the Huntington's disease Pathway

33 Genes that were differentially expressed at 3 months in AR100 mouse muscle were classified under the Huntington's disease pathway. Central to this pathway is oxidative phosphorylation, highlighted in yellow.

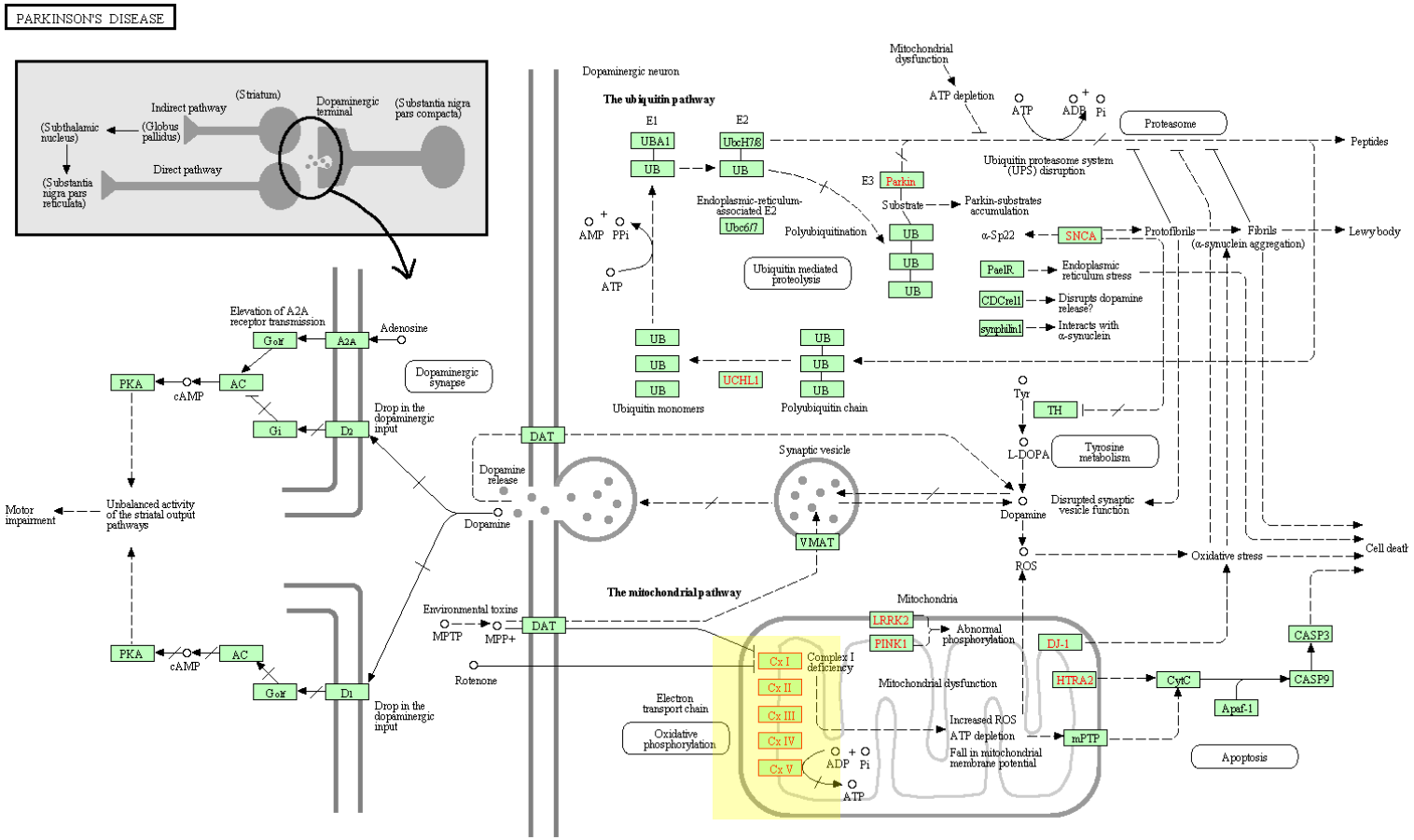

Figure 71 Dysregulated gene expression in TA muscles of AR100 mice at 3 months of age: analysis of the Parkingson's disease Pathway

33 Genes that were differentially expressed at 3 months in AR100 mouse muscle were classified under the Huntington's disease pathway. Central to this pathway is oxidative phosphorylation, highlighted in yellow.

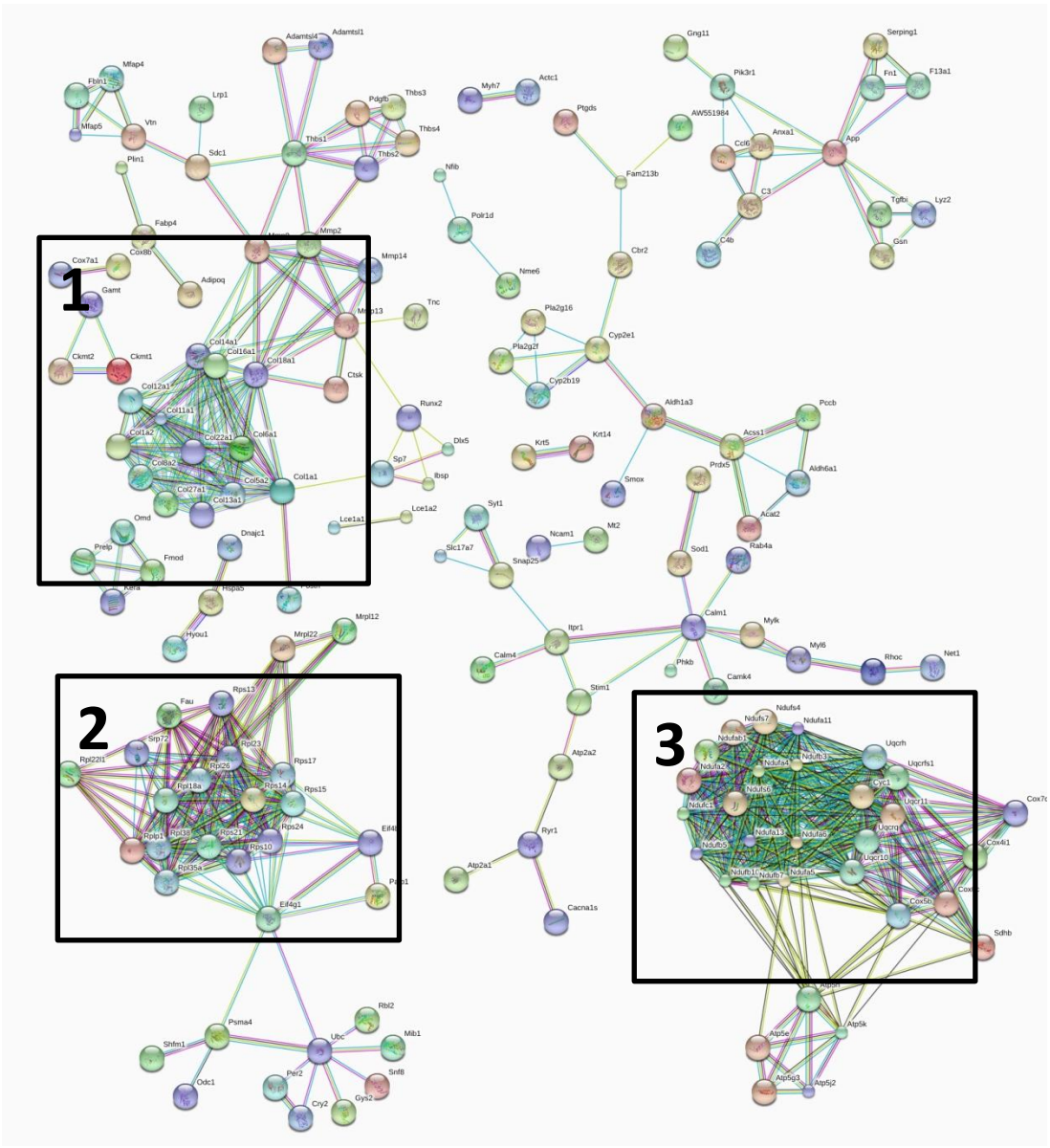

Figure 72 Three Month STRING protein interaction analysis of differential gene expression in TA muscles of 3 month old AR100 mice.

STRING Protein analysis showing connections between all 514 genes differentially expressed in the TA muscles of AR100 mice at 3 months. Three main clusters of protein interaction were identified- shown in selections **1-3**.

Cluster 1

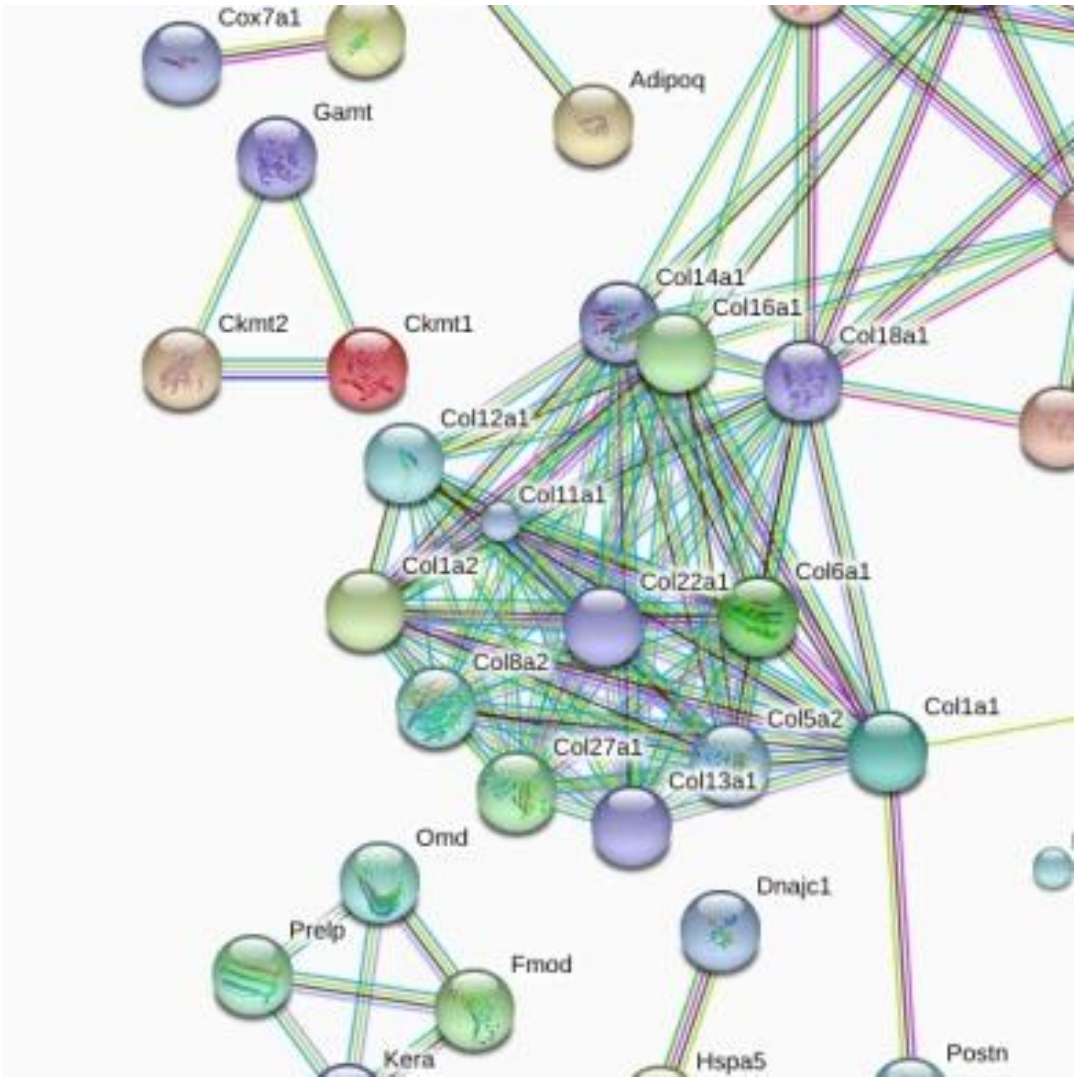

Figure 73 Cluster 1- STRING protein interaction analysis: Collagens

STRING analysis identified Collagens as one of the clusters of protein-protein interaction dysregulated in TA muscles of 3 month old AR100 mice.

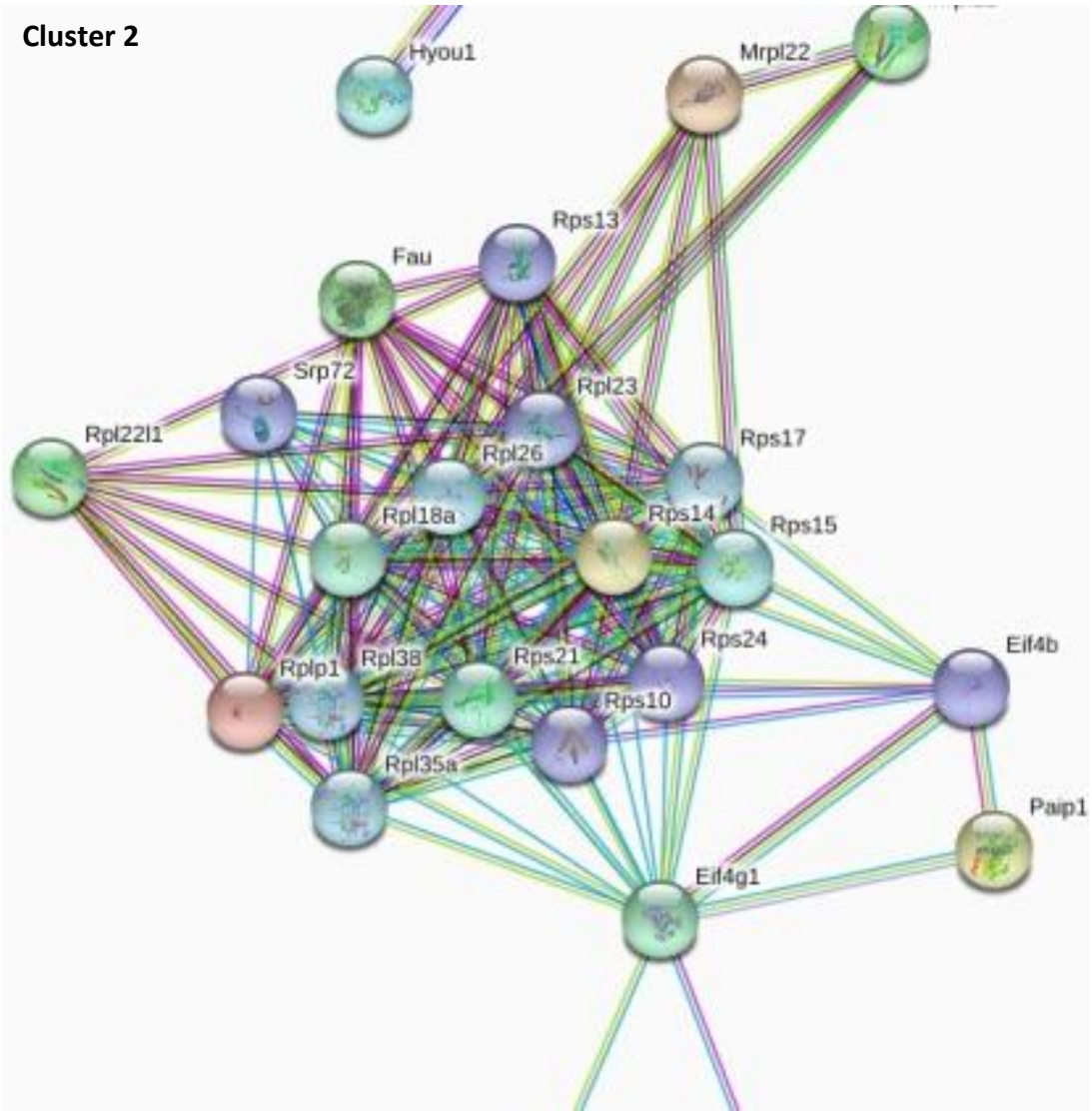

Figure 74 Cluster 2- STRING protein interaction analysis: Ribosomal proteins

STRING analysis identified Ribosomal proteins as one of the clusters of protein-protein interaction dysregulated in TA muscles of 3 month old AR100 mice.

Cluster 3

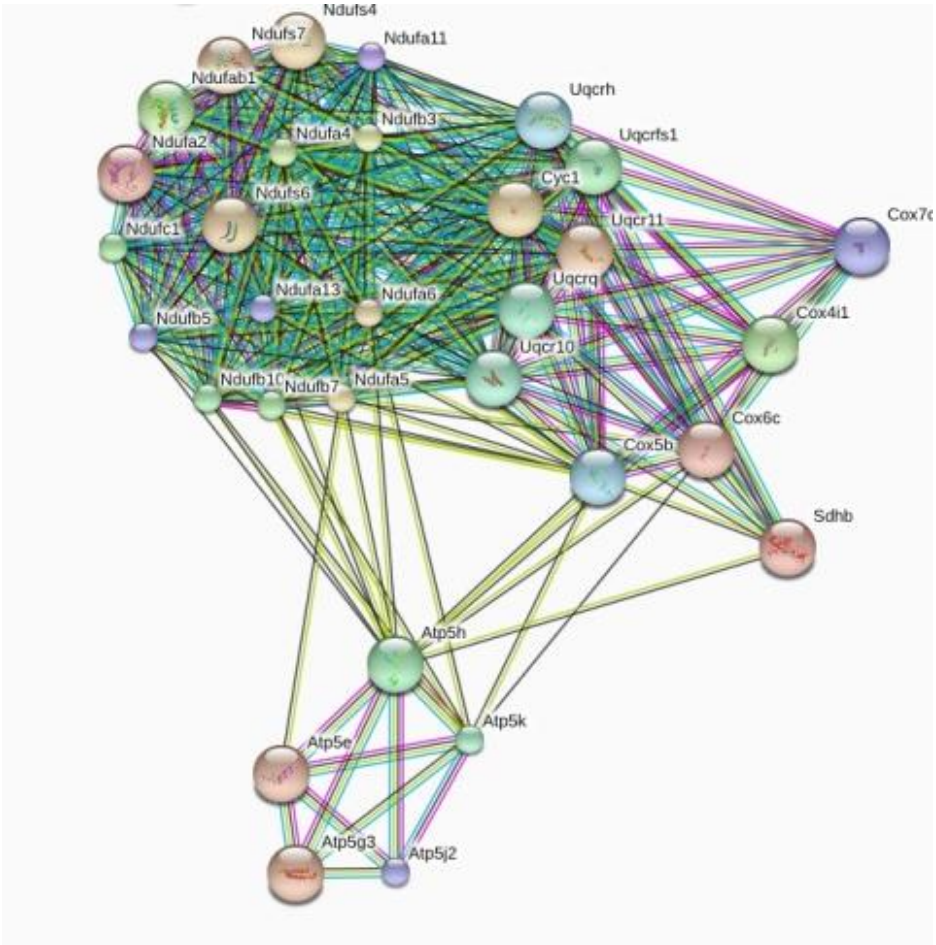

Figure 75 Cluster 3- STRING protein interaction analysis: NADH dehydrogenases

STRING analysis identified NADH dehydrogenases as one of the clusters of protein-protein interaction that was dysregulated in TA muscles of 3 month old AR100 mice.

4.3.4 Western blot Validation of Pathway analysis of differential gene expression in TA muscles of 3 month old mice

RNA-seq and pathway analysis enrichment showed that at the mRNA level, the oxidative phosphorylation pathway was significantly dysregulated in AR100 muscle TA muscle in comparison to AR20 TA muscle. The oxidative phosphorylation electron transport chain contributes to dysregulation of a number of pathways (Figure 68 to Figure 71). Next, I analysed the protein expression levels of components of Oxidative Phosphorylation by western blot, to determine if there was a significant difference in this pathway at the protein level in the TA muscles of AR100 mice throughout disease progression.

I examined levels of multiple complex II subunits (Figure 76), particularly as SDH staining of TA muscle shows a possible increase in SDH by 18 months (See Figure 44). I blotted for SDHa and SDHb, to deterimine if there could be significant changes in one complex subunit whilst other subunits were unaffected. I found that on the whole there was no significant difference in AR100 muscle at any stage of disease progression for either subunit. However, surprisingly at 3 Months there was significantly higher levels of SDHa in AR20 muscle. Furthermore, at 6 and 18 months there was significantly less SDHb in AR20 muscle. This finding illustrates how different subunits can be changed within the same complex and perhaps more thorough analysis of of mitochondrial complex subunits is required.

I next examined the levels of Cytochrome C (Figure 77) , the electon carrier between complex III and IV, and a mediator of apoptosis. There was no significant difference between any genotype at any stage of disease, most likely due to the high variability between samples. I next went on to investigate markers of mitchondrial homeostasis, such as PTEN-induced kinase 1 (PINK), a marker of mitophagy (Figure 78) and Caspase 9 which increases as a mediator of mitochondrial induced apopotosis (Figure 79). I found no signicant change in the levels of these two proteins although there was a trend for increased caspase 9 expression at symptomatic stages of disease.

Figure 76

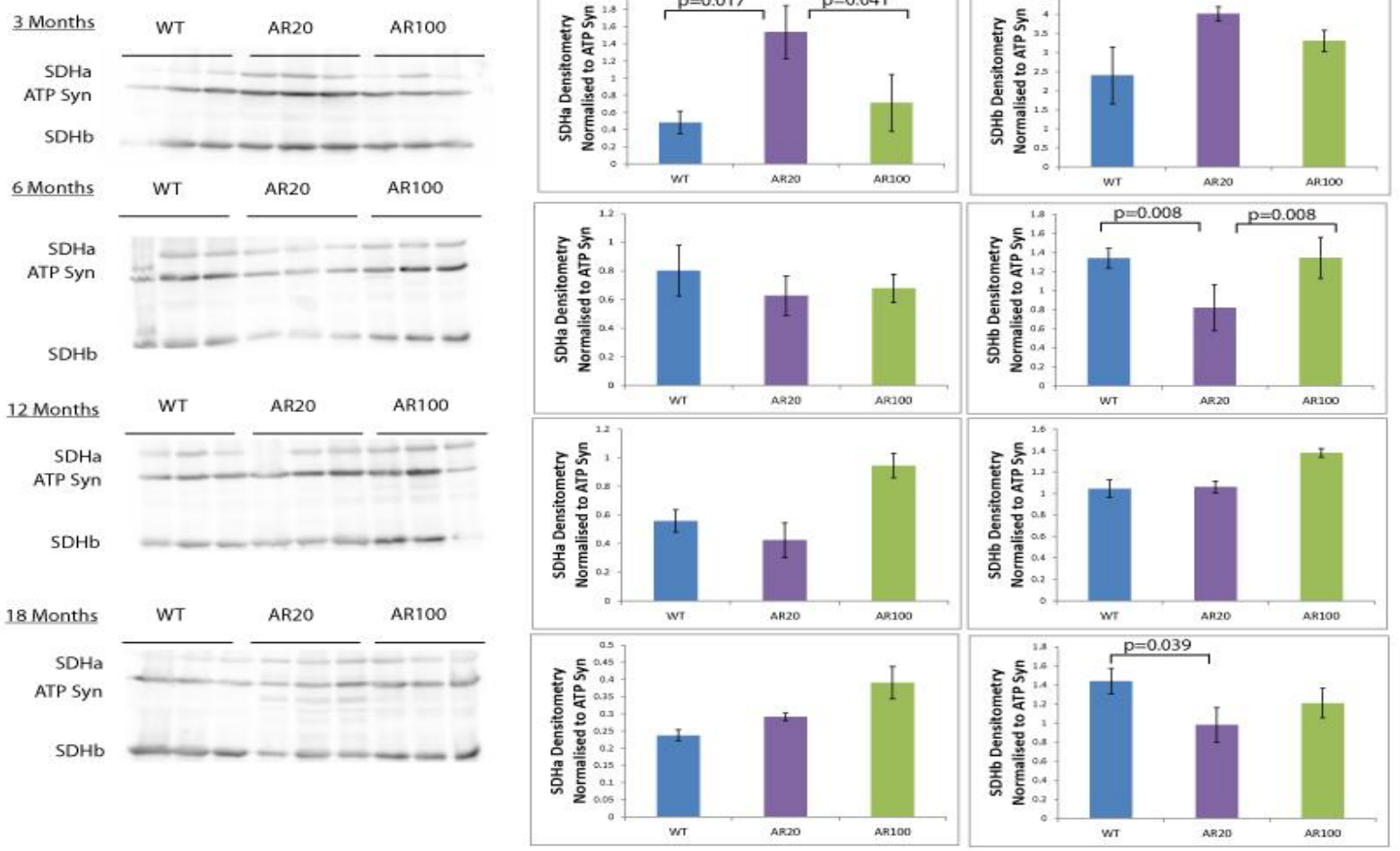
3 Months
WT
AR20
AR100
SDHa
ATP Syn
SDHb
6 Months
12 Months
18 Months
SDHa Densitometry Normalised to ATP Syn
SDHb Densitometry Normalised to ATP Syn
p=0.017
p=0.041
p=0.008
p=0.008
p=0.039

Figure 76 Mitochondrial Complexes II and V WB in Adult muscle

Mitochondrial Complexes II (SDHa and SDHb) and V (ATP Synthase) WB in Adult TA muscle of 3, 6 12 and 18 months. At three months there is significantly more SDHa in AR20 muscle in comparison to WT or AR100. At 6 months there is significantly less SDHb in AR20 muscle and at 18 months there is significantly less SDHb in AR20 muscle in comparison to WT. Statistical analysis was performed using one-way ANOVA and Tukey's HSD post-hoc test ($n=3$, $p<0.05$). Error bars=SEM

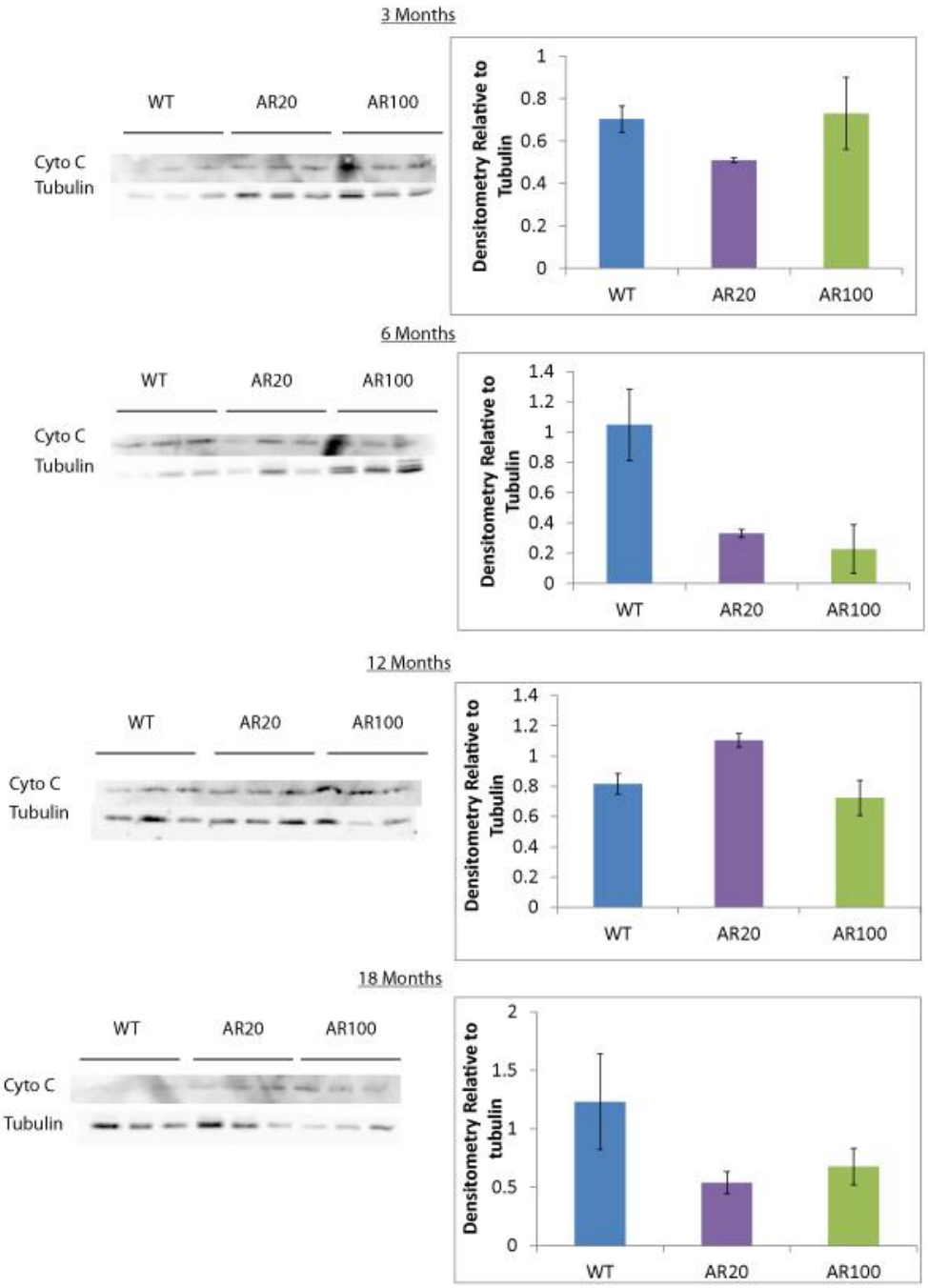

Figure 77 WB analysis of Cytochrome C levels in adult TA Muscle

WB for Cytochrome C in TA muscle Homogenate at pre-symptomatic 3 months of age, symptom onset 6 months, fully symptomatic disease -12 months and disease end stage of 18 months in WT, AR20 and AR100 mice. There are no significant differences between AR20 and AR100 muscle samples Statistical analysis was performed using one-way ANOVA and Tukey's HSD post-hoc test ($n=3$, $p<0.05$). Error bars=SEM

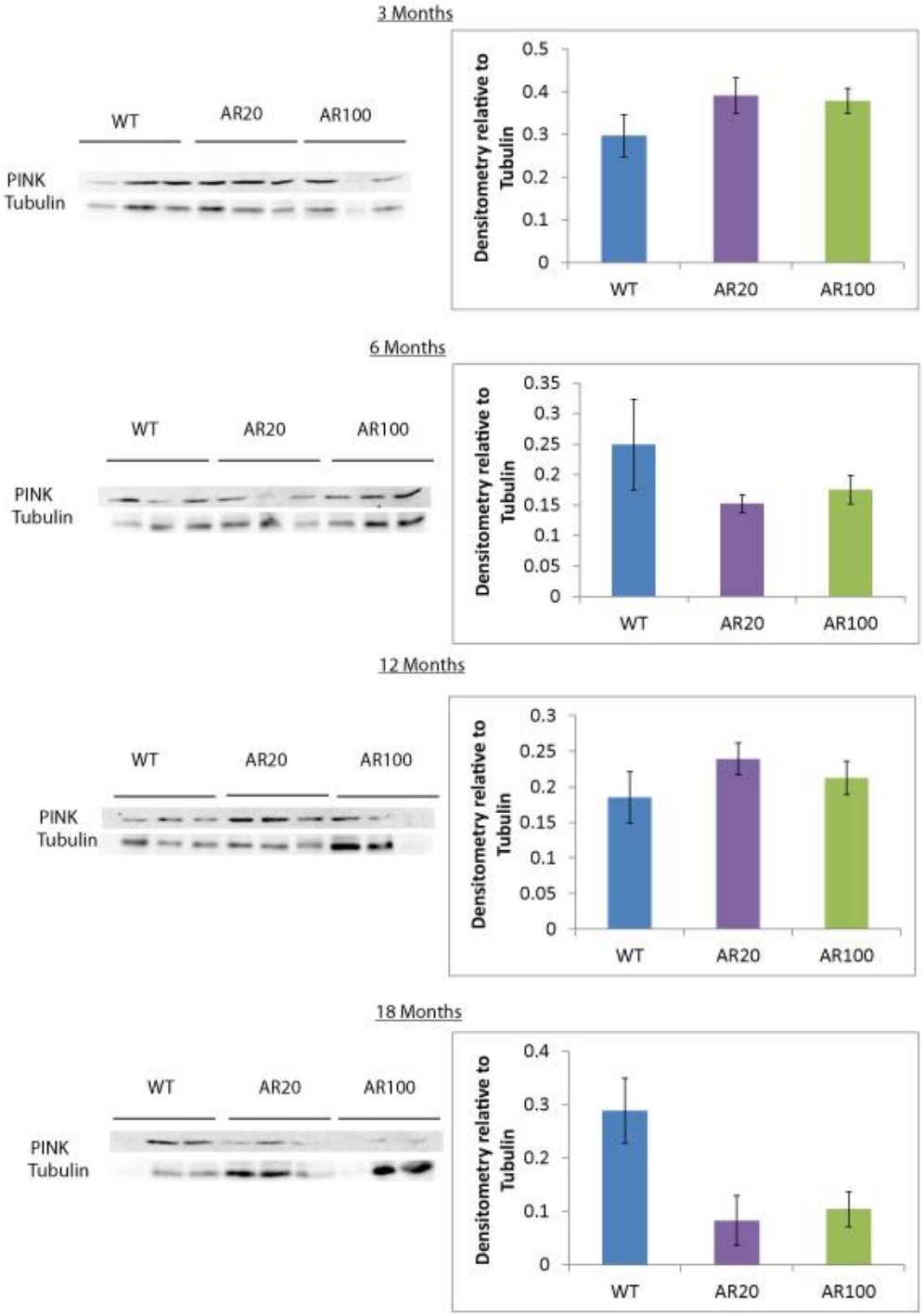

Figure 78 WB Analysis of PINK Protein levels in adult TA muscle

Western Blot Analysis of TA muscle from WT, AR20 and AR100 for PINK. There was no significant difference at all ages in PINK protein expression. Statistical analysis was performed using one-way ANOVA and Tukey's HSD post-hoc test (n=3, $p<0.05$). Error bars= SEM.

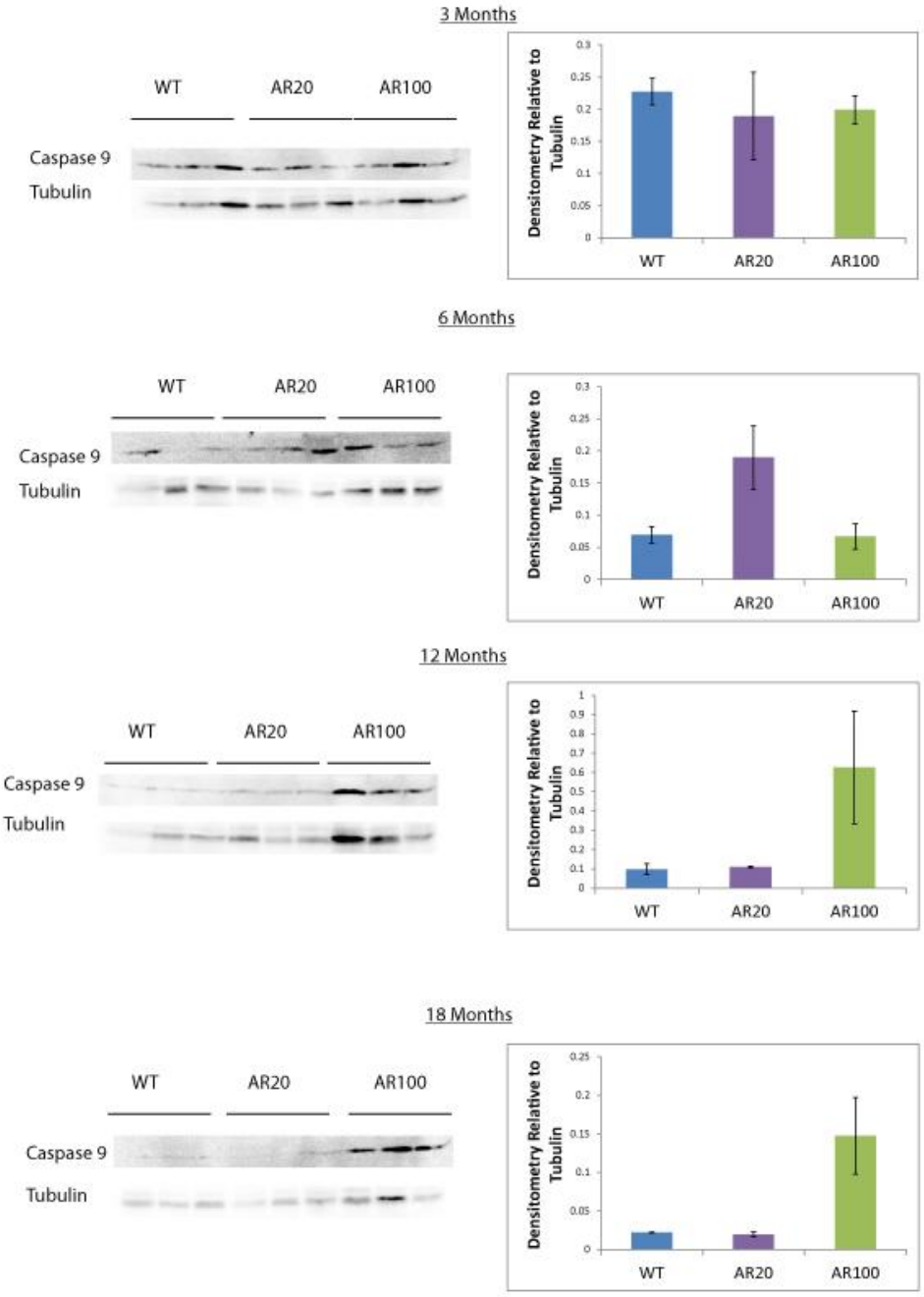

Figure 79 WB analysis of Caspase 9 levels in adult TA Muscle

Western Blot Analysis of TA muscle from WT, AR20 and AR100 for total caspase 9. There was no significant difference at all ages in caspase 9 protein expression. Statistical analysis was performed using one-way ANOVA and Tukey's HSD post-hoc test ($n=3$, $p<0.05$).

4.3.5 Twelve Month Pathway analysis of differential gene expression in AR100 TA muscles

WEB GESTALT and DAVID pathway enrichment was performed on a total of 5962 genes dysregulated in 12 Month AR100 TA muscle in comparison to AR20. Using Go slim analysis the top biological, molecular function and cellular component categories found to be altered were metabolic processes, protein binding and the cell membrane respectively (Figure 80). The top specific pathways identified (for a full list see Appendix III) were pathways in Cancer, where 124 genes were differentially expressed (Figure 81), focal adhesion, where 116 genes were differentially expressed (Figure 82), and MAPK Signalling pathway, where 101 genes were differentially expressed (Figure 83). MAPK signalling was central to the other pathways that were dysregulated, and is highlighted in the relevant figures. Regulation of the actin cytoskeleton pathway showed 97 genes differentially expressed (Figure 84), the Insulin signalling pathway, showed 67 genes differentially expressed (Figure 81) and Protein processing in the ER pathway had 70 genes differentially expressed (Figure 86). The Insulin signalling pathway and ER stress (highlighted in the pathway figures below) were analysed further by Western Blotting.

4.3.6 Eighteen Month Pathway analysis of differential gene expression in AR100 TA muscles

The pathways found to be dysregulated at 18 months in the TA muscles of AR100 mice were broadly the same as those investigated at 12 months of age. A list of the Top 100 dysregulated genes in AR100 TA muscle, compared to AR20 muscle can be found in Appendix I. A list of dysregulated genes compared to AR20 and WT is presented in Appendix II and a full list of dysregulated pathways at 18 months can be found in Appendix III.

Figure 80

A

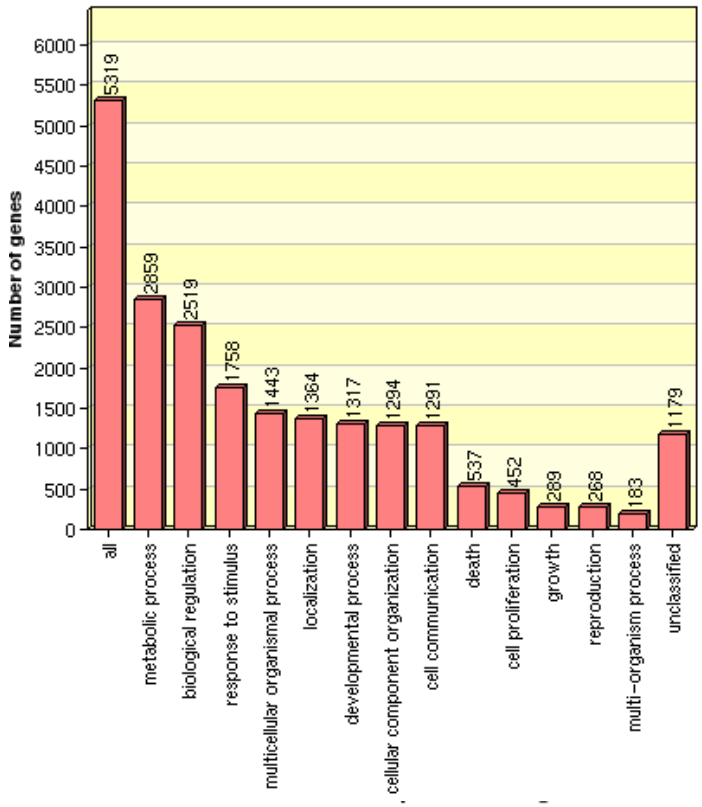
Number of genes
6000
5500
5000
4500
4000
3500
3000
2500
2000
1500
1000
500
0
5319
2859
2519
1758
1443
1364
1317
1294
1291
537
452
289
268
183
1179
all
metabolic process
biological regulation
response to stimulus
multicellular organismal process
localization
developmental process
cellular component organization
cell communication
death
cell proliferation
growth
reproduction
multi-organism process
unclassified

B

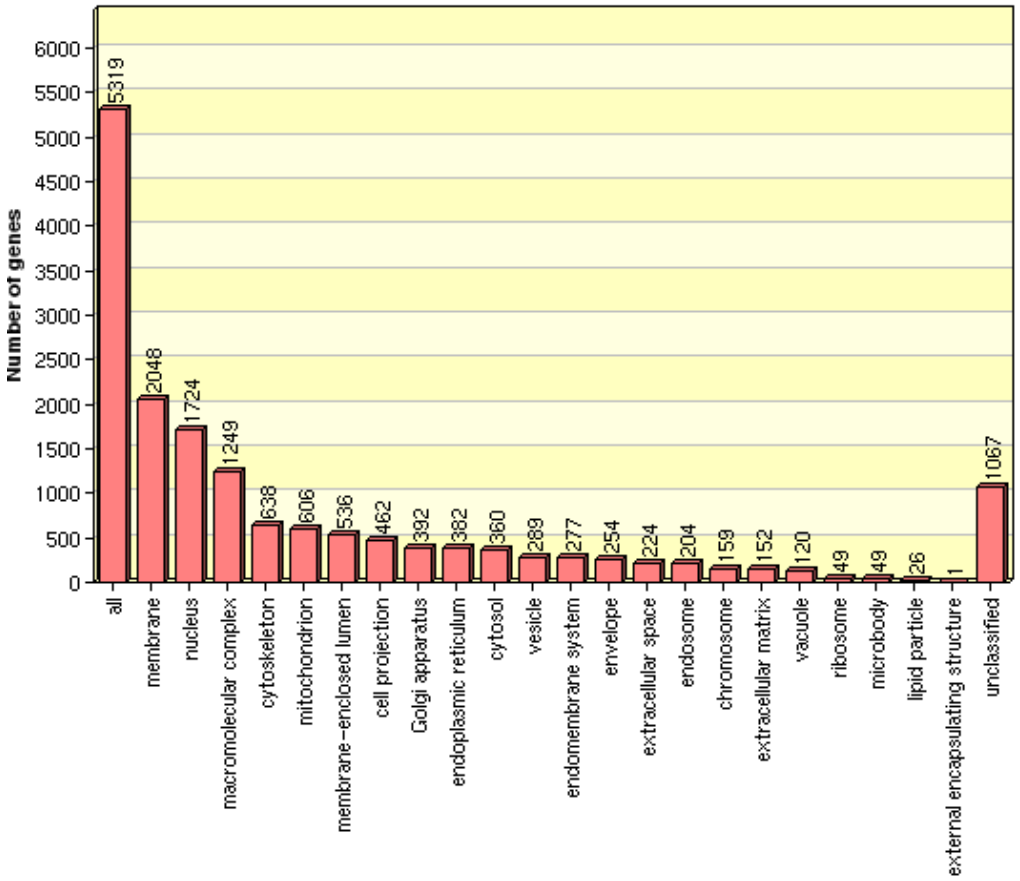
Number of genes
6000
5500
5000
4500
4000
3500
3000
2500
2000
1500
1000
500
0
5319
2048
1724
1249
638
606
536
462
392
382
360
289
277
254
224
204
159
152
120
49
49
26
1
1067
all
membrane
nucleus
macromolecular complex
cytoskeleton
mitochondrion
membrane-enclosed lumen
cell projection
Golgi apparatus
endoplasmic reticulum
cytosol
vesicle
endomembrane system
envelope
extracellular space
endosome
chromosome
extracellular matrix
vacuole
ribosome
microbody
lipid particle
external encapsulating structure
unclassified

C

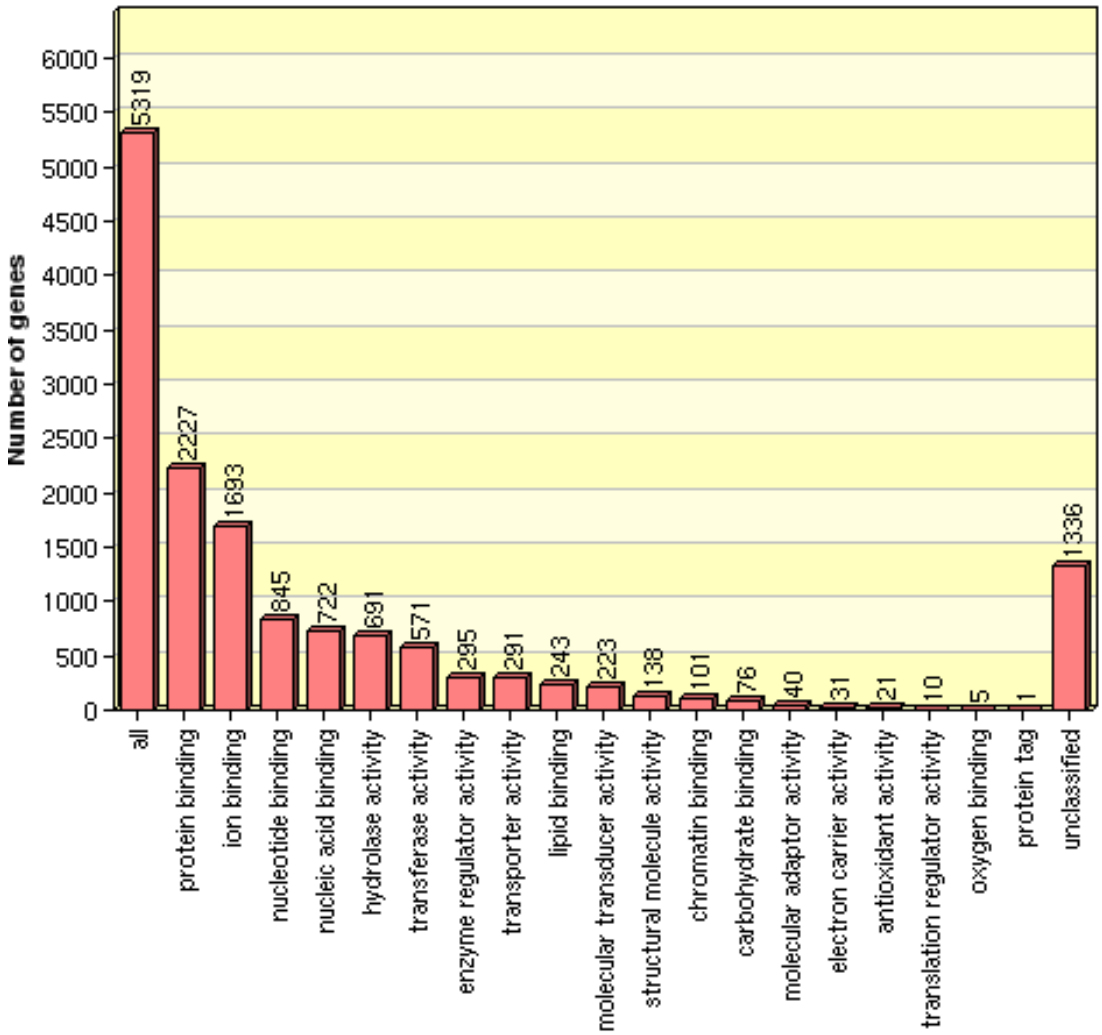

Figure 80 Classification of Altered Genes in 12 Month TA Muscle using Go Slim Analysis

Classification of 5962 genes using Go slim analysis identified **A**) the Biological Process to be most dysregulated as 'Metabolic processes'. **B**) The Molecular function most disturbed was 'Protein binding'. **C**) The Cellular compartment most disturbed was identified as the cell membrane.

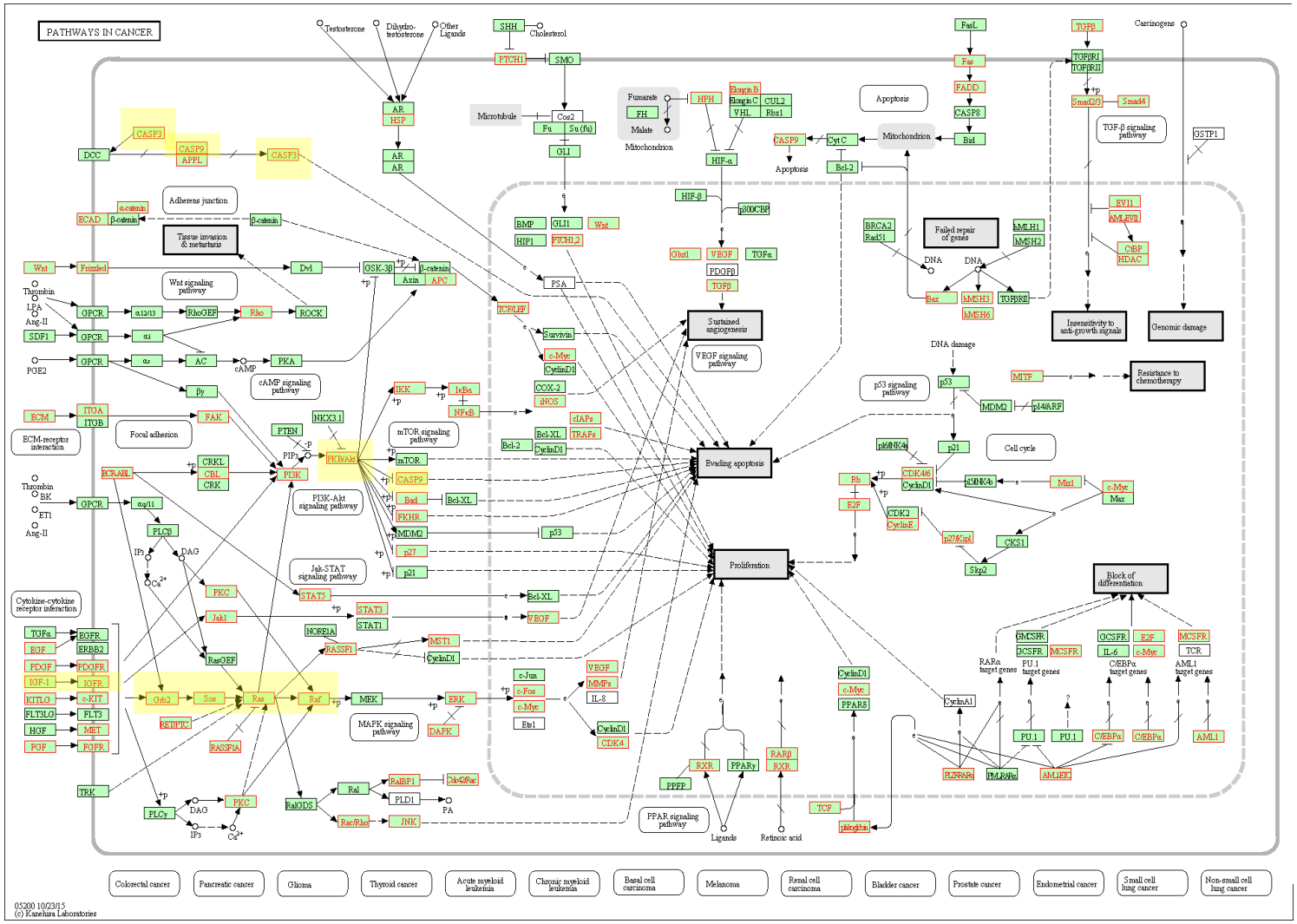

Figure 81 Dysregulated gene expression in TA muscle of 12 month old AR100 mice: Pathways in Cancer

124 genes identified as differentially regulated in 12 Month AR100 muscle, in comparison to AR20 muscle, fell under the category of pathways in cancer. Highlighted in yellow are MAPK signalling and AKT signalling central to multiple KEGG Pathways identified.

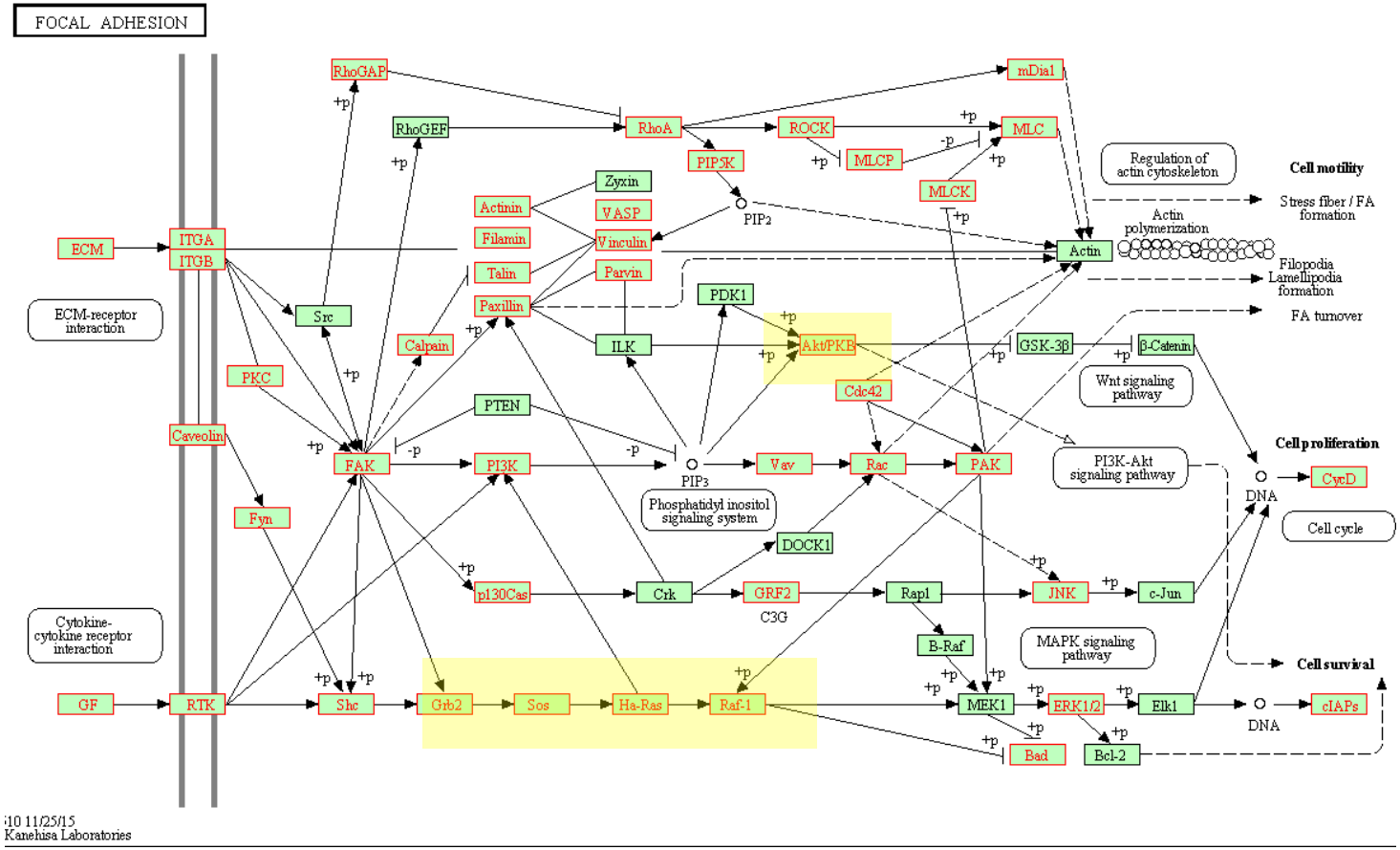

Figure 82 Dysregulated gene expression in TA muscle of 12 month old AR100 mice: Focal Adhesion

116 genes identified differentially regulated in 12 Month AR100 muscle, in comparison to AR20, fell under the category of Focal Adhesion. Highlighted in yellow are MAPK signalling and AKT signalling central to multiple KEGG Pathways identified

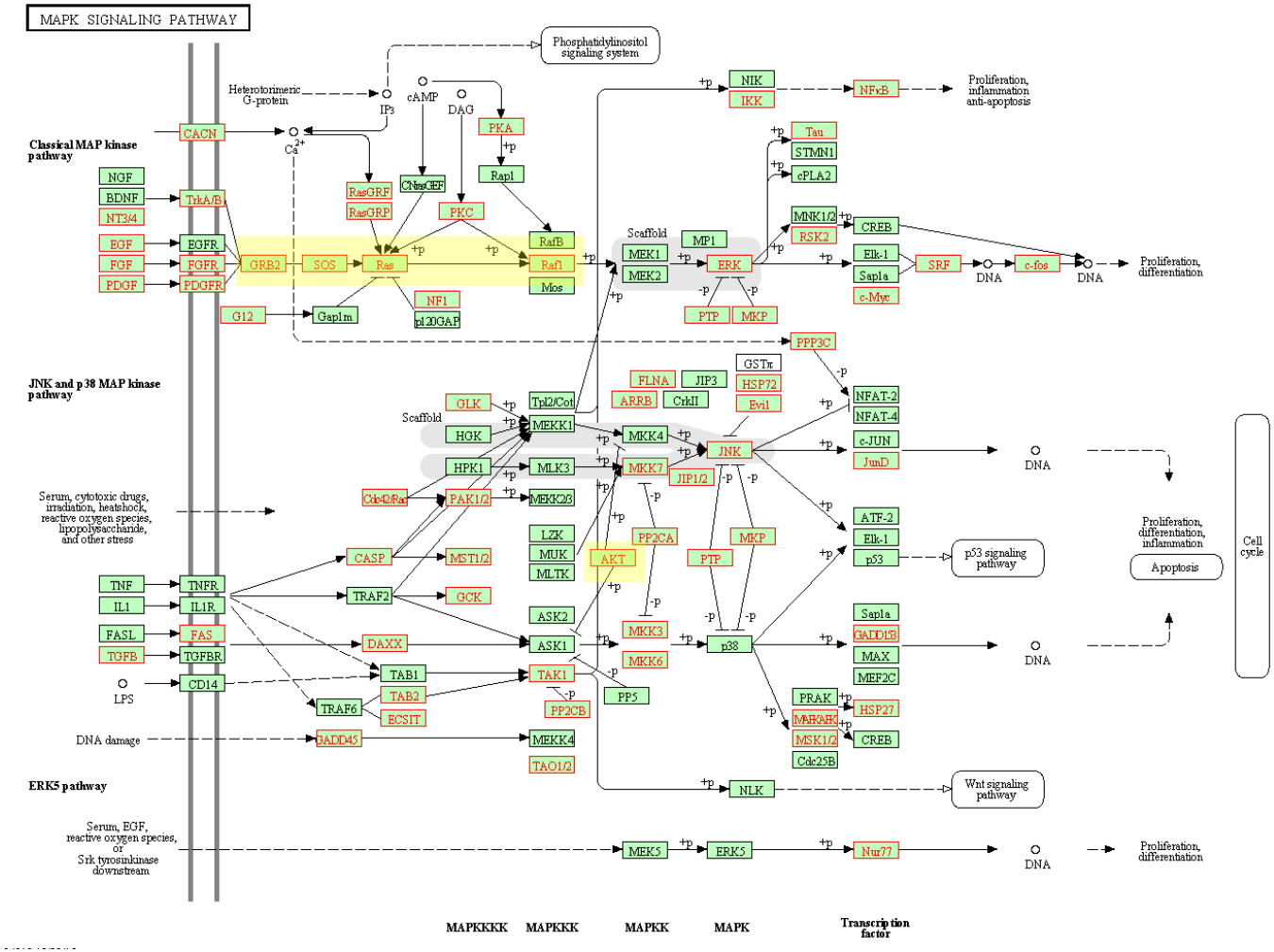

Figure 83 Dysregulated gene expression in TA muscle of 12 month old AR100 mice: MAPK Signalling

101 genes within the MAPK signalling pathway were differentially expressed in the TA muscle of AR100 muscle in comparison to AR20 at 12 months of age. Highlighted in green is the Sos-Ras-Raf component of this pathway, central to many signalling pathways as well as AKT, a key signalling protein in multiple pathways

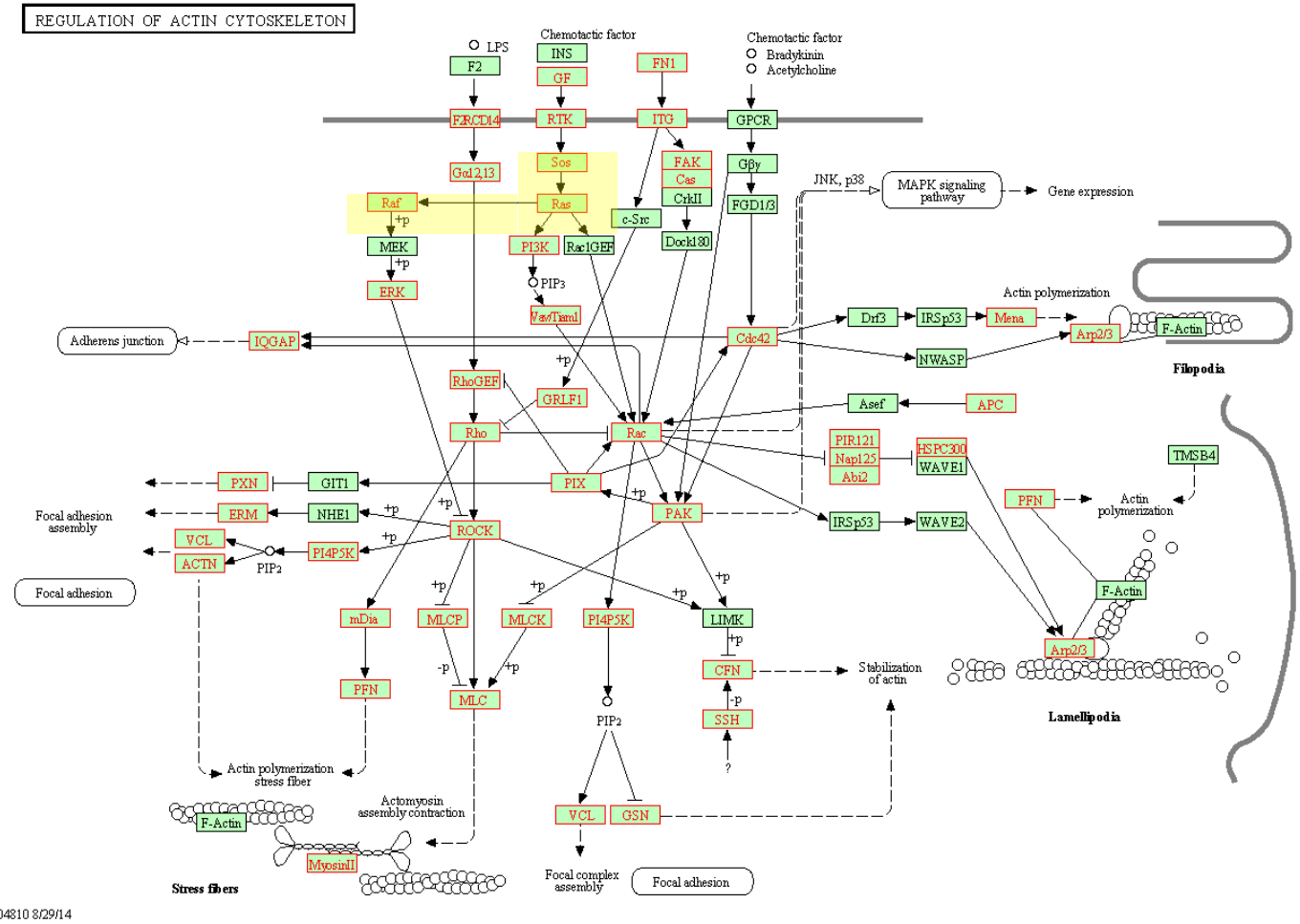

Figure 84 Dysregulated gene expression in TA muscle of 12 month old AR100 mice: Regulation of the actin cytoskeleton

97 genes which have a role in the regulation of the actin cytoskeleton were identified as differentially expressed in 12 month old AR100 TA muscle in comparison to AR20. Highlighted in yellow is the Sos-Ras Raf pathway also a component of MAPK signalling.

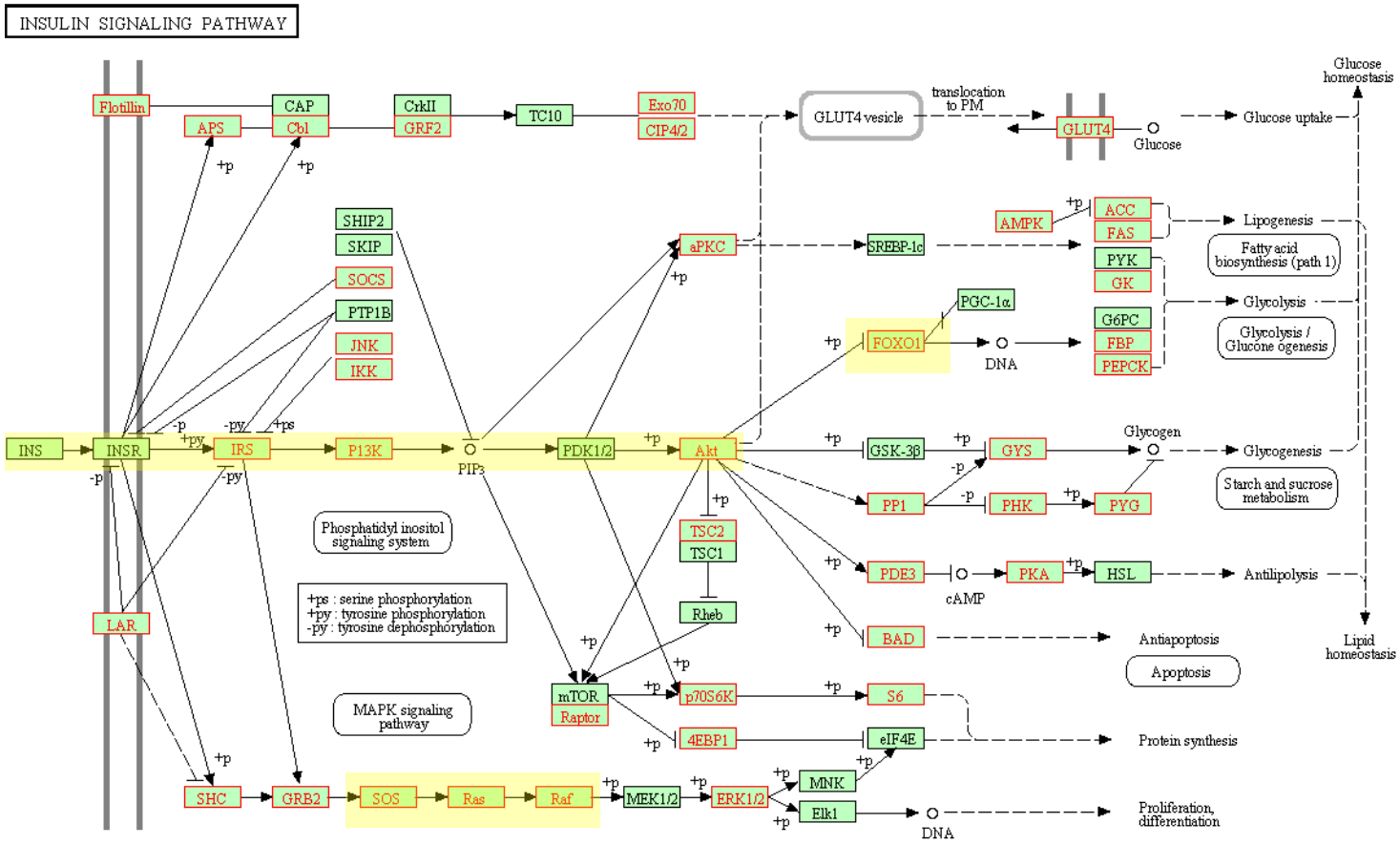

Figure 85

Dysregulated gene expression in TA muscle of 12 month old AR100 mice: The Insulin Signalling Pathway

67 genes with a role of Insulin signalling were found to be differentially expressed in 12 month AR100 muscle in comparison to AR20. Highlighted in yellow is the Sos-Ras Raf pathway, also a component of MAPK signalling, AKT a multifunctional signalling protein and FOXO1, an important mediator of muscle atrophy

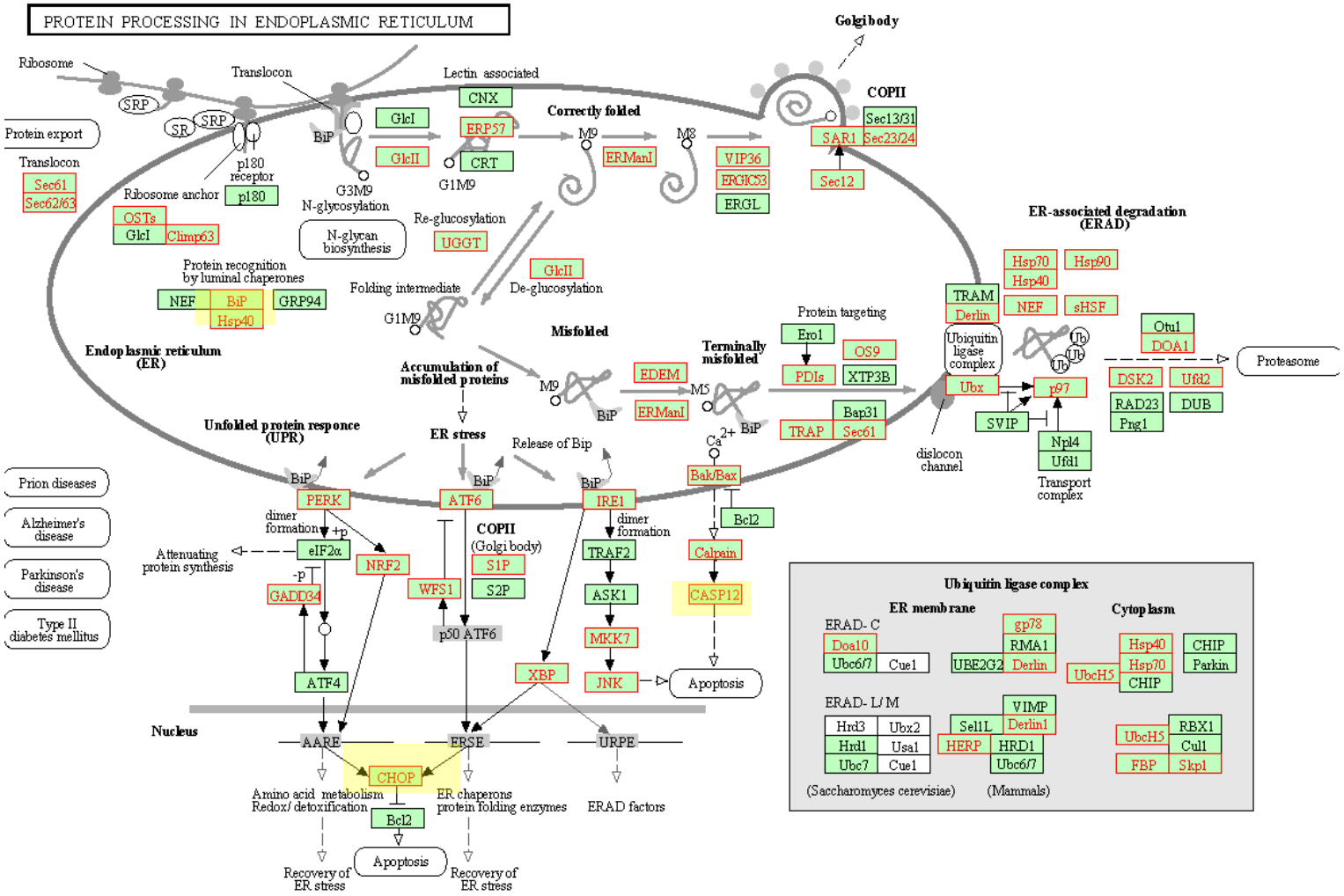

Figure 86 Dysregulated gene expression in TA muscle of 12 month old AR100 mice: Protein Processing in the Endoplasmic Reticulum

70 genes with a role of Protein processing were found to be differentially expressed in 12 month AR100 muscle in comparison to AR20. Highlighted in yellow are the genes I confirmed using WB.

4.3.7 Western blot validation of RNA sequencing pathway analysis of TA muscles of 12 month old AR100 mice.

As a result of the pathway analysis performed on RNA sequencing gene list, the pathways I confirmed at the protein level via Western blotting were the Insulin signalling pathway (Figure 85) and the Protein Processing in the ER (Figure 86), pathways that have previously been implicated to play a role in SBMA pathogenesis (Palazzolo et al., 2009, Montague et al., 2014).

4.3.7.1 IGF-1 Downstream muscle atrophy pathway

Significant differences in protein expression were largely limited to muscles of mice aged 18 months. Western blot analysis of AR100 mouse muscle revealed lower levels of phosphorylated Insulin like growth factor 1 (IGF1) receptor at 18 months (Figure 87). I also observed higher Protein Kinase B (PKB/AKT) levels in AR100 muscle (Figure 88) but lower activated phosphorylated AKT at 18 months of age (Figure 89). Surprisingly differences in Fork head box protein (Fox01) were seen prior to symptom onset, with significantly higher Fox01 levels at 3 months of age. No significant differences were seen in Fox01 levels at symptomatic stages (Figure 90). Western blotting revealed that there was a significantly higher Peroxisome proliferator-activated receptor gamma coactivator 1-alpha (PGC1α) level in 18 month AR100 muscle (Figure 91).

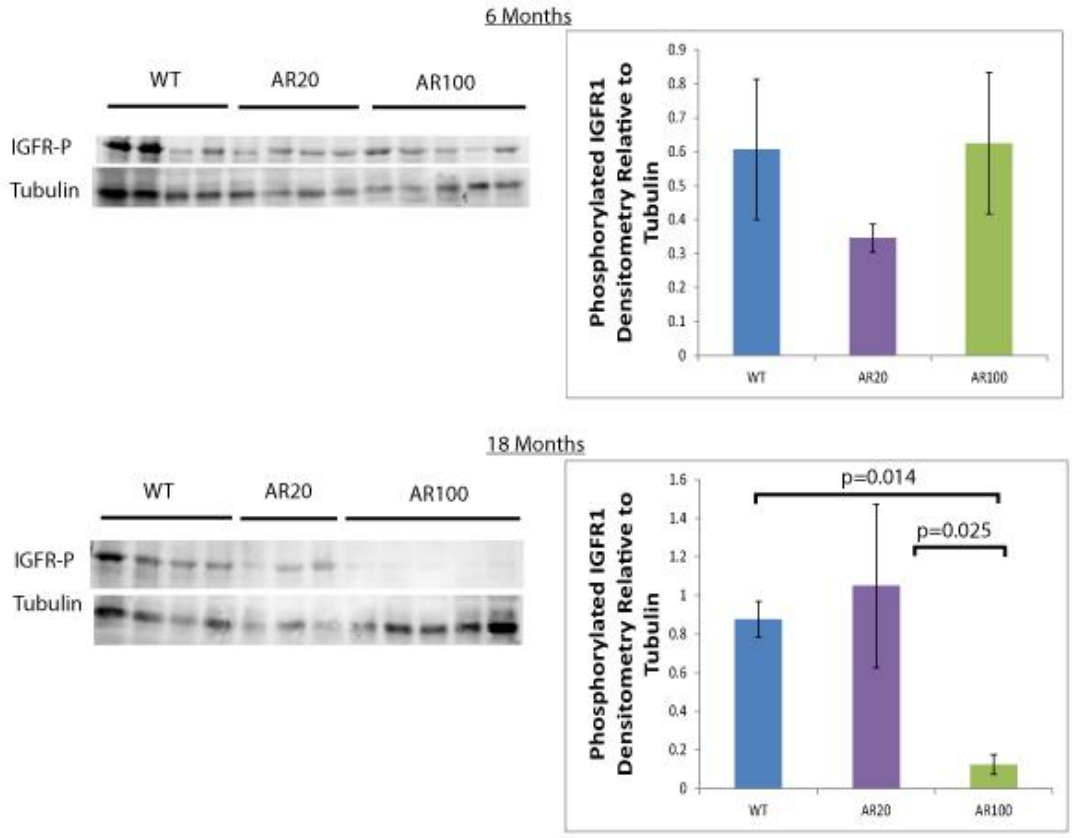

Figure 87 Western Blot analysis of Phosphorylated IGF1 receptor in adult TA muscles of WT AR20 and AR100 mice

WB of TA muscles from AR100 mice shows a significant reduction in the expression level of phosphorylated IGF1 receptor at 18 months. Statistical analysis was performed using one-way ANOVA and Tukey's HSD post-hoc test for 6 month data ($n \geq 3$, $p<0.05$). For 18 months analysis, as there was a non-normal distribution a Kruskall Wallis test was used ($p=0.016$) and post hoc Mann- Whitney U tests ($n \geq 3$; $p=0.014$; $p=0.025$). There is significantly lower phosphorylated IGF1 receptor in AR100 TA muscle at 18 months of age. Error bars = SEM.

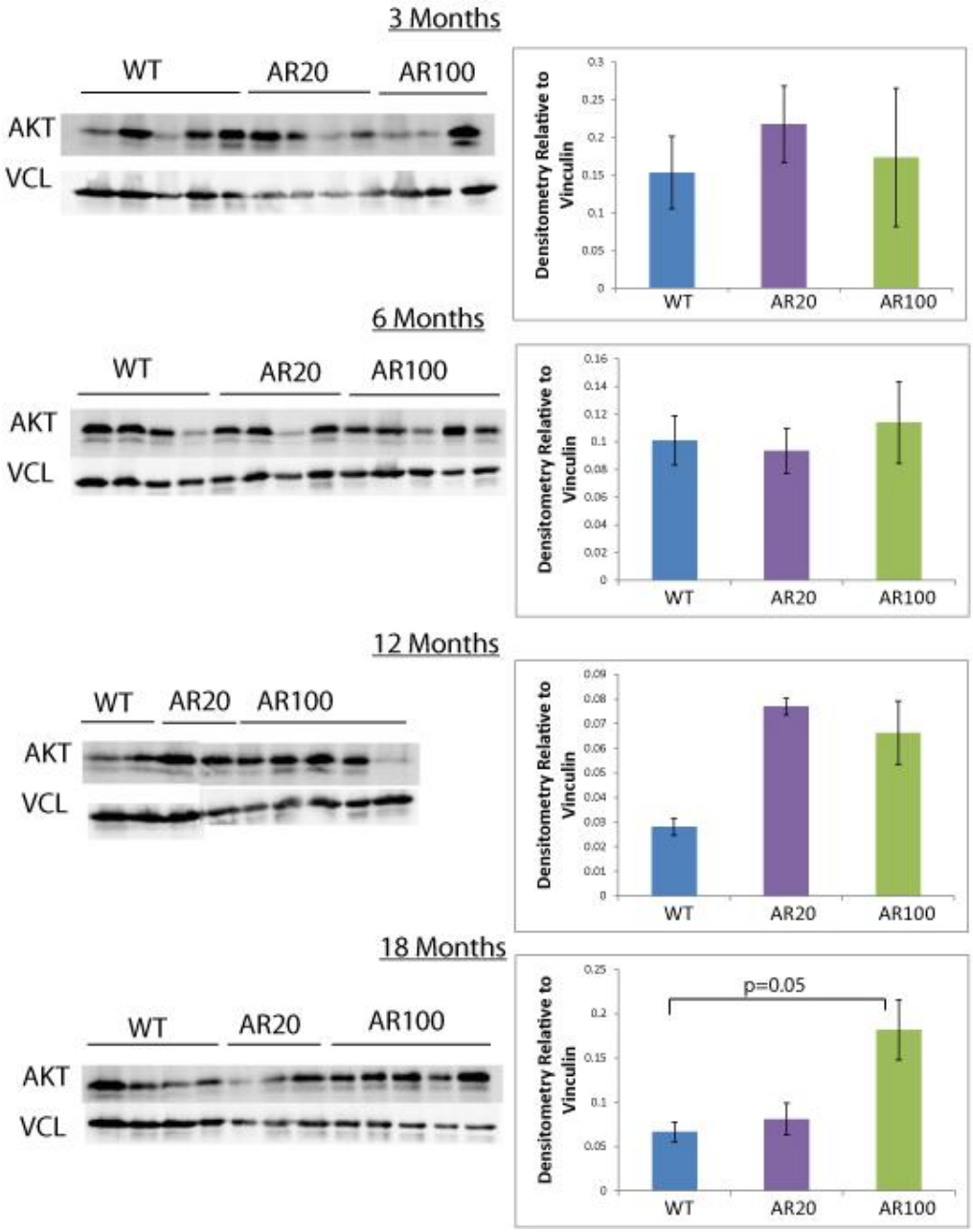

Figure 88 Western Blot Analysis of Total AKT in TA muscles of WT, AR20 and AR100 mice

Western Blot analysis of 3, 6, 12 and 18 month WT, AR20 and AR100 TA muscle for Total AKT. Band densitometry is calculated relative to Vinculin. At 18 months there is a significant increase in Total AKT levels in TA muscles of AR100 mice muscle in comparison to WT mice. Statistical analysis was performed using one-way ANOVA and Tukey's HSD post-hoc test ($n \geq 3$, $p < 0.05$) Error bars= SEM

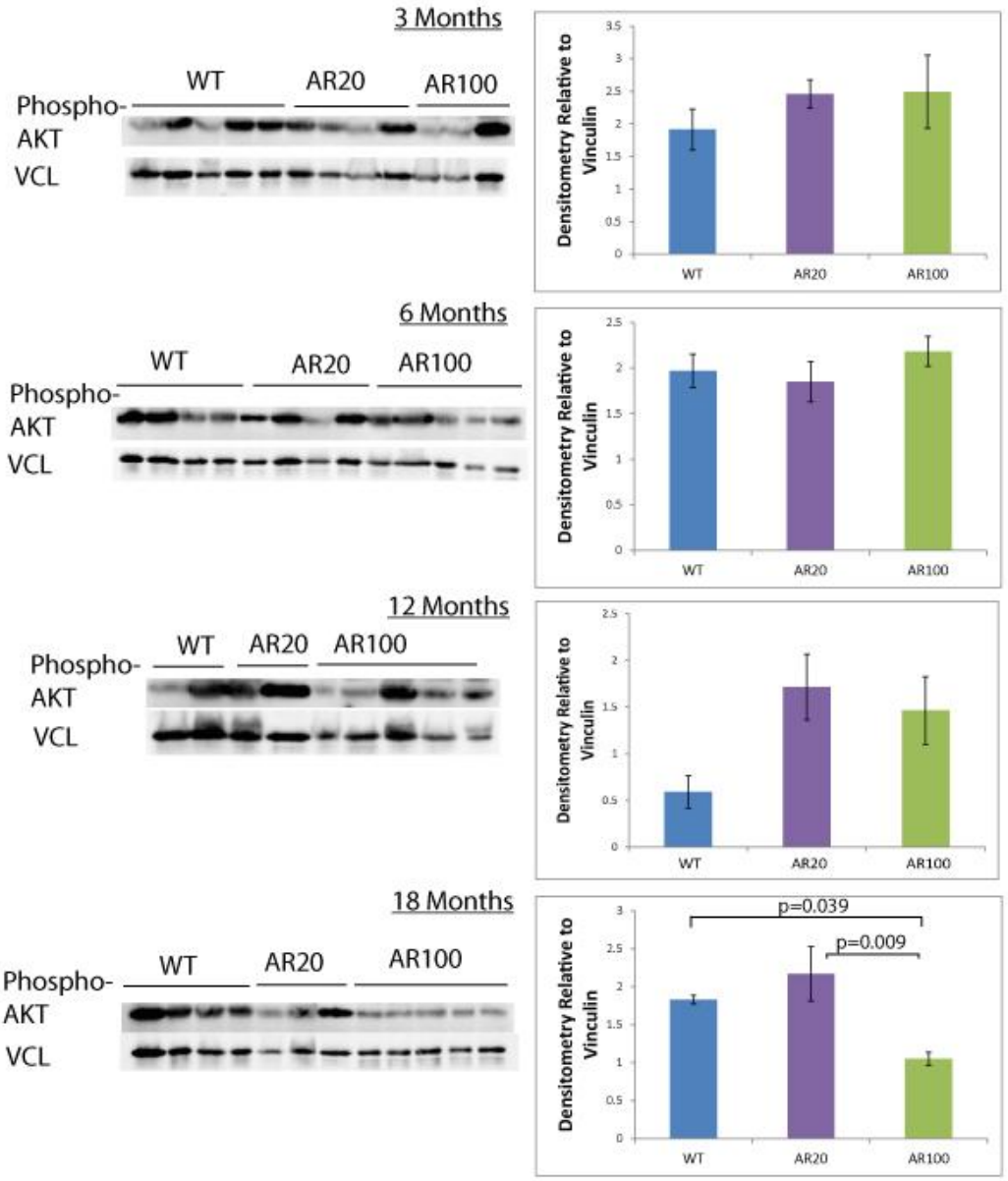

Figure 89 Western Blot Analysis of Phosphorylated AKT in TA muscles of WT AR20 and AR100 mice

Western Blot analysis of 3, 6, 12 and 18 month WT, AR20 and AR100 TA muscle for AKT phosphorylated at Thr 308. Band densitometry is calculated relative to Vinculin. At 18 months there is a significant decrease in Phosphorylated AKT levels in TA muscle of AR100 mice in comparison to WT and AR20 mice. Statistical analysis was performed using one-way ANOVA and Tukey's HSD post-hoc test ($n \geq 3$, $p < 0.05$). Error bars= SEM

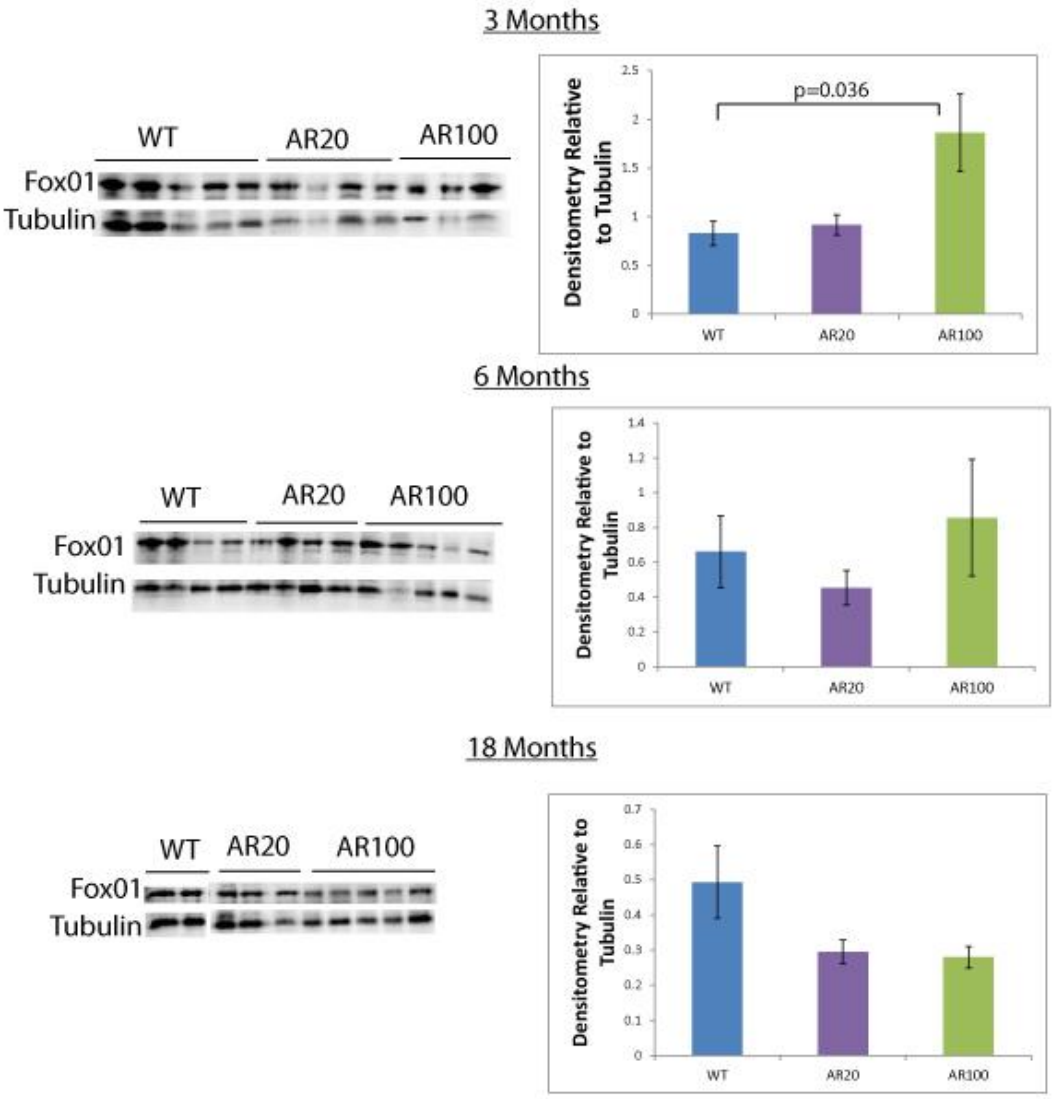

Figure 90 WB Analysis of Fox01 in AR100 mouse TA muscle

Western Blot and densitometry analysis of Fork head box protein O1 (Fox01) levels in the TA muscle of WT, AR20 and AR100 mice. There is a significantly higher Fox01 level in TA muscles of AR100 mice in comparison to WT mice at 3 months of age. Statistical analysis was performed using one-way ANOVA and Tukey's HSD post-hoc test (n=3, $p<0.05$). Error bars= SEM

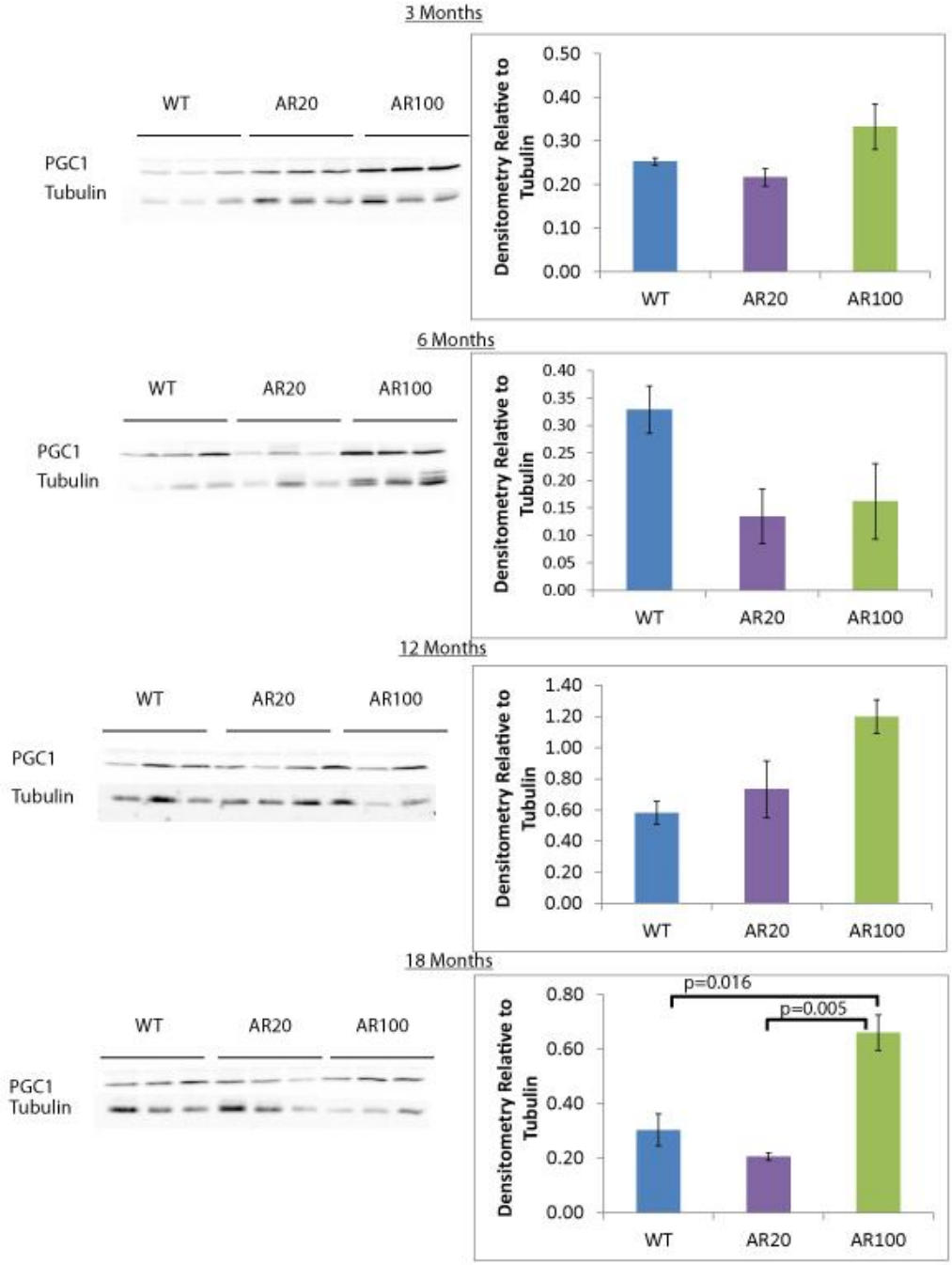

Figure 91 WB Analysis of PGC1 α in TA Muscles of WT, AR20 and AR100 mice

Western Blotting for PGC1 α in TA muscles in 3, 6, 12 and 18 month old WT, AR20 and AR100 mice. There is a significant increase in PGC1 α expression in TA muscles of AR100 mice at 18 months. Statistical analysis was performed using one-way ANOVA and Tukey's HSD post-hoc test (n=3, $p<0.05$). Error bars= SEM.

4.3.7.2 Analysis of the ER stress pathway in TA muscle of AR100 mice

I was lastly interested in the KEGG 'protein processing in the ER' pathway identified by WEB GESTALT and DAVID as being significantly changed in muscle of AR100 mice. Additionally, ER stress related pathways in motor neurons were examined in vitro and in the spinal cord of AR100 mice in Chapter 2. Although this pathway is significantly dysregulated at the RNA level, I found no significant difference in the ER stress marker BiP until 18 months of age (Figure 92), when there was a significant decline in BiP. Furthermore ER stress mediated apoptotic proteins such as CHOP, (Figure 93 A) cleaved caspase 12 (Figure 93 B) and cleaved caspase 3 (Figure 93 C) were undetectable via western blot. It was therefore not possible to determine whether this pathway was altered in AR100 mouse muscle.

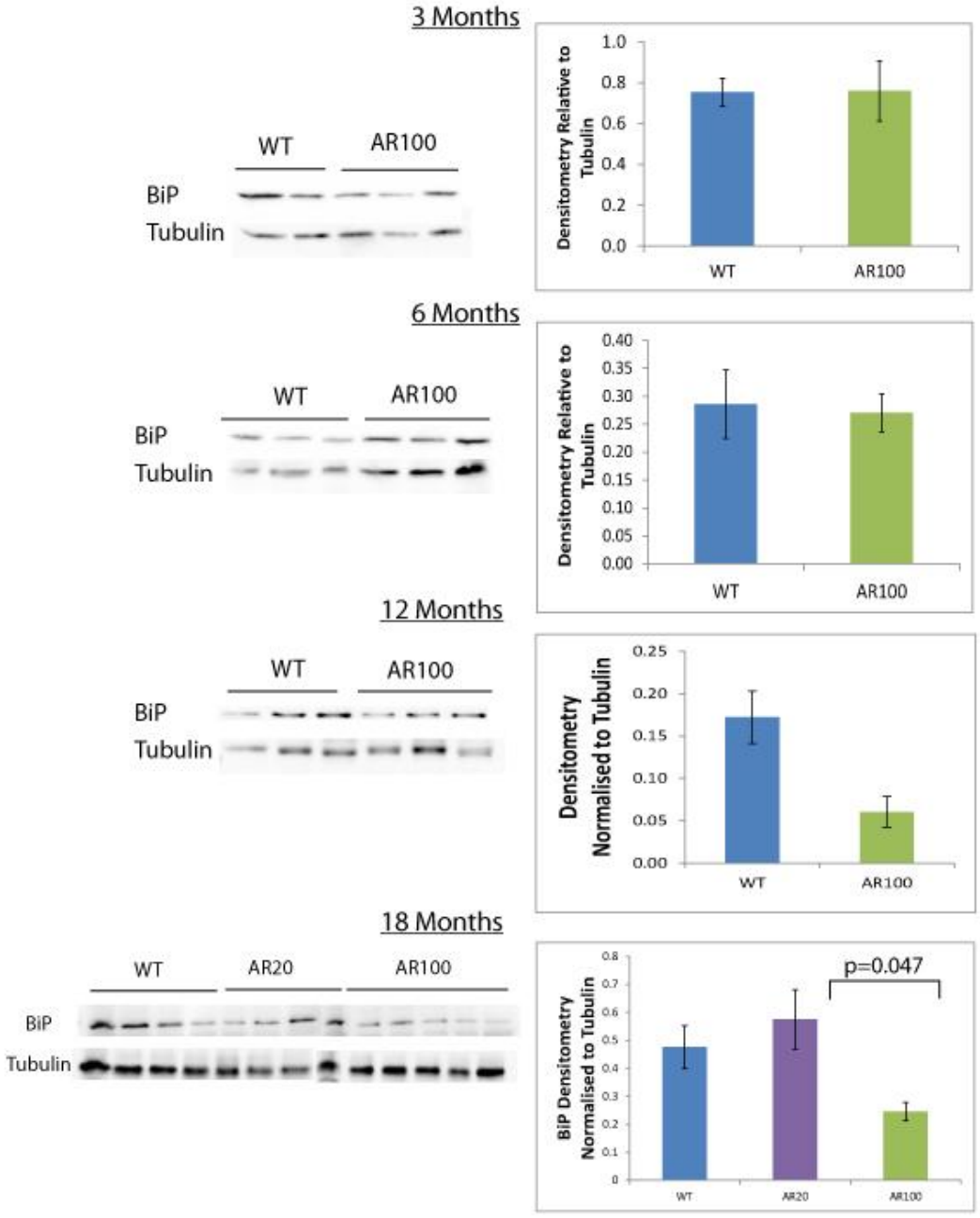

Figure 92 BiP Expression in TA Muscles of WT, AR20 and AR100 mice

WB and densitometry analysis of BiP expression in the TA muscles of WT, AR20 and AR100 mice at 3, 6, 12 and 18 months of age. There is a significant decline in BiP protein expression in the TA of AR100 mice. Statistical analysis was performed using one-way ANOVA and Tukey's HSD post-hoc test ($n \geq 3$, $p < 0.05$). Error bars=SEM.

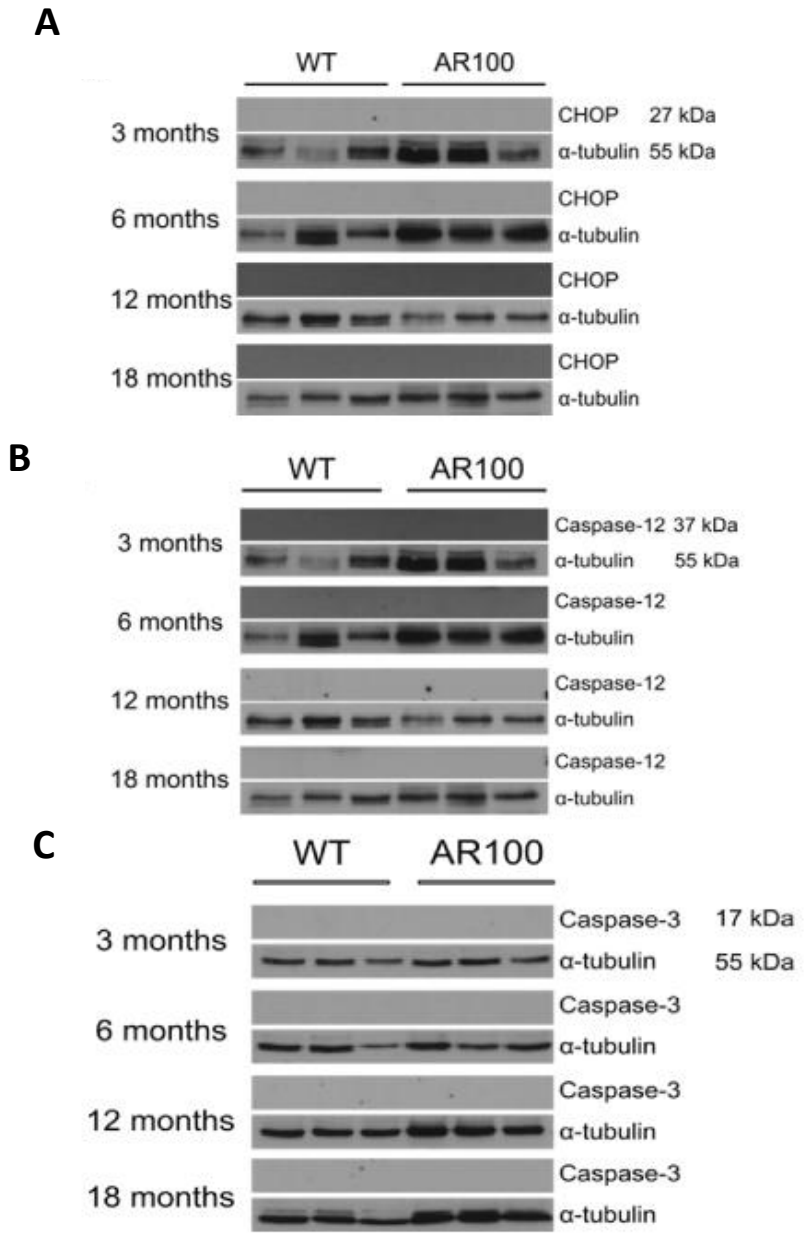

Figure 93 WB analysis of ER stress induced cell death markers in TA muscles of WT and AR100 mice

Western Blot Analysis of TA muscle from WT and AR100 mice for **A)** CHOP, **B**) Activated Caspase 12 and **C)** Activated caspase 3. All three western blots were negative for the expression of these cell death markers. Western blots performed by MSc Student Marta Budzinska under my co-supervision.

4.4 Discussion

In this Chapter I carried out RNA sequencing analysis of AR100 muscle as well as pathway analysis enrichment in order to determine the underlying molecular causative changes in SBMA. I then performed western blot analysis of AR100 mouse TA muscle to identify if the changes seen at the RNA level were reflected at the protein level. The key themes of investigation were Myogenic Regulatory factors, Oxidative phosphorylation, Insulin like growth factor signalling, MAPK signalling and Protein processing within the ER. As summarised in Table 10, largely no significant differences at the protein level were observed. It was not until disease end stage that statistically significant changes were detected in MyoD, Myogenin, Phosphorylated IGFR-1, AKT, phosphorylated AKT, PGC1α and BiP.

4.4.1 There are no significant changes in MyoD and Myogenin expression until disease end stage in TA muscles of AR100 mice

I began by western blotting for two candidate proteins which have been shown to be key regulators of muscle homeostasis (Park et al., 2013, Galbiati et al., 2012, Mielcarek et al., 2015). I found that there was no significant difference in MyoD levels in the TA until 18 months of age, when MyoD levels decreased in muscles of AR100 mice (Figure 62). Furthermore, analysis of myogenin levels showed a significant decrease in AR100 TA in comparison to WT TA muscles (Figure 63). This suggests that changes in myogenic regulatory factors such as MyoD and myogenin are unlikely to play a causative role in SBMA. However, it has previously been shown that MyoD mRNA levels are increased in the muscle of the knock-in model of SBMA (Yu et al., 2006). However, this study did not quantify levels of myogenin protein. I have found using RNA sequencing, discussed below, that MyoD has down-regulated RNA levels at 12 months of age, whereas myogenin is up-regulated at 12 and 18 months in AR100 mouse TA muscle. This shows that changes at the mRNA level are not always mirrored at the protein level.

Table 10 Summary of Significant Changes in WB marker expression in AR100 TA muscle

	Age			
Marker	3 Months	6 Months	12 Months	18 Months
MyoD	NA	■	■	▼
Myogenin	■	■	■	▼
SDHa	▼	■	■	■
SDHb	■	▲	■	■
Cytochrome C	■	■	■	■
PINK	■	■	■	■
Caspase 9	■	■	■	■
Phospho-IGFR-1	NA	■	NA	▼
AKT	■	■	■	▲
Phospho-AKT	■	■	■	▼
Fox01	▲	■	NA	■
PGC1α	■	■	■	▲
BiP	■	■	■	▼
CHOP	NA	NA	NA	NA
Caspase 12	NA	NA	NA	NA
Caspase 3	NA	NA	NA	NA

Key	
Change	**Symbol**
Increased	▲
Decreased	▼
Unchanged	■
Unknown	NA

4.4.2 Abnormal Oxidative phosphorylation is an early pathogenic feature of SBMA muscle

RNA Sequencing and pathway enrichment analysis revealed the electron transport chain as a site of significant dysregulation at 3 months in AR100 mouse TA muscle (Figure 69), a pre-symptomatic stage in the AR100 mouse model of SBMA. Thus this change may play a causative role in the pathology of SBMA. To date there has been

limited focus on mitochondrial function in SBMA (Finsterer et al., 2015). Interestingly in 1999, the first pathogenic mechanism in SBMA proposed, was linked to mitochondria (Stenoien et al., 1999). This study showed that polyQ aggregates sequestered mitochondria within inclusions. This lead to the conclusion that the process of aggregate formation is highly energy consuming (Stenoien et al., 1999). It has also been shown that the formation of AR aggregates within the cytoplasm can disrupt mitochondria distribution (Piccioni et al., 2002). Additionally, it has been shown that AR, in its mutated form, interacts differently with cytochrome C oxidase. Upon the addition of ligand, WT AR forms stronger associations with cytochrome C oxidase subunit Vb therefore further highlighting mitochondrial disruption as a cause of pathology (Beauchemin et al., 2001). Recently, it has been reported by Ranganathan and colleagues that there are mitochondrial abnormalities in neuronal cell lines expressing polyQ AR, as shown by a depolarised mitochondrial membrane potential and an increase in mitochondrial apoptosis marker caspase 9 (Ranganathan et al., 2009). They additionally confirmed that the AR associates with mitochondria with polyQ AR forming a greater association.

To date, mitochondrial involvement in SBMA muscle has not been extensively studied. However, at the protein level, I did not find that there was a significant difference in mitochondrial- related proteins. Components of complex II, SDHa and SDHb were only significantly different to WT in the non-pathogenic AR20 mouse TA. Furthermore, analysis of proteins associated with mitochondrial homeostasis, such as cytochrome C and PTEN-induced kinase 1 (PINK), a marker of mitophagy, were also unchanged in AR100 muscle, although Cytochrome C and PINK were reduced in AR20 and AR100 muscles at 18 months, compared to WT (Figure 77 and Figure 78). There was a clear increase in caspase 9 expression in AR100 muscle at 12 and 18 months. However, this was not statistically significant (Figure 79). Surprisingly, there were a few differences at the protein level for any of the candidates assessed at 3 months, although this may have been due to the inherit variability within the technique, or the ability of RNA sequencing to detect more subtle changes in expression.

Despite the absence of significant changes in mitochondrial related pathways at the protein level, targeting mitochondria as a therapeutic strategy should still be considered. Indeed, in the AR97Q mouse model of SBMA, the drug Pioglitazone which acts by stimulating mitochondrial biogenesis has been shown to decrease cytotoxicity (Iida et al., 2014).

4.4.3 MAPK signalling is a fundamental component of disease in SBMA muscle at symptomatic stages

Although a number of pathways are dysregulated in the TA muscles of AR100 mice TA, a central component of these pathways is oxidative phosphorylation (Figure 68 to Figure 71) and MAPK signalling (Figure 81 to Figure 85), which underpin most, if not all of these pathways. The MAPK signalling pathway provides an interesting point for further investigation, as it is a component of many regulatory pathways. Genistein has been shown to disrupt p44/p42 MAPK causing dissociation of AR from one of its co-regulators and treatment with Genistein has been shown to be beneficial in AR-97Q mice, increasing motor capability and increasing survival (Qiang et al., 2013).

4.4.4 IGF-1 downstream pathways in AR100 mouse muscle

Results from RNA sequencing and pathway analysis revealed that the Insulin signalling pathway may be affected in AR100 mouse muscle (Figure 85). The Insulin signalling pathway is also activated by Insulin like Growth factor 1 (IGF1). In Chapter 3, I found that there is a decreased frequency of IGF-1 positive muscle fibres in the AR100 muscle at 12 months of age. Western blot analysis showed that at disease end stage there was clear involvement of IGF-1 associated pathways. Not only was there a significant decrease in the activated form of the IGF-1 receptor, as quantified by western blot (Figure 87), but there was a significant increase in a component of this signalling pathway- Protein Kinase B (PKB/AKT), (Figure 88), although its activated form was significantly decreased (Figure 89). The increased AKT in its dormant state could perhaps be compensatory for the fact that there are lower levels of phosphorylated Akt. It has been shown that AKT and the AR directly

interact with AKT, phosphorylating the AR and reducing ligand binding in motor neuron like cell lines (Palazzolo et al., 2007).

Interestingly, there was no significant difference in levels of Fork head box protein O1 (Fox01) at symptomatic stages, yet at very early pre-symptomatic in the AR100 mice, there were significantly higher levels of Fox01 in AR100 mouse muscle at 3 months (Figure 90). Fox01 could therefore play a role in SBMA pathology, as there are significant changes in its protein levels prior to symptom onset. As Fox01 has a major role in muscle homeostasis (Bentzinger et al., 2013), this could be highly relevant in SBMA pathogenesis. Evidence presented in this Chapter suggests that Fox01 is working in an IGF-1 independent manner. Downstream in the Insulin signalling pathway is the key mitochondrial regulation transcription factor, Peroxisome proliferator-activated receptor gamma co-activator 1-alpha (PGC1α). I found that there were significantly higher PGC1α levels at 18 months of age in the AR100 mouse TA muscle by analysis with WB (Figure 91). In contrast to results presented in this Chapter, it has been previously shown that PGC1β is reduced in the knock in mouse model of SBMA but there was no change in PGC1α (Ranganathan et al., 2009).

Despite the western blot analysis indicated that IGF-1 downstream proteins are only significantly changed at disease end stage, in other mouse models of SBMA, it has been shown that targeting IGF-1 signalling has beneficial effects (Palazzolo et al., 2009). Indeed, a clinical trial in SBMA patients evaluating the effect of IGF-1 treatment using a Novartis drug known as BVS857 is currently underway.

4.4.5 ER stress in AR100 mouse muscle

The final pathway of interest in this study was the 'protein processing in the endoplasmic reticulum' identified to be dysregulated by RNA sequencing and pathway analysis (Figure 86). As I had studied ER stress related pathways in Chapter 2, it was of particular interest to analyse the involvement of ER stress regulating proteins in muscle as both my results and previous work in the Greensmith had

mainly focused on ER stress in primary motor neurons and the spinal cord as a cause of pathology in SBMA (Montague et al., 2014).

Western blot analysis of AR100 mouse muscle showed that there was no significant difference in the ER chaperone BiP until 18 months of age (Figure 92), when protein levels were significantly reduced. Levels of BiP increase upon ER stress as it is responsible for sensing a state of 'overload' within the ER (Hetz and Mollereau, 2014). Furthermore, is has been shown in the AR97Q model of SBMA that BiP levels rise in the muscle and co-localised with the AR (Yang et al., 2013). This surprising decline in BiP protein may be a result of the muscles inability to regulate protein synthesis at this late stage of disease. Further analysis of ER stress regulating proteins was largely inconclusive as levels of CHOP, active Caspase 12 and Caspase 3 could not be detected using WB of whole muscle lysate (Figure 93). Although these models could not be quantified using WB the more sensitive methods of RNA sequencing and pathway analysis has identified this pathway as dysregulated in AR100 mouse muscle at the RNA level.

4.4.6 Summary

In this Chapter I have identified candidate pathways for future investigation into the pathogenic mechanisms within the muscle of SBMA. RNA sequencing and pathway analysis were more sensitive at identifying candidates for future investigation. Western blot analysis largely agreed with the results of RNA sequencing and pathway analysis, however changes in blot densitometry were often not significant until 18 months of age. The key pathways of future interest for SBMA pathology identified from the results presented in this Chapter are Oxidative phosphorylation, shown to be dysregulated early in disease pathogenesis, as well as pathways such as MAPK signalling and IGF-1 signalling which are clearly dysregulated later in disease pathogenesis.

Chapter 5 Conclusion

Conclusion

In this Thesis I have studied the pathophysiology of SBMA muscle and spinal cord using the AR100 mouse model. I have worked on primary MNs to investigate cell death, I have provided an in depth analysis of AR100 mouse muscle and I have used RNA sequencing techniques to propose molecular pathways that may underpin pathogenesis in the muscle of SBMA.

5.1 Cell death pathways characterised in ALS MNs are not broadly relevant in SBMA

I began by investigating the Fas/NO cell death pathway previously demonstrated to signal MN death in a more severe model of MND- the mtSOD1 mouse models of ALS (Bernard-Marissal et al., 2012). These authors found that in primary MNs and the spinal cord of mtSOD1 mice there was a reduction in the ER chaperone Calreticulin (CRT). They observed that treatment of primary MNs with cell stressors, DetaNONOate (an NO donor) and sFasL, lead to a decrease in CRT causing ER stress and eventual apoptosis. As the AR100 mouse model had previously been demonstrated to show evidence of ER stress within the spinal cord and in primary MN culture (Montague et al., 2014), I examined whether this pathway also played a role in MN death in SBMA.

Using both manual and automated cell counting techniques I did not observe an increased vulnerability of AR100 MNs to any cell stressors tested- Thapsigargin, DetaNONOate or sFasL. This is surprising, particularly in regard to Thapsigargin, as AR100 primary MNs have already been reported to show ER stress in the Greensmith lab (Montague et al., 2014). The lack of a significant difference seen between WT and AR100 MNs could be due to SBMA being androgen dependent. As I did not observe a change in the localisation of the AR in response to Dihydrotestosterone (DHT) treatment, this may be the underlying cause of the lack of difference observed *in vitro*.

I therefore attempted to validate my cell counting techniques using $SOD1^{G93A}$ MNs. I found no significant difference between WT and $SOD1^{G93A}$ MNs in all measures of cell survival. However, there was a clear variability in cell counts in these experiments, irrespective of genotype. This variability may have masked any underlying differences in cell survival between WT and SBMA MNs. This has led me to question the applicability of assessing MN cell survival using *in vitro* cell counting techniques. Additionally MN death is actually a late stage occurrence in MNDs, and perhaps MN dysfunction plays a more fundamental role in pathology. It may be more applicable to assess primary MNs using more sensitive techniques. For example, it has been shown that AR100 primary MNs show evidence of Ca^{2+} mishandling (Montague et al., 2014), and changes in mitochondrial membrane potential (K. Montague, PhD Thesis 2012).

To further investigate the possible involvement of the pathway proposed by Bernard-Marissal et al. (2012), I went on to analyse levels of CRT in primary MNs as well as in the spinal cord of both SBMA and ALS model mice. I was able to replicate some of the results reported in Bernard-Marissal et al. (2012), with a reduction in CRT expression in $SOD1^{G93A}$ primary MNs in comparison to WT. However, I also found a significant reduction in baseline CRT levels in $SOD1^{G93A}$ MNs, independent of any exogenous stressor treatment. This suggests CRT may have a role in $SOD1^{G93A}$ MNs independent of the Fas/NO pathway. I also investigated the levels of CRT in the AR100 mouse. In spinal cords I found an increase in CRT in SBMA mice in comparison to WT mice at postnatal day 5. Interestingly, this is the opposite change to that reported to Bernard-Marissal et al. (2012) in mtSOD1 mice. It may be the case that in AR100 MNs, an increase in CRT is detrimental to the viability of primary MNs, as this has also been reported in HeLa cells (Nakamura et al., 2000). Alternatively, as CRT has many other ER- independent roles (Gold et al., 2010), it may be possible that the increase in CRT observed may actually be compensatory, particularly as CRT has been shown to play a role in AR receptor export from the nucleus (Dedhar et al., 1994, Nguyen et al., 2009). As a significant increase in CRT in AR100 spinal cords was observed at P5, it is possible that CRT has a role in delaying pathology early in development.

Taken together, these results show that it is not possible to extrapolate the Fas/NO cell death pathway in $SOD1^{G93A}$ MNs to AR100 MNs. This pathway is likely to be a highly specific pathway, not only just being present in mtSOD1 ALS but also restricted to fast fatigable MNs- those of which show an increased vulnerability to ER stress (Saxena et al., 2009). Furthermore, it has recently been shown that CRT may not have such a detrimental role in mtSOD1 as suggested since crossing $SOD1^{G93A}$ mice with CRT heterozygous knock out mice had a very limited effect on pathology (Bernard-Marissal et al., 2014).

5.2 The AR100 mouse model shows signs of muscle pathology earlier than spinal cord degeneration

SBMA is typically considered a MND, thus the majority of earlier research has focused on the spinal cord. However, recent developments in SBMA research have shown that peripheral treatment is sufficient to ablate symptoms in SBMA model mice (Cortes et al., 2014a, Lieberman et al., 2014). The question of whether pathology arises in the muscle or the spinal cord is by no means a new one (Jordan and Lieberman, 2008), particularly as different mouse models of disease have shown muscle and MN pathology in varying extents. Furthermore, owing to the different stages of diagnosis in patients (Finsterer and Soraru, 2015), it is problematic to come to a definitive conclusion of where pathology arises in patients.

In order to investigate muscle pathology in SBMA, I began by completing a longitudinal physiology analysis of AR20 mouse muscle. AR20 mice are the correct control for AR100 mice as they contain the same yeast artificial chromosome (YAC) however, the AR repeat length is of a non-pathological length (Sopher et al., 2004). I found that AR20 mice do not display a degenerative phenotype allowing us to conclude that the pathology seen in AR100 mice is due to the polyglutamine expansion rather than the presence of the YAC containing the human AR.

I next examined AR100 primary myotubes in culture. To date there is limited analysis of SBMA myotubes *in vitro.* Malena et al. (2013) has previously shown

defects in patient myocytes ability to fuse into myotubes as well as ultrastructural disorganisation, even at this early stage of development. In my investigation, AR100 primary myotubes did appear smaller in comparison to WT myotubes. However, I did not find a quantifiable significant difference between WT and AR100 cells. Thus although there may be differences between WT and AR100 myotubes early in *in vitro* development, similar to my *in vitro* analysis of primary MNs, a very sensitive mode of analysis is required to explore these differences further.

Studies on the AR100 mouse model of SBMA have largely focused on spinal cord pathogenesis. By performing histopathology on the TA muscle of AR100 mice, I observed muscle hypertrophy as early as 3 months, long before any signs of spinal cord degeneration. I suggest this early finding may be compensatory because by 6 months muscle atrophy was present. This evidence of muscle atrophy coincides with the first signs of muscle weakness in the AR100 mouse (A. Gray, PhD Thesis 2015). It is now clear that in the AR100 mouse model, muscle atrophy and weakness precedes any MN degeneration as a reduction in the number of sciatic pool MNs is not seen until 18 months of age (Malik et al., 2013).

Through H&E, SDH and Van Gieson histology I observed areas of negative staining, in the AR100 mouse TA muscle, evident between 6 and 12 months of age. This suggests muscle fibre loss is present early in the TA muscle of AR100 mice. However, there was no significant reduction in the number of muscle fibres in AR100 muscle, even at disease end stage. This lack of a significant decline in muscle fibre number may contribute to the somewhat mild symptoms of SBMA as a disease, in comparison to other neuromuscular diseases.

SDH staining of the TA muscle also allowed me to conclude that there was a shift to a higher oxidative capacity of AR100 mouse muscle fibres at disease end stage, indicative of an increase in the number of slow twitch muscle fibres. Furthermore, muscle fibre typing confirmed that as early as 6 months of age, the AR100 TA has an increase in the number of slow twitch type 2A muscle fibres in comparison to WT TA muscle. Interestingly, H&E staining revealed mainly signs of myogenic

degeneration at 12 months of age in the AR100 TA muscle, yet further analysis of the neuromuscular junction and innervation marker Nogo-A confirmed there is indeed a neurogenic component in pathology. However, this was more evident later in disease development. These results suggest that SBMA has both a myogenic and a neurogenic component but they may cause different pathogenic features and may occur at different stages of disease progression (Giorgetti and Lieberman, 2016).

In addition H&E staining revealed an apparent lack of internalised nuclei in the AR100 TA muscle at 12 months of age. It was not until 18 months that this sign of muscle regeneration was observed. Furthermore, IGF-1 staining revealed a lack of intensely stained muscle fibres in AR100 mouse TA, suggesting that this marker of satellite cell activation is absent. These results suggest there may be a component of SBMA pathology that may be due to defective muscle regeneration. It would be of interest to perform muscle injury experiments and determine the AR100 mouse models ability to regenerate in comparison to WT muscle. It would also be of interest to compare the response of AR100 mouse muscle to that of a mouse model of muscular dystrophy as there is an increasing viewpoint that SBMA may indeed be a form of myotonic dystrophy (Oki et al., 2013).

5.3 A number of already established molecular pathways may be relevant to SBMA muscle pathology

RNA sequencing data revealed a high number of dysregulated genes in the muscle of AR100 mice throughout disease progression. Interestingly, the highest number of genes were dysregulated at 12 months of age, in comparison to 3 months (a presymptomatic stage of disease in AR100 mice), or 18 months of age (disease end stage. At 12 months of age AR100 mice are fully symptomatic it is difficult to conclude which gene changes are causative at this stage. Similarly, one cannot fully deduce that all gene changes occurring at 3 months are causative as they may in fact be compensatory. As the RNA sequencing study presented in this Thesis largely allows correlation of gene changes throughout disease, it may be of interest to supplement this with knock-down/ knock-out or constitutive expression of the genes identified in order to determine whether the gene changes seen are

causative, compensatory or accessory to pathogenesis in the AR100 mouse model of SBMA.

Pathway analysis of RNA Sequencing data of AR100 muscle revealed a large number of molecular pathways already established in degenerative diseases that may also play a role in muscular degeneration in SBMA. As the electron transport chain was a component of a number of the pathways identified to be dysregulated at 3 months it is possible that dysregulated mitochondrial pathways may underpin important role early muscle pathology in SBMA.

As ATP formation is fundamental for muscle twitch it is not surprising that mitochondria are involved in the degeneration of muscle in SBMA. In fact, one of the first models of SBMA identified that polyQ aggregates sequestered mitochondria within inclusions (Stenoien et al., 1999). The continued investigation of the role of mitochondria in SBMA muscle is warranted. However, as the electron transport chain is highly complicated with the different complexes having a number of subunits, the western blotting techniques used in this Thesis may not be the most effective way to further investigate its involvement.

I also investigated the protein level of different mitochondrial function markers including Cytochrome C, PINK and Caspase 9. Due to having n=3 per group, results largely fell short of statistical significance. In most cases changes in protein expression via western blotting could only be observed at disease end stage, whereas RNA sequencing clearly showed there was an involvement of these markers, at a gene level, early in disease progression in the AR100 mice. This could suggest that there is a delay in the molecular changes at the protein- functional level.

RNA sequencing and pathway analysis on AR100 muscle at a symptomatic stage of disease revealed IGF-1 related pathways may have a role in the dysfunction in AR100 muscle. It has already been shown using an alternative mouse model of SBMA that increasing levels of IGF-1 can be beneficial (Palazzolo et al., 2009, Rinaldi

et al., 2012). It may be an advantage to dissect IGF-1 regulated pathways in more detail as in other neuromuscular diseases reduction of IGF-1 can be beneficial (Biondi et al., 2015).

I further analysed IGF-1 regulated pathways by western blotting for the activated form of the IGF-1 receptor, AKT- both active and dormant, Fox01 and PGC1α. As with my mitochondrial function western blot analysis, I did not see significant differences until disease end stage, with the exception of Fox01. At 3 months there was a significant increase in the Fox01 protein levels in AR100 muscle. This suggests a compensatory role of Fox01 in AR100 muscle that may be acting in an IGF-1 independent manner, as RNA sequencing only identified IGF-1 mediated pathways are dysregulated at 12 and 18 months of age. I did observe a last stage involvement of other proteins downstream to IGF-1 through western blotting. There was a significant decrease in phosphorylated AKT and an increase in AKT. However, this signalling molecule plays a vast role in a number of pathways so it may not be a targeted approach for therapeutics. Levels of PGC1α, a mitochondrial biogenesis marker, were found to be upregulated at 18 months of age. This suggests even at disease end stage there are compensatory processes occurring in the AR100 mouse TA muscle.

The final pathway I investigated was protein processing in the ER. In the Greensmith lab, ER stress has been observed in the spinal cord of AR100 mice (Montague et al., 2014). Therefore it was of interest to determine if this pathway too played a role in AR100 muscle degeneration. Although RNA sequencing and pathway analysis methods identified the involvement of ER stress late in AR100 pathology, at the protein level evidence for increased markers of ER stress was lacking. Indeed, at 18 months of age I observed a significant decrease in ER stress sensing protein BiP. BiP is responsible for sensing a high protein loads in the ER, therefore typically BiP levels increase in conditions of ER stress, leading to either a reduction of protein synthesis or apoptosis (Hetz, 2012). This suggests that protein load in the AR100 muscle is actually reduced at disease end stage- perhaps a compensatory feature. In contrast in AR100 spinal cord, early in disease development, an increase in BiP is

observed (Montague et al., 2014). These two contrasting findings suggest that different mechanisms may underpin the pathophysiology of SBMA in muscle and in spinal cord. Although they both play a part in pathology, different processes appear to be a result of the polyglutamine expansion in the AR in SBMA.

5.4 Concluding remarks

In this Thesis, I have shown that cell death pathways, such as the Fas/NO and Calreticulin pathway, responsible for MN apoptosis in severe neuromuscular disease may not all be a pathogenic feature of SBMA. This may be, at least in part, due to the causative protein of SBMA- the polyglutamine expanded androgen receptor, directly binding to Calreticulin and Calreticulin's many other functions. My analysis of AR100 muscle has clearly shown that the muscle is a primary site for pathogenesis in SBMA, and my RNA sequencing and pathway analysis study has identified a number of additional molecular pathways for further investigation into muscle pathogenesis.

Chapter 6 Appendices

Appendix I: AR100 Mouse Tibialis anterior changed gene expression in comparison to AR20

6.1 Top 100 up regulated genes in AR100 Mouse Tibialis Anterior Muscle at 3 Months

Gene Symbol	Gene Name	FC	FDR P value
Pkp1	plakophilin 1	350.575	0.009
Podnl1	podocan-like 1	340.978	0.003
Fcgbp	Fc fragment of IgG binding protein	276.689	0.000
Crct1	cysteine-rich C-terminal 1	228.256	0.002
Klk7	kallikrein related-peptidase 7 (chymotryptic, stratum corneum)	215.685	0.013
Tmem181b-ps	transmembrane protein 181B, pseudogene	213.884	0.011
Hal	histidine ammonia lyase	208.227	0.007
Ackr4	atypical chemokine receptor 4	206.212	0.005
Chit1	chitinase 1 (chitotriosidase)	198.279	0.000
Atp6v0d2	ATPase, H+ transporting, lysosomal V0 subunit D2	193.300	0.023
Lce1c	late cornified envelope 1C	189.811	0.011
Ckmt1	creatine kinase, mitochondrial 1, ubiquitous	189.444	0.024
Kprp	keratinocyte expressed, proline-rich	181.978	0.025
Lce1a1	late cornified envelope 1A1	152.842	0.000
Cyp2b19	cytochrome P450, family 2, subfamily b, polypeptide 19	152.133	0.045
Krt14	keratin 14	151.378	0.013
Tacstd2	tumor-associated calcium signal transducer 2	148.495	0.005
Krt77	keratin 77	145.430	0.001
Cdsn	corneodesmosin	138.084	0.000
Pla2g2f	phospholipase A2, group IIF	137.161	0.000
Pdzk1ip1	PDZK1 interacting protein 1	133.170	0.000
Lad1	ladinin	121.030	0.016
Serpina12	serine (or cysteine) peptidase inhibitor, clade A (alpha-1 antiproteinase, antitrypsin), member 12	116.419	0.000

Nrxn1	neurexin I	115.797	0.021
Mmp13	matrix metallopeptidase 13	114.165	0.000
Lce1a2	late cornified envelope 1A2	109.400	0.000
Dlx5	distal-less homeobox 5	102.808	0.002
Dsp	desmoplakin	95.731	0.008
Bbox1	butyrobetaine (gamma), 2-oxoglutarate dioxygenase 1 (gamma-butyrobetaine hydroxylase)	91.069	0.006
Tnn	tenascin N	70.043	0.001
Capn11	calpain 11	57.769	0.000
Flg2	filaggrin family member 2	50.716	0.032
Ibsp	integrin binding sialoprotein	45.534	0.000
Ano9	anoctamin 9	44.265	0.003
Orm1	orosomucoid 1	41.440	0.000
Trim29	tripartite motif-containing 29	39.265	0.016
2310050c09rik	RIKEN cDNA 2310050C09 gene	35.886	0.031
Dsg1a	desmoglein 1 alpha	33.939	0.000
Acan	aggrecan	32.882	0.001
Dmkn	dermokine	30.708	0.001
Col12a1	collagen, type XII, alpha 1	28.733	0.000
Krt15	keratin 15	25.670	0.001
Mrgprg	MAS-related GPR, member G	25.435	0.023
Krt5	keratin 5	24.016	0.000
Prss35	protease, serine, 35	23.468	0.000
1500015o10rik	RIKEN cDNA 1500015O10 gene	21.371	0.002
Syt1	synaptotagmin I	20.857	0.023
Ptgds	prostaglandin D2 synthase (brain)	20.605	0.013
Col11a1	collagen, type XI, alpha 1	19.808	0.015
Sfrp4	secreted frizzled-related protein 4	14.704	0.000
Anxa8	annexin A8	14.353	0.000
Postn	periostin, osteoblast specific factor	13.494	0.014
Sp7	Sp7 transcription factor 7	13.446	0.004

Edil3	EGF-like repeats and discoidin I-like domains 3	11.879	0.000
Asprv1	aspartic peptidase, retroviral-like 1	11.589	0.014
Lrrc15	leucine rich repeat containing 15	11.502	0.000
Acp5	acid phosphatase 5, tartrate resistant	11.441	0.011
Sfrp2	secreted frizzled-related protein 2	11.428	0.000
Cdh11	cadherin 11	10.698	0.001
Plekhg4	pleckstrin homology domain containing, family G (with RhoGef domain) member 4	10.176	0.000
Calm4	calmodulin 4	9.713	0.005
Tnc	tenascin C	9.122	0.002
Slc17a7	solute carrier family 17 (sodium-dependent inorganic phosphate cotransporter), member 7	9.078	0.007
Comp	cartilage oligomeric matrix protein	9.040	0.000
Snap25	synaptosomal-associated protein 25	8.878	0.013
Col8a2	collagen, type VIII, alpha 2	7.942	0.039
Aw551984	expressed sequence AW551984	7.748	0.011
Camk4	calcium/calmodulin-dependent protein kinase IV	7.203	0.002
Wif1	Wnt inhibitory factor 1	7.044	0.005
Ltbp2	latent transforming growth factor beta binding protein 2	6.853	0.031
Thbs2	thrombospondin 2	6.520	0.008
Angptl7	angiopoietin-like 7	6.459	0.014
Omd	osteomodulin	6.400	0.012
Mmp9	matrix metallopeptidase 9	6.280	0.000
Chad	chondroadherin	6.280	0.034
Slit2	slit homolog 2 (Drosophila)	5.518	0.019
Col16a1	collagen, type XVI, alpha 1	5.513	0.005
Col6a5	collagen, type VI, alpha 5	5.315	0.016
Kera	keratocan	5.257	0.000
Adam12	a disintegrin and metallopeptidase domain 12 (meltrin alpha)	5.201	0.011
Fbln1	fibulin 1	4.736	0.003
Fmod	fibromodulin	4.637	0.002
Igsf10	immunoglobulin superfamily, member 10	4.477	0.010

Runx2	runt related transcription factor 2	4.416	0.025
Dkk3	dickkopf homolog 3 (Xenopus laevis)	4.387	0.000
Itgbl1	integrin, beta-like 1	4.321	0.014
Ptn	pleiotrophin	4.298	0.002
Aldh1a3	aldehyde dehydrogenase family 1, subfamily A3	4.279	0.020
Cilp2	cartilage intermediate layer protein 2	4.200	0.000
Wisp2	WNT1 inducible signaling pathway protein 2	4.026	0.000
Pamr1	peptidase domain containing associated with muscle regeneration 1	4.018	0.016
Ctsk	cathepsin K	3.845	0.000
Clec11a	C-type lectin domain family 11, member a	3.678	0.042
Qpct	glutaminyl-peptide cyclotransferase (glutaminyl cyclase)	3.648	0.039
Thbs1	thrombospondin 1	3.603	0.004
Pcsk5	proprotein convertase subtilisin/kexin type 5	3.569	0.026
Plin1	perilipin 1	3.555	0.005
Mt2	metallothionein 2	3.548	0.000
Vit	vitrin	3.473	0.000
Perp	PERP, TP53 apoptosis effector	3.443	0.043

6.2 Top 100 down regulated genes in AR100 mouse Tibialis Anterior Muscle at 3 Months

Gene Symbol	Gene Name	FC	FC-	FDR P value
Gys2	glycophorin C	0.087	-11.552	0.013
Gm12671	glyceraldehyde-3-phosphate dehydrogenase pseudogene	0.281	-3.557	0.000
Gm14029	cytochrome c oxidase subunit 2-like	0.302	-3.310	0.044
Gm29216	predicted gene 28661	0.321	-3.114	0.032
Htra4	hemoglobin alpha, adult chain 2	0.332	-3.015	0.000
Gm28661	predicted gene 28438	0.332	-3.008	0.015
Gm28438	predicted gene 28437	0.334	-2.990	0.004
Gm28437	glyceraldehyde-3-phosphate dehydrogenase pseudogene	0.342	-2.928	0.000
Gm10925	guanidinoacetate methyltransferase	0.350	-2.860	0.002
Gm2606	predicted gene 23935	0.412	-2.427	0.002
Bdh1	cDNA sequence BC029214	0.428	-2.336	0.006
Pfkfb3	platelet derived growth factor, B polypeptide	0.448	-2.233	0.020
Csrp3	cytochrome c oxidase, subunit VIc	0.479	-2.086	0.001
B230312c02rik	ADP-ribosyltransferase 5	0.484	-2.066	0.044
Pim1	6-phosphofructo-2-kinase/fructose-2,6-biphosphatase 3	0.486	-2.059	0.003
Irx3os	immunoglobulin heavy constant mu	0.489	-2.045	0.003
Gm23935	predicted gene 15543	0.508	-1.968	0.002
Npr3	nicotinamide nucleotide transhydrogenase	0.517	-1.934	0.001
Btnl9	3-hydroxybutyrate dehydrogenase, type 1	0.526	-1.902	0.004
Ighm	HtrA serine peptidase 4	0.526	-1.900	0.036
1700001o22rik	RIKEN cDNA 1700001O22 gene	0.527	-1.899	0.000
D330023k18rik	cytochrome P450, family 4, subfamily f, polypeptide 39	0.537	-1.863	0.041
Cldn5	Cbp/p300-interacting transactivator, with Glu/Asp-rich carboxy-terminal domain, 4	0.540	-1.853	0.000
Ankrd2	ARP3 actin-related protein 3B	0.565	-1.770	0.013
Mettl21c	LSM8 homolog, U6 small nuclear RNA associated (S. cerevisiae)	0.578	-1.729	0.007

Hba-a2	glycogen synthase 2	0.582	-1.717	0.002
Actc1	RAB4A, member RAS oncogene family	0.583	-1.717	0.000
Gm13341	predicted gene 13340	0.586	-1.706	0.013
Mir99ahg	methyltransferase like 21C	0.590	-1.695	0.016
Cacna2d4	butyrophilin-like 9	0.591	-1.693	0.000
Tmem100	transmembrane protein 100	0.597	-1.675	0.000
Cited4	calcium channel, voltage-dependent, alpha 2/delta subunit 4	0.602	-1.661	0.034
Actr3b	actin, alpha, cardiac muscle 1	0.619	-1.614	0.000
Plekho1	proviral integration site 1	0.630	-1.588	0.032
Nnt	NADH dehydrogenase (ubiquinone) 1 alpha subcomplex, 5	0.633	-1.581	0.000
Ppp1r27	protein phosphatase 1, regulatory (inhibitor) subunit 11	0.646	-1.548	0.000
Sbk2	SH3-binding domain kinase family, member 2	0.646	-1.548	0.000
Gm12286	predicted gene 10925	0.647	-1.546	0.000
Lrtm2	lectin, galactose binding, soluble 1	0.648	-1.542	0.000
Dera	differentially expressed in B16F10 1	0.657	-1.522	0.000
Nudt6	natriuretic peptide receptor 3	0.663	-1.508	0.021
Gm13340	glyceraldehyde-3-phosphate dehydrogenase pseudogene	0.663	-1.508	0.001
Smim4	small integral membrane protein 4	0.681	-1.468	0.003
Fabp4	dual specificity phosphatase 26 (putative)	0.690	-1.449	0.014
Odc1	nudix (nucleoside diphosphate linked moiety X)-type motif 6	0.692	-1.445	0.000
Cyp4f39	cystatin E/M	0.694	-1.442	0.004
Ubc	ubiquitin C	0.697	-1.436	0.017
Gm15543	predicted gene 14029	0.701	-1.428	0.000
Gng11	predicted gene 29216	0.703	-1.423	0.000
Lsm8	leucine-rich repeats and transmembrane domains 2	0.708	-1.412	0.005
Six4	sine oculis-related homeobox 4	0.722	-1.384	0.028
Gamt	F-box protein 32	0.723	-1.383	0.006
Siva1	SIVA1, apoptosis-inducing factor	0.724	-1.381	0.022
Stbd1	starch binding domain 1	0.729	-1.372	0.004
Mrln	Mir99a and Mirlet7c-1 host gene (non-protein coding)	0.735	-1.361	0.045

2310001h17rik	RIKEN cDNA 2310001H17 gene	0.742	-1.347	0.004
Arhgef15	ankyrin repeat domain 2 (stretch responsive muscle)	0.743	-1.345	0.020
Gypc	guanine nucleotide binding protein (G protein), gamma 11	0.744	-1.344	0.036
Rab4a	protein phosphatase 1, regulatory subunit 27	0.748	-1.337	0.003
Tomm5	translocase of outer mitochondrial membrane 5 homolog (yeast)	0.748	-1.336	0.008
Fbxo32	family with sequence similarity 213, member B	0.748	-1.336	0.015
Slc38a4	solute carrier family 38, member 4	0.752	-1.329	0.011
Rpl38	ribosomal protein L38	0.755	-1.325	0.000
Pdgfb	ornithine decarboxylase, structural 1	0.755	-1.324	0.006
Relt	RELT tumor necrosis factor receptor	0.756	-1.324	0.018
Smim8	small integral membrane protein 8	0.757	-1.322	0.009
Bc029214	BBSome interacting protein 1	0.758	-1.320	0.008
Tpt1-ps3	tumor protein, translationally-controlled, pseudogene 3	0.758	-1.319	0.000
Lgals1	ketohexokinase	0.759	-1.318	0.004
Itgb1bp1	iron-sulfur cluster assembly 2 homolog (S. cerevisiae)	0.762	-1.313	0.038
Cst6	cysteine and glycine-rich protein 3	0.765	-1.307	0.018
Fam213b	fatty acid binding protein 4, adipocyte	0.766	-1.305	0.042
Rpl22l1	ribosomal protein L22 like 1	0.766	-1.305	0.033
Bbip1	RIKEN cDNA B230312C02 gene	0.766	-1.305	0.034
Ppp1r11	processing of precursor 5, ribonuclease P/MRP family (S. cerevisiae)	0.767	-1.304	0.001
Art5	Rho guanine nucleotide exchange factor (GEF) 15	0.767	-1.304	0.007
Zswim7	zinc finger, SWIM-type containing 7	0.769	-1.301	0.004
Mrpl22	mitochondrial ribosomal protein L12	0.769	-1.300	0.000
Vamp8	vesicle-associated membrane protein 8	0.769	-1.300	0.026
Smox	spermine oxidase	0.769	-1.300	0.011
Dusp26	2-deoxyribose-5-phosphate aldolase homolog (C. elegans)	0.770	-1.299	0.036
Deb1	RIKEN cDNA D330023K18 gene	0.771	-1.298	0.001
2310065f04rik	RIKEN cDNA 2310065F04 gene	0.774	-1.292	0.010
Snf8	SNF8, ESCRT-II complex subunit, homolog (S. cerevisiae)	0.774	-1.292	0.033
Smim11	small integral membrane protein 11	0.775	-1.290	0.017

Pop5	pleckstrin homology domain containing, family O member 1	0.776	-1.289	0.005
Tmem256	transmembrane protein 256	0.776	-1.288	0.000
Cox6c	claudin 5	0.778	-1.286	0.001
Ndufa2	mitochondrial ribosomal protein L22	0.779	-1.283	0.000
Vamp5	vesicle-associated membrane protein 5	0.781	-1.281	0.005
Tmem160	transmembrane protein 160	0.781	-1.280	0.022
Isca2	iron-sulfur cluster assembly 2 homolog (S. cerevisiae)	0.783	-1.277	0.009
Ndufa5	NADH dehydrogenase (ubiquinone) 1 alpha subcomplex, 2	0.786	-1.273	0.011
Itpr1	integrin beta 1 binding protein 1	0.787	-1.270	0.002
Vtn	vitronectin	0.789	-1.267	0.031
Mrpl12	myoregulin	0.792	-1.263	0.000
Use1	unconventional SNARE in the ER 1 homolog (S. cerevisiae)	0.793	-1.261	0.004
Timmdc1	translocase of inner mitochondrial membrane domain containing 1	0.794	-1.259	0.014
Rps17	ribosomal protein S17	0.795	-1.258	0.031
Khk	inositol 1,4,5-trisphosphate receptor 1	0.796	-1.257	0.000

6.3 Top 100 up regulated genes at in AR100 Mouse Tibialis Anterior Muscle 12 Months

Gene Symbol	Gene Name	FC	FDR P value
Ltf	lactotransferrin	683.494	0.001
Lhx1	LIM homeobox protein 1	264.981	0.000
Chi3l3	chitinase 3-like 3	198.500	0.000
Gata4	GATA binding protein 4	198.172	0.000
Pax6	paired box gene 6	93.164	0.000
Ngp	neutrophilic granule protein	83.313	0.026
Pax2	paired box gene 2	50.180	0.000
Sln	sarcolipin	45.557	0.000
Muc15	mucin 15	30.684	0.000
Krt18	keratin 18	29.875	0.000

Uchl1	ubiquitin carboxy-terminal hydrolase L1	25.654	0.000
Rab15	RAB15, member RAS oncogene family	23.609	0.000
Foxf2	forkhead box F2	21.939	0.000
Fam171b	family with sequence similarity 171, member B	21.769	0.000
Clca6	chloride channel calcium activated 6	21.333	0.000
Ttc9	tetratricopeptide repeat domain 9	19.423	0.000
Ect2l	epithelial cell transforming sequence 2 oncogene-like	18.057	0.000
Acsm5	acyl-CoA synthetase medium-chain family member 5	16.553	0.000
Zfp365	zinc finger protein 365	16.347	0.000
Ano3	anoctamin 3	15.385	0.000
S100a9	S100 calcium binding protein A9 (calgranulin B)	15.278	0.006
Ces5a	carboxylesterase 5A	14.750	0.000
Edar	ectodysplasin-A receptor	14.587	0.000
Retnlg	resistin like gamma	14.489	0.012
Cntnap4	contactin associated protein-like 4	14.405	0.001
Espnl	espin-like	13.276	0.000
Heatr8	HEAT repeat containing 8	13.163	0.000
Sh2d4a	SH2 domain containing 4A	12.345	0.000
Cidea	cell death-inducing DNA fragmentation factor, alpha subunit-like effector A	12.261	0.000
Enkur	enkurin, TRPC channel interacting protein	12.119	0.000
Ifltd1	intermediate filament tail domain containing 1	10.916	0.002
1700024P16Rik	RIKEN cDNA 1700024P16 gene	10.315	0.000
Dync1i1	dynein cytoplasmic 1 intermediate chain 1	9.718	0.001
Zp2	zona pellucida glycoprotein 2	9.569	0.000
Rab13	RAB13, member RAS oncogene family	9.395	0.000
Myom3	myomesin family, member 3	9.363	0.000
Gldn	gliomedin	9.127	0.000
Scel	sciellin	9.089	0.000
Mogat1	monoacylglycerol O-acyltransferase 1	9.087	0.009
Tdrd9	tudor domain containing 9	8.377	0.000

Tmem202	transmembrane protein 202	8.356	0.000
1810041L15Rik	RIKEN cDNA 1810041L15 gene	8.328	0.000
Acox2	acyl-Coenzyme A oxidase 2, branched chain	8.231	0.000
Gsdma	gasdermin A	7.992	0.043
Kcnj3	potassium inwardly-rectifying channel, subfamily J, member 3	7.972	0.000
Shbg	sex hormone binding globulin	7.879	0.000
Nrcam	neuron-glia-CAM-related cell adhesion molecule	7.870	0.000
Rtkn2	rhotekin 2	7.678	0.000
March. 09	membrane-associated ring finger (C3HC4) 9	7.663	0.000
Ddc	dopa decarboxylase	7.647	0.000
Tmem53	transmembrane protein 53	7.628	0.000
Chrna1	cholinergic receptor, nicotinic, alpha polypeptide 1 (muscle)	7.557	0.000
Crybb1	crystallin, beta B1	7.174	0.000
BC061194	cDNA sequence BC061194	7.166	0.000
Shroom3	shroom family member 3	7.077	0.000
Musk	muscle, skeletal, receptor tyrosine kinase	6.948	0.000
Serpinb1a	serine (or cysteine) peptidase inhibitor, clade B, member 1a	6.741	0.000
Ctla4	cytotoxic T-lymphocyte-associated protein 4	6.707	0.004
Slc1a2	solute carrier family 1 (glial high affinity glutamate transporter), member 2	6.686	0.039
Aldh1b1	aldehyde dehydrogenase 1 family, member B1	6.445	0.001
Odf3l1	outer dense fiber of sperm tails 3-like 1	6.408	0.001
D430019H16Rik	RIKEN cDNA D430019H16 gene	6.322	0.003
1700027A23Rik	RIKEN cDNA 1700027A23 gene	6.075	0.014
Cpne2	copine II	6.048	0.000
Slc16a5	solute carrier family 16 (monocarboxylic acid transporters), member 5	6.025	0.019
Rrad	Ras-related associated with diabetes	6.017	0.000
Slc37a1	solute carrier family 37 (glycerol-3-phosphate transporter), member 1	5.988	0.000
Slc7a5	solute carrier family 7 (cationic amino acid transporter, y+ system), member 5	5.886	0.000
1700010I14Rik	RIKEN cDNA 1700010I14 gene	5.843	0.000
Ntn5	netrin 5	5.830	0.000

Dok5	docking protein 5	5.617	0.000
Runx1	runt related transcription factor 1	5.605	0.000
Actc1	actin, alpha, cardiac muscle 1	5.538	0.000
Smtnl1	smoothelin-like 1	5.527	0.000
1700040L02Rik	RIKEN cDNA 1700040L02 gene	5.507	0.017
Foxq1	forkhead box Q1	5.477	0.020
Rnf165	ring finger protein 165	5.442	0.002
Lix1	limb expression 1 homolog (chicken)	5.426	0.000
Kcnk1	potassium channel, subfamily K, member 1	5.317	0.004
Casq2	calsequestrin 2	5.312	0.000
Gm684	predicted gene 684	5.277	0.000
Tlr4	toll-like receptor 4	5.256	0.000
Srrm4	serine/arginine repetitive matrix 4	5.164	0.000
Prelid2	PRELI domain containing 2	5.097	0.000
Ankrd1	ankyrin repeat domain 1 (cardiac muscle)	5.063	0.000
Scube2	signal peptide, CUB domain, EGF-like 2	5.001	0.000
Lamc2	laminin, gamma 2	4.894	0.000
Glrb	glycine receptor, beta subunit	4.848	0.016
Chrdl2	chordin-like 2	4.847	0.000
Klhdc8a	kelch domain containing 8A	4.763	0.000
Cnga3	cyclic nucleotide gated channel alpha 3	4.739	0.000
Ahnak2	AHNAK nucleoprotein 2	4.696	0.000
Slc1a1	solute carrier family 1 (neuronal/epithelial high affinity glutamate transporter, system Xag), member 1	4.681	0.000
Rsph1	radial spoke head 1 homolog (Chlamydomonas)	4.661	0.000
Kif11	kinesin family member 11	4.647	0.000
Arpp21	cyclic AMP-regulated phosphoprotein, 21	4.593	0.000
1700016C15Rik	RIKEN cDNA 1700016C15 gene	4.471	0.009
Dpp6	dipeptidylpeptidase 6	4.446	0.000
Wbscr27	Williams Beuren syndrome chromosome region 27 (human)	4.440	0.000
Cd6	CD6 antigen	4.431	0.012

6.4 Top 100 down regulated genes at in AR100 Mouse Tibialis Anterior Muscle 12 Months

Gene Symbol	Gene Name	FC	FC-	FDR P value
Krt71	keratin 71	0.000	-4333.072	0.009
Krt25	keratin 25	0.000	-3336.518	0.009
Krt27	keratin 27	0.000	-2318.208	0.009
5430421N21Rik	RIKEN cDNA 5430421N21 gene	0.001	-1325.706	0.009
Krtap7-1	keratin associated protein 7-1	0.001	-1090.257	0.011
Krtap8-1	keratin associated protein 8-1	0.001	-982.649	0.014
Prr9	proline rich 9	0.001	-949.867	0.001
Krt72-ps	keratin 72, pseudogene	0.001	-917.022	0.010
Krt28	keratin 28	0.001	-905.356	0.011
Krt35	keratin 35	0.001	-870.368	0.011
Krt31	keratin 31	0.001	-737.648	0.010
Krt81	keratin 81	0.001	-691.167	0.012
Krt86	keratin 86	0.002	-642.070	0.013
Krt34	keratin 34	0.002	-590.686	0.027
Krtap11-1	keratin associated protein 11-1	0.002	-588.689	0.019
Krt33b	keratin 33B	0.002	-446.833	0.024
Krtap22-2	keratin associated protein 22-2	0.002	-424.078	0.028
Krtap1-5	keratin associated protein 1-5	0.003	-379.998	0.024
Esrp1	epithelial splicing regulatory protein 1	0.003	-378.825	0.010
Krtap6-1	keratin associated protein 6-1	0.003	-343.012	0.019
Crnn	cornulin	0.003	-334.304	0.032
Krtap3-1	keratin associated protein 3-1	0.003	-328.639	0.018
Krtap4-7	keratin associated protein 4-7	0.003	-323.058	0.016
Mmrn1	multimerin 1	0.003	-313.605	0.000
Krtap3-3	keratin associated protein 3-3	0.003	-298.000	0.028
Krtap9-3	keratin associated protein 9-3	0.003	-291.350	0.015

Krtap6-5	keratin associated protein 6-5	0.004	-241.442	0.001
Gm11562	predicted gene 11562	0.004	-229.297	0.001
Fam19a4	family with sequence similarity 19, member A4	0.004	-222.633	0.000
Krtap4-1	keratin associated protein 4-1	0.005	-216.978	0.035
Krt17	keratin 17	0.008	-127.487	0.007
Trim29	tripartite motif-containing 29	0.009	-110.606	0.005
Dsp	desmoplakin	0.010	-99.406	0.045
Fgfbp1	fibroblast growth factor binding protein 1	0.011	-91.305	0.000
Krt75	keratin 75	0.011	-88.593	0.005
Zmynd17	zinc finger, MYND domain containing 17	0.013	-78.645	0.000
Tnn	tenascin N	0.016	-64.415	0.000
Tchh	trichohyalin	0.018	-55.624	0.010
Krt26	keratin 26	0.019	-53.572	0.000
Gprc5d	G protein-coupled receptor, family C, group 5, member D	0.019	-52.485	0.040
Dsc3	desmocollin 3	0.025	-39.688	0.001
Gys2	glycogen synthase 2	0.032	-31.515	0.001
Mrgprg	MAS-related GPR, member G	0.032	-30.904	0.007
Dkk3	dickkopf homolog 3 (Xenopus laevis)	0.038	-26.622	0.000
Dapl1	death associated protein-like 1	0.040	-25.124	0.049
Lrrc15	leucine rich repeat containing 15	0.044	-22.968	0.000
Pkp3	plakophilin 3	0.044	-22.495	0.002
Dmkn	dermokine	0.045	-22.006	0.006
Calm4	calmodulin 4	0.050	-19.943	0.000
Crct1	cysteine-rich C-terminal 1	0.057	-17.485	0.000
Syt9	synaptotagmin IX	0.058	-17.139	0.000
Grem2	gremlin 2 homolog, cysteine knot superfamily (Xenopus laevis)	0.059	-17.029	0.000
Krt5	keratin 5	0.059	-16.884	0.040
Rmi2	RMI2, RecQ mediated genome instability 2, homolog (S. cerevisiae)	0.062	-16.117	0.000
Hcn4	hyperpolarization-activated, cyclic nucleotide-gated K+ 4	0.064	-15.619	0.000
Krt79	keratin 79	0.066	-15.096	0.000

Evpl	envoplakin	0.066	-15.072	0.005
1700001O22Rik	RIKEN cDNA 1700001O22 gene	0.067	-14.819	0.000
Fat3	FAT tumor suppressor homolog 3 (Drosophila)	0.074	-13.426	0.000
Cdsn	corneodesmosin	0.079	-12.583	0.001
Krtdap	keratinocyte differentiation associated protein	0.080	-12.424	0.014
Pla2g5	phospholipase A2, group V	0.082	-12.221	0.000
Nek5	NIMA (never in mitosis gene a)-related expressed kinase 5	0.083	-12.121	0.000
Aoah	acyloxyacyl hydrolase	0.083	-12.068	0.001
Pfkfb3	6-phosphofructo-2-kinase/fructose-2,6-biphosphatase 3	0.084	-11.965	0.000
Fam57b	family with sequence similarity 57, member B	0.084	-11.909	0.000
Gyltl1b	glycosyltransferase-like 1B	0.088	-11.406	0.014
Mylk4	myosin light chain kinase family, member 4	0.089	-11.215	0.000
BC048355	cDNA sequence BC048355	0.089	-11.185	0.000
Rasd2	RASD family, member 2	0.090	-11.100	0.000
C2cd4a	C2 calcium-dependent domain containing 4A	0.091	-11.026	0.002
Odf3l2	outer dense fiber of sperm tails 3-like 2	0.098	-10.211	0.000
Tgm1	transglutaminase 1, K polypeptide	0.106	-9.459	0.028
Cdh3	cadherin 3	0.109	-9.190	0.024
Pon1	paraoxonase 1	0.110	-9.101	0.000
Ppm1n	protein phosphatase, Mg2+/Mn2+ dependent, 1N (putative)	0.110	-9.052	0.000
Cuzd1	CUB and zona pellucida-like domains 1	0.112	-8.905	0.000
Orm1	orosomucoid 1	0.112	-8.890	0.016
S100a14	S100 calcium binding protein A14	0.117	-8.533	0.012
Sfrp2	secreted frizzled-related protein 2	0.122	-8.180	0.004
Car3	carbonic anhydrase 3	0.123	-8.140	0.000
Adamts8	a disintegrin-like and metallopeptidase (reprolysin type) with thrombospondin type 1 motif, 8	0.125	-8.020	0.000
Lep	leptin	0.127	-7.870	0.003
Plin1	perilipin 1	0.127	-7.846	0.010
Prima1	proline rich membrane anchor 1	0.127	-7.844	0.000
Otog	otogelin	0.128	-7.840	0.000

Aebp1	AE binding protein 1	0.128	-7.807	0.000
Mrgprb1	MAS-related GPR, member B1	0.129	-7.781	0.000
Col9a1	collagen, type IX, alpha 1	0.129	-7.724	0.000
Smox	spermine oxidase	0.130	-7.679	0.000
Tpx2	TPX2, microtubule-associated protein homolog (Xenopus laevis)	0.132	-7.587	0.000
Htra4	HtrA serine peptidase 4	0.136	-7.367	0.000
Gm4980	predicted gene 4980	0.140	-7.147	0.000
Tiam1	T cell lymphoma invasion and metastasis 1	0.144	-6.933	0.000
Tmem45b	transmembrane protein 45b	0.148	-6.779	0.000
Irf5	interferon regulatory factor 5	0.149	-6.696	0.000
Sytl1	synaptotagmin-like 1	0.154	-6.507	0.008
St14	suppression of tumorigenicity 14 (colon carcinoma)	0.155	-6.459	0.005
Kcnc1	potassium voltage gated channel, Shaw-related subfamily, member 1	0.158	-6.331	0.000
Atp1a4	ATPase, Na+/K+ transporting, alpha 4 polypeptide	0.160	-6.257	0.001

6.5 Top 100 up regulated genes at in AR100 Mouse Tibialis Anterior Muscle 18 Months

Gene Symbol	Gene Name	FC	FDR P value
Syt8	synaptotagmin VIII	17.83808	0.002
Doc2b	double C2, beta	14.52198	0.002
Ddit4	DNA-damage-inducible transcript 4	10.65074	0.000
Odf3l2	outer dense fiber of sperm tails 3-like 2	10.29318	0.000
8430408G22Rik	RIKEN cDNA 8430408G22 gene	9.529894	0.000
Arrdc2	arrestin domain containing 2	8.344727	0.001
Nek5	NIMA (never in mitosis gene a)-related expressed kinase 5	7.265924	0.000
Chac1	ChaC, cation transport regulator 1	6.890642	0.000
Kcnf1	potassium voltage-gated channel, subfamily F, member 1	5.78918	0.000
Gck	glucokinase	5.509411	0.000

Tmem132b	transmembrane protein 132B	5.486828	0.000
Fat3	FAT tumor suppressor homolog 3 (Drosophila)	5.392127	0.002
Prima1	proline rich membrane anchor 1	5.176436	0.006
Calm4	calmodulin 4	5.022388	0.008
Slc10a6	solute carrier family 10 (sodium/bile acid cotransporter family), member 6	4.878722	0.000
Car1	carbonic anhydrase 1	4.760295	0.030
Nr4a3	nuclear receptor subfamily 4, group A, member 3	4.753808	0.000
Uts2d	urotensin 2 domain containing	4.445818	0.014
Snca	synuclein, alpha	4.365791	0.019
Hcn4	hyperpolarization-activated, cyclic nucleotide-gated K+ 4	4.255479	0.038
Amd2	S-adenosylmethionine decarboxylase 2	4.228902	0.002
Wdr62	WD repeat domain 62	4.091838	0.000
Stc1	stanniocalcin 1	3.978641	0.001
Fbxo32	F-box protein 32	3.976043	0.007
Pdk4	pyruvate dehydrogenase kinase, isoenzyme 4	3.954181	0.000
Pcdhb20	protocadherin beta 20	3.90065	0.012
Kcnk5	potassium channel, subfamily K, member 5	3.81525	0.001
Pck1	phosphoenolpyruvate carboxykinase 1, cytosolic	3.789319	0.005
Agbl1	ATP/GTP binding protein-like 1	3.716518	0.000
Ppp1r3c	protein phosphatase 1, regulatory (inhibitor) subunit 3C	3.574042	0.000
Klhl38	kelch-like 38 (Drosophila)	3.520629	0.000
Slc25a25	solute carrier family 25 (mitochondrial carrier, phosphate carrier), member 25	3.504886	0.033
Map3k6	mitogen-activated protein kinase kinase kinase 6	3.492723	0.000
Gadd45g	growth arrest and DNA-damage-inducible 45 gamma	3.462259	0.000

4921507P07Rik	RIKEN cDNA 4921507P07 gene	3.414259	0.009
Pla2g7	phospholipase A2, group VII (platelet-activating factor acetylhydrolase, plasma)	3.405307	0.025
Cilp	cartilage intermediate layer protein, nucleotide pyrophosphohydrolase	3.357833	0.004
Amd1	S-adenosylmethionine decarboxylase 1	3.327013	0.000
Papln	papilin, proteoglycan-like sulfated glycoprotein	3.318197	0.025
Fam107a	family with sequence similarity 107, member A	3.291195	0.001
Gen1	Gen homolog 1, endonuclease (Drosophila)	3.231787	0.026
Otub2	OTU domain, ubiquitin aldehyde binding 2	3.214601	0.000
Klf10	Kruppel-like factor 10	3.194383	0.000
Asns	asparagine synthetase	3.159274	0.000
Xylt1	xylosyltransferase 1	3.053551	0.002
Kcnab1	potassium voltage-gated channel, shaker-related subfamily, beta member 1	3.03535	0.007
Mfsd7b	major facilitator superfamily domain containing 7B	3.020066	0.000
Tekt1	tektin 1	3.009025	0.000
Slc2a3	solute carrier family 2 (facilitated glucose transporter), member 3	3.004972	0.000
Ces1d	carboxylesterase 1D	2.947511	0.040
Nt5c1a	5'-nucleotidase, cytosolic IA	2.900609	0.000
Gm9766	predicted gene 9766	2.880411	0.001
Ctla2b	cytotoxic T lymphocyte-associated protein 2 beta	2.862841	0.000
Mafb	v-maf musculoaponeurotic fibrosarcoma oncogene family, protein B (avian)	2.856215	0.000
4933415F23Rik	RIKEN cDNA 4933415F23 gene	2.845656	0.015
Fkbp5	FK506 binding protein 5	2.827713	0.018
Gdpd5	glycerophosphodiester phosphodiesterase domain containing 5	2.819746	0.000
Vldlr	very low density lipoprotein receptor	2.811793	0.000
Trim63	tripartite motif-containing 63	2.774028	0.021

Myh4	myosin, heavy polypeptide 4, skeletal muscle	2.76355	0.015
Adra1a	adrenergic receptor, alpha 1a	2.763107	0.042
Timp4	tissue inhibitor of metalloproteinase 4	2.71305	0.000
Glb1l2	galactosidase, beta 1-like 2	2.705831	0.002
Ntsr2	neurotensin receptor 2	2.687357	0.033
Cyp2e1	cytochrome P450, family 2, subfamily e, polypeptide 1	2.673173	0.013
Tob2	transducer of ERBB2, 2	2.647384	0.000
Mib1	mindbomb homolog 1 (Drosophila)	2.627491	0.043
Slc40a1	solute carrier family 40 (iron-regulated transporter), member 1	2.626267	0.000
Pgf	placental growth factor	2.6237	0.009
Apoh	apolipoprotein H	2.623475	0.038
Rai14	retinoic acid induced 14	2.614426	0.000
Rhpn2	rhophilin, Rho GTPase binding protein 2	2.60351	0.001
Rapgef5	Rap guanine nucleotide exchange factor (GEF) 5	2.598726	0.000
Adipoq	adiponectin, C1Q and collagen domain containing	2.59841	0.007
Serpine1	serine (or cysteine) peptidase inhibitor, clade E, member 1	2.594099	0.000
Slc52a3	solute carrier protein family 52, member 3	2.593809	0.014
Rnf32	ring finger protein 32	2.576949	0.004
S1pr1	sphingosine-1-phosphate receptor 1	2.556521	0.000
Exph5	exophilin 5	2.521679	0.026
Ucp3	uncoupling protein 3 (mitochondrial, proton carrier)	2.51364	0.000
Ccne2	cyclin E2	2.507572	0.002
Gucy2g	guanylate cyclase 2g	2.49591	0.016
Atp13a5	ATPase type 13A5	2.487041	0.000
Shc2	SHC (Src homology 2 domain containing) transforming protein 2	2.450333	0.001
Slc6a17	solute carrier family 6 (neurotransmitter transporter), member 17	2.445827	0.025

Cfd	complement factor D (adipsin)	2.443226	0.001
Adamts8	a disintegrin-like and metallopeptidase (reprolysin type) with thrombospondin type 1 motif, 8	2.414385	0.007
Slc38a4	solute carrier family 38, member 4	2.314312	0.000
Kcnq5	potassium voltage-gated channel, subfamily Q, member 5	2.31411	0.000
A930016O22Rik	RIKEN cDNA A930016O22 gene	2.31369	0.008
Slc43a1	solute carrier family 43, member 1	2.307351	0.009
Npc1	Niemann Pick type C1	2.303053	0.000
Vav3	vav 3 oncogene	2.278918	0.003
Sema7a	sema domain, immunoglobulin domain (Ig), and GPI membrane anchor, (semaphorin) 7A	2.271953	0.000
Slc16a3	solute carrier family 16 (monocarboxylic acid transporters), member 3	2.255496	0.001
Catsper4	cation channel, sperm associated 4	2.246601	0.012
Acer2	alkaline ceramidase 2	2.236422	0.016

6.6 Top 100 down regulated genes at in AR100 Mouse Tibialis Anterior Muscle 18 Months

Gene Symbol	Gene Name	FC	FC-	FDR P value
Hoxd13	homeobox D13	0.000912	-1095.94	0.000
Gata4	GATA binding protein 4	0.001098	-910.412	0.012
Muc15	mucin 15	0.00112	-892.7	0.000
Lhx1	LIM homeobox protein 1	0.001749	-571.597	0.000
Otx1	orthodenticle homolog 1 (Drosophila)	0.00304	-328.965	0.001
Pax2	paired box gene 2	0.003318	-301.386	0.000
Lhx8	LIM homeobox protein 8	0.003345	-298.941	0.000
Fcrl5	Fc receptor-like 5	0.003446	-290.189	0.002

Nkx2-3	NK2 transcription factor related, locus 3 (Drosophila)	0.00352	-284.106	0.002
Pdcd1	programmed cell death 1	0.003922	-254.958	0.001
Kynu	kynureninase (L-kynurenine hydrolase)	0.004214	-237.301	0.006
Folr4	folate receptor 4 (delta)	0.004539	-220.316	0.004
Isl1	ISL1 transcription factor, LIM/homeodomain	0.010074	-99.2646	0.003
Sall3	sal-like 3 (Drosophila)	0.016513	-60.5586	0.001
Igj	immunoglobulin joining chain	0.018618	-53.7117	0.000
Ptpn7	protein tyrosine phosphatase, non-receptor type 7	0.021203	-47.1622	0.001
Zic2	zinc finger protein of the cerebellum 2	0.022447	-44.5491	0.004
Krtdap	keratinocyte differentiation associated protein	0.023176	-43.1483	0.015
Slamf6	SLAM family member 6	0.024787	-40.3433	0.012
Ms4a4b	membrane-spanning 4-domains, subfamily A, member 4B	0.027405	-36.4892	0.000
Cntnap4	contactin associated protein-like 4	0.027421	-36.469	0.012
Dtl	denticleless homolog (Drosophila)	0.028232	-35.4211	0.000
Serpina3g	serine (or cysteine) peptidase inhibitor, clade A, member 3G	0.028403	-35.2079	0.000
Krt18	keratin 18	0.031692	-31.5538	0.000
Bcl11a	B cell CLL/lymphoma 11A (zinc finger protein)	0.032854	-30.4377	0.010
Tfap2a	transcription factor AP-2, alpha	0.033321	-30.011	0.001
Uchl1	ubiquitin carboxy-terminal hydrolase L1	0.034205	-29.2353	0.000
Foxf2	forkhead box F2	0.036285	-27.5594	0.000
Cd5	CD5 antigen	0.038011	-26.3084	0.008
Rasal3	RAS protein activator like 3	0.039291	-25.4511	0.000
Rab15	RAB15, member RAS oncogene family	0.040473	-24.7078	0.000
Cd8a	CD8 antigen, alpha chain	0.040691	-24.5757	0.001
Ccl8	chemokine (C-C motif) ligand 8	0.046068	-21.7069	0.000

Ces5a	carboxylesterase 5A	0.046703	-21.412	0.000
Cd4	CD4 antigen	0.048741	-20.5166	0.000
Fcgr4	Fc receptor, IgG, low affinity IV	0.050444	-19.824	0.000
Fam171b	family with sequence similarity 171, member B	0.052255	-19.1371	0.000
Gsdma	gasdermin A	0.052606	-19.0091	0.000
Ltb	lymphotoxin B	0.053662	-18.6351	0.019
Ikzf3	IKAROS family zinc finger 3	0.054051	-18.5009	0.001
Ly6c2	lymphocyte antigen 6 complex, locus C2	0.056049	-17.8415	0.003
Batf	basic leucine zipper transcription factor, ATF-like	0.056308	-17.7595	0.031
Ccl12	chemokine (C-C motif) ligand 12	0.056345	-17.7477	0.028
Pax6	paired box gene 6	0.057603	-17.3603	0.007
Cidea	cell death-inducing DNA fragmentation factor, alpha subunit-like effector A	0.057892	-17.2734	0.000
Ccl5	chemokine (C-C motif) ligand 5	0.058128	-17.2033	0.000
Clspn	claspin	0.058988	-16.9527	0.023
Dmrta2	doublesex and mab-3 related transcription factor like family A2	0.062089	-16.1059	0.012
Gzmk	granzyme K	0.06319	-15.8254	0.027
Il21r	interleukin 21 receptor	0.063213	-15.8196	0.004
Cd72	CD72 antigen	0.064189	-15.579	0.037
Ttc9	tetratricopeptide repeat domain 9	0.065572	-15.2505	0.000
Sln	sarcolipin	0.069215	-14.4477	0.001
Dnase1l3	deoxyribonuclease 1-like 3	0.069771	-14.3325	0.000
Cd79a	CD79A antigen (immunoglobulin-associated alpha)	0.07062	-14.1604	0.008
Cd22	CD22 antigen	0.070657	-14.1528	0.003
Ctla4	cytotoxic T-lymphocyte-associated protein 4	0.070752	-14.1338	0.000

2010001M09Rik	RIKEN cDNA 2010001M09 gene	0.071555	-13.9753	0.003
Cd3g	CD3 antigen, gamma polypeptide	0.07197	-13.8946	0.000
Cd2	CD2 antigen	0.072053	-13.8786	0.000
Il2rb	interleukin 2 receptor, beta chain	0.073228	-13.6561	0.003
Odf3l1	outer dense fiber of sperm tails 3-like 1	0.074442	-13.4332	0.004
Derl3	Der1-like domain family, member 3	0.074738	-13.3801	0.001
Nuf2	NUF2, NDC80 kinetochore complex component, homolog (S. cerevisiae)	0.075024	-13.3291	0.017
Il7r	interleukin 7 receptor	0.077025	-12.9827	0.010
Glipr1	GLI pathogenesis-related 1 (glioma)	0.078756	-12.6974	0.008
Enkur	enkurin, TRPC channel interacting protein	0.079766	-12.5367	0.001
Gldn	gliomedin	0.079949	-12.508	0.000
Pou2af1	POU domain, class 2, associating factor 1	0.082594	-12.1074	0.001
En1	engrailed 1	0.082647	-12.0996	0.000
Rac2	RAS-related C3 botulinum substrate 2	0.083404	-11.9898	0.000
Lax1	lymphocyte transmembrane adaptor 1	0.083693	-11.9485	0.001
Rhoh	ras homolog gene family, member H	0.086053	-11.6208	0.000
Tnfrsf13c	tumor necrosis factor receptor superfamily, member 13c	0.086336	-11.5826	0.020
Sh2d4a	SH2 domain containing 4A	0.086493	-11.5616	0.000
Tnfsf8	tumor necrosis factor (ligand) superfamily, member 8	0.087455	-11.4344	0.028
Ect2l	epithelial cell transforming sequence 2 oncogene-like	0.09071	-11.0241	0.000
Itgax	integrin alpha X	0.090955	-10.9944	0.000
Cd52	CD52 antigen	0.091342	-10.9479	0.000
Cd6	CD6 antigen	0.091456	-10.9342	0.000
Cd180	CD180 antigen	0.091786	-10.8949	0.004
Serpina3f	serine (or cysteine) peptidase inhibitor, clade A, member 3F	0.092401	-10.8224	0.029

Dync1i1	dynein cytoplasmic 1 intermediate chain 1	0.092592	-10.8001	0.000
Ly9	lymphocyte antigen 9	0.094412	-10.5919	0.006
Fcgr1	Fc receptor, IgG, high affinity I	0.09453	-10.5786	0.006
Spib	Spi-B transcription factor (Spi-1/PU.1 related)	0.095906	-10.4269	0.001
Galnt6	UDP-N-acetyl-alpha-D-galactosamine:polypeptide N-acetylgalactosaminyltransferase 6	0.096288	-10.3855	0.020
Cela1	chymotrypsin-like elastase family, member 1	0.096657	-10.3459	0.002
Scel	sciellin	0.097779	-10.2271	0.005
Cd8b1	CD8 antigen, beta chain 1	0.098388	-10.1638	0.017
Edar	ectodysplasin-A receptor	0.098428	-10.1597	0.000
Rnf165	ring finger protein 165	0.09862	-10.1399	0.005
1700024P16Rik	RIKEN cDNA 1700024P16 gene	0.09903	-10.0979	0.000
Kcnj3	potassium inwardly-rectifying channel, subfamily J, member 3	0.09996	-10.004	0.000
Dusp5	dual specificity phosphatase 5	0.100456	-9.95456	0.000
H2-Oa	histocompatibility 2, O region alpha locus	0.102586	-9.74789	0.015
Ly6d	lymphocyte antigen 6 complex, locus D	0.102615	-9.74514	0.006

Appendix II: Three Genotype Changed Gene List Comparison in WT, AR20 and AR100 Tibialis Anterior Muscle

6.7 Three Month Common Gene comparison- Up regulated Genes

Gene Symbol	Gene Name
Art5	ADP-ribosyltransferase 5
Atp5k	ATP synthase, H+ transporting, mitochondrial F1F0 complex, subunit e
Ckmt2	creatine kinase, mitochondrial 2
Cox4i1	cytochrome c oxidase subunit IV isoform 1
Cox5b	cytochrome c oxidase, subunit Vb
Gm13340	
Lmod3	leiomodin 3 (fetal)
Minos1	mitochondrial inner membrane organizing system 1
Mrln	Myoregulin
Ndufa11	NADH dehydrogenase (ubiquinone) 1 alpha subcomplex 11
Ndufa5	NADH dehydrogenase (ubiquinone) 1 alpha subcomplex, 5
Ndufb10	NADH dehydrogenase (ubiquinone) 1 beta subcomplex, 10
Ndufb7	NADH dehydrogenase (ubiquinone) 1 beta subcomplex, 7
Ndufs4	NADH dehydrogenase (ubiquinone) Fe-S protein 4
Pop5	processing of precursor 5, ribonuclease P/MRP family (S. cerevisiae)
Prdx5	peroxiredoxin 5
Rps21	ribosomal protein S21
Slc25a3	solute carrier family 25 (mitochondrial carrier, phosphate carrier), member 3
Uqcrq	ubiquinol-cytochrome c reductase, complex III subunit VII
Use1	unconventional SNARE in the ER 1 homolog (S. cerevisiae)
Vamp5	vesicle-associated membrane protein 5

6.8 Three Month Common Gene comparison- Down regulated Genes

Gene Symbol	Gene Name
Adam9	a disintegrin and metallopeptidase domain 9 (meltrin gamma)
Cacna1s	calcium channel, voltage-dependent, L type, alpha 1S subunit
Phf2	PHD finger protein 2
Ryr1	ryanodine receptor 1, skeletal muscle
Sympk	symplekin

6.9 Twelve Month Common Gene comparison- all genes

Gene Symbol	Gene Name
Abi2	abl-interactor 2
Sorbs3	sorbin and SH3 domain containing 3
Ssu72	Ssu72 RNA polymerase II CTD phosphatase homolog (yeast)
Nt5dc3	5'-nucleotidase domain containing 3
Plekhg2	pleckstrin homology domain containing, family G (with RhoGef domain) member 2
Mettl13	methyltransferase like 13
Ifrd2	interferon-related developmental regulator 2
Arpc1a	actin related protein 2/3 complex, subunit 1A
Gm9162	glyceraldehyde-3-phosphate dehydrogenase pseudogene
Prosc	proline synthetase co-transcribed
Arrdc4	arrestin domain containing 4
Pdp2	pyruvate dehyrogenase phosphatase catalytic subunit 2
Usp20	ubiquitin specific peptidase 20
Scrib	scribbled homolog (Drosophila)
Pkia	protein kinase inhibitor, alpha
Bcl7a	B cell CLL/lymphoma 7A
Bnip3l	BCL2/adenovirus E1B interacting protein 3-like
Shc2	SHC (Src homology 2 domain containing) transforming protein 2
Dnajc21	DnaJ (Hsp40) homolog, subfamily C, member 21
Pcdh1	protocadherin 1
Rif1	Rap1 interacting factor 1 homolog (yeast)
Kcnq5	potassium voltage-gated channel, subfamily Q, member 5
Cyb5r3	cytochrome b5 reductase 3
Snip1	Smad nuclear interacting protein 1
Lrig2	leucine-rich repeats and immunoglobulin-like domains 2
Ppia	peptidylprolyl isomerase A
Blvrb	biliverdin reductase B (flavin reductase (NADPH))
Dysf	dysferlin
Tmem8	transmembrane protein 8 (five membrane-spanning domains)
Zbed4	zinc finger, BED domain containing 4
Mbnl1	muscleblind-like 1 (Drosophila)
Dctn3	dynactin 3
Faf2	Fas associated factor family member 2
Abcd4	ATP-binding cassette, sub-family D (ALD), member 4
Tmco4	transmembrane and coiled-coil domains 4
Nkain1	Na+/K+ transporting ATPase interacting 1
Hsd17b4	hydroxysteroid (17-beta) dehydrogenase 4
Atg13	autophagy related 13
Mettl9	methyltransferase like 9

1700010I14Rik	RIKEN cDNA 1700010I14 gene
Psmd11	proteasome (prosome, macropain) 26S subunit, non-ATPase, 11
Ubxn4	UBX domain protein 4
Psph	phosphoserine phosphatase
Kpna1	karyopherin (importin) alpha 1
Dhrs7b	dehydrogenase/reductase (SDR family) member 7B
Tnfaip1	tumor necrosis factor, alpha-induced protein 1 (endothelial)
Steap3	STEAP family member 3
Ctps	cytidine 5'-triphosphate synthase
Slc41a3	solute carrier family 41, member 3
Cox11	COX11 homolog, cytochrome c oxidase assembly protein (yeast)
Trappc3	trafficking protein particle complex 3
Nek6	NIMA (never in mitosis gene a)-related expressed kinase 6
Myo1b	myosin IB
Rnf187	ring finger protein 187
Tmem53	transmembrane protein 53
Setd3	SET domain containing 3
Rnf115	ring finger protein 115
Ppm1l	protein phosphatase 1 (formerly 2C)-like
Atp1a1	ATPase, Na+/K+ transporting, alpha 1 polypeptide
Lzts1	leucine zipper, putative tumor suppressor 1
2310008N11Rik	RIKEN cDNA 2310008N11 gene
Mllt10	myeloid/lymphoid or mixed-lineage leukemia (trithorax homolog, Drosophila); translocated to, 10
Sspn	sarcospan
Etfa	electron transferring flavoprotein, alpha polypeptide
Slc39a13	solute carrier family 39 (metal ion transporter), member 13
Kat2a	K(lysine) acetyltransferase 2A
Pqlc2	PQ loop repeat containing 2
B430212C06Rik	RIKEN cDNA B430212C06 gene
6030458C11Rik	RIKEN cDNA 6030458C11 gene
Tmem104	transmembrane protein 104
Snx24	sorting nexing 24
Usp2	ubiquitin specific peptidase 2
Pmm1	phosphomannomutase 1
Vps4b	vacuolar protein sorting 4b (yeast)
Kcnj2	potassium inwardly-rectifying channel, subfamily J, member 2
Clpb	ClpB caseinolytic peptidase B
Bbx	bobby sox homolog (Drosophila)
Srl	sarcalumenin

Rpia	ribose 5-phosphate isomerase A
2610306M01Rik	RIKEN cDNA 2610306M01 gene
Nrcam	neuron-glia-CAM-related cell adhesion molecule
Nmt1	N-myristoyltransferase 1
Txndc5	thioredoxin domain containing 5
Klhl2	kelch-like 2, Mayven (Drosophila)
Ttc39c	tetratricopeptide repeat domain 39C
Nup210	nucleoporin 210
Klhl21	kelch-like 21 (Drosophila)
Cdk5	cyclin-dependent kinase 5
Sync	syncoilin
Sod2	superoxide dismutase 2, mitochondrial
Gm17068	glyceraldehyde-3-phosphate dehydrogenase pseudogene
Tubb6	tubulin, beta 6 class V
Fam195b	family with sequence similarity 195, member B
Ctdspl	CTD (carboxy-terminal domain, RNA polymerase II, polypeptide A) small phosphatase-like
Tmem184c	transmembrane protein 184C
Cdon	cell adhesion molecule-related/down-regulated by oncogenes
Riok3	RIO kinase 3 (yeast)
Sgk1	serum/glucocorticoid regulated kinase 1
Aig1	androgen-induced 1
A430046D13Rik	Riken cDNA A430046D13 gene
Ppp1r2	protein phosphatase 1, regulatory (inhibitor) subunit 2
Atp6v1e1	ATPase, H+ transporting, lysosomal V1 subunit E1
Adal	adenosine deaminase-like
Snapc3	small nuclear RNA activating complex, polypeptide 3
Ppp1r37	protein phosphatase 1, regulatory subunit 37
Disp1	dispatched homolog 1 (Drosophila)
Chd6	chromodomain helicase DNA binding protein 6
Cbfb	core binding factor beta
Gm3200	glyceraldehyde-3-phosphate dehydrogenase pseudogene
Chek2	checkpoint kinase 2
Jkamp	JNK1/MAPK8-associated membrane protein
Rev3l	REV3-like, catalytic subunit of DNA polymerase zeta RAD54 like (S. cerevisiae)
A130014A01Rik	RIKEN cDNA A130014A01 gene
Fgd5	FYVE, RhoGEF and PH domain containing 5
Zbtb16	zinc finger and BTB domain containing 16
Synpo2l	synaptopodin 2-like

Gm13292	glyceraldehyde-3-phosphate dehydrogenase pseudogene
Exosc1	exosome component 1
Hs1bp3	HCLS1 binding protein 3
Qser1	glutamine and serine rich 1
Cstb	cystatin B
Kit	kit oncogene
Sult1a1	sulfotransferase family 1A, phenol-preferring, member 1
Flywch1	FLYWCH-type zinc finger 1
Lrrc8d	leucine rich repeat containing 8D
Zcchc24	zinc finger, CCHC domain containing 24
Cacfd1	calcium channel flower domain containing 1
Vamp2	vesicle-associated membrane protein 2
Smox	spermine oxidase
Grem2	gremlin 2 homolog, cysteine knot superfamily (Xenopus laevis)
Rab12	RAB12, member RAS oncogene family
Hdgfrp2	hepatoma-derived growth factor, related protein 2
Pfkl	phosphofructokinase, liver, B-type
Adam17	a disintegrin and metallopeptidase domain 17
4931428F04Rik	RIKEN cDNA 4931428F04 gene
Pacsin2	protein kinase C and casein kinase substrate in neurons 2
Napb	N-ethylmaleimide sensitive fusion protein attachment protein beta
Mtl5	metallothionein-like 5, testis-specific (tesmin)
4921524J17Rik	RIKEN cDNA 4921524J17 gene
2310015A10Rik	RIKEN cDNA 2310015A10 gene
Ldhb	lactate dehydrogenase B
Clint1	clathrin interactor 1
Nmi	N-myc (and STAT) interactor
Eif3c	eukaryotic translation initiation factor 3, subunit C
Vgll4	vestigial like 4 (Drosophila)
Glyr1	glyoxylate reductase 1 homolog (Arabidopsis)
Tet2	tet methylcytosine dioxygenase 2
Gm4980	predicted gene 4980
Mrpl38	mitochondrial ribosomal protein L38
Slc25a29	solute carrier family 25 (mitochondrial carrier, palmitoylcarnitine transporter), member 29
Det1	de-etiolated homolog 1 (Arabidopsis)
Mdp1	magnesium-dependent phosphatase 1
Eftud2	elongation factor Tu GTP binding domain containing 2
Oma1	OMA1 homolog, zinc metallopeptidase (S. cerevisiae)
Mfsd8	major facilitator superfamily domain containing 8
Dnajc7	DnaJ (Hsp40) homolog, subfamily C, member 7

Pdia3	protein disulfide isomerase associated 3
Ndufa4l2	NADH dehydrogenase (ubiquinone) 1 alpha subcomplex, 4-like 2
Tor3a	torsin family 3, member A
Ccdc134	coiled-coil domain containing 134
Gp1ba	glycoprotein 1b, alpha polypeptide
Nsa2	NSA2 ribosome biogenesis homolog (S. cerevisiae)
Slc35b1	solute carrier family 35, member B1
Scn4b	sodium channel, type IV, beta
Rpp14	ribonuclease P 14 subunit (human)
Pi4k2a	phosphatidylinositol 4-kinase type 2 alpha
Rbms2	RNA binding motif, single stranded interacting protein 2
Ankrd37	ankyrin repeat domain 37
Srfbp1	serum response factor binding protein 1
Itga6	integrin alpha 6
Rab3a	RAB3A, member RAS oncogene family
Aggf1	angiogenic factor with G patch and FHA domains 1
Myc	myelocytomatosis oncogene
Itpkb	inositol 1,4,5-trisphosphate 3-kinase B
Wls	wntless homolog (Drosophila)
Larp7	La ribonucleoprotein domain family, member 7
Aida	axin interactor, dorsalization associated
Ctsf	cathepsin F
Casp12	caspase 12
Lpin3	lipin 3
Pdcl	phosducin-like
Manbal	mannosidase, beta A, lysosomal-like
Rbm33	RNA binding motif protein 33
Mir1b	microRNA 1b
Rhobtb2	Rho-related BTB domain containing 2
Mnt	max binding protein
Rab3gap1	RAB3 GTPase activating protein subunit 1
Ptprs	protein tyrosine phosphatase, receptor type, S
Myo5a	myosin VA
Fam49b	family with sequence similarity 49, member B
Rnaseh2b	ribonuclease H2, subunit B
Rab11fip3	RAB11 family interacting protein 3 (class II)
Trip4	thyroid hormone receptor interactor 4
Nr6a1	nuclear receptor subfamily 6, group A, member 1
Lta4h	leukotriene A4 hydrolase
Acox2	acyl-Coenzyme A oxidase 2, branched chain
Zdhhc5	zinc finger, DHHC domain containing 5
Smyd2	SET and MYND domain containing 2
Calu	calumenin

C1qbp	complement component 1, q subcomponent binding protein
Cpd	carboxypeptidase D
Ppp1r9a	protein phosphatase 1, regulatory (inhibitor) subunit 9A
Eef2	eukaryotic translation elongation factor 2
Rasgrp2	RAS, guanyl releasing protein 2
2310016G11Rik	RIKEN cDNA 2310016G11 gene
Sephs1	selenophosphate synthetase 1
Mrrf	mitochondrial ribosome recycling factor
Stx4a	syntaxin 4A (placental)
Setbp1	SET binding protein 1
Tmem106b	transmembrane protein 106B
Mpv17l	Mpv17 transgene, kidney disease mutant-like
1190002N15Rik	RIKEN cDNA 1190002N15 gene
Poldip3	polymerase (DNA-directed), delta interacting protein 3
Cmtm7	CKLF-like MARVEL transmembrane domain containing 7
Slc9a2	solute carrier family 9 (sodium/hydrogen exchanger), member 2
Bcl6b	B cell CLL/lymphoma 6, member B
Slc2a4	solute carrier family 2 (facilitated glucose transporter), member 4
Klc4	kinesin light chain 4
Eif2a	eukaryotic translation initiation factor 2A
Cnpy2	canopy 2 homolog (zebrafish)
Syt9	synaptotagmin IX
Gm10605	predicted gene 10605
Clcn7	chloride channel 7
Prmt10	protein arginine methyltransferase 10 (putative)
Lrrc59	leucine rich repeat containing 59
Mettl21a	methyltransferase like 21A
Trp53bp2	transformation related protein 53 binding protein 2
Sf3a2	splicing factor 3a, subunit 2
D11Wsu47e	DNA segment, Chr 11, Wayne State University 47, expressed
Ttll4	tubulin tyrosine ligase-like family, member 4
Ppp2r5b	protein phosphatase 2, regulatory subunit B (B56), beta isoform
Mppe1	metallophosphoesterase 1
Ldha-ps2	lactate dehydrogenase A, pseudogene 2
Tmem132b	transmembrane protein 132B

Hlcs	holocarboxylase synthetase (biotin- [propriony-Coenzyme A-carboxylase (ATP-hydrolysing)] ligase)
Crybb1	crystallin, beta B1
Oraov1	oral cancer overexpressed 1
Cuzd1	CUB and zona pellucida-like domains 1
Espnl	espin-like
Cstf2t	cleavage stimulation factor, 3' pre-RNA subunit 2, tau
Stk4	serine/threonine kinase 4
Snx7	sorting nexin 7
Lamc2	laminin, gamma 2
Cdkl2	cyclin-dependent kinase-like 2 (CDC2-related kinase)
Tmem127	transmembrane protein 127
Nos3	nitric oxide synthase 3, endothelial cell
Mustn1	musculoskeletal, embryonic nuclear protein 1
Mdm4	transformed mouse 3T3 cell double minute 4
Pex11a	peroxisomal biogenesis factor 11 alpha
Tmtc4	transmembrane and tetratricopeptide repeat containing 4
1700109H08Rik	RIKEN cDNA 1700109H08 gene
Amigo3	adhesion molecule with Ig like domain 3
Scarb1	scavenger receptor class B, member 1
Dot1l	DOT1-like, histone H3 methyltransferase (S. cerevisiae)
Kif26a	kinesin family member 26A
Fas	Fas (TNF receptor superfamily member 6)
Uba2	ubiquitin-like modifier activating enzyme 2
Eogt	EGF domain-specific O-linked N-acetylglucosamine (GlcNAc) transferase
Rab40b	Rab40b, member RAS oncogene family
Rnf166	ring finger protein 166
Card6	caspase recruitment domain family, member 6
Bloc1s6	biogenesis of organelles complex-1, subunit 6, pallidin
Trim24	tripartite motif-containing 24
Arvcf	armadillo repeat gene deleted in velo-cardio-facial syndrome
2810403A07Rik	RIKEN cDNA 2810403A07 gene
Bet1l	blocked early in transport 1 homolog (S. cerevisiae)-like

Mtfr1	mitochondrial fission regulator 1
Fancd2	Fanconi anemia, complementation group D2
Pon2	paraoxonase 2
Metrn	meteorin, glial cell differentiation regulator
Ehhadh	enoyl-Coenzyme A, hydratase/3-hydroxyacyl Coenzyme A dehydrogenase
Kif3c	kinesin family member 3C
Tfap4	transcription factor AP4
Mboat7	membrane bound O-acyltransferase domain containing 7
C2cd2	C2 calcium-dependent domain containing 2
Scamp1	secretory carrier membrane protein 1
Rnf170	ring finger protein 170
Esco1	establishment of cohesion 1 homolog 1 (S. cerevisiae)
Cadm1	cell adhesion molecule 1
Slc2a4rg-ps	Slc2a4 regulator, pseudogene
Prpf6	PRP6 pre-mRNA splicing factor 6 homolog (yeast)
Asl	argininosuccinate lyase
Naa20	N(alpha)-acetyltransferase 20, NatB catalytic subunit
Rgmb	RGM domain family, member B
Mboat1	membrane bound O-acyltransferase domain containing 1
Fam135a	family with sequence similarity 135, member A
Fam173b	family with sequence similarity 173, member B
Slc3a2	solute carrier family 3 (activators of dibasic and neutral amino acid transport), member 2
Rfwd2	ring finger and WD repeat domain 2
Sh2b2	SH2B adaptor protein 2
Arhgef5	Rho guanine nucleotide exchange factor (GEF) 5
Ccdc68	coiled-coil domain containing 68
Mt1	metallothionein 1
Mkrn2	makorin, ring finger protein, 2
Mark2	MAP/microtubule affinity-regulating kinase 2
Dhrs11	dehydrogenase/reductase (SDR family) member 11
Ube4a	ubiquitination factor E4A, UFD2 homolog (S. cerevisiae)
Thpo	thrombopoietin
Etohd2	ethanol decreased 2
Prom1	prominin 1

Cmya5	cardiomyopathy associated 5
Znrf3	zinc and ring finger 3
5730455P16Rik	RIKEN cDNA 5730455P16 gene
Zfp385b	zinc finger protein 385B
Atic	5-aminoimidazole-4-carboxamide ribonucleotide formyltransferase/IMP cyclohydrolase
Yipf1	Yip1 domain family, member 1
Trnau1ap	tRNA selenocysteine 1 associated protein 1
Sdf4	stromal cell derived factor 4
Megf8	multiple EGF-like-domains 8
2700029M09Rik	RIKEN cDNA 2700029M09 gene
Hey1	hairy/enhancer-of-split related with YRPW motif 1
Tbl3	transducin (beta)-like 3
1700052K11Rik	RIKEN cDNA 1700052K11 gene
Pkn1	protein kinase N1
Sfxn2	sideroflexin 2
Gm5559	glyceraldehyde-3-phosphate dehydrogenase pseudogene
Ap4s1	adaptor-related protein complex AP-4, sigma 1
Kctd15	potassium channel tetramerisation domain containing 15
Ccdc32	coiled-coil domain containing 32
Cd82	CD82 antigen
Sh3glb1	SH3-domain GRB2-like B1 (endophilin)
Lmod1	leiomodin 1 (smooth muscle)
Pnpla3	patatin-like phospholipase domain containing 3
Paf1	Paf1, RNA polymerase II associated factor, homolog (S. cerevisiae)
Camk1	calcium/calmodulin-dependent protein kinase I
Vps11	vacuolar protein sorting 11 (yeast)
Vcp	valosin containing protein
Dhx32	DEAH (Asp-Glu-Ala-His) box polypeptide 32
Cc2d2a	coiled-coil and C2 domain containing 2A
Taf6l	TAF6-like RNA polymerase II, p300/CBP-associated factor (PCAF)-associated factor
Irf3	interferon regulatory factor 3
1700001O22Rik	RIKEN cDNA 1700001O22 gene

Mtpap	mitochondrial poly(A) polymerase
Lrrc32	leucine rich repeat containing 32
H2-T22	histocompatibility 2, T region locus 22
Gm7507	glyceraldehyde-3-phosphate dehydrogenase pseudogene
Parp3	poly (ADP-ribose) polymerase family, member 3
Sema4d	sema domain, immunoglobulin domain (Ig), transmembrane domain (TM) and short cytoplasmic domain, (semaphorin) 4D
Gm3636	predicted gene 3636
Kcna5	potassium voltage-gated channel, shaker-related subfamily, member 5
Got1	glutamate oxaloacetate transaminase 1, soluble
Rpn1	ribophorin I
Phf10	PHD finger protein 10
Zfp28	zinc finger protein 28
Eng	endoglin
Tbcel	tubulin folding cofactor E-like
Msh3	mutS homolog 3 (E. coli)
B3galnt2	UDP-GalNAc:betaGlcNAc beta 1,3-galactosaminyltransferase, polypeptide 2
Arhgap31	Rho GTPase activating protein 31
Fkbp15	FK506 binding protein 15
Serpinb6a	serine (or cysteine) peptidase inhibitor, clade B, member 6a
As3mt	arsenic (+3 oxidation state) methyltransferase
Abhd11	abhydrolase domain containing 11
Cd38	CD38 antigen
Top1mt	DNA topoisomerase 1, mitochondrial
Six1	sine oculis-related homeobox 1
Scaf1	SR-related CTD-associated factor 1
1700123M08Rik	RIKEN cDNA 1700123M08 gene
Brk1	BRICK1, SCAR/WAVE actin-nucleating complex subunit
C030037D09Rik	RIKEN cDNA C030037D09 gene
Taf1b	TATA box binding protein (Tbp)-associated factor, RNA polymerase I, B
Ppp4r1	protein phosphatase 4, regulatory subunit 1
Npl	N-acetylneuraminate pyruvate lyase
Mx2	myxovirus (influenza virus) resistance 2

D330023K18Rik	RIKEN cDNA D330023K18 gene
Hoxc11	homeobox C11
Dusp7	dual specificity phosphatase 7
Gpr146	G protein-coupled receptor 146
Gpr137	G protein-coupled receptor 137
Tut1	terminal uridylyl transferase 1, U6 snRNA-specific
Fut10	fucosyltransferase 10
Trim41	tripartite motif-containing 41
Trdc	T cell receptor delta, constant region
Mfn1	mitofusin 1
Vegfa	vascular endothelial growth factor A
Qrsl1	glutaminyl-tRNA synthase (glutamine-hydrolyzing)-like 1
Foxf2	forkhead box F2
Acadsb	acyl-Coenzyme A dehydrogenase, short/branched chain
Atat1	alpha tubulin acetyltransferase 1
Mylip	myosin regulatory light chain interacting protein
Stam	signal transducing adaptor molecule (SH3 domain and ITAM motif) 1
Myd88	myeloid differentiation primary response gene 88
Trafd1	TRAF type zinc finger domain containing 1
Osbpl1a	oxysterol binding protein-like 1A
Crip2	cysteine rich protein 2
Alas1	aminolevulinic acid synthase 1
Zfp260	zinc finger protein 260
Slc7a5	solute carrier family 7 (cationic amino acid transporter, y+ system), member 5
Flrt2	fibronectin leucine rich transmembrane protein 2
Dok7	docking protein 7
Ormdl3	ORM1-like 3 (S. cerevisiae)
Ripk2	receptor (TNFRSF)-interacting serine-threonine kinase 2
Prepl	prolyl endopeptidase-like
Sort1	sortilin 1
Sacs	sacsin
9530068E07Rik	RIKEN cDNA 9530068E07 gene
Atp8a2	ATPase, aminophospholipid transporter-like, class I, type 8A, member 2

Gdap10	ganglioside-induced differentiation-associated-protein 10
Smad4	SMAD family member 4
Adrbk2	adrenergic receptor kinase, beta 2
Sgk3	serum/glucocorticoid regulated kinase 3
Papss2	3'-phosphoadenosine 5'-phosphosulfate synthase 2
4931406C07Rik	RIKEN cDNA 4931406C07 gene
Shmt2	serine hydroxymethyltransferase 2 (mitochondrial)
Cebpg	CCAAT/enhancer binding protein (C/EBP), gamma
Dync1li2	dynein, cytoplasmic 1 light intermediate chain 2
Otud6b	OTU domain containing 6B
Zfp612	zinc finger protein 612
Pip5k1a	phosphatidylinositol-4-phosphate 5-kinase, type 1 alpha
Mettl16	methyltransferase like 16
Trmt12	tRNA methyltranferase 12 homolog (S. cerevisiae)
Prkab2	protein kinase, AMP-activated, beta 2 non-catalytic subunit
Crem	cAMP responsive element modulator
Cpt1a	carnitine palmitoyltransferase 1a, liver
Msrb2	methionine sulfoxide reductase B2
Hmcn1	hemicentin 1
Arl6ip5	ADP-ribosylation factor-like 6 interacting protein 5
C130074G19Rik	RIKEN cDNA C130074G19 gene
F2r	coagulation factor II (thrombin) receptor
Tnk2	tyrosine kinase, non-receptor, 2
Rb1	retinoblastoma 1
Pcbp4	poly(rC) binding protein 4
Vamp8	vesicle-associated membrane protein 8
Decr2	2-4-dienoyl-Coenzyme A reductase 2, peroxisomal
Fbxw7	F-box and WD-40 domain protein 7
Pld3	phospholipase D family, member 3
Chst15	carbohydrate (N-acetylgalactosamine 4-sulfate 6-O) sulfotransferase 15
Xrcc6	X-ray repair complementing defective repair in Chinese hamster cells 6

Snta1	syntrophin, acidic 1
Eid2	EP300 interacting inhibitor of differentiation 2
Wsb1	WD repeat and SOCS box-containing 1
Ccdc28b	coiled coil domain containing 28B
Acvr2a	activin receptor IIA
Sgcb	sarcoglycan, beta (dystrophin-associated glycoprotein)
Tm9sf4	transmembrane 9 superfamily protein member 4
Dpyd	dihydropyrimidine dehydrogenase
2810032G03Rik	RIKEN cDNA 2810032G03 gene
Cep68	centrosomal protein 68
Ptp4a3	protein tyrosine phosphatase 4a3
Ccnl2	cyclin L2
Prelid2	PRELI domain containing 2
Gm9658	glyceraldehyde-3-phosphate dehydrogenase pseudogene
Tep1	telomerase associated protein 1
Rgs5	regulator of G-protein signaling 5
Atp1a2	ATPase, Na+/K+ transporting, alpha 2 polypeptide
Atrnl1	attractin like 1
Rrp1	ribosomal RNA processing 1 homolog (S. cerevisiae)
Mapre3	microtubule-associated protein, RP/EB family, member 3
Crmp1	collapsin response mediator protein 1
Jak2	Janus kinase 2
Ghitm	growth hormone inducible transmembrane protein
Ppp2r3d	protein phosphatase 2 (formerly 2A), regulatory subunit B'', delta
1700020I14Rik	RIKEN cDNA 1700020I14 gene
Tinagl1	tubulointerstitial nephritis antigen-like 1
Ppargc1b	peroxisome proliferative activated receptor, gamma, coactivator 1 beta
Mtap	methylthioadenosine phosphorylase
Dll4	delta-like 4 (Drosophila)
Cuedc1	CUE domain containing 1
Trim72	tripartite motif-containing 72
Mfap1a	microfibrillar-associated protein 1A
Camta1	calmodulin binding transcription activator 1
Cnrip1	cannabinoid receptor interacting protein 1

Map3k9	mitogen-activated protein kinase kinase kinase 9
Musk	muscle, skeletal, receptor tyrosine kinase
Gsk3a	glycogen synthase kinase 3 alpha
Heatr3	HEAT repeat containing 3
Fam73a	family with sequence similarity 73, member A
Erg	avian erythroblastosis virus E-26 (v-ets) oncogene related
Rptor	regulatory associated protein of MTOR, complex 1
Gm10604	predicted gene 10604
Snap47	synaptosomal-associated protein, 47
Idnk	idnK gluconokinase homolog (E. coli)
Phyh	phytanoyl-CoA hydroxylase
Atp6v1g2	ATPase, H+ transporting, lysosomal V1 subunit G2
Vps39	vacuolar protein sorting 39 (yeast)
1700120C14Rik	RIKEN cDNA 1700120C14 gene
Prrc1	proline-rich coiled-coil 1
Pmm2	phosphomannomutase 2
Cox15	COX15 homolog, cytochrome c oxidase assembly protein (yeast)
Fbxo4	F-box protein 4
Mest	mesoderm specific transcript
Itfg2	integrin alpha FG-GAP repeat containing 2
Aldoc	aldolase C, fructose-bisphosphate
Sbno2	strawberry notch homolog 2 (Drosophila)
Fam118b	family with sequence similarity 118, member B
Ppp1r16a	protein phosphatase 1, regulatory (inhibitor) subunit 16A
Rnf20	ring finger protein 20
Fbxo45	F-box protein 45
Avil	advillin
Tsen34	tRNA splicing endonuclease 34 homolog (S. cerevisiae)
Sh3rf2	SH3 domain containing ring finger 2
Adra1a	adrenergic receptor, alpha 1a
Oasl1	2'-5' oligoadenylate synthetase-like 1
Gm5864	PDZ and LIM domain protein 1 pseudogene
Nedd1	neural precursor cell expressed, developmentally down-regulated gene 1
Gm3695	glyceraldehyde-3-phosphate dehydrogenase pseudogene
Zfp513	zinc finger protein 513

Gstm7	glutathione S-transferase, mu 7
Fam171b	family with sequence similarity 171, member B
Ndn	necdin
Ilvbl	ilvB (bacterial acetolactate synthase)-like
Gm2a	GM2 ganglioside activator protein
Gm17501	predicted gene, 17501
Csnk1g3	casein kinase 1, gamma 3
Nipa2	non imprinted in Prader-Willi/Angelman syndrome 2 homolog (human)
Ccdc101	coiled-coil domain containing 101
Smu1	smu-1 suppressor of mec-8 and unc-52 homolog (C. elegans)
Tmem252	transmembrane protein 252
Pik3ca	phosphatidylinositol 3-kinase, catalytic, alpha polypeptide
Phf2	PHD finger protein 2
Fcgrt	Fc receptor, IgG, alpha chain transporter
Pde4d	phosphodiesterase 4D, cAMP specific
P2ry1	purinergic receptor P2Y, G-protein coupled 1
Tbc1d22a	TBC1 domain family, member 22a
Nup153	nucleoporin 153
Adcy4	adenylate cyclase 4
Dhrs7	dehydrogenase/reductase (SDR family) member 7
Chmp4b	charged multivesicular body protein 4B
Slco4a1	solute carrier organic anion transporter family, member 4a1
Rars2	arginyl-tRNA synthetase 2, mitochondrial
Lama5	laminin, alpha 5
Wfdc1	WAP four-disulfide core domain 1
Per3	period homolog 3 (Drosophila)
Nkiras2	NFKB inhibitor interacting Ras-like protein 2
Nr1d1	nuclear receptor subfamily 1, group D, member 1
Copg2	coatomer protein complex, subunit gamma 2
Eif6	eukaryotic translation initiation factor 6
Apoa1bp	apolipoprotein A-I binding protein
Xrcc6bp1	XRCC6 binding protein 1
Znrd1as	ZNRD1 antisense RNA
Tnip2	TNFAIP3 interacting protein 2
Mthfd1	methylenetetrahydrofolate dehydrogenase (NADP+ dependent), methenyltetrahydrofolate cyclohydrolase, formyltetrahydrofolate synthase

Coro7	coronin 7
Gpt2	glutamic pyruvate transaminase (alanine aminotransferase) 2
Adig	adipogenin
Prrt3	proline-rich transmembrane protein 3
Nf2	neurofibromatosis 2
Psmd5	proteasome (prosome, macropain) 26S subunit, non-ATPase, 5
Pank1	pantothenate kinase 1
Dnmt1	DNA methyltransferase (cytosine-5) 1
Rapgef3	Rap guanine nucleotide exchange factor (GEF) 3
A430105I19Rik	RIKEN cDNA A430105I19 gene
2210016F16Rik	RIKEN cDNA 2210016F16 gene
Dpp3	dipeptidylpeptidase 3
Tspan31	tetraspanin 31
Fam102b	family with sequence similarity 102, member B
Tcte2	t-complex-associated testis expressed 2
Fscn2	fascin homolog 2, actin-bundling protein, retinal (Strongylocentrotus purpuratus)
Scyl1	SCY1-like 1 (S. cerevisiae)
Rtn3	reticulon 3
Sdpr	serum deprivation response
Agtrap	angiotensin II, type I receptor-associated protein
Ggt7	gamma-glutamyltransferase 7
Os9	amplified in osteosarcoma
Trim11	tripartite motif-containing 11
Mpped2	metallophosphoesterase domain containing 2
Ik	IK cytokine
Gramd1a	GRAM domain containing 1A
Cpne2	copine II
Hspa12b	heat shock protein 12B
AI464131	expressed sequence AI464131
Habp2	hyaluronic acid binding protein 2
Tma16	translation machinery associated 16 homolog (S. cerevisiae)
Pdlim5	PDZ and LIM domain 5
Eid1	EP300 interacting inhibitor of differentiation 1
Cebpz	CCAAT/enhancer binding protein zeta
Dnase1	deoxyribonuclease I
Odf3l1	outer dense fiber of sperm tails 3-like 1
Zfand1	zinc finger, AN1-type domain 1

Htatip2	HIV-1 tat interactive protein 2, homolog (human)
Sema6b	sema domain, transmembrane domain (TM), and cytoplasmic domain, (semaphorin) 6B
Farsb	phenylalanyl-tRNA synthetase, beta subunit
Acap3	ArfGAP with coiled-coil, ankyrin repeat and PH domains 3
Cc2d1b	coiled-coil and C2 domain containing 1B
Kcnj8	potassium inwardly-rectifying channel, subfamily J, member 8
Shisa4	shisa homolog 4 (Xenopus laevis)
Apcdd1	adenomatosis polyposis coli down-regulated 1
Aldh1l2	aldehyde dehydrogenase 1 family, member L2
Sctr	secretin receptor
Hlf	hepatic leukemia factor
Vezf1	vascular endothelial zinc finger 1
Ppp1r3a	protein phosphatase 1, regulatory (inhibitor) subunit 3A
Phkb	phosphorylase kinase beta
Gdf11	growth differentiation factor 11
Chmp7	charged multivesicular body protein 7
Acsf3	acyl-CoA synthetase family member 3
Vgll3	vestigial like 3 (Drosophila)
Tmem205	transmembrane protein 205
Dnajc18	DnaJ (Hsp40) homolog, subfamily C, member 18
Atf5	activating transcription factor 5
En1	engrailed 1
Dmpk	dystrophia myotonica-protein kinase
Ube3c	ubiquitin protein ligase E3C
Sec14l5	SEC14-like 5 (S. cerevisiae)
Trib2	tribbles homolog 2 (Drosophila)
Naca	nascent polypeptide-associated complex alpha polypeptide
Pgrmc2	progesterone receptor membrane component 2
Spag5	sperm associated antigen 5
Map4k2	mitogen-activated protein kinase kinase kinase kinase 2
Cdc42ep3	CDC42 effector protein (Rho GTPase binding) 3
Tsc22d4	TSC22 domain family, member 4
Ell2	elongation factor RNA polymerase II 2

2310015D24Rik	RIKEN cDNA 2310015D24 gene
Tmem246	transmembrane protein 246
Parp12	poly (ADP-ribose) polymerase family, member 12
Cdkn2aipnl	CDKN2A interacting protein N-terminal like
Asrgl1	asparaginase like 1
Tob1	transducer of ErbB-2.1
Fbxo30	F-box protein 30
Fam193b	family with sequence similarity 193, member B
Marveld2	MARVEL (membrane-associating) domain containing 2
Copb1	coatomer protein complex, subunit beta 1
Ccdc85a	coiled-coil domain containing 85A
Epm2a	epilepsy, progressive myoclonic epilepsy, type 2 gene alpha
Rnf165	ring finger protein 165
Fam26e	family with sequence similarity 26, member E
Auts2	autism susceptibility candidate 2
Creb5	cAMP responsive element binding protein 5
Cacna2d1	calcium channel, voltage-dependent, alpha2/delta subunit 1
Gtf3c1	general transcription factor III C 1
Gas6	growth arrest specific 6
2610035D17Rik	RIKEN cDNA 2610035D17 gene
Dcaf8	DDB1 and CUL4 associated factor 8
Car8	carbonic anhydrase 8
Gfer	growth factor, erv1 (S. cerevisiae)-like (augmenter of liver regeneration)
Col24a1	collagen, type XXIV, alpha 1
Clcc1	chloride channel CLIC-like 1
Alg14	asparagine-linked glycosylation 14
Nom1	nucleolar protein with MIF4G domain 1
Lman2	lectin, mannose-binding 2
Cdc5l	cell division cycle 5-like (S. pombe)
Nrtn	neurturin
Car1	carbonic anhydrase 1
March 6	membrane-associated ring finger (C3HC4) 6
BC029722	cDNA sequence BC029722
Rmnd5a	required for meiotic nuclear division 5 homolog A (S. cerevisiae)

Smoc2	SPARC related modular calcium binding 2
Nktr	natural killer tumor recognition sequence
Klhdc3	kelch domain containing 3
Scamp5	secretory carrier membrane protein 5
Mmd	monocyte to macrophage differentiation-associated
Macrod2	MACRO domain containing 2
Asb10	ankyrin repeat and SOCS box-containing 10
Card11	caspase recruitment domain family, member 11
Cdnf	cerebral dopamine neurotrophic factor
Adck5	aarF domain containing kinase 5
Atp6v0e2	ATPase, H+ transporting, lysosomal V0 subunit E2
Smarcd3	SWI/SNF related, matrix associated, actin dependent regulator of chromatin, subfamily d, member 3
Mpp6	membrane protein, palmitoylated 6 (MAGUK p55 subfamily member 6)
Rcan1	regulator of calcineurin 1
Pmpca	peptidase (mitochondrial processing) alpha
Nt5c	5',3'-nucleotidase, cytosolic
Leo1	Leo1, Paf1/RNA polymerase II complex component, homolog (S. cerevisiae)
Tle1	transducin-like enhancer of split 1, homolog of Drosophila E(spl)
Kcnma1	potassium large conductance calcium-activated channel, subfamily M, alpha member 1
Fam83d	family with sequence similarity 83, member D
Ankrd32	ankyrin repeat domain 32
Stx6	syntaxin 6
Eif3l	eukaryotic translation initiation factor 3, subunit L
Snx4	sorting nexin 4
A930004D18Rik	RIKEN cDNA A930004D18 gene
Pcyt2	phosphate cytidylyltransferase 2, ethanolamine
Brap	BRCA1 associated protein
Tecta	tectorin alpha
Odf2	outer dense fiber of sperm tails 2
Ect2l	epithelial cell transforming sequence 2 oncogene-like
Ift80	intraflagellar transport 80
Cenpc1	centromere protein C1

Tmem56	transmembrane protein 56
Bri3	brain protein I3
Unc13b	unc-13 homolog B (C. elegans)
Ephb4	Eph receptor B4
Pds5b	PDS5, regulator of cohesion maintenance, homolog B (S. cerevisiae)
Wnk2	WNK lysine deficient protein kinase 2
Rnf130	ring finger protein 130
Plk3	polo-like kinase 3
Als2cl	ALS2 C-terminal like
Cda	cytidine deaminase
Prkcz	protein kinase C, zeta
B4galt5	UDP-Gal:betaGlcNAc beta 1,4-galactosyltransferase, polypeptide 5
Klhdc1	kelch domain containing 1
Txnl1	thioredoxin-like 1
1700030K09Rik	RIKEN cDNA 1700030K09 gene
Mcm6	minichromosome maintenance deficient 6 (MIS5 homolog, S. pombe) (S. cerevisiae)
Slc27a1	solute carrier family 27 (fatty acid transporter), member 1
Entpd6	ectonucleoside triphosphate diphosphohydrolase 6
Plekhm2	pleckstrin homology domain containing, family M (with RUN domain) member 2
Aqp7	aquaporin 7
Tbx1	T-box 1
Oxld1	oxidoreductase like domain containing 1
Tmem234	transmembrane protein 234
Tubg2	tubulin, gamma 2
Pphln1	periphilin 1
Med25	mediator of RNA polymerase II transcription, subunit 25 homolog (yeast)
Tbkbp1	TBK1 binding protein 1
Arpc3	actin related protein 2/3 complex, subunit 3
Plekho1	pleckstrin homology domain containing, family O member 1
Polr3b	polymerase (RNA) III (DNA directed) polypeptide B
Dazap2	DAZ associated protein 2
Cdk5rap3	CDK5 regulatory subunit associated protein 3
Slc43a3	solute carrier family 43, member 3
Bace1	beta-site APP cleaving enzyme 1

Slc37a1	solute carrier family 37 (glycerol-3-phosphate transporter), member 1
Lix1	limb expression 1 homolog (chicken)
Prdm16	PR domain containing 16
Ypel2	yippee-like 2 (Drosophila)
Itgb3bp	integrin beta 3 binding protein (beta3-endonexin)
Rnf10	ring finger protein 10
Ift27	intraflagellar transport 27
Kbtbd13	kelch repeat and BTB (POZ) domain containing 13
Wdr7	WD repeat domain 7
C330006A16Rik	RIKEN cDNA C330006A16 gene
Parp4	poly (ADP-ribose) polymerase family, member 4
Phf7	PHD finger protein 7
Tspan2	tetraspanin 2
Rhoa	ras homolog gene family, member A
Osmr	oncostatin M receptor
Arhgef25	Rho guanine nucleotide exchange factor (GEF) 25
Kctd2	potassium channel tetramerisation domain containing 2
Bst2	bone marrow stromal cell antigen 2
Serpinb1a	serine (or cysteine) peptidase inhibitor, clade B, member 1a
P2ry6	pyrimidinergic receptor P2Y, G-protein coupled, 6
Trip10	thyroid hormone receptor interactor 10
Ltbp1	latent transforming growth factor beta binding protein 1
1110008L16Rik	RIKEN cDNA 1110008L16 gene
Fam110a	family with sequence similarity 110, member A
Slc35a1	solute carrier family 35 (CMP-sialic acid transporter), member 1
Cdk4	cyclin-dependent kinase 4
Cand1	cullin associated and neddylation disassociated 1
Npc1	Niemann Pick type C1
Hspa5	heat shock protein 5
Golga3	golgi autoantigen, golgin subfamily a, 3
Zscan2	zinc finger and SCAN domain containing 2
Popdc3	popeye domain containing 3

Gm16470	glyceraldehyde-3-phosphate dehydrogenase pseudogene
Pxn	paxillin
Mta2	metastasis-associated gene family, member 2
Fat3	FAT tumor suppressor homolog 3 (Drosophila)
Sbk1	SH3-binding kinase 1
Pts	6-pyruvoyl-tetrahydropterin synthase
Ccdc90b	coiled-coil domain containing 90B
Cyb5rl	cytochrome b5 reductase-like
Palmd	palmdelphin
Rangap1	RAN GTPase activating protein 1
Sdc3	syndecan 3
Lrrc8c	leucine rich repeat containing 8 family, member C
2310057M21Rik	RIKEN cDNA 2310057M21 gene
Ctf1	cardiotrophin 1
Tk1	thymidine kinase 1
Bhlhe40	basic helix-loop-helix family, member e40
Cct3	chaperonin containing Tcp1, subunit 3 (gamma)
Pdcd7	programmed cell death 7
Mybbp1a	MYB binding protein (P160) 1a
Cth	cystathionase (cystathionine gamma-lyase)
Tnfrsf12a	tumor necrosis factor receptor superfamily, member 12a
Pgm2l1	phosphoglucomutase 2-like 1
Dusp27	dual specificity phosphatase 27 (putative)
Gmip	Gem-interacting protein
Tmem173	transmembrane protein 173
Atg16l2	autophagy related 16-like 2 (S. cerevisiae)
Cndp2	CNDP dipeptidase 2 (metallopeptidase M20 family)
Riok2	RIO kinase 2 (yeast)
Abce1	ATP-binding cassette, sub-family E (OABP), member 1
Pacsin3	protein kinase C and casein kinase substrate in neurons 3
Jak1	Janus kinase 1
Ocel1	occludin/ELL domain containing 1
Ifi44	interferon-induced protein 44
Trappc1	trafficking protein particle complex 1
Metap2	methionine aminopeptidase 2
Obfc1	oligonucleotide/oligosaccharide-binding fold containing 1

Mul1	mitochondrial ubiquitin ligase activator of NFKB 1
Runx1	runt related transcription factor 1
Fadd	Fas (TNFRSF6)-associated via death domain
Stbd1	starch binding domain 1
B3galt6	UDP-Gal:betaGal beta 1,3-galactosyltransferase, polypeptide 6
Nfyb	nuclear transcription factor-Y beta
1810037I17Rik	RIKEN cDNA 1810037I17 gene
Ammecr1l	AMME chromosomal region gene 1-like
Cdk10	cyclin-dependent kinase 10
Tet3	tet methylcytosine dioxygenase 3
Ppa2	pyrophosphatase (inorganic) 2
Rnf103	ring finger protein 103
Pigs	phosphatidylinositol glycan anchor biosynthesis, class S
Serp1	stress-associated endoplasmic reticulum protein 1
Lrrc28	leucine rich repeat containing 28
Hsp90ab1	heat shock protein 90 alpha (cytosolic), class B member 1
Acss3	acyl-CoA synthetase short-chain family member 3
Tomm20	translocase of outer mitochondrial membrane 20 homolog (yeast)
Cebpd	CCAAT/enhancer binding protein (C/EBP), delta
Noa1	nitric oxide associated 1
Aimp2	aminoacyl tRNA synthetase complex-interacting multifunctional protein 2
Phf1	PHD finger protein 1
Eftud1	elongation factor Tu GTP binding domain containing 1
Nek5	NIMA (never in mitosis gene a)-related expressed kinase 5
Tollip	toll interacting protein
Tmf1	TATA element modulatory factor 1
Sf3a1	splicing factor 3a, subunit 1
Panx1	pannexin 1
Banp	BTG3 associated nuclear protein
Vcpip1	valosin containing protein (p97)/p47 complex interacting protein 1

Arhgap23	Rho GTPase activating protein 23
Arl8a	ADP-ribosylation factor-like 8A
Tph1	tryptophan hydroxylase 1
Slc25a34	solute carrier family 25, member 34
Oxnad1	oxidoreductase NAD-binding domain containing 1
Midn	midnolin
Zscan18	zinc finger and SCAN domain containing 18
Sh3bp1	SH3-domain binding protein 1
Golm1	golgi membrane protein 1
Cidea	cell death-inducing DNA fragmentation factor, alpha subunit-like effector A
Zdhhc1	zinc finger, DHHC domain containing 1
Adam22	a disintegrin and metallopeptidase domain 22
Bche	butyrylcholinesterase
Tiprl	TIP41, TOR signalling pathway regulator-like (S. cerevisiae)
L2hgdh	L-2-hydroxyglutarate dehydrogenase
Mfsd7b	major facilitator superfamily domain containing 7B
Smyd1	SET and MYND domain containing 1
Ephb6	Eph receptor B6
Smarca2	SWI/SNF related, matrix associated, actin dependent regulator of chromatin, subfamily a, member 2
Top2b	topoisomerase (DNA) II beta
Stk35	serine/threonine kinase 35
Vps29	vacuolar protein sorting 29 (S. pombe)
Lbh	limb-bud and heart
Nrp2	neuropilin 2
Retsat	retinol saturase (all trans retinol 13,14 reductase)
Vps4a	vacuolar protein sorting 4a (yeast)
Golph3	golgi phosphoprotein 3
Zfp512	zinc finger protein 512
Rusc2	RUN and SH3 domain containing 2
2700046G09Rik	RIKEN cDNA 2700046G09 gene
Ccnt1	cyclin T1
Peo1	progressive external ophthalmoplegia 1 (human)
2610001J05Rik	RIKEN cDNA 2610001J05 gene
Fam168a	family with sequence similarity 168, member A

Gm8756	glyceraldehyde-3-phosphate dehydrogenase pseudogene
Ybx2	Y box protein 2
Ppm1k	protein phosphatase 1K (PP2C domain containing)
Acads	acyl-Coenzyme A dehydrogenase, short chain
Cbr3	carbonyl reductase 3
Gm6316	glyceraldehyde-3-phosphate dehydrogenase pseudogene
Slc39a12	solute carrier family 39 (zinc transporter), member 12
Rdx	radixin
Azi2	5-azacytidine induced gene 2
Nudt22	nudix (nucleoside diphosphate linked moiety X)-type motif 22
2810414N06Rik	RIKEN cDNA 2810414N06 gene
Sept 7	septin 7
Zfyve27	zinc finger, FYVE domain containing 27
Tmem2	transmembrane protein 2
Kcnb1	potassium voltage gated channel, Shab-related subfamily, member 1
Hipk4	homeodomain interacting protein kinase 4
Tmtc1	transmembrane and tetratricopeptide repeat containing 1
Ptgr2	prostaglandin reductase 2
Blmh	bleomycin hydrolase
Dennd3	DENN/MADD domain containing 3
Mettl8	methyltransferase like 8
Atp13a2	ATPase type 13A2
Mcc	mutated in colorectal cancers
Tbc1d19	TBC1 domain family, member 19
Gsr	glutathione reductase
Zfp637	zinc finger protein 637
Gm8825	glyceraldehyde-3-phosphate dehydrogenase pseudogene
Odf3l2	outer dense fiber of sperm tails 3-like 2
Zbtb46	zinc finger and BTB domain containing 46
Trappc4	trafficking protein particle complex 4
Nek7	NIMA (never in mitosis gene a)-related expressed kinase 7
Cdipt	CDP-diacylglycerol--inositol 3-phosphatidyltransferase (phosphatidylinositol synthase)

Nr3c1	nuclear receptor subfamily 3, group C, member 1
Ing2	inhibitor of growth family, member 2
Tmem123	transmembrane protein 123
Gm14290	predicted gene 14290
Traip	TRAF-interacting protein
Slc38a2	solute carrier family 38, member 2
Plb1	phospholipase B1
Npepl1	aminopeptidase-like 1
Kdm1b	lysine (K)-specific demethylase 1B
Sumf1	sulfatase modifying factor 1
Ercc5	excision repair cross-complementing rodent repair deficiency, complementation group 5
Cdc23	CDC23 cell division cycle 23
Lman1	lectin, mannose-binding, 1
Tec	tec protein tyrosine kinase
Hoxa7	homeobox A7
Sf3b1	splicing factor 3b, subunit 1
Impad1	inositol monophosphatase domain containing 1
Man2a2	mannosidase 2, alpha 2
Zfp358	zinc finger protein 358
Usp3	ubiquitin specific peptidase 3
Xpo7	exportin 7
Ttll12	tubulin tyrosine ligase-like family, member 12
Qsox1	quiescin Q6 sulfhydryl oxidase 1
Shank3	SH3/ankyrin domain gene 3
Mphosph8	M-phase phosphoprotein 8
Cdk19	cyclin-dependent kinase 19
Idh3b	isocitrate dehydrogenase 3 (NAD+) beta
Aldh1b1	aldehyde dehydrogenase 1 family, member B1
Kbtbd8	kelch repeat and BTB (POZ) domain containing 8
Helb	helicase (DNA) B
Rhbdl3	rhomboid, veinlet-like 3 (Drosophila)
Sgpl1	sphingosine phosphate lyase 1
Gm17552	predicted gene, 17552
Mcm2	minichromosome maintenance deficient 2 mitotin (S. cerevisiae)
Ring1	ring finger protein 1
D930016D06Rik	RIKEN cDNA D930016D06 gene
Prdm4	PR domain containing 4

Cyp4f13	cytochrome P450, family 4, subfamily f, polypeptide 13
Khsrp	KH-type splicing regulatory protein
Ttc19	tetratricopeptide repeat domain 19
Trp53inp2	transformation related protein 53 inducible nuclear protein 2
Camk2a	calcium/calmodulin-dependent protein kinase II alpha
Sh2b3	SH2B adaptor protein 3
Ech1	enoyl coenzyme A hydratase 1, peroxisomal
Pole4	polymerase (DNA-directed), epsilon 4 (p12 subunit)
Ldoc1l	leucine zipper, down-regulated in cancer 1-like
Tor1aip1	torsin A interacting protein 1
Kras	v-Ki-ras2 Kirsten rat sarcoma viral oncogene homolog
Gm8055	glyceraldehyde-3-phosphate dehydrogenase pseudogene
Pcgf5	polycomb group ring finger 5
Fgfr1	fibroblast growth factor receptor 1
Fam136a	family with sequence similarity 136, member A
Wdyhv1	WDYHV motif containing 1
Elp6	elongator acetyltransferase complex subunit 6
Pitx3	paired-like homeodomain transcription factor 3
Abcb8	ATP-binding cassette, sub-family B (MDR/TAP), member 8
Cyld	cylindromatosis (turban tumor syndrome)
Znrf1	zinc and ring finger 1
Thoc6	THO complex 6 homolog (Drosophila)
Rnmt	RNA (guanine-7-) methyltransferase
Cabyr	calcium-binding tyrosine-(Y)-phosphorylation regulated (fibrousheathin 2)
Gm12295	predicted gene 12295
Tmem143	transmembrane protein 143
H2-M6-ps	histocompatibility 2, M region locus 6, pseudogene
Acsm5	acyl-CoA synthetase medium-chain family member 5
Snai3	snail homolog 3 (Drosophila)
Aebp2	AE binding protein 2
Mkrn1	makorin, ring finger protein, 1
Ptpn21	protein tyrosine phosphatase, non-receptor type 21

Gtpbp6	GTP binding protein 6 (putative)
Sox9	SRY-box containing gene 9
Prdm2	PR domain containing 2, with ZNF domain
Klf6	Kruppel-like factor 6
Exosc9	exosome component 9
Shf	Src homology 2 domain containing F
Gfm2	G elongation factor, mitochondrial 2
Tspan4	tetraspanin 4
Rsrc2	arginine/serine-rich coiled-coil 2
Gpr157	G protein-coupled receptor 157
Gm14148	glyceraldehyde-3-phosphate dehydrogenase pseudogene
A730011C13Rik	RIKEN cDNA A730011C13 gene
Plekho2	pleckstrin homology domain containing, family O member 2
Mdh1	malate dehydrogenase 1, NAD (soluble)
Papln	papilin, proteoglycan-like sulfated glycoprotein
Mapre1	microtubule-associated protein, RP/EB family, member 1
Ttyh3	tweety homolog 3 (Drosophila)
Hax1	HCLS1 associated X-1
Arfgap3	ADP-ribosylation factor GTPase activating protein 3
Cpt2	carnitine palmitoyltransferase 2
Btnl9	butyrophilin-like 9
Cfdp1	craniofacial development protein 1
Brd1	bromodomain containing 1
Vps35	vacuolar protein sorting 35
Lemd2	LEM domain containing 2
Ccl2	chemokine (C-C motif) ligand 2
St3gal6	ST3 beta-galactoside alpha-2,3-sialyltransferase 6
Pax2	paired box gene 2
Klf4	Kruppel-like factor 4 (gut)
Galnt11	UDP-N-acetyl-alpha-D-galactosamine:polypeptide N-acetylgalactosaminyltransferase 11
Prkrir	protein-kinase, interferon-inducible double stranded RNA dependent inhibitor, repressor of (P58 repressor)
Nedd9	neural precursor cell expressed, developmentally down-regulated gene 9
Hars	histidyl-tRNA synthetase

Gm684	predicted gene 684
Fam19a4	family with sequence similarity 19, member A4
Tmem161b	transmembrane protein 161B
Stxbp4	syntaxin binding protein 4
Ifit1	interferon-induced protein with tetratricopeptide repeats 1
Gsta4	glutathione S-transferase, alpha 4
Sh3glb2	SH3-domain GRB2-like endophilin B2
Srgap2	SLIT-ROBO Rho GTPase activating protein 2
Kif2a	kinesin family member 2A
Caskin2	CASK-interacting protein 2
Mthfsd	methenyltetrahydrofolate synthetase domain containing
Gnl2	guanine nucleotide binding protein-like 2 (nucleolar)
Arhgdia	Rho GDP dissociation inhibitor (GDI) alpha
Aga	aspartylglucosaminidase
Myo6	myosin VI
Ass1	argininosuccinate synthetase 1
Acox3	acyl-Coenzyme A oxidase 3, pristanoyl
Gm11658	glyceraldehyde-3-phosphate dehydrogenase pseudogene
Crnkl1	Crn, crooked neck-like 1 (Drosophila)
Zkscan6	zinc finger with KRAB and SCAN domains 6
Igfbp5	insulin-like growth factor binding protein 5
Arhgap12	Rho GTPase activating protein 12
Zfp280b	zinc finger protein 280B
3632451O06Rik	RIKEN cDNA 3632451O06 gene
Napg	N-ethylmaleimide sensitive fusion protein attachment protein gamma
Wdr70	WD repeat domain 70
Clip4	CAP-GLY domain containing linker protein family, member 4
Rhobtb3	Rho-related BTB domain containing 3
Ppp1r26	protein phosphatase 1, regulatory subunit 26
Dars	aspartyl-tRNA synthetase
Hectd3	HECT domain containing 3
Sec23b	SEC23B (S. cerevisiae)
Gm15179	predicted gene 15179
Ankmy2	ankyrin repeat and MYND domain containing 2
Actr1a	ARP1 actin-related protein 1A, centractin alpha
Irgm1	immunity-related GTPase family M member 1

Sema6d	sema domain, transmembrane domain (TM), and cytoplasmic domain, (semaphorin) 6D
Ccdc102a	coiled-coil domain containing 102A
Med11	mediator of RNA polymerase II transcription, subunit 11 homolog (S. cerevisiae)
Col9a1	collagen, type IX, alpha 1
Shox2	short stature homeobox 2
Jup	junction plakoglobin
Trp53bp1	transformation related protein 53 binding protein 1
Tmem106c	transmembrane protein 106C
Serf1	small EDRK-rich factor 1
Gypc	glycophorin C
Nek1	NIMA (never in mitosis gene a)-related expressed kinase 1
Cdv3	carnitine deficiency-associated gene expressed in ventricle 3
Zfp768	zinc finger protein 768
Ccne2	cyclin E2
Rgl2	ral guanine nucleotide dissociation stimulator-like 2
Fer	ferris
Slc30a9	solute carrier family 30 (zinc transporter), member 9
Rad52	RAD52 homolog (S. cerevisiae)
Rbm38	RNA binding motif protein 38
Ppp2r5c	protein phosphatase 2, regulatory subunit B (B56), gamma isoform
Ctage5	CTAGE family, member 5
Serpinb9	serine (or cysteine) peptidase inhibitor, clade B, member 9
Mc5r	melanocortin 5 receptor
Vtn	vitronectin
Ppp6c	protein phosphatase 6, catalytic subunit
Adprh	ADP-ribosylarginine hydrolase
Rbm18	RNA binding motif protein 18
Eif2s2	eukaryotic translation initiation factor 2, subunit 2 (beta)
Uba3	ubiquitin-like modifier activating enzyme 3
Mfsd6	major facilitator superfamily domain containing 6
Pbxip1	pre B cell leukemia transcription factor interacting protein 1
Desi2	desumoylating isopeptidase 2

Rab33b	RAB33B, member of RAS oncogene family
Cmtm8	CKLF-like MARVEL transmembrane domain containing 8
Cops3	COP9 (constitutive photomorphogenic) homolog, subunit 3 (Arabidopsis thaliana)
Lrrn1	leucine rich repeat protein 1, neuronal
Fam32a	family with sequence similarity 32, member A
Rnf157	ring finger protein 157
Ints4	integrator complex subunit 4
Eapp	E2F-associated phosphoprotein
Il11ra1	interleukin 11 receptor, alpha chain 1
Gm6498	glyceraldehyde-3-phosphate dehydrogenase pseudogene
Chordc1	cysteine and histidine-rich domain (CHORD)-containing, zinc-binding protein 1
Rps6ka1	ribosomal protein S6 kinase polypeptide 1
Tubd1	tubulin, delta 1
Nosip	nitric oxide synthase interacting protein
Msto1	misato homolog 1 (Drosophila)
Mrpl3	mitochondrial ribosomal protein L3
Pthlh	parathyroid hormone-like peptide
Irx5	Iroquois related homeobox 5 (Drosophila)
Tbc1d16	TBC1 domain family, member 16
Arf5	ADP-ribosylation factor 5
Zdhhc17	zinc finger, DHHC domain containing 17
Plin4	perilipin 4
Dicer1	dicer 1, ribonuclease type III
Nckap1	NCK-associated protein 1
Pex3	peroxisomal biogenesis factor 3
Dnm3	dynamin 3
Ppp2r3a	protein phosphatase 2, regulatory subunit B'', alpha
Grb2	growth factor receptor bound protein 2
Chmp3	charged multivesicular body protein 3
Prkd2	protein kinase D2
Kcnv2	potassium channel, subfamily V, member 2
Hddc3	HD domain containing 3
Pqlc1	PQ loop repeat containing 1
Vsig10	V-set and immunoglobulin domain containing 10
Atp6v1h	ATPase, H+ transporting, lysosomal V1 subunit H
Dennd2c	DENN/MADD domain containing 2C

P4ha2	procollagen-proline, 2-oxoglutarate 4-dioxygenase (proline 4-hydroxylase), alpha II polypeptide
Ninj1	ninjurin 1
Gm6283	predicted gene 6283
Ifi35	interferon-induced protein 35
Slc2a3	solute carrier family 2 (facilitated glucose transporter), member 3
Gtf3a	general transcription factor III A
Gna12	guanine nucleotide binding protein, alpha 12
Ets2	E26 avian leukemia oncogene 2, 3' domain
Hivep3	human immunodeficiency virus type I enhancer binding protein 3
Rai14	retinoic acid induced 14
Gucy2g	guanylate cyclase 2g
Mapk1	mitogen-activated protein kinase 1
Tomm34	translocase of outer mitochondrial membrane 34
1110002E22Rik	RIKEN cDNA 1110002E22 gene
Tmem5	transmembrane protein 5
Usp22	ubiquitin specific peptidase 22
Ppfia4	protein tyrosine phosphatase, receptor type, f polypeptide (PTPRF), interacting protein (liprin), alpha 4
Plekhg4	pleckstrin homology domain containing, family G (with RhoGef domain) member 4
Aspscr1	alveolar soft part sarcoma chromosome region, candidate 1 (human)
Adam9	a disintegrin and metallopeptidase domain 9 (meltrin gamma)
Cry2	cryptochrome 2 (photolyase-like)
Foxp4	forkhead box P4
Tshz1	teashirt zinc finger family member 1
Ccar1	cell division cycle and apoptosis regulator 1
Ighm	immunoglobulin heavy constant mu
Lrp12	low density lipoprotein-related protein 12
Calml4	calmodulin-like 4
Pprc1	peroxisome proliferative activated receptor, gamma, coactivator-related 1
Abhd4	abhydrolase domain containing 4
Ift172	intraflagellar transport 172
Hspa9	heat shock protein 9
Pias3	protein inhibitor of activated STAT 3

Nfatc3	nuclear factor of activated T cells, cytoplasmic, calcineurin dependent 3
Dock7	dedicator of cytokinesis 7
Arap1	ArfGAP with RhoGAP domain, ankyrin repeat and PH domain 1
Prima1	proline rich membrane anchor 1
Mfap1b	microfibrillar-associated protein 1B
Chid1	chitinase domain containing 1
Rad21	RAD21 homolog (S. pombe)
Pvr	poliovirus receptor
Prep	prolyl endopeptidase
Pdgfb	platelet derived growth factor, B polypeptide
Psmd6	proteasome (prosome, macropain) 26S subunit, non-ATPase, 6
Gins4	GINS complex subunit 4 (Sld5 homolog)
Zfp704	zinc finger protein 704
Gata4	GATA binding protein 4
Kitl	kit ligand
Abcf3	ATP-binding cassette, sub-family F (GCN20), member 3
Slc25a20	solute carrier family 25 (mitochondrial carnitine/acylcarnitine translocase), member 20
Sema3c	sema domain, immunoglobulin domain (Ig), short basic domain, secreted, (semaphorin) 3C
Dnajc8	DnaJ (Hsp40) homolog, subfamily C, member 8
Zfp597	zinc finger protein 597
Smg9	smg-9 homolog, nonsense mediated mRNA decay factor (C. elegans)
Jarid2	jumonji, AT rich interactive domain 2
Dbnl	drebrin-like
Gm9892	eukaryotic translation initiation factor 2, subunit 2 (beta) pseudogene
Dnajb4	DnaJ (Hsp40) homolog, subfamily B, member 4
Nemf	nuclear export mediator factor
Irgq	immunity-related GTPase family, Q
2810013P06Rik	RIKEN cDNA 2810013P06 gene
March 4	membrane-associated ring finger (C3HC4) 4
Crocc	ciliary rootlet coiled-coil, rootletin
Fam57b	family with sequence similarity 57, member B
Slc26a6	solute carrier family 26, member 6
Zfr2	zinc finger RNA binding protein 2
Gpd2	glycerol phosphate dehydrogenase 2, mitochondrial

Bmp6	bone morphogenetic protein 6
Btbd9	BTB (POZ) domain containing 9
Blcap	bladder cancer associated protein homolog (human)
Mt3	metallothionein 3
Lifr	leukemia inhibitory factor receptor
Stoml1	stomatin-like 1
Paip2b	poly(A) binding protein interacting protein 2B
Ext2	exostoses (multiple) 2
Igf1r	insulin-like growth factor I receptor
Slc28a2	solute carrier family 28 (sodium-coupled nucleoside transporter), member 2
Spop	speckle-type POZ protein
Atp13a5	ATPase type 13A5
Mbtps1	membrane-bound transcription factor peptidase, site 1
Chmp1a	charged multivesicular body protein 1A
Ppif	peptidylprolyl isomerase F (cyclophilin F)
Mypn	myopalladin
Lgals8	lectin, galactose binding, soluble 8
Kifc3	kinesin family member C3
D830032E09Rik	RIKEN cDNA D830032E09 gene
Ppm1n	protein phosphatase, Mg2+/Mn2+ dependent, 1N (putative)
Socs6	suppressor of cytokine signaling 6
Nol8	nucleolar protein 8
Kdm1a	lysine (K)-specific demethylase 1A
Sestd1	SEC14 and spectrin domains 1
Cacng7	calcium channel, voltage-dependent, gamma subunit 7
Mn1	meningioma 1
Samd8	sterile alpha motif domain containing 8
Nup107	nucleoporin 107
Tbc1d10c	TBC1 domain family, member 10c
Pddc1	Parkinson disease 7 domain containing 1
Stat5b	signal transducer and activator of transcription 5B
Rrm2b	ribonucleotide reductase M2 B (TP53 inducible)
Hmgn2	high mobility group nucleosomal binding domain 2
Bag3	BCL2-associated athanogene 3
Slc40a1	solute carrier family 40 (iron-regulated transporter), member 1
Atg10	autophagy related 10

Abca5	ATP-binding cassette, sub-family A (ABC1), member 5
Kars	lysyl-tRNA synthetase
Fitm2	fat storage-inducing transmembrane protein 2
Setd7	SET domain containing (lysine methyltransferase) 7
Ing1	inhibitor of growth family, member 1
Bloc1s5	biogenesis of organelles complex-1, subunit 5, muted
Polk	polymerase (DNA directed), kappa
Tanc1	tetratricopeptide repeat, ankyrin repeat and coiled-coil containing 1
Myl6b	myosin, light polypeptide 6B
Ltv1	LTV1 homolog (S. cerevisiae)
Cd2bp2	CD2 antigen (cytoplasmic tail) binding protein 2
Fam69a	family with sequence similarity 69, member A
Zcchc11	zinc finger, CCHC domain containing 11
Gldn	gliomedin
Ppp2r5d	protein phosphatase 2, regulatory subunit B (B56), delta isoform
Fam169b	family with sequence similarity 169, member B
Dok4	docking protein 4
Fbxw8	F-box and WD-40 domain protein 8
Cdr2	cerebellar degeneration-related 2
Tiam2	T cell lymphoma invasion and metastasis 2
Sec23a	SEC23A (S. cerevisiae)
Lman2l	lectin, mannose-binding 2-like
A330094K24Rik	RIKEN cDNA A330094K24 gene
Ccnl1	cyclin L1
Adamtsl1	ADAMTS-like 1
Plaa	phospholipase A2, activating protein
Dync1li1	dynein cytoplasmic 1 light intermediate chain 1
Ralbp1	ralA binding protein 1
Socs2	suppressor of cytokine signaling 2
Hp1bp3	heterochromatin protein 1, binding protein 3
Rilpl1	Rab interacting lysosomal protein-like 1
Ifngr2	interferon gamma receptor 2
Ogfr	opioid growth factor receptor
Foxl2os	forkhead box L2 opposite strand transcript
Iws1	IWS1 homolog (S. cerevisiae)
Taok1	TAO kinase 1
Gm5507	glyceraldehyde-3-phosphate dehydrogenase pseudogene

Tm9sf3	transmembrane 9 superfamily member 3
Ikbip	IKBKB interacting protein
Grpel1	GrpE-like 1, mitochondrial
Tax1bp1	Tax1 (human T cell leukemia virus type I) binding protein 1
Rnf114	ring finger protein 114
Zfp654	zinc finger protein 654
Gdi2	guanosine diphosphate (GDP) dissociation inhibitor 2
Lyn	Yamaguchi sarcoma viral (v-yes-1) oncogene homolog
Shq1	SHQ1 homolog (S. cerevisiae)
Noc2l	nucleolar complex associated 2 homolog (S. cerevisiae)
Eef2k	eukaryotic elongation factor-2 kinase
Cpped1	calcineurin-like phosphoesterase domain containing 1
Tlr6	toll-like receptor 6
Ndufs1	NADH dehydrogenase (ubiquinone) Fe-S protein 1
Gpcpd1	glycerophosphocholine phosphodiesterase GDE1 homolog (S. cerevisiae)
Gzf1	GDNF-inducible zinc finger protein 1
Vps13a	vacuolar protein sorting 13A (yeast)
Slc25a47	solute carrier family 25, member 47
Leprot	leptin receptor overlapping transcript
4930577N17Rik	RIKEN cDNA 4930577N17 gene
Crtc2	CREB regulated transcription coactivator 2
Ckap4	cytoskeleton-associated protein 4
Gm3671	glyceraldehyde-3-phosphate dehydrogenase pseudogene
Clk1	CDC-like kinase 1
B4galt6	UDP-Gal:betaGlcNAc beta 1,4-galactosyltransferase, polypeptide 6
Gm826	predicted gene 826
Elmo3	engulfment and cell motility 3
Pogk	pogo transposable element with KRAB domain
Osbpl6	oxysterol binding protein-like 6
Lrrc49	leucine rich repeat containing 49
Far1	fatty acyl CoA reductase 1
Nfkb2	nuclear factor of kappa light polypeptide gene enhancer in B cells 2, p49/p100
Atxn7l3	ataxin 7-like 3
Cul4a	cullin 4A

Ncbp2	nuclear cap binding protein subunit 2
Smpdl3b	sphingomyelin phosphodiesterase, acid-like 3B
Fbxo38	F-box protein 38
Coq3	coenzyme Q3 homolog, methyltransferase (yeast)
Kbtbd12	kelch repeat and BTB (POZ) domain containing 12
Abcb1b	ATP-binding cassette, sub-family B (MDR/TAP), member 1B
Rfx7	regulatory factor X, 7
Tmem204	transmembrane protein 204
Dixdc1	DIX domain containing 1
Dctn5	dynactin 5
Eaf1	ELL associated factor 1
Tubg1	tubulin, gamma 1
Pip4k2c	phosphatidylinositol-5-phosphate 4-kinase, type II, gamma
Atf6	activating transcription factor 6
Usp16	ubiquitin specific peptidase 16
Sema6c	sema domain, transmembrane domain (TM), and cytoplasmic domain, (semaphorin) 6C
Kdm4c	lysine (K)-specific demethylase 4C
Stard4	StAR-related lipid transfer (START) domain containing 4
Zmynd19	zinc finger, MYND domain containing 19
Eprs	glutamyl-prolyl-tRNA synthetase
Tmem168	transmembrane protein 168
Nuak1	NUAK family, SNF1-like kinase, 1
Zswim6	zinc finger, SWIM domain containing 6
E530011L22Rik	RIKEN cDNA E530011L22 gene
Vps33b	vacuolar protein sorting 33B (yeast)
Nle1	notchless homolog 1 (Drosophila)
Spryd4	SPRY domain containing 4
Mfap3l	microfibrillar-associated protein 3-like
Shisa3	shisa homolog 3 (Xenopus laevis)
Rap1gds1	RAP1, GTP-GDP dissociation stimulator 1
Hsp90aa1	heat shock protein 90, alpha (cytosolic), class A member 1
Appl1	adaptor protein, phosphotyrosine interaction, PH domain and leucine zipper containing 1
Tbce	tubulin-specific chaperone E

Myh8	myosin, heavy polypeptide 8, skeletal muscle, perinatal
Cat	catalase
Aldh16a1	aldehyde dehydrogenase 16 family, member A1
Jmjd1c	jumonji domain containing 1C
Ddx23	DEAD (Asp-Glu-Ala-Asp) box polypeptide 23
Pigk	phosphatidylinositol glycan anchor biosynthesis, class K
Get4	golgi to ER traffic protein 4 homolog (S. cerevisiae)
Pax6	paired box gene 6
Nr4a1	nuclear receptor subfamily 4, group A, member 1
Ptk2	PTK2 protein tyrosine kinase 2
Dgka	diacylglycerol kinase, alpha
Ambra1	autophagy/beclin 1 regulator 1
Tfip11	tuftelin interacting protein 11
Rftn1	raftlin lipid raft linker 1
Ahi1	Abelson helper integration site 1
Tmem59	transmembrane protein 59
Gm5187	predicted gene 5187
Rin3	Ras and Rab interactor 3
Dlg1	discs, large homolog 1 (Drosophila)
Zfp454	zinc finger protein 454
Cryzl1	crystallin, zeta (quinone reductase)-like 1
Gba	glucosidase, beta, acid
Csrp1	cysteine and glycine-rich protein 1
Gcnt2	glucosaminyl (N-acetyl) transferase 2, I-branching enzyme
D430041D05Rik	RIKEN cDNA D430041D05 gene
Fam20b	family with sequence similarity 20, member B
Rpgrip1l	Rpgrip1-like
Dusp14	dual specificity phosphatase 14
Cd59a	CD59a antigen
Mat2a	methionine adenosyltransferase II, alpha
Pmvk	phosphomevalonate kinase
Skil	SKI-like
March 5	membrane-associated ring finger (C3HC4) 5
Cbx4	chromobox 4
Klk1b26	kallikrein 1-related petidase b26
Rbpms	RNA binding protein gene with multiple splicing
Lmna	lamin A

Ptges2	prostaglandin E synthase 2
Ighg2b	immunoglobulin heavy constant gamma 2B
Cryab	crystallin, alpha B
Sypl	synaptophysin-like protein
Amd1	S-adenosylmethionine decarboxylase 1
Syt11	synaptotagmin XI
Il34	interleukin 34
Chmp2b	charged multivesicular body protein 2B
Adrbk1	adrenergic receptor kinase, beta 1
Sec22c	SEC22 vesicle trafficking protein homolog C (S. cerevisiae)
Capn2	calpain 2
Commd7	COMM domain containing 7
Psme3	proteaseome (prosome, macropain) 28 subunit, 3
Styx	serine/threonine/tyrosine interaction protein
Nudt7	nudix (nucleoside diphosphate linked moiety X)-type motif 7
Lin9	lin-9 homolog (C. elegans)
Map2k6	mitogen-activated protein kinase kinase 6
Tppp3	tubulin polymerization-promoting protein family member 3
Srm	spermidine synthase
Car2	carbonic anhydrase 2
Btrc	beta-transducin repeat containing protein
Cyfip1	cytoplasmic FMR1 interacting protein 1
Zfp365	zinc finger protein 365
Acp2	acid phosphatase 2, lysosomal
Sbds	Shwachman-Bodian-Diamond syndrome homolog (human)
Ahcyl1	S-adenosylhomocysteine hydrolase-like 1
Slc12a2	solute carrier family 12, member 2
Arl4a	ADP-ribosylation factor-like 4A
Ppcs	phosphopantothenoylcysteine synthetase
Kcnj11	potassium inwardly rectifying channel, subfamily J, member 11
Sart3	squamous cell carcinoma antigen recognized by T cells 3
Klhl33	kelch-like 33 (Drosophila)
Tmub2	transmembrane and ubiquitin-like domain containing 2
Patl1	protein associated with topoisomerase II homolog 1 (yeast)
Pitpnc1	phosphatidylinositol transfer protein, cytoplasmic 1

Gimap6	GTPase, IMAP family member 6
Acvr1b	activin A receptor, type 1B
Csnk1e	casein kinase 1, epsilon
N6amt1	N-6 adenine-specific DNA methyltransferase 1 (putative)
Mis12	MIS12 homolog (yeast)
Plekha3	pleckstrin homology domain-containing, family A (phosphoinositide binding specific) member 3
Adk	adenosine kinase
Vps37a	vacuolar protein sorting 37A (yeast)
Fnip1	folliculin interacting protein 1
Sepp1	selenoprotein P, plasma, 1
Appbp2	amyloid beta precursor protein (cytoplasmic tail) binding protein 2
Raf1	v-raf-leukemia viral oncogene 1
Arpp21	cyclic AMP-regulated phosphoprotein, 21
Fv1	Friend virus susceptibility 1
BB218582	expressed sequence BB218582
N4bp2l2	NEDD4 binding protein 2-like 2
Vasp	vasodilator-stimulated phosphoprotein
Fam63b	family with sequence similarity 63, member B
Rora	RAR-related orphan receptor alpha
Aar2	AAR2 splicing factor homolog (S. cerevisiae)
Ncln	nicalin homolog (zebrafish)
Gm12182	glyceraldehyde-3-phosphate dehydrogenase pseudogene
Aldh5a1	aldhehyde dehydrogenase family 5, subfamily A1
Zfp180	zinc finger protein 180
Cnnm2	cyclin M2
Fam19a5	family with sequence similarity 19, member A5
Luc7l2	LUC7-like 2 (S. cerevisiae)
Zdhhc3	zinc finger, DHHC domain containing 3
Angptl4	angiopoietin-like 4
BC037034	cDNA sequence BC037034
Prkaa1	protein kinase, AMP-activated, alpha 1 catalytic subunit
Pabpc1	poly(A) binding protein, cytoplasmic 1
Gnl1	guanine nucleotide binding protein-like 1
Zfp639	zinc finger protein 639
Plin3	perilipin 3
Nagk	N-acetylglucosamine kinase

Bcas3	breast carcinoma amplified sequence 3
Ssr1	signal sequence receptor, alpha
Dlat	dihydrolipoamide S-acetyltransferase (E2 component of pyruvate dehydrogenase complex)
Inpp5j	inositol polyphosphate 5-phosphatase J
Micu1	mitochondrial calcium uptake 1
Cdk2ap2	CDK2-associated protein 2
Rngtt	RNA guanylyltransferase and 5'-phosphatase
Cd200	CD200 antigen
Rab3gap2	RAB3 GTPase activating protein subunit 2
9330104G04Rik	RIKEN cDNA 9330104G04 gene
Inpp5a	inositol polyphosphate-5-phosphatase A
Mir133a-1	microRNA 133a-1
Srpk2	serine/arginine-rich protein specific kinase 2
Car3	carbonic anhydrase 3
2410127L17Rik	RIKEN cDNA 2410127L17 gene
Kctd9	potassium channel tetramerisation domain containing 9
Zc3h14	zinc finger CCCH type containing 14
Apobec3	apolipoprotein B mRNA editing enzyme, catalytic polypeptide 3
Arcn1	archain 1
Arfgef1	ADP-ribosylation factor guanine nucleotide-exchange factor 1(brefeldin A-inhibited)
Egln1	EGL nine homolog 1 (C. elegans)
Adamts9	a disintegrin-like and metallopeptidase (reprolysin type) with thrombospondin type 1 motif, 9
Igkv12-44	immunoglobulin kappa variable 12-44
Tpx2	TPX2, microtubule-associated protein homolog (Xenopus laevis)
Cd24a	CD24a antigen
Sdad1	SDA1 domain containing 1
Rbp7	retinol binding protein 7, cellular
Arhgef15	Rho guanine nucleotide exchange factor (GEF) 15
Prpf31	PRP31 pre-mRNA processing factor 31 homolog (yeast)
Dld	dihydrolipoamide dehydrogenase

Nit1	nitrilase 1
A430005L14Rik	RIKEN cDNA A430005L14 gene
Abhd14b	abhydrolase domain containing 14b
Gm10390	predicted gene 10390
Gm5617	predicted gene 5617
Amfr	autocrine motility factor receptor
Pdgfrb	platelet derived growth factor receptor, beta polypeptide
Epb4.1	erythrocyte protein band 4.1
Eps15l1	epidermal growth factor receptor pathway substrate 15-like 1
Myl12a	myosin, light chain 12A, regulatory, non-sarcomeric
Cyb5r1	cytochrome b5 reductase 1
Nudcd1	NudC domain containing 1
2310039L15Rik	RIKEN cDNA 2310039L15 gene
Myo5c	myosin VC
Iffo1	intermediate filament family orphan 1
Stau1	staufen (RNA binding protein) homolog 1 (Drosophila)
Camk2b	calcium/calmodulin-dependent protein kinase II, beta
Pla2g5	phospholipase A2, group V
Atp6v0a1	ATPase, H+ transporting, lysosomal V0 subunit A1
Cox10	COX10 homolog, cytochrome c oxidase assembly protein, heme A: farnesyltransferase (yeast)
Pfdn2	prefoldin 2
Ssbp3	single-stranded DNA binding protein 3
Ulk1	unc-51 like kinase 1
Sept 10	septin 10
Hsf2bp	heat shock transcription factor 2 binding protein
1810041L15Rik	RIKEN cDNA 1810041L15 gene
Cpsf3	cleavage and polyadenylation specificity factor 3
Lats1	large tumor suppressor
Zp2	zona pellucida glycoprotein 2
Prdm15	PR domain containing 15
Xpo1	exportin 1, CRM1 homolog (yeast)
Tmed2	transmembrane emp24 domain trafficking protein 2
Ist1	increased sodium tolerance 1 homolog (yeast)

Stk3	serine/threonine kinase 3
Bmpr2	bone morphogenetic protein receptor, type II (serine/threonine kinase)
Hspa1l	heat shock protein 1-like
Srcin1	SRC kinase signaling inhibitor 1
S100a13	S100 calcium binding protein A13
Stau2	staufen (RNA binding protein) homolog 2 (Drosophila)
Tbx15	T-box 15
Tbl1xr1	transducin (beta)-like 1X-linked receptor 1
Pepd	peptidase D
A830052D11Rik	RIKEN cDNA A830052D11 gene
Tmem88	transmembrane protein 88
Acad12	acyl-Coenzyme A dehydrogenase family, member 12
Dnajb12	DnaJ (Hsp40) homolog, subfamily B, member 12
Atp8b2	ATPase, class I, type 8B, member 2
Bbc3	BCL2 binding component 3
Spa17	sperm autoantigenic protein 17
Tmem129	transmembrane protein 129
Spg21	spastic paraplegia 21 homolog (human)
Prkab1	protein kinase, AMP-activated, beta 1 non-catalytic subunit
Tmem170b	transmembrane protein 170B
Jam2	junction adhesion molecule 2
Slc25a11	solute carrier family 25 (mitochondrial carrier oxoglutarate carrier), member 11
2310011J03Rik	RIKEN cDNA 2310011J03 gene
Sln	sarcolipin
Sdc4	syndecan 4
Nmnat3	nicotinamide nucleotide adenylyltransferase 3
Snx2	sorting nexin 2
Lhx1	LIM homeobox protein 1
Polr1d	polymerase (RNA) I polypeptide D
Slc1a1	solute carrier family 1 (neuronal/epithelial high affinity glutamate transporter, system Xag), member 1
Jrk	jerky
Pes1	pescadillo homolog 1, containing BRCT domain (zebrafish)

Tmx4	thioredoxin-related transmembrane protein 4
Acaa1a	acetyl-Coenzyme A acyltransferase 1A
Ntmt1	N-terminal Xaa-Pro-Lys N-methyltransferase 1
Dscr3	Down syndrome critical region gene 3
Gm8116	predicted gene 8116
Inf2	inverted formin, FH2 and WH2 domain containing
Ticam1	toll-like receptor adaptor molecule 1
Insig2	insulin induced gene 2
Rnpepl1	arginyl aminopeptidase (aminopeptidase B)-like 1
Rbm45	RNA binding motif protein 45
Dazl	deleted in azoospermia-like
Itpr1	inositol 1,4,5-trisphosphate receptor 1
4933404O12Rik	RIKEN cDNA 4933404O12 gene
Klf9	Kruppel-like factor 9
Brox	BRO1 domain and CAAX motif containing
Tmem144	transmembrane protein 144
Rnf122	ring finger protein 122
2310020H05Rik	RIKEN cDNA 2310020H05 gene
Cdc42se1	CDC42 small effector 1
Cirbp	cold inducible RNA binding protein
Casp9	caspase 9
Ap1ar	adaptor-related protein complex 1 associated regulatory protein
Arl4d	ADP-ribosylation factor-like 4D
Dynll1	dynein light chain LC8-type 1
Tcf7l1	transcription factor 7 like 1 (T cell specific, HMG box)
Parp6	poly (ADP-ribose) polymerase family, member 6
Stk10	serine/threonine kinase 10
Slc9a3r2	solute carrier family 9 (sodium/hydrogen exchanger), member 3 regulator 2
Tiam1	T cell lymphoma invasion and metastasis 1
Afg3l1	AFG3(ATPase family gene 3)-like 1 (yeast)
Dchs1	dachsous 1 (Drosophila)
Sipa1l1	signal-induced proliferation-associated 1 like 1
Alg9	asparagine-linked glycosylation 9 (alpha 1,2 mannosyltransferase)
Mccc1	methylcrotonoyl-Coenzyme A carboxylase 1 (alpha)

Amd-ps3	S-adenosylmethionine decarboxylase, pseudogene 3
Crtc1	CREB regulated transcription coactivator 1
Hars2	histidyl-tRNA synthetase 2, mitochondrial (putative)
Trim12a	tripartite motif-containing 12A
Sacm1l	SAC1 (suppressor of actin mutations 1, homolog)-like (S. cerevisiae)
Gfm1	G elongation factor, mitochondrial 1
Wbscr17	Williams-Beuren syndrome chromosome region 17 homolog (human)
Hook1	hook homolog 1 (Drosophila)
Thbs4	thrombospondin 4
Slc7a2	solute carrier family 7 (cationic amino acid transporter, y+ system), member 2
Slc16a3	solute carrier family 16 (monocarboxylic acid transporters), member 3
Pmpcb	peptidase (mitochondrial processing) beta
Tcta	T cell leukemia translocation altered gene
Cdh4	cadherin 4
Scn3b	sodium channel, voltage-gated, type III, beta
Ip6k2	inositol hexaphosphate kinase 2
Zfp9	zinc finger protein 9
Tmem186	transmembrane protein 186
Kctd1	potassium channel tetramerisation domain containing 1
Evi5	ecotropic viral integration site 5
Intu	inturned planar cell polarity effector homolog (Drosophila)
Ly6c1	lymphocyte antigen 6 complex, locus C1
Gle1	GLE1 RNA export mediator (yeast)
Vrk3	vaccinia related kinase 3
Ubac2	ubiquitin associated domain containing 2
Lnx1	ligand of numb-protein X 1
Fgfr3	fibroblast growth factor receptor 3
Mcl1	myeloid cell leukemia sequence 1
Tspan15	tetraspanin 15
Gm8318	glyceraldehyde-3-phosphate dehydrogenase pseudogene
Dnajc13	DnaJ (Hsp40) homolog, subfamily C, member 13
1600002K03Rik	RIKEN cDNA 1600002K03 gene
Grwd1	glutamate-rich WD repeat containing 1

Ptger1	prostaglandin E receptor 1 (subtype EP1)
Clasp1	CLIP associating protein 1
Opa3	optic atrophy 3
Xab2	XPA binding protein 2
Aspa	aspartoacylase
Cog7	component of oligomeric golgi complex 7
Nol3	nucleolar protein 3 (apoptosis repressor with CARD domain)
Rfk	riboflavin kinase
Myo1d	myosin ID
Bad	BCL2-associated agonist of cell death
Wrnip1	Werner helicase interacting protein 1
Prkrip1	Prkr interacting protein 1 (IL11 inducible)
Kcnc3	potassium voltage gated channel, Shaw-related subfamily, member 3
Cox19	COX19 cytochrome c oxidase assembly homolog (S. cerevisiae)
Slc39a1	solute carrier family 39 (zinc transporter), member 1
Dync1i2	dynein cytoplasmic 1 intermediate chain 2
Tbx4	T-box 4
Shmt1	serine hydroxymethyltransferase 1 (soluble)
Dnajc14	DnaJ (Hsp40) homolog, subfamily C, member 14
Pfkfb3	6-phosphofructo-2-kinase/fructose-2,6-biphosphatase 3
Ky	kyphoscoliosis peptidase
Gabrr2	gamma-aminobutyric acid (GABA) C receptor, subunit rho 2
Oplah	5-oxoprolinase (ATP-hydrolysing)
Gm5532	predicted gene 5532
Tmbim6	transmembrane BAX inhibitor motif containing 6
Cetn3	centrin 3
Pard3	par-3 (partitioning defective 3) homolog (C. elegans)
Plin2	perilipin 2
Hk2	hexokinase 2
Emc9	ER membrane protein complex subunit 9
Atp1a4	ATPase, Na+/K+ transporting, alpha 4 polypeptide
Fzd7	frizzled homolog 7 (Drosophila)
Rab6a	RAB6A, member RAS oncogene family
Reps1	RalBP1 associated Eps domain containing protein

Desi1	desumoylating isopeptidase 1
Gm10327	glyceraldehyde-3-phosphate dehydrogenase pseudogene
Rit1	Ras-like without CAAX 1
Igsf8	immunoglobulin superfamily, member 8
Ldlr	low density lipoprotein receptor
Arf4	ADP-ribosylation factor 4
6330403A02Rik	RIKEN cDNA 6330403A02 gene
Fbxl22	F-box and leucine-rich repeat protein 22
Calcrl	calcitonin receptor-like
Lrrc24	leucine rich repeat containing 24
Lingo3	leucine rich repeat and Ig domain containing 3
Myl4	myosin, light polypeptide 4
Tmem117	transmembrane protein 117
Smad6	SMAD family member 6
Rabgef1	RAB guanine nucleotide exchange factor (GEF) 1
Nacc1	nucleus accumbens associated 1, BEN and BTB (POZ) domain containing
Cry1	cryptochrome 1 (photolyase-like)
Dnase2a	deoxyribonuclease II alpha
Itgav	integrin alpha V
Murc	muscle-related coiled-coil protein
Zfyve9	zinc finger, FYVE domain containing 9
March 9	membrane-associated ring finger (C3HC4) 9
2310015K22Rik	RIKEN cDNA 2310015K22 gene
Agap3	ArfGAP with GTPase domain, ankyrin repeat and PH domain 3
Parg	poly (ADP-ribose) glycohydrolase
Dhrs4	dehydrogenase/reductase (SDR family) member 4
Pold2	polymerase (DNA directed), delta 2, regulatory subunit
Tmem135	transmembrane protein 135
Prodh	proline dehydrogenase
Nudt13	nudix (nucleoside diphosphate linked moiety X)-type motif 13
Naa40	N(alpha)-acetyltransferase 40, NatD catalytic subunit, homolog (S. cerevisiae)
Bach1	BTB and CNC homology 1
Kin	antigenic determinant of rec-A protein

Pdcd6ip	programmed cell death 6 interacting protein
Tef	thyrotroph embryonic factor
Wdr26	WD repeat domain 26
Angpt1	angiopoietin 1
Plxdc1	plexin domain containing 1
Kcng4	potassium voltage-gated channel, subfamily G, member 4
Tgoln1	trans-golgi network protein
Slc4a3	solute carrier family 4 (anion exchanger), member 3
Baiap2l2	BAI1-associated protein 2-like 2
Ntf5	neurotrophin 5
Ccdc132	coiled-coil domain containing 132
Emc2	ER membrane protein complex subunit 2
Gca	grancalcin
Pde7a	phosphodiesterase 7A
Rbbp4	retinoblastoma binding protein 4
Brd7	bromodomain containing 7
Larp4	La ribonucleoprotein domain family, member 4
Ttc12	tetratricopeptide repeat domain 12
Tmem150c	transmembrane protein 150C
Klhl12	kelch-like 12 (Drosophila)
Tmx3	thioredoxin-related transmembrane protein 3
Arhgap27	Rho GTPase activating protein 27
Otud3	OTU domain containing 3
Agap1	ArfGAP with GTPase domain, ankyrin repeat and PH domain 1
Dbp	D site albumin promoter binding protein
Dnajb5	DnaJ (Hsp40) homolog, subfamily B, member 5
Nsf	N-ethylmaleimide sensitive fusion protein
AU040320	expressed sequence AU040320
Exd1	exonuclease 3'-5' domain containing 1
4930512H18Rik	RIKEN cDNA 4930512H18 gene
Cpm	carboxypeptidase M
Helq	helicase, POLQ-like
4632428C04Rik	RIKEN cDNA 4632428C04 gene
Gm15706	predicted gene 15706
Klhl26	kelch-like 26 (Drosophila)
4930430F08Rik	RIKEN cDNA 4930430F08 gene

Tm9sf2	transmembrane 9 superfamily member 2
Rab10	RAB10, member RAS oncogene family
Xpr1	xenotropic and polytropic retrovirus receptor 1
Gps2	G protein pathway suppressor 2
Ints3	integrator complex subunit 3
Prpf19	PRP19/PSO4 pre-mRNA processing factor 19 homolog (S. cerevisiae)
Twf2	twinfilin, actin-binding protein, homolog 2 (Drosophila)
Slc25a13	solute carrier family 25 (mitochondrial carrier, adenine nucleotide translocator), member 13
Prkar1a	protein kinase, cAMP dependent regulatory, type I, alpha
Gm2308	glyceraldehyde-3-phosphate dehydrogenase pseudogene
Neto2	neuropilin (NRP) and tolloid (TLL)-like 2
Arhgef7	Rho guanine nucleotide exchange factor (GEF7)
Hes6	hairy and enhancer of split 6 (Drosophila)
Psip1	PC4 and SFRS1 interacting protein 1
D8Ertd82e	DNA segment, Chr 8, ERATO Doi 82, expressed
Lgmn	legumain
Eif4b	eukaryotic translation initiation factor 4B
Gm166	predicted gene 166
Tlr3	toll-like receptor 3
Aco1	aconitase 1
Dlc1	deleted in liver cancer 1
Hspa4	heat shock protein 4
Skap2	src family associated phosphoprotein 2
Prss55	protease, serine, 55
Cabin1	calcineurin binding protein 1
Rgl3	ral guanine nucleotide dissociation stimulator-like 3
Nog	noggin
Rab23	RAB23, member RAS oncogene family
C78197	expressed sequence C78197
Tmpo	thymopoietin
St8sia5	ST8 alpha-N-acetyl-neuraminide alpha-2,8-sialyltransferase 5
Glud1	glutamate dehydrogenase 1
Ephx2	epoxide hydrolase 2, cytoplasmic
D430019H16Rik	RIKEN cDNA D430019H16 gene
Ap1g2	adaptor protein complex AP-1, gamma 2 subunit

Slc25a23	solute carrier family 25 (mitochondrial carrier; phosphate carrier), member 23
Sap130	Sin3A associated protein
Cad	carbamoyl-phosphate synthetase 2, aspartate transcarbamylase, and dihydroorotase
Gm8174	glyceraldehyde-3-phosphate dehydrogenase pseudogene
Nup93	nucleoporin 93
Mgat4b	mannoside acetylglucosaminyltransferase 4, isoenzyme B
Pdzd7	PDZ domain containing 7
Hdac11	histone deacetylase 11
Igfals	insulin-like growth factor binding protein, acid labile subunit
Itga4	integrin alpha 4
Pax3	paired box gene 3
Shc4	SHC (Src homology 2 domain containing) family, member 4
Speg	SPEG complex locus
Adam15	a disintegrin and metallopeptidase domain 15 (metargidin)
Actr2	ARP2 actin-related protein 2
Snx17	sorting nexin 17
Cdc40	cell division cycle 40
Ces1d	carboxylesterase 1D
Fbxo40	F-box protein 40
Ap3b1	adaptor-related protein complex 3, beta 1 subunit
Acot7	acyl-CoA thioesterase 7
Zbtb43	zinc finger and BTB domain containing 43
Peli1	pellino 1
Sesn1	sestrin 1
Mpzl3	myelin protein zero-like 3
Tle4	transducin-like enhancer of split 4, homolog of Drosophila E(spl)
Rac1	RAS-related C3 botulinum substrate 1
Ash2l	ash2 (absent, small, or homeotic)-like (Drosophila)
Sun2	Sad1 and UNC84 domain containing 2
Actr10	ARP10 actin-related protein 10
Insig1	insulin induced gene 1
Slc9a9	solute carrier family 9 (sodium/hydrogen exchanger), member 9
Ostf1	osteoclast stimulating factor 1

Tmem202	transmembrane protein 202
Kat5	K(lysine) acetyltransferase 5
Wdr1	WD repeat domain 1
Acsm3	acyl-CoA synthetase medium-chain family member 3
Atxn7l1	ataxin 7-like 1
Zdhhc13	zinc finger, DHHC domain containing 13
Fgfbp1	fibroblast growth factor binding protein 1
Pstpip2	proline-serine-threonine phosphatase-interacting protein 2
Akap7	A kinase (PRKA) anchor protein 7
Nqo1	NAD(P)H dehydrogenase, quinone 1
Xbp1	X-box binding protein 1
Ndufaf4	NADH dehydrogenase (ubiquinone) 1 alpha subcomplex, assembly factor 4
Tmem167b	transmembrane protein 167B
Timm22	translocase of inner mitochondrial membrane 22 homolog (yeast)
Npepps	aminopeptidase puromycin sensitive
Nhej1	nonhomologous end-joining factor 1
Sertad3	SERTA domain containing 3
2310022A10Rik	RIKEN cDNA 2310022A10 gene
9830004L10Rik	RIKEN cDNA 9830004L10 gene
Dpp9	dipeptidylpeptidase 9
Tpd52l1	tumor protein D52-like 1
9430015G10Rik	RIKEN cDNA 9430015G10 gene
Tbck	TBC1 domain containing kinase
Fam174b	family with sequence similarity 174, member B
Ifit3	interferon-induced protein with tetratricopeptide repeats 3
Akirin2	akirin 2
Gpr155	G protein-coupled receptor 155
Ccni	cyclin I
Dnajc28	DnaJ (Hsp40) homolog, subfamily C, member 28
Hltf	helicase-like transcription factor
Casc4	cancer susceptibility candidate 4
Ddr1	discoidin domain receptor family, member 1
1810014B01Rik	RIKEN cDNA 1810014B01 gene

Tfrc	transferrin receptor
Ddx54	DEAD (Asp-Glu-Ala-Asp) box polypeptide 54
Zmat3	zinc finger matrin type 3
Rprd1a	regulation of nuclear pre-mRNA domain containing 1A
Fxyd6	FXYD domain-containing ion transport regulator 6
Ung	uracil DNA glycosylase
Casr	calcium-sensing receptor
Adh1	alcohol dehydrogenase 1 (class I)
Rwdd3	RWD domain containing 3
Sh3bp2	SH3-domain binding protein 2
Mafk	v-maf musculoaponeurotic fibrosarcoma oncogene family, protein K (avian)
Tspo	translocator protein
Ssb	Sjogren syndrome antigen B
Mettl21c	methyltransferase like 21C
Ramp1	receptor (calcitonin) activity modifying protein 1
Cacna1a	calcium channel, voltage-dependent, P/Q type, alpha 1A subunit
Snx1	sorting nexin 1
Htra1	HtrA serine peptidase 1
Kank2	KN motif and ankyrin repeat domains 2
BC035947	cDNA sequence BC035947
Hsd17b7	hydroxysteroid (17-beta) dehydrogenase 7
St8sia4	ST8 alpha-N-acetyl-neuraminide alpha-2,8-sialyltransferase 4
Cnga3	cyclic nucleotide gated channel alpha 3
Rbfox2	RNA binding protein, fox-1 homolog (C. elegans) 2
Ap1m1	adaptor-related protein complex AP-1, mu subunit 1
Pcnt	pericentrin (kendrin)
Cd151	CD151 antigen
Usp36	ubiquitin specific peptidase 36
Meaf6	MYST/Esa1-associated factor 6
Lmbr1	limb region 1
4930429F24Rik	RIKEN cDNA 4930429F24 gene
Mttp	microsomal triglyceride transfer protein
Ccrn4l	CCR4 carbon catabolite repression 4-like (S. cerevisiae)

Bloc1s4	biogenesis of organelles complex-1, subunit 4, cappuccino
Tspan14	tetraspanin 14
Pdlim1	PDZ and LIM domain 1 (elfin)
Snrnp200	small nuclear ribonucleoprotein 200 (U5)
Prox1	prospero-related homeobox 1
Spint2	serine protease inhibitor, Kunitz type 2
Ccdc88c	coiled-coil domain containing 88C
Usp19	ubiquitin specific peptidase 19
Spcs2	signal peptidase complex subunit 2 homolog (S. cerevisiae)
Suox	sulfite oxidase
Dzip3	DAZ interacting protein 3, zinc finger
Hsbp1l1	heat shock factor binding protein 1-like 1
4632404H12Rik	RIKEN cDNA 4632404H12 gene
Eif2b1	eukaryotic translation initiation factor 2B, subunit 1 (alpha)
Sec22b	SEC22 vesicle trafficking protein homolog B (S. cerevisiae)
Mgrn1	mahogunin, ring finger 1
Mettl1	methyltransferase like 1
Uxs1	UDP-glucuronate decarboxylase 1
Pogz	pogo transposable element with ZNF domain
Ube2o	ubiquitin-conjugating enzyme E2O
Zfp574	zinc finger protein 574
Wipi1	WD repeat domain, phosphoinositide interacting 1
Prkcd	protein kinase C, delta
Pfn1	profilin 1
Plcd1	phospholipase C, delta 1
Sh3bgrl3	SH3 domain binding glutamic acid-rich protein-like 3
Ube3a	ubiquitin protein ligase E3A
Cd300lg	CD300 antigen like family member G
Stip1	stress-induced phosphoprotein 1
Pgpep1l	pyroglutamyl-peptidase I-like
Mast2	microtubule associated serine/threonine kinase 2
Mapk9	mitogen-activated protein kinase 9
Ccdc146	coiled-coil domain containing 146
Ift52	intraflagellar transport 52
Atp6v1a	ATPase, H+ transporting, lysosomal V1 subunit A

Celsr2	cadherin, EGF LAG seven-pass G-type receptor 2 (flamingo homolog, Drosophila)
Smc3	structural maintenance of chromosomes 3
Psmd12	proteasome (prosome, macropain) 26S subunit, non-ATPase, 12
Aebp1	AE binding protein 1
Kif3a	kinesin family member 3A
Ntsr2	neurotensin receptor 2
Hdac1	histone deacetylase 1
Setd8	SET domain containing (lysine methyltransferase) 8
Mlph	melanophilin
Prkaa2	protein kinase, AMP-activated, alpha 2 catalytic subunit
Dock8	dedicator of cytokinesis 8
C530008M17Rik	RIKEN cDNA C530008M17 gene
Slc25a28	solute carrier family 25, member 28
Atp6v0e	ATPase, H+ transporting, lysosomal V0 subunit E
Rfng	RFNG O-fucosylpeptide 3-beta-N-acetylglucosaminyltransferase
Pde4b	phosphodiesterase 4B, cAMP specific
B3galt2	UDP-Gal:betaGlcNAc beta 1,3-galactosyltransferase, polypeptide 2
Cul3	cullin 3
Exoc3	exocyst complex component 3
Nr3c2	nuclear receptor subfamily 3, group C, member 2
Gzmm	granzyme M (lymphocyte met-ase 1)
Rph3al	rabphilin 3A-like (without C2 domains)
Nipal3	NIPA-like domain containing 3
Ywhag	tyrosine 3-monooxygenase/tryptophan 5-monooxygenase activation protein, gamma polypeptide
Synpo2	synaptopodin 2
Sox17	SRY-box containing gene 17
Vps52	vacuolar protein sorting 52 (yeast)
Nkain2	Na+/K+ transporting ATPase interacting 2
Sdcbp	syndecan binding protein
Cap2	CAP, adenylate cyclase-associated protein, 2 (yeast)
Frmd6	FERM domain containing 6
Ccdc57	coiled-coil domain containing 57
Ankrd44	ankyrin repeat domain 44

F11r	F11 receptor
Fam71e1	family with sequence similarity 71, member E1
Zfp35	zinc finger protein 35
Zfp598	zinc finger protein 598
Snx6	sorting nexin 6
Gpbp1l1	GC-rich promoter binding protein 1-like 1
Sec61a2	Sec61, alpha subunit 2 (S. cerevisiae)
Slc43a1	solute carrier family 43, member 1
Gnb4	guanine nucleotide binding protein (G protein), beta 4
Ednrb	endothelin receptor type B
Naglu	alpha-N-acetylglucosaminidase (Sanfilippo disease IIIB)
4921531C22Rik	RIKEN cDNA 4921531C22 gene
Ranbp10	RAN binding protein 10
Commd6	COMM domain containing 6
Ppp2r5e	protein phosphatase 2, regulatory subunit B (B56), epsilon isoform
Ube2e1	ubiquitin-conjugating enzyme E2E 1
Aldh6a1	aldehyde dehydrogenase family 6, subfamily A1
Pdzrn3	PDZ domain containing RING finger 3
Hps5	Hermansky-Pudlak syndrome 5 homolog (human)
Fkbp4	FK506 binding protein 4
Slc25a46	solute carrier family 25, member 46
Gnptab	N-acetylglucosamine-1-phosphate transferase, alpha and beta subunits
Hif1an	hypoxia-inducible factor 1, alpha subunit inhibitor
Fam122a	family with sequence similarity 122, member A
Ctnna1	catenin (cadherin associated protein), alpha 1
Arrdc2	arrestin domain containing 2
Eif5	eukaryotic translation initiation factor 5
Aptx	aprataxin
Socs7	suppressor of cytokine signaling 7
Arl16	ADP-ribosylation factor-like 16
Mef2d	myocyte enhancer factor 2D
Notch4	notch 4
Cog6	component of oligomeric golgi complex 6
Fbxo47	F-box protein 47
Amigo1	adhesion molecule with Ig like domain 1
Prdx6	peroxiredoxin 6
Evi5l	ecotropic viral integration site 5 like

Neo1	neogenin
Srrm4	serine/arginine repetitive matrix 4
9030624J02Rik	RIKEN cDNA 9030624J02 gene
Ndnl2	necdin-like 2
Prrg2	proline-rich Gla (G-carboxyglutamic acid) polypeptide 2
1700016C15Rik	RIKEN cDNA 1700016C15 gene
Atp6v0d1	ATPase, H+ transporting, lysosomal V0 subunit D1
Polr3k	polymerase (RNA) III (DNA directed) polypeptide K
Preb	prolactin regulatory element binding
Xpnpep1	X-prolyl aminopeptidase (aminopeptidase P) 1, soluble
Igkc	immunoglobulin kappa constant
Mras	muscle and microspikes RAS
Pisd-ps1	phosphatidylserine decarboxylase, pseudogene 1
Dennd4b	DENN/MADD domain containing 4B
Cox8a	cytochrome c oxidase, subunit VIIIa
Dmrt2	doublesex and mab-3 related transcription factor 2
Tdrkh	tudor and KH domain containing protein
2310016D23Rik	RIKEN cDNA 2310016D23 gene
Shbg	sex hormone binding globulin
Hgsnat	heparan-alpha-glucosaminide N-acetyltransferase
Ccnd3	cyclin D3
Eif4ebp1	eukaryotic translation initiation factor 4E binding protein 1
Pcnxl4	pecanex-like 4 (Drosophila)
Exoc4	exocyst complex component 4
Usp4	ubiquitin specific peptidase 4 (proto-oncogene)
Sema3b	sema domain, immunoglobulin domain (Ig), short basic domain, secreted, (semaphorin) 3B
Psme4	proteasome (prosome, macropain) activator subunit 4
Ankrd13a	ankyrin repeat domain 13a
Fabp4	fatty acid binding protein 4, adipocyte
Btbd1	BTB (POZ) domain containing 1

Abcf2	ATP-binding cassette, sub-family F (GCN20), member 2
Mib1	mindbomb homolog 1 (Drosophila)
Tsc2	tuberous sclerosis 2
Ugp2	UDP-glucose pyrophosphorylase 2
Robo4	roundabout homolog 4 (Drosophila)
Gm8100	glyceraldehyde-3-phosphate dehydrogenase pseudogene
Esam	endothelial cell-specific adhesion molecule
Wwp1	WW domain containing E3 ubiquitin protein ligase 1
St6galnac6	ST6 (alpha-N-acetyl-neuraminyl-2,3-beta-galactosyl-1,3)-N-acetylgalactosaminide alpha-2,6-sialyltransferase 6
Prkaca	protein kinase, cAMP dependent, catalytic, alpha
Irs2	insulin receptor substrate 2
Parn	poly(A)-specific ribonuclease (deadenylation nuclease)
Stim2	stromal interaction molecule 2
Gm5835	ribosomal protein L4 pseudogene
Irs1	insulin receptor substrate 1
Mapkapk2	MAP kinase-activated protein kinase 2
Ppp1r3c	protein phosphatase 1, regulatory (inhibitor) subunit 3C
Azin1	antizyme inhibitor 1
Meox2	mesenchyme homeobox 2
Slc44a2	solute carrier family 44, member 2
Tmem100	transmembrane protein 100
P4hb	prolyl 4-hydroxylase, beta polypeptide
6330416G13Rik	RIKEN cDNA 6330416G13 gene
Mthfr	5,10-methylenetetrahydrofolate reductase
Dusp3	dual specificity phosphatase 3 (vaccinia virus phosphatase VH1-related)
Flt4	FMS-like tyrosine kinase 4
Dnm2	dynamin 2
Hmgn1	high mobility group nucleosomal binding domain 1
Pfkm	phosphofructokinase, muscle
Ablim2	actin-binding LIM protein 2
Adamtsl4	ADAMTS-like 4

Dok5	docking protein 5
Gm9903	predicted gene 9903
Ptch1	patched homolog 1
Gabarapl1	gamma-aminobutyric acid (GABA) A receptor-associated protein-like 1
Jag2	jagged 2
Bcl6	B cell leukemia/lymphoma 6
Elf2	E74-like factor 2
Cav1	caveolin 1, caveolae protein
Cnbp	cellular nucleic acid binding protein
Kifap3	kinesin-associated protein 3
Rbm8a	RNA binding motif protein 8a
Atg7	autophagy related 7
Galnt1	UDP-N-acetyl-alpha-D-galactosamine:polypeptide N-acetylgalactosaminyltransferase 1
Eny2	enhancer of yellow 2 homolog (Drosophila)
Fem1a	feminization 1 homolog a (C. elegans)
Tcn2	transcobalamin 2
Fbxw5	F-box and WD-40 domain protein 5
Impdh1	inosine 5'-phosphate dehydrogenase 1
Urm1	ubiquitin related modifier 1 homolog (S. cerevisiae)
Rcsd1	RCSD domain containing 1
Cib1	calcium and integrin binding 1 (calmyrin)
Ctsc	cathepsin C
Fxn	frataxin
Cdc42bpg	CDC42 binding protein kinase gamma (DMPK-like)
Dpy19l3	dpy-19-like 3 (C. elegans)
Mtmr14	myotubularin related protein 14
Ak4	adenylate kinase 4
Tmem126b	transmembrane protein 126B
Gm4929	glyceraldehyde-3-phosphate dehydrogenase pseudogene
Ift43	intraflagellar transport 43 homolog (Chlamydomonas)
Sdha	succinate dehydrogenase complex, subunit A, flavoprotein (Fp)
Casp3	caspase 3
Ppp3cc	protein phosphatase 3, catalytic subunit, gamma isoform
Golga7b	golgi autoantigen, golgin subfamily a, 7B
Mtif3	mitochondrial translational initiation factor 3

Txnrd3	thioredoxin reductase 3
Cyb5b	cytochrome b5 type B
Ttn	titin
Fut8	fucosyltransferase 8
Aox1	aldehyde oxidase 1
Ddx41	DEAD (Asp-Glu-Ala-Asp) box polypeptide 41
Rassf1	Ras association (RalGDS/AF-6) domain family member 1
Oacyl	O-acyltransferase like
Btbd10	BTB (POZ) domain containing 10
Ptprq	protein tyrosine phosphatase, receptor type, Q
BC048679	cDNA sequence BC048679
Actr3	ARP3 actin-related protein 3
Grasp	GRP1 (general receptor for phosphoinositides 1)-associated scaffold protein
Itpa	inosine triphosphatase (nucleoside triphosphate pyrophosphatase)
Trim55	tripartite motif-containing 55
Use1	unconventional SNARE in the ER 1 homolog (S. cerevisiae)
Ctla4	cytotoxic T-lymphocyte-associated protein 4
Egflam	EGF-like, fibronectin type III and laminin G domains
Ptpmt1	protein tyrosine phosphatase, mitochondrial 1
Zfp410	zinc finger protein 410
Asb13	ankyrin repeat and SOCS box-containing 13
Cmpk2	cytidine monophosphate (UMP-CMP) kinase 2, mitochondrial
Capn7	calpain 7
Tada3	transcriptional adaptor 3
Gm11814	lactate dehydrogenase A pseudogene
Fam134a	family with sequence similarity 134, member A
Cnot6	CCR4-NOT transcription complex, subunit 6
Gm11557	glyceraldehyde-3-phosphate dehydrogenase pseudogene
Pibf1	progesterone immunomodulatory binding factor 1
Tppp	tubulin polymerization promoting protein
D6Wsu163e	DNA segment, Chr 6, Wayne State University 163, expressed
Sntb1	syntrophin, basic 1
Mmp15	matrix metallopeptidase 15
BC024978	cDNA sequence BC024978

Vdac3-ps1	voltage-dependent anion channel 3, pseudogene 1
Slc7a1	solute carrier family 7 (cationic amino acid transporter, y+ system), member 1
Efcab6	EF-hand calcium binding domain 6
Spcs3	signal peptidase complex subunit 3 homolog (S. cerevisiae)
Ube2q2	ubiquitin-conjugating enzyme E2Q (putative) 2
Tmem9	transmembrane protein 9
Irf8	interferon regulatory factor 8
Ppp1r7	protein phosphatase 1, regulatory (inhibitor) subunit 7
Car13	carbonic anhydrase 13
Ifitm2	interferon induced transmembrane protein 2
Gm3534	glyceraldehyde-3-phosphate dehydrogenase pseudogene
Sec62	SEC62 homolog (S. cerevisiae)
Hsf2	heat shock factor 2
Pias2	protein inhibitor of activated STAT 2
Zfp446	zinc finger protein 446
Ptx3	pentraxin related gene
4930556M19Rik	RIKEN cDNA 4930556M19 gene
Myoz3	myozenin 3
Spryd3	SPRY domain containing 3
Evc	Ellis van Creveld gene syndrome
Pter	phosphotriesterase related
1110008F13Rik	RIKEN cDNA 1110008F13 gene
Stxbp2	syntaxin binding protein 2
Rab1b	RAB1B, member RAS oncogene family
Gdpd5	glycerophosphodiester phosphodiesterase domain containing 5
Asb7	ankyrin repeat and SOCS box-containing 7
Decr1	2,4-dienoyl CoA reductase 1, mitochondrial
Nars	asparaginyl-tRNA synthetase
Eps15	epidermal growth factor receptor pathway substrate 15
Mavs	mitochondrial antiviral signaling protein
Rev1	REV1 homolog (S. cerevisiae)
4930552P12Rik	RIKEN cDNA 4930552P12 gene
Gm11185	glyceraldehyde-3-phosphate dehydrogenase pseudogene
Cyth2	cytohesin 2

Etnk1	ethanolamine kinase 1
Traf3ip3	TRAF3 interacting protein 3
BC005537	cDNA sequence BC005537
Elp2	elongator acetyltransferase complex subunit 2
Gm15676	predicted gene 15676
Ppp6r2	protein phosphatase 6, regulatory subunit 2
Ppat	phosphoribosyl pyrophosphate amidotransferase
Gm10293	glyceraldehyde-3-phosphate dehydrogenase pseudogene
Pgp	phosphoglycolate phosphatase
Fmnl2	formin-like 2
Ddo	D-aspartate oxidase
Zfp954	zinc finger protein 954
Snx10	sorting nexin 10
A830019P07Rik	RIKEN cDNA A830019P07 gene
Ankrd6	ankyrin repeat domain 6
Dnm1l	dynamin 1-like
Pkig	protein kinase inhibitor, gamma
Ccdc50	coiled-coil domain containing 50
Ttc38	tetratricopeptide repeat domain 38
Slc25a17	solute carrier family 25 (mitochondrial carrier, peroxisomal membrane protein), member 17
Cpsf7	cleavage and polyadenylation specific factor 7
Taf8	TAF8 RNA polymerase II, TATA box binding protein (TBP)-associated factorq
Rrad	Ras-related associated with diabetes
Dbt	dihydrolipoamide branched chain transacylase E2
Plrg1	pleiotropic regulator 1, PRL1 homolog (Arabidopsis)
Telo2	TEL2, telomere maintenance 2, homolog (S. cerevisiae)
Armc10	armadillo repeat containing 10
Vps16	vacuolar protein sorting 16 (yeast)
Cog1	component of oligomeric golgi complex 1
Pbld2	phenazine biosynthesis-like protein domain containing 2
0610040J01Rik	RIKEN cDNA 0610040J01 gene
2310067B10Rik	RIKEN cDNA 2310067B10 gene
Piwil2	piwi-like homolog 2 (Drosophila)

Rfc1	replication factor C (activator 1) 1
Parp9	poly (ADP-ribose) polymerase family, member 9
Gltp	glycolipid transfer protein
Hnmt	histamine N-methyltransferase
Hgs	HGF-regulated tyrosine kinase substrate
Hrasls	HRAS-like suppressor
Spg20	spastic paraplegia 20, spartin (Troyer syndrome) homolog (human)
Ccl25	chemokine (C-C motif) ligand 25
1700024P16Rik	RIKEN cDNA 1700024P16 gene
Stxbp6	syntaxin binding protein 6 (amisyn)
Atpaf1	ATP synthase mitochondrial F1 complex assembly factor 1
Hnrnpl	heterogeneous nuclear ribonucleoprotein L
Ip6k3	inositol hexaphosphate kinase 3
Mllt11	myeloid/lymphoid or mixed-lineage leukemia (trithorax homolog, Drosophila); translocated to, 11
1500017E21Rik	RIKEN cDNA 1500017E21 gene
Eln	elastin
Hadhb	hydroxyacyl-Coenzyme A dehydrogenase/3-ketoacyl-Coenzyme A thiolase/enoyl-Coenzyme A hydratase (trifunctional protein), beta subunit
Ranbp9	RAN binding protein 9
Rom1	rod outer segment membrane protein 1
Creld1	cysteine-rich with EGF-like domains 1
Pafah1b2	platelet-activating factor acetylhydrolase, isoform 1b, subunit 2
Gm2076	glyceraldehyde-3-phosphate dehydrogenase pseudogene
Man2c1	mannosidase, alpha, class 2C, member 1
Syn3	synapsin III
Uvrag	UV radiation resistance associated gene
Spice1	spindle and centriole associated protein 1
Acox1	acyl-Coenzyme A oxidase 1, palmitoyl
Rras	Harvey rat sarcoma oncogene, subgroup R
Ap3s2	adaptor-related protein complex 3, sigma 2 subunit
Foxk2	forkhead box K2
D030056L22Rik	RIKEN cDNA D030056L22 gene

2310030G06Rik	RIKEN cDNA 2310030G06 gene
Gm18859	glyceraldehyde-3-phosphate dehydrogenase pseudogene
March 08	membrane-associated ring finger (C3HC4) 8
AI597479	expressed sequence AI597479
Bpnt1	bisphosphate 3'-nucleotidase 1
Arl4c	ADP-ribosylation factor-like 4C
Prkra	protein kinase, interferon inducible double stranded RNA dependent activator
Snx32	sorting nexin 32
Angpt2	angiopoietin 2
Fam161b	family with sequence similarity 161, member B
Mrpl10	mitochondrial ribosomal protein L10
4930513N10Rik	RIKEN cDNA 4930513N10 gene
Ksr1	kinase suppressor of ras 1
Wscd1	WSC domain containing 1
Tsc22d1	TSC22 domain family, member 1
Rragd	Ras-related GTP binding D
Dpm2	dolichol-phosphate (beta-D) mannosyltransferase 2
Exoc1	exocyst complex component 1
Fchsd2	FCH and double SH3 domains 2
Asb4	ankyrin repeat and SOCS box-containing 4
E2f4	E2F transcription factor 4
Zfp68	zinc finger protein 68
Gm17586	predicted gene, 17586
Mef2a	myocyte enhancer factor 2A
Prpf18	PRP18 pre-mRNA processing factor 18 homolog (yeast)
Tmem80	transmembrane protein 80
Fam120aos	family with sequence similarity 120A opposite strand
Edem2	ER degradation enhancer, mannosidase alpha-like 2
Btaf1	BTAF1 RNA polymerase II, B-TFIID transcription factor-associated, (Mot1 homolog, S. cerevisiae)
Naa50	N(alpha)-acetyltransferase 50, NatE catalytic subunit
Anxa6	annexin A6
Dclre1c	DNA cross-link repair 1C, PSO2 homolog (S. cerevisiae)
Dand5	DAN domain family, member 5

Psme2	proteasome (prosome, macropain) 28 subunit, beta
Etf1	eukaryotic translation termination factor 1
Dguok	deoxyguanosine kinase
Rhoh	ras homolog gene family, member H
Edar	ectodysplasin-A receptor
Sec22a	SEC22 vesicle trafficking protein homolog A (S. cerevisiae)
Galk2	galactokinase 2
Endog	endonuclease G
Bcar3	breast cancer anti-estrogen resistance 3
Atp6v1c1	ATPase, H+ transporting, lysosomal V1 subunit C1
Nudt16	nudix (nucleoside diphosphate linked moiety X)-type motif 16
Vps36	vacuolar protein sorting 36 (yeast)
N4bp2	NEDD4 binding protein 2
Kdelr1	KDEL (Lys-Asp-Glu-Leu) endoplasmic reticulum protein retention receptor 1
Tdrd9	tudor domain containing 9
Usp1	ubiquitin specific peptidase 1
Tcp11l1	t-complex 11 like 1
Sparcl1	SPARC-like 1
Mlx	MAX-like protein X
Izumo4	IZUMO family member 4
Fggy	FGGY carbohydrate kinase domain containing
Shc1	src homology 2 domain-containing transforming protein C1
Hsph1	heat shock 105kDa/110kDa protein 1
Rock1	Rho-associated coiled-coil containing protein kinase 1
Enkur	enkurin, TRPC channel interacting protein
Sec24a	Sec24 related gene family, member A (S. cerevisiae)
Gatsl3	GATS protein-like 3
Abcd3	ATP-binding cassette, sub-family D (ALD), member 3
Spsb4	splA/ryanodine receptor domain and SOCS box containing 4
Cbx8	chromobox 8
Acadl	acyl-Coenzyme A dehydrogenase, long-chain
Itfg1	integrin alpha FG-GAP repeat containing 1
Ttll1	tubulin tyrosine ligase-like 1
Ldb2	LIM domain binding 2
Npr2	natriuretic peptide receptor 2

BC029214	cDNA sequence BC029214
Cxxc5	CXXC finger 5
Muc15	mucin 15
Utp6	UTP6, small subunit (SSU) processome component, homolog (yeast)
Rhoc	ras homolog gene family, member C
Zw10	ZW10 homolog (Drosophila), centromere/kinetochore protein
Fzr1	fizzy/cell division cycle 20 related 1 (Drosophila)
Sin3b	transcriptional regulator, SIN3B (yeast)
Btbd2	BTB (POZ) domain containing 2
Ano3	anoctamin 3
Zfp157	zinc finger protein 157
Ivns1abp	influenza virus NS1A binding protein
Zdbf2	zinc finger, DBF-type containing 2
Terf2ip	telomeric repeat binding factor 2, interacting protein
1700037C18Rik	RIKEN cDNA 1700037C18 gene
Bach2	BTB and CNC homology 2
Hspb11	heat shock protein family B (small), member 11
Mir133a-2	microRNA 133a-2
Nmrk2	nicotinamide riboside kinase 2
Ccdc127	coiled-coil domain containing 127
Gm17396	predicted gene, 17396
Pradc1	protease-associated domain containing 1
Galns	galactosamine (N-acetyl)-6-sulfate sulfatase
Stard7	START domain containing 7
Usp28	ubiquitin specific peptidase 28
Ctla2a	cytotoxic T lymphocyte-associated protein 2 alpha
Tpm4	tropomyosin 4
Naa15	N(alpha)-acetyltransferase 15, NatA auxiliary subunit
Kcnj3	potassium inwardly-rectifying channel, subfamily J, member 3
Fscn1	fascin homolog 1, actin bundling protein (Strongylocentrotus purpuratus)
St13	suppression of tumorigenicity 13
Fam53a	family with sequence similarity 53, member A
Ift122	intraflagellar transport 122
Myot	myotilin

Pcgf3	polycomb group ring finger 3
Cdk5rap1	CDK5 regulatory subunit associated protein 1
Haus8	4HAUS augmin-like complex, subunit 8
Fn3k	fructosamine 3 kinase
Hspa4l	heat shock protein 4 like
Lrrfip2	leucine rich repeat (in FLII) interacting protein 2
Cyb5r2	cytochrome b5 reductase 2
Prune	prune homolog (Drosophila)
Gltscr2	glioma tumor suppressor candidate region gene 2
Trp63	transformation related protein 63
Myog	myogenin
Pdk1	pyruvate dehydrogenase kinase, isoenzyme 1
Vwa5a	von Willebrand factor A domain containing 5A
Taf2	TAF2 RNA polymerase II, TATA box binding protein (TBP)-associated factor
Rtkn2	rhotekin 2
Tcf15	transcription factor 15
Ulk2	unc-51 like kinase 2
Bbs4	Bardet-Biedl syndrome 4 (human)
Tab2	TGF-beta activated kinase 1/MAP3K7 binding protein 2
Sept 11	septin 11
Zfyve16	zinc finger, FYVE domain containing 16
D1Ertd622e	DNA segment, Chr 1, ERATO Doi 622, expressed
Rasd2	RASD family, member 2
Lrp3	low density lipoprotein receptor-related protein 3
Iqcc	IQ motif containing C
Dstn	destrin
Trim39	tripartite motif-containing 39
Polm	polymerase (DNA directed), mu
Ugcg	UDP-glucose ceramide glucosyltransferase
Adamts20	a disintegrin-like and metallopeptidase (reprolysin type) with thrombospondin type 1 motif, 20
Ppm1b	protein phosphatase 1B, magnesium dependent, beta isoform
Necap2	NECAP endocytosis associated 2
Tex261	testis expressed gene 261
Sart1	squamous cell carcinoma antigen recognized by T cells 1

BC031181	cDNA sequence BC031181
Slit1	slit homolog 1 (Drosophila)
Cdh23	cadherin 23 (otocadherin)
Ush1g	Usher syndrome 1G
Ogdhl	oxoglutarate dehydrogenase-like
Hspa2	heat shock protein 2
Dach1	dachshund 1 (Drosophila)
Stmn4	stathmin-like 4
Fbxo25	F-box protein 25
Mtss1l	metastasis suppressor 1-like
9130023H24Rik	RIKEN cDNA 9130023H24 gene
Igfn1	immunoglobulin-like and fibronectin type III domain containing 1
Fbxo10	F-box protein 10
Tex10	testis expressed gene 10
Dip2a	DIP2 disco-interacting protein 2 homolog A (Drosophila)
Trpc3	transient receptor potential cation channel, subfamily C, member 3
Tmed9	transmembrane emp24 protein transport domain containing 9
Lyar	Ly1 antibody reactive clone
Ankrd13b	ankyrin repeat domain 13b
Usp38	ubiquitin specific peptidase 38
Ddost	dolichyl-di-phosphooligosaccharide-protein glycotransferase
Clptm1l	CLPTM1-like
Ddah1	dimethylarginine dimethylaminohydrolase 1
Sox12	SRY-box containing gene 12
Mtx2	metaxin 2
Paqr9	progestin and adipoQ receptor family member IX
Arhgap15	Rho GTPase activating protein 15
Dyrk2	dual-specificity tyrosine-(Y)-phosphorylation regulated kinase 2
Nod1	nucleotide-binding oligomerization domain containing 1
Btf3l4	basic transcription factor 3-like 4
Coro6	coronin 6
Med15	mediator complex subunit 15

Adcyap1r1	adenylate cyclase activating polypeptide 1 receptor 1
Baalc	brain and acute leukemia, cytoplasmic
Cntnap4	contactin associated protein-like 4
Lin52	lin-52 homolog (C. elegans)
Hnrnpc	heterogeneous nuclear ribonucleoprotein C
Sh3tc2	SH3 domain and tetratricopeptide repeats 2
Itgb6	integrin beta 6
Mios	missing oocyte, meiosis regulator, homolog (Drosophila)
Pnpla8	patatin-like phospholipase domain containing 8
Dock4	dedicator of cytokinesis 4
Ampd2	adenosine monophosphate deaminase 2
Dtna	dystrobrevin alpha
Nsmce2	non-SMC element 2 homolog (MMS21, S. cerevisiae)
Rpusd1	RNA pseudouridylate synthase domain containing 1
Ptrf	polymerase I and transcript release factor
Vta1	Vps20-associated 1 homolog (S. cerevisiae)
Chrnb1	cholinergic receptor, nicotinic, beta polypeptide 1 (muscle)
Rad50	RAD50 homolog (S. cerevisiae)
Ciz1	CDKN1A interacting zinc finger protein 1
Nucb1	nucleobindin 1
Mrpl39	mitochondrial ribosomal protein L39
Itfg3	integrin alpha FG-GAP repeat containing 3
Nomo1	nodal modulator 1
Ube2w	ubiquitin-conjugating enzyme E2W (putative)
Sgms1	sphingomyelin synthase 1
Ccnyl1	cyclin Y-like 1
Hist1h1e	histone cluster 1, H1e
Tbc1d20	TBC1 domain family, member 20
Gpatch8	G patch domain containing 8
Sft2d2	SFT2 domain containing 2
Cacna1s	calcium channel, voltage-dependent, L type, alpha 1S subunit
2410131K14Rik	RIKEN cDNA 2410131K14 gene
Gm13375	predicted gene 13375
Slc4a7	solute carrier family 4, sodium bicarbonate cotransporter, member 7
Smap2	stromal membrane-associated GTPase-activating protein 2

Arhgap10	Rho GTPase activating protein 10
Tmbim1	transmembrane BAX inhibitor motif containing 1
Rbm28	RNA binding motif protein 28
Atp11b	ATPase, class VI, type 11B
Cnksr1	connector enhancer of kinase suppressor of Ras 1
Hps1	Hermansky-Pudlak syndrome 1 homolog (human)
Vldlr	very low density lipoprotein receptor
Plekhh2	pleckstrin homology domain containing, family H (with MyTH4 domain) member 2
Clasp2	CLIP associating protein 2
Gsdma	gasdermin A
1700040L02Rik	RIKEN cDNA 1700040L02 gene
Hdac10	histone deacetylase 10
Col27a1	collagen, type XXVII, alpha 1
Isg15	ISG15 ubiquitin-like modifier
2410022M11Rik	RIKEN cDNA 2410022M11 gene
Tm4sf1	transmembrane 4 superfamily member 1
Nipa1	non imprinted in Prader-Willi/Angelman syndrome 1 homolog (human)
Dctn4	dynactin 4
Wwp2	WW domain containing E3 ubiquitin protein ligase 2
Mkl1	MKL (megakaryoblastic leukemia)/myocardin-like 1
Pgd	phosphogluconate dehydrogenase
Cul5	cullin 5
Nudt12	nudix (nucleoside diphosphate linked moiety X)-type motif 12
Pcmtd1	protein-L-isoaspartate (D-aspartate) O-methyltransferase domain containing 1
AI118078	expressed sequence AI118078
Aqp1	aquaporin 1
Rragc	Ras-related GTP binding C
Itpkc	inositol 1,4,5-trisphosphate 3-kinase C
Tmem201	transmembrane protein 201
Iba57	IBA57, iron-sulfur cluster assembly homolog (S. cerevisiae)
Mdfi	MyoD family inhibitor

Dync1i1	dynein cytoplasmic 1 intermediate chain 1
Btd	biotinidase
Rbm20	RNA binding motif protein 20
Rxra	retinoid X receptor alpha
Scap	SREBF chaperone
Ppp3cb	protein phosphatase 3, catalytic subunit, beta isoform
Ppil1	peptidylprolyl isomerase (cyclophilin)-like 1
A930018M24Rik	RIKEN cDNA A930018M24 gene
Hdgfrp3	hepatoma-derived growth factor, related protein 3
Otub2	OTU domain, ubiquitin aldehyde binding 2
Plekhg5	pleckstrin homology domain containing, family G (with RhoGef domain) member 5
BC067074	cDNA sequence BC067074
Parm1	prostate androgen-regulated mucin-like protein 1
Sf3a3	splicing factor 3a, subunit 3
Heatr1	HEAT repeat containing 1
Gm9061	glyceraldehyde-3-phosphate dehydrogenase pseudogene
Ubap2l	ubiquitin associated protein 2-like
Abcb4	ATP-binding cassette, sub-family B (MDR/TAP), member 4
Phb	prohibitin
Ube2z	ubiquitin-conjugating enzyme E2Z (putative)
Nek9	NIMA (never in mitosis gene a)-related expressed kinase 9
Aen	apoptosis enhancing nuclease
Sobp	sine oculis-binding protein homolog (Drosophila)
Papolg	poly(A) polymerase gamma
Jagn1	jagunal homolog 1 (Drosophila)
Zbed3	zinc finger, BED domain containing 3
Ppp1cc	protein phosphatase 1, catalytic subunit, gamma isoform
Tbca	tubulin cofactor A
Pkdcc	protein kinase domain containing, cytoplasmic
Mapk4	mitogen-activated protein kinase 4
Wdr25	WD repeat domain 25
Zfp697	zinc finger protein 697
Bcl9	B cell CLL/lymphoma 9

Rmi2	RMI2, RecQ mediated genome instability 2, homolog (S. cerevisiae)
Synm	synemin, intermediate filament protein
Sdccag3	serologically defined colon cancer antigen 3
Ddb1	damage specific DNA binding protein 1
5730419F03Rik	RIKEN cDNA 5730419F03 gene
Apbb1	amyloid beta (A4) precursor protein-binding, family B, member 1
Zbtb44	zinc finger and BTB domain containing 44
Ttc7	tetratricopeptide repeat domain 7
Ncam1	neural cell adhesion molecule 1
Ccdc6	coiled-coil domain containing 6
Nudt4	nudix (nucleoside diphosphate linked moiety X)-type motif 4
Zfp532	zinc finger protein 532
Hmox2	heme oxygenase (decycling) 2
Tmem37	transmembrane protein 37
Gpd1l	glycerol-3-phosphate dehydrogenase 1-like
Lcmt2	leucine carboxyl methyltransferase 2
BC052040	cDNA sequence BC052040
Shroom3	shroom family member 3
Ablim3	actin binding LIM protein family, member 3
Ap2b1	adaptor-related protein complex 2, beta 1 subunit
Tlr4	toll-like receptor 4
Sgcg	sarcoglycan, gamma (dystrophin-associated glycoprotein)
Dmxl2	Dmx-like 2
C330011M18Rik	RIKEN cDNA C330011M18 gene
Vash1	vasohibin 1
Tal2	T cell acute lymphocytic leukemia 2
Pacrg	PARK2 co-regulated
Eif4h	eukaryotic translation initiation factor 4H
Bmpr1b	bone morphogenetic protein receptor, type 1B
Camta2	calmodulin binding transcription activator 2
Stx12	syntaxin 12
Eml4	echinoderm microtubule associated protein like 4
B4galt4	UDP-Gal:betaGlcNAc beta 1,4-galactosyltransferase, polypeptide 4
Fzd9	frizzled homolog 9 (Drosophila)

Igf2bp2	insulin-like growth factor 2 mRNA binding protein 2
Ppfia1	protein tyrosine phosphatase, receptor type, f polypeptide (PTPRF), interacting protein (liprin), alpha 1
Ncoa5	nuclear receptor coactivator 5
Gm10032	predicted gene 10032
Fuca1	fucosidase, alpha-L- 1, tissue
Fastkd1	FAST kinase domains 1
Aifm2	apoptosis-inducing factor, mitochondrion-associated 2
Rhog	ras homolog gene family, member G
Sike1	suppressor of IKBKE 1
Tada2a	transcriptional adaptor 2A
Exoc2	exocyst complex component 2
Mgll	monoglyceride lipase
Tada2b	transcriptional adaptor 2B
Smc4	structural maintenance of chromosomes 4
Ints9	integrator complex subunit 9
Lrsam1	leucine rich repeat and sterile alpha motif containing 1
Dnajc3	DnaJ (Hsp40) homolog, subfamily C, member 3
Rnf150	ring finger protein 150
Card14	caspase recruitment domain family, member 14
Myh14	myosin, heavy polypeptide 14
Kank3	KN motif and ankyrin repeat domains 3
Coq5	coenzyme Q5 homolog, methyltransferase (yeast)
Gm10643	predicted gene 10643
Wnk1	WNK lysine deficient protein kinase 1
1810058I24Rik	RIKEN cDNA 1810058I24 gene
Nkd2	naked cuticle 2 homolog (Drosophila)
Pea15a	phosphoprotein enriched in astrocytes 15A
Siva1	SIVA1, apoptosis-inducing factor
Rabgap1l	RAB GTPase activating protein 1-like
5830444B04Rik	RIKEN cDNA 5830444B04 gene
Casd1	CAS1 domain containing 1
Got2	glutamate oxaloacetate transaminase 2, mitochondrial
Tle6	transducin-like enhancer of split 6, homolog of Drosophila E(spl)

4930458D05Rik	RIKEN cDNA 4930458D05 gene
Lyrm2	LYR motif containing 2
Esd	esterase D/formylglutathione hydrolase
Comt	catechol-O-methyltransferase
Gm4335	glyceraldehyde-3-phosphate dehydrogenase pseudogene
Sat2	spermidine/spermine N1-acetyl transferase 2
Myod1	myogenic differentiation 1
Elp4	elongation protein 4 homolog (S. cerevisiae)
Rnf126	ring finger protein 126
Pik3ip1	phosphoinositide-3-kinase interacting protein 1
Vwa7	von Willebrand factor A domain containing 7
Sars	seryl-aminoacyl-tRNA synthetase
R3hdm1	R3H domain 1 (binds single-stranded nucleic acids)
Apbb2	amyloid beta (A4) precursor protein-binding, family B, member 2
Snx21	sorting nexin family member 21
Rpp40	ribonuclease P 40 subunit (human)
Rgma	RGM domain family, member A
Mb	myoglobin
Cited2	Cbp/p300-interacting transactivator, with Glu/Asp-rich carboxy-terminal domain, 2
Hcn4	hyperpolarization-activated, cyclic nucleotide-gated K+ 4
Frk	fyn-related kinase
Fam160b2	family with sequence similarity 160, member B2
1810026J23Rik	RIKEN cDNA 1810026J23 gene
Cbwd1	COBW domain containing 1
Sh2b1	SH2B adaptor protein 1
Foxo3	forkhead box O3
Kank1	KN motif and ankyrin repeat domains 1
E030030I06Rik	RIKEN cDNA E030030I06 gene
Man1b1	mannosidase, alpha, class 1B, member 1
Rundc1	RUN domain containing 1
Hnrnpul1	heterogeneous nuclear ribonucleoprotein U-like 1
Ube2e2	ubiquitin-conjugating enzyme E2E 2
Efcab2	EF-hand calcium binding domain 2
Tbcc	tubulin-specific chaperone C

Snx5	sorting nexin 5
Ehd4	EH-domain containing 4
Kif11	kinesin family member 11
Itm2c	integral membrane protein 2C
Haghl	hydroxyacylglutathione hydrolase-like
Ascc2	activating signal cointegrator 1 complex subunit 2
Uap1l1	UDP-N-acteylglucosamine pyrophosphorylase 1-like 1
Epha2	Eph receptor A2
Birc3	baculoviral IAP repeat-containing 3
Ptdss1	phosphatidylserine synthase 1
Ier3	immediate early response 3
Fkbp7	FK506 binding protein 7
Cnst	consortin, connexin sorting protein
Chac1	ChaC, cation transport regulator 1
Ccdc159	coiled-coil domain containing 159
Ddc	dopa decarboxylase
Gm6288	predicted gene 6288
Pgpep1	pyroglutamyl-peptidase I
Sap30bp	SAP30 binding protein
Fbxo18	F-box protein 18
Zfp641	zinc finger protein 641
Arf6	ADP-ribosylation factor 6
Zfp286	zinc finger protein 286
Vipas39	VPS33B interacting protein, apical-basolateral polarity regulator, spe-39 homolog
Rorc	RAR-related orphan receptor gamma
Drg2	developmentally regulated GTP binding protein 2
Cherp	calcium homeostasis endoplasmic reticulum protein
Gpt	glutamic pyruvic transaminase, soluble
Wipi2	WD repeat domain, phosphoinositide interacting 2
Serpine2	serine (or cysteine) peptidase inhibitor, clade E, member 2
Lgals3bp	lectin, galactoside-binding, soluble, 3 binding protein
Naa16	N(alpha)-acetyltransferase 16, NatA auxiliary subunit
E130308A19Rik	RIKEN cDNA E130308A19 gene
Pex13	peroxisomal biogenesis factor 13
Rbl1	retinoblastoma-like 1 (p107)

Asb8	ankyrin repeat and SOCS box-containing 8
Tnfrsf21	tumor necrosis factor receptor superfamily, member 21
Slmo2	slowmo homolog 2 (Drosophila)
Ubqln4	ubiquilin 4
Traf4	TNF receptor associated factor 4
6030419C18Rik	RIKEN cDNA 6030419C18 gene
Cbx2	chromobox 2
Ifit2	interferon-induced protein with tetratricopeptide repeats 2
Fam129b	family with sequence similarity 129, member B
Ebag9	estrogen receptor-binding fragment-associated gene 9
Emcn	endomucin
Itgb5	integrin beta 5
Gm4654	glyceraldehyde-3-phosphate dehydrogenase pseudogene
Mylk4	myosin light chain kinase family, member 4
Gpatch4	G patch domain containing 4
Ntn5	netrin 5
Gramd1b	GRAM domain containing 1B
Clcnkb	chloride channel Kb
Asb1	ankyrin repeat and SOCS box-containing 1
Pelp1	proline, glutamic acid and leucine rich protein 1
Dyrk1a	dual-specificity tyrosine-(Y)-phosphorylation regulated kinase 1a
Adcy2	adenylate cyclase 2
Tm6sf1	transmembrane 6 superfamily member 1
Tspan13	tetraspanin 13
Ppil2	peptidylprolyl isomerase (cyclophilin)-like 2
Pak4	p21 protein (Cdc42/Rac)-activated kinase 4
Nes	nestin
Cpeb3	cytoplasmic polyadenylation element binding protein 3
Stambp	STAM binding protein
Fastkd3	FAST kinase domains 3
Nceh1	arylacetamide deacetylase-like 1
0610009L18Rik	RIKEN cDNA 0610009L18 gene
Ccdc86	coiled-coil domain containing 86
Rab2a	RAB2A, member RAS oncogene family
Sel1l3	sel-1 suppressor of lin-12-like 3 (C. elegans)
Lars	leucyl-tRNA synthetase

Mtrf1	mitochondrial translational release factor 1
Xrn2	5'-3' exoribonuclease 2
Vps37c	vacuolar protein sorting 37C (yeast)
Tfdp1	transcription factor Dp 1
Slc2a1	solute carrier family 2 (facilitated glucose transporter), member 1
Lmo7	LIM domain only 7
Ccz1	CCZ1 vacuolar protein trafficking and biogenesis associated
Gpc1	glypican 1
Ap3m1	adaptor-related protein complex 3, mu 1 subunit
Tmem71	transmembrane protein 71
Trabd	TraB domain containing
Larp1b	La ribonucleoprotein domain family, member 1B
2010107G23Rik	RIKEN cDNA 2010107G23 gene
Thumpd1	THUMP domain containing 1
Rasa3	RAS p21 protein activator 3
Cbfa2t2	core-binding factor, runt domain, alpha subunit 2, translocated to, 2 (human)
Cttnbp2nl	CTTNBP2 N-terminal like
Ushbp1	Usher syndrome 1C binding protein 1
Eif2ak2	eukaryotic translation initiation factor 2-alpha kinase 2
Rbfox1	RNA binding protein, fox-1 homolog (C. elegans) 1
Eci2	enoyl-Coenzyme A delta isomerase 2
Stx7	syntaxin 7
E130317F20Rik	RIKEN cDNA E130317F20 gene
Slc18a1	solute carrier family 18 (vesicular monoamine), member 1
Chmp5	charged multivesicular body protein 5
Dhps	deoxyhypusine synthase
Cttn	cortactin
Inppl1	inositol polyphosphate phosphatase-like 1
Slc25a37	solute carrier family 25, member 37
Limd1	LIM domains containing 1
Oxct1	3-oxoacid CoA transferase 1
Pias1	protein inhibitor of activated STAT 1
Tcp11l2	t-complex 11 (mouse) like 2

Anapc7	anaphase promoting complex subunit 7
Klhl38	kelch-like 38 (Drosophila)
Mast4	microtubule associated serine/threonine kinase family member 4
Zranb2	zinc finger, RAN-binding domain containing 2
Scarf1	scavenger receptor class F, member 1
Nxn	nucleoredoxin
Sephs2	selenophosphate synthetase 2
Phf20l1	PHD finger protein 20-like 1
Gnl3	guanine nucleotide binding protein-like 3 (nucleolar)
Gata2	GATA binding protein 2
Cnot7	CCR4-NOT transcription complex, subunit 7
Ipmk	inositol polyphosphate multikinase
Hnrnpa1	heterogeneous nuclear ribonucleoprotein A1
Taok3	TAO kinase 3
Msrb3	methionine sulfoxide reductase B3
Actr6	ARP6 actin-related protein 6
Tnfrsf4	tumor necrosis factor receptor superfamily, member 4
Sf3b2	splicing factor 3b, subunit 2
Fam96b	family with sequence similarity 96, member B
Mdfic	MyoD family inhibitor domain containing
Ubtf	upstream binding transcription factor, RNA polymerase I
Cog2	component of oligomeric golgi complex 2
Bsdc1	BSD domain containing 1
Gorasp1	golgi reassembly stacking protein 1
Mettl11b	methyltransferase like 11B
Siah2	seven in absentia 2
Enoph1	enolase-phosphatase 1
Pcyt1a	phosphate cytidylyltransferase 1, choline, alpha isoform
Frat2	frequently rearranged in advanced T cell lymphomas 2
Gpx3	glutathione peroxidase 3
Hspb3	heat shock protein 3
Phtf2	putative homeodomain transcription factor 2
Stc1	stanniocalcin 1
Sec63	SEC63-like (S. cerevisiae)
Ikzf5	IKAROS family zinc finger 5
Ube2d3	ubiquitin-conjugating enzyme E2D 3
Rint1	RAD50 interactor 1
Pusl1	pseudouridylate synthase-like 1
Igsf3	immunoglobulin superfamily, member 3

Rrm1	ribonucleotide reductase M1
Plin5	perilipin 5
Endov	endonuclease V
2310075C17Rik	RIKEN cDNA 2310075C17 gene
Klhdc8a	kelch domain containing 8A
Fbxo44	F-box protein 44
Twsg1	twisted gastrulation homolog 1 (Drosophila)
P2rx5	purinergic receptor P2X, ligand-gated ion channel, 5
Pef1	penta-EF hand domain containing 1
Wdr6	WD repeat domain 6
Wars	tryptophanyl-tRNA synthetase
Cpn1	carboxypeptidase N, polypeptide 1
Cd86	CD86 antigen
Ube2q1	ubiquitin-conjugating enzyme E2Q (putative) 1
Gnptg	N-acetylglucosamine-1-phosphotransferase, gamma subunit
Ppp2r4	protein phosphatase 2A, regulatory subunit B (PR 53)
Ptms	parathymosin
Gab2	growth factor receptor bound protein 2-associated protein 2
Ces5a	carboxylesterase 5A
4930544D05Rik	RIKEN cDNA 4930544D05 gene
Gm7293	glyceraldehyde-3-phosphate dehydrogenase pseudogene
Bag6	BCL2-associated athanogene 6
Ppme1	protein phosphatase methylesterase 1
Osgin1	oxidative stress induced growth inhibitor 1
Trim35	tripartite motif-containing 35
Rab8a	RAB8A, member RAS oncogene family
Cdkn2c	cyclin-dependent kinase inhibitor 2C (p18, inhibits CDK4)
Dock9	dedicator of cytokinesis 9
Kdm5b	lysine (K)-specific demethylase 5B
Dnajb6	DnaJ (Hsp40) homolog, subfamily B, member 6
Arpp19	cAMP-regulated phosphoprotein 19
Ythdf2	YTH domain family 2
Eps8l1	EPS8-like 1
Paqr8	progestin and adipoQ receptor family member VIII
0610010F05Rik	RIKEN cDNA 0610010F05 gene

Lrrn3	leucine rich repeat protein 3, neuronal
Hsf1	heat shock factor 1
Pecam1	platelet/endothelial cell adhesion molecule 1
Tbc1d23	TBC1 domain family, member 23
Guf1	GUF1 GTPase homolog (S. cerevisiae)
Usp14	ubiquitin specific peptidase 14
C1qtnf9	C1q and tumor necrosis factor related protein 9
Rab21	RAB21, member RAS oncogene family
AI854703	expressed sequence AI854703
Uspl1	ubiquitin specific peptidase like 1
Sppl3	signal peptide peptidase 3
Lactb	lactamase, beta
Hist1h4h	histone cluster 1, H4h
Fsd1l	fibronectin type III and SPRY domain containing 1-like
Enah	enabled homolog (Drosophila)
Ift20	intraflagellar transport 20
Pan3	PAN3 polyA specific ribonuclease subunit homolog (S. cerevisiae)
Setdb1	SET domain, bifurcated 1
Homer1	homer homolog 1 (Drosophila)
Slbp	stem-loop binding protein
Aars	alanyl-tRNA synthetase
Tmem43	transmembrane protein 43
Alg3	asparagine-linked glycosylation 3 (alpha-1,3-mannosyltransferase)
Anp32a	acidic (leucine-rich) nuclear phosphoprotein 32 family, member A
Aagab	alpha- and gamma-adaptin binding protein
Grip2	glutamate receptor interacting protein 2
Pik3cd	phosphatidylinositol 3-kinase catalytic delta polypeptide
Kpna4	karyopherin (importin) alpha 4
Sphk2	sphingosine kinase 2
Cdyl2	chromodomain protein, Y chromosome-like 2
Coq9	coenzyme Q9 homolog (yeast)
Atp5a1	ATP synthase, H+ transporting, mitochondrial F1 complex, alpha subunit 1
Wbp4	WW domain binding protein 4
Pik3r2	phosphatidylinositol 3-kinase, regulatory subunit, polypeptide 2 (p85 beta)
Mall	mal, T cell differentiation protein-like
Ctc1	CTS telomere maintenance complex component 1
E2f2	E2F transcription factor 2

2310001H17Rik	RIKEN cDNA 2310001H17 gene
Gm4819	glyceraldehyde-3-phosphate dehydrogenase pseudogene
Pmepa1	prostate transmembrane protein, androgen induced 1
Usp5	ubiquitin specific peptidase 5 (isopeptidase T)
Exoc6	exocyst complex component 6
Lamp1	lysosomal-associated membrane protein 1
Rsph3b	radial spoke 3B homolog (Chlamydomonas)
Tob2	transducer of ERBB2, 2
Aldh2	aldehyde dehydrogenase 2, mitochondrial
Cbr1	carbonyl reductase 1
Aldoart2	aldolase 1 A retrogene 2
Fbxo32	F-box protein 32
Nckipsd	NCK interacting protein with SH3 domain
Evc2	Ellis van Creveld syndrome 2
N4bp1	NEDD4 binding protein 1
Bbs1	Bardet-Biedl syndrome 1 (human)
K230010J24Rik	RIKEN cDNA K230010J24 gene
Actr1b	ARP1 actin-related protein 1B, centractin beta
Vgll2	vestigial like 2 homolog (Drosophila)
Prelid1	PRELI domain containing 1
Dhx36	DEAH (Asp-Glu-Ala-His) box polypeptide 36
Gm7251	glyceraldehyde-3-phosphate dehydrogenase pseudogene
Slc29a1	solute carrier family 29 (nucleoside transporters), member 1
Nfe2l2	nuclear factor, erythroid derived 2, like 2
Lrrc14	leucine rich repeat containing 14
Fuom	fucose mutarotase
Arhgap19	Rho GTPase activating protein 19
2010111I01Rik	RIKEN cDNA 2010111I01 gene
Nup155	nucleoporin 155
Cav2	caveolin 2
Grsf1	G-rich RNA sequence binding factor 1
Kat2b	K(lysine) acetyltransferase 2B
Leprotl1	leptin receptor overlapping transcript-like 1
Zfp110	zinc finger protein 110
Arih2	ariadne homolog 2 (Drosophila)
Bcar1	breast cancer anti-estrogen resistance 1
Fbxo31	F-box protein 31

Rfxank	regulatory factor X-associated ankyrin-containing protein
Sept9	septin 9
Cd93	CD93 antigen
Lmod3	leiomodin 3 (fetal)
Pxmp4	peroxisomal membrane protein 4
Maea	macrophage erythroblast attacher
Cul9	cullin 9

6.10 Eighteen Month Common Gene comparison- Up regulated Genes

Gene Symbol	Gene Name
4930481A15Rik	RIKEN cDNA 4930481A15 gene
8430408G22Rik	RIKEN cDNA 8430408G22 gene
Dock9	dedicator of cytokinesis 9
Gja1	gap junction protein, alpha 1
Jun	Jun oncogene
Kcna5	Potassium Channel, Voltage Gated Shaker Related Subfamily A, Member 5
Klhl38	kelch-like 38 (Drosophila)
Per1	period homolog 1 (Drosophila)
Slc10a6	solute carrier family 10 (sodium/bile acid cotransporter family), member 6
Slc38a2	solute carrier family 38, member 2
Ucp3	Uncoupling Protein 3 (Mitochondrial, Proton Carrier)
Wdr62	WD Repeat Domain 62

6.11 Eighteen Month Common Gene comparison- Down regulated Genes

Gene Symbol	Gene Name
Adap1	ArfGAP with dual PH domains 1
Aif1	allograft inflammatory factor 1
Ccl5	chemokine (C-C motif) ligand 5
Cd22	CD22 antigen
Cd37	CD37 antigen
Cd3g	CD3 antigen, gamma polypeptide
Cd6	CD6 antigen
Cd79b	CD79B antigen
Cd83	CD83 antigen
Chia1	chitinase, acidic 1
Ddc	dopa decarboxylase
Dock8	dedicator of cytokinesis 8
Gm10053	cytochrome c, somatic pseudogene

H2-Ob	histocompatibility 2, O region beta locus
Ighg3	Immunoglobulin heavy constant gamma 3
Ighv14-4	immunoglobulin heavy variable 14-4
Ighv1-53	immunoglobulin heavy variable 1-53
Ighv1-55	immunoglobulin heavy variable 1-55
Ighv1-64	immunoglobulin heavy variable 1-64
Ighv1-85	immunoglobulin heavy variable 1-85
Ighv3-6	immunoglobulin heavy variable V3-6
Ighv8-12	immunoglobulin heavy variable V8-12
Igkc	Immunoglobulin Kappa Constant
Igkv10-96	immunoglobulin kappa variable 10-96
Igkv17-121	immunoglobulin kappa variable 17-121
Igkv2-109	immunoglobulin kappa variable 2-109
Igkv3-1	immunoglobulin kappa variable 3-1
Igkv3-10	immunoglobulin kappa variable 3-10
Igkv3-2	immunoglobulin kappa variable 3-2
Igkv3-5	immunoglobulin kappa chain variable 3-5
Igkv4-55	immunoglobulin kappa variable 4-55
Igkv4-57	immunoglobulin kappa variable 4-57
Igkv4-68	immunoglobulin kappa variable 4-68
Igkv4-91	immunoglobulin kappa chain variable 4-91
Igkv5-39	immunoglobulin kappa variable 5-39
Igkv6-20	immunoglobulin kappa variable 6-20
Igkv6-23	immunoglobulin kappa variable 6-23
Igkv6-32	immunoglobulin kappa variable 6-32
Iglc1	immunoglobulin lambda constant 1
Iglc3	immunoglobulin lambda constant 3
Iglv1	immunoglobulin lambda variable 1
Il9r	interleukin 9 receptor
Irf4	interferon regulatory factor 4
Jchain	Joining Chain Of Multimeric IgA And IgM
Lag3	lymphocyte-activation gene 3
Mki67	antigen identified by monoclonal antibody Ki 67
Ms4a1	membrane-spanning 4-domains, subfamily A, member 1
Mzb1	Marginal Zone B And B1 Cell-Specific Protein
Nuf2	NUF2, NDC80 kinetochore complex component, homolog (S. cerevisiae)
Pax5	paired box gene 5
Pdcd1	programmed cell death 1
Pou2af1	POU domain, class 2, associating factor 1
Ptpn22	protein tyrosine phosphatase, non-receptor type 22 (lymphoid)
Rrad	Ras-related associated with diabetes
Slamf6	SLAM family member 6
Spib	Spi-B transcription factor (Spi-1/PU.1 related)
Stxbp2	syntaxin binding protein 2
Sytl2	synaptotagmin-like 2

Tnfrsf13b	tumor necrosis factor receptor superfamily, member 13b
Trac	T cell receptor alpha constant
Trbc2	T cell receptor beta, constant 2
Zc3h12d	zinc finger CCCH type containing 12D

Appendix III : Top KEGG Pathways deregulated

6.12 Three Month Top KEGG Pathways Deregulated

Term	Number of Genes	% of Genes	P-Value	Benjamini
Alzheimer's disease	40	8.7	0.000000	0.00000
Oxidative phosphorylation	34	7.4	0.000000	0.00000
Parkinson's disease	31	6.7	0.000000	0.00000
Huntington's disease	32	6.9	0.000000	0.00000
Cardiac muscle contraction	18	3.9	0.000000	0.00000
ECM-receptor interaction	17	3.7	0.000000	0.00000
Ribosome	15	3.3	0.000001	0.00002
Focal adhesion	19	4.1	0.000068	0.00110

6.13 Twelve Month Top KEGG Pathways Deregulated

Term	Number of Genes	% of Genes	P-Value	Benjamini
Focal adhesion	115	2.1	0.00000	0.00000
Regulation of actin cytoskeleton	96	1.8	0.00000	0.00002
Insulin signalling pathway	65	1.2	0.00000	0.00012
ECM-receptor interaction	44	0.8	0.00000	0.00013
Chronic myeloid leukemia	41	0.8	0.00000	0.00014
Hypertrophic cardiomyopathy (HCM)	43	0.8	0.00001	0.00037
Pathways in cancer	125	2.3	0.00001	0.00037
Dilated cardiomyopathy	45	0.8	0.00003	0.00072
Ubiquitin mediated proteolysis	60	1.1	0.00006	0.00120
Small cell lung cancer	41	0.8	0.00011	0.00210
Neurotrophin signaling pathway	57	1.1	0.00011	0.00190
Axon guidance	57	1.1	0.00014	0.00230
Endocytosis	81	1.5	0.00014	0.00210
Purine metabolism	65	1.2	0.00026	0.00350
Arrhythmogenic right ventricular cardiomyopathy (ARVC)	36	0.7	0.00035	0.00450
Tight junction	57	1.1	0.00036	0.00440
VEGF signalling pathway	36	0.7	0.00047	0.00540
Acute myeloid leukemia	29	0.5	0.00047	0.00510
MAPK signaling pathway	99	1.8	0.00053	0.00540
Vascular smooth muscle contraction	51	0.9	0.00065	0.00630
Arginine and proline metabolism	27	0.5	0.00077	0.00710
Glioma	31	0.6	0.00082	0.00720
Proteasome	24	0.4	0.00160	0.01300
Adipocytokine signaling pathway	31	0.6	0.00200	0.01600
ErbB signaling pathway	38	0.7	0.00200	0.01600
Prostate cancer	39	0.7	0.00210	0.01600
Renal cell carcinoma	32	0.6	0.00210	0.01500

mTOR signaling pathway	26	0.5	0.00270	0.01900
Non-small cell lung cancer	26	0.5	0.00270	0.01900
Pyruvate metabolism	21	0.4	0.00330	0.02200
Glutathione metabolism	25	0.5	0.00340	0.02200
Aminoacyl-tRNA biosynthesis	21	0.4	0.00470	0.02900
Oocyte meiosis	46	0.9	0.00510	0.03100
Inositol phosphate metabolism	25	0.5	0.00620	0.03600
Colorectal cancer	36	0.7	0.00630	0.03500
Fc gamma R-mediated phagocytosis	40	0.7	0.00630	0.03500
Chemokine signaling pathway	67	1.2	0.00690	0.03700
Pancreatic cancer	31	0.6	0.00740	0.03800
Alanine, aspartate and glutamate metabolism	16	0.3	0.00790	0.04000
Spliceosome	48	0.9	0.00860	0.04200
Wnt signaling pathway	56	1	0.00880	0.04200
Cysteine and methionine metabolism	17	0.3	0.00890	0.04200
Adherens junction	32	0.6	0.00940	0.04300
Leukocyte transendothelial migration	46	0.9	0.01000	0.04600
Lysosome	46	0.9	0.01000	0.04600
Glycolysis / Gluconeogenesis	29	0.5	0.01100	0.04900

6.14 Eighteen Month Top KEGG Pathways Deregulated

Term	Number of Genes	% of genes	P-Value	Benjamini
Focal adhesion	48	2.2	0.00000	0.00033
Hematopoietic cell lineage	25	1.1	0.00003	0.00250
p53 signalling pathway	22	1	0.00003	0.00190
B cell receptor signalling pathway	24	1.1	0.00004	0.00170
Pathways in cancer	64	2.9	0.00004	0.00140
Cell adhesion molecules (CAMs)	37	1.7	0.00004	0.00130
Dilated cardiomyopathy	26	1.2	0.00005	0.00120
Regulation of actin cytoskeleton	46	2.1	0.00011	0.00260
Natural killer cell mediated cytotoxicity	30	1.4	0.00017	0.00350
T cell receptor signalling pathway	29	1.3	0.00023	0.00420
Hypertrophic cardiomyopathy (HCM)	23	1	0.00024	0.00400
Glycolysis / Gluconeogenesis	20	0.9	0.00026	0.00390
Leukocyte transendothelial migration	29	1.3	0.00027	0.00370
Primary immunodeficiency	13	0.6	0.00063	0.00820
Galactose metabolism	11	0.5	0.00069	0.00850
Calcium signalling pathway	39	1.8	0.00089	0.01000
MAPK signalling pathway	50	2.3	0.00098	0.01100
Chemokine signalling pathway	37	1.7	0.00130	0.01400
Amino sugar and nucleotide sugar metabolism	14	0.6	0.00140	0.01300
Prion diseases	12	0.5	0.00180	0.01700
Chronic myeloid leukaemia	19	0.9	0.00300	0.02600
Insulin signalling pathway	29	1.3	0.00300	0.02500

Tight junction	28	1.3	0.00440	0.03500
GnRH signalling pathway	22	1	0.00440	0.03300
Endocytosis	38	1.7	0.00470	0.03400
Glioma	16	0.7	0.00710	0.04900

References

ABEL, A., WALCOTT, J., WOODS, J., DUDA, J. & MERRY, D. E. 2001. Expression of expanded repeat androgen receptor produces neurologic disease in transgenic mice. *Hum Mol Genet,* 10**,** 107-16.

ADACHI, H., KATSUNO, M., MINAMIYAMA, M., SANG, C., PAGOULATOS, G., ANGELIDIS, C., KUSAKABE, M., YOSHIKI, A., KOBAYASHI, Y., DOYU, M. & SOBUE, G. 2003. Heat shock protein 70 chaperone overexpression ameliorates phenotypes of the spinal and bulbar muscular atrophy transgenic mouse model by reducing nuclear-localized mutant androgen receptor protein. *J Neurosci,* 23**,** 2203-11.

ADACHI, H., KATSUNO, M., MINAMIYAMA, M., WAZA, M., SANG, C., NAKAGOMI, Y., KOBAYASHI, Y., TANAKA, F., DOYU, M., INUKAI, A., YOSHIDA, M., HASHIZUME, Y. & SOBUE, G. 2005. Widespread nuclear and cytoplasmic accumulation of mutant androgen receptor in SBMA patients. *Brain,* 128**,** 659-70.

ADACHI, H., KUME, A., LI, M., NAKAGOMI, Y., NIWA, H., DO, J., SANG, C., KOBAYASHI, Y., DOYU, M. & SOBUE, G. 2001. Transgenic mice with an expanded CAG repeat controlled by the human AR promoter show polyglutamine nuclear inclusions and neuronal dysfunction without neuronal cell death. *Hum Mol Genet,* 10**,** 1039-48.

ALUR, M., NGUYEN, M. M., EGGENER, S. E., JIANG, F., DADRAS, S. S., STERN, J., KIMM, S., ROEHL, K., KOZLOWSKI, J., PINS, M., MICHALAK, M., DHIR, R. & WANG, Z. 2009. Suppressive roles of calreticulin in prostate cancer growth and metastasis. *Am J Pathol,* 175**,** 882-90.

ARAI, T. 2014. Significance and limitation of the pathological classification of TDP-43 proteinopathy. *Neuropathology,* 34**,** 578-88.

ARAKI, K., NAKANISHI, H., NAKAMURA, T., ATSUTA, N., YAMADA, S., HIJIKATA, Y., HASHIZUME, A., SUZUKI, K., KATSUNO, M. & SOBUE, G. 2015. Myotonia-like symptoms in a patient with spinal and bulbar muscular atrophy. *Neuromuscul Disord*.

ARBER, S., HAN, B., MENDELSOHN, M., SMITH, M., JESSELL, T. M. & SOCKANATHAN, S. 1999. Requirement for the homeobox gene Hb9 in the consolidation of motor neuron identity. *Neuron,* 23**,** 659-74.

ATKIN, J. D., SCOTT, R. L., WEST, J. M., LOPES, E., QUAH, A. K. & CHEEMA, S. S. 2005. Properties of slow- and fast-twitch muscle fibres in a mouse model of amyotrophic lateral sclerosis. *Neuromuscul Disord,* 15**,** 377-88.

ATWAL, R. S. & TRUANT, R. 2008. A stress sensitive ER membrane-association domain in Huntingtin protein defines a potential role for Huntingtin in the regulation of autophagy. *Autophagy,* 4**,** 91-3.

BAILEY, C. K., ANDRIOLA, I. F., KAMPINGA, H. H. & MERRY, D. E. 2002. Molecular chaperones enhance the degradation of expanded polyglutamine repeat androgen receptor in a cellular model of spinal and bulbar muscular atrophy. *Hum Mol Genet,* 11**,** 515-23.

BANNO, H., KATSUNO, M., SUZUKI, K., TAKEUCHI, Y., KAWASHIMA, M., SUGA, N., TAKAMORI, M., ITO, M., NAKAMURA, T., MATSUO, K., YAMADA, S., OKI, Y., ADACHI, H., MINAMIYAMA, M., WAZA, M., ATSUTA, N., WATANABE, H., FUJIMOTO, Y., NAKASHIMA, T., TANAKA, F., DOYU, M. & SOBUE, G. 2009. Phase 2 trial of leuprorelin in patients with spinal and bulbar muscular atrophy. *Ann Neurol,* 65**,** 140-50.

BEAUCHEMIN, A. M., GOTTLIEB, B., BEITEL, L. K., ELHAJI, Y. A., PINSKY, L. & TRIFIRO, M. A. 2001. Cytochrome c oxidase subunit Vb interacts with human androgen receptor: a

potential mechanism for neurotoxicity in spinobulbar muscular atrophy. *Brain Res Bull,* 56**,** 285-97.

BEITEL, L. K., ALVARADO, C., MOKHTAR, S., PALIOURAS, M. & TRIFIRO, M. 2013. Mechanisms mediating spinal and bulbar muscular atrophy: investigations into polyglutamine-expanded androgen receptor function and dysfunction. *Front Neurol,* 4**,** 53.

BENTZINGER, C. F., LIN, S., ROMANINO, K., CASTETS, P., GURIDI, M., SUMMERMATTER, S., HANDSCHIN, C., TINTIGNAC, L. A., HALL, M. N. & RUEGG, M. A. 2013. Differential response of skeletal muscles to mTORC1 signaling during atrophy and hypertrophy. *Skelet Muscle,* 3**,** 6.

BERKES, C. A. & TAPSCOTT, S. J. 2005. MyoD and the transcriptional control of myogenesis. *Semin Cell Dev Biol,* 16**,** 585-95.

BERNARD-MARISSAL, N., MOUMEN, A., SUNYACH, C., PELLEGRINO, C., DUDLEY, K., HENDERSON, C. E., RAOUL, C. & PETTMANN, B. 2012. Reduced calreticulin levels link endoplasmic reticulum stress and Fas-triggered cell death in motoneurons vulnerable to ALS. *J Neurosci,* 32**,** 4901-12.

BERNARD-MARISSAL, N., SUNYACH, C., MARISSAL, T., RAOUL, C. & PETTMANN, B. 2014. Calreticulin levels determine onset of early muscle denervation by fast motoneurons of ALS model mice. *Neurobiol Dis*.

BILSLAND, L. G., SAHAI, E., KELLY, G., GOLDING, M., GREENSMITH, L. & SCHIAVO, G. 2010. Deficits in axonal transport precede ALS symptoms in vivo. *Proc Natl Acad Sci U S A,* 107**,** 20523-8.

BINGHAM, P. M., SCOTT, M. O., WANG, S., MCPHAUL, M. J., WILSON, E. M., GARBERN, J. Y., MERRY, D. E. & FISCHBECK, K. H. 1995. Stability of an expanded trinucleotide repeat in the androgen receptor gene in transgenic mice. *Nat Genet,* 9**,** 191-6.

BIONDI, O., BRANCHU, J., BEN SALAH, A., HOUDEBINE, L., BERTIN, L., CHALI, F., DESSEILLE, C., WEILL, L., SANCHEZ, G., LANCELIN, C., AID, S., LOPES, P., PARISET, C., LECOLLE, S., COTE, J., HOLZENBERGER, M., CHANOINE, C., MASSAAD, C. & CHARBONNIER, F. 2015. IGF-1R Reduction Triggers Neuroprotective Signaling Pathways in Spinal Muscular Atrophy Mice. *J Neurosci,* 35**,** 12063-79.

BLAU, H. M., COSGROVE, B. D. & HO, A. T. V. 2015. The central role of muscle stem cells in regenerative failure with aging. *Nat Med,* 21**,** 854-862.

BLOEMBERG, D. & QUADRILATERO, J. 2012. Rapid determination of myosin heavy chain expression in rat, mouse, and human skeletal muscle using multicolor immunofluorescence analysis. *PLoS One,* 7**,** e35273.

BOYCE, M., BRYANT, K. F., JOUSSE, C., LONG, K., HARDING, H. P., SCHEUNER, D., KAUFMAN, R. J., MA, D., COEN, D. M., RON, D. & YUAN, J. 2005. A selective inhibitor of eIF2alpha dephosphorylation protects cells from ER stress. *Science,* 307**,** 935-9.

BRAUBACH, P., ORYNBAYEV, M., ANDRONACHE, Z., HERING, T., LANDWEHRMEYER, G. B., LINDENBERG, K. S. & MELZER, W. 2014. Altered Ca2+ signaling in skeletal muscle fibers of the R6/2 mouse, a model of Huntington's disease. *J Gen Physiol,* 144**,** 393-413.

BROOKS, B. P., PAULSON, H. L., MERRY, D. E., SALAZAR-GRUESO, E. F., BRINKMANN, A. O., WILSON, E. M. & FISCHBECK, K. H. 1997. Characterization of an expanded glutamine repeat androgen receptor in a neuronal cell culture system. *Neurobiol Dis,* 3**,** 313-23.

BROS-FACER, V., KRULL, D., TAYLOR, A., DICK, J. R., BATES, S. A., CLEVELAND, M. S., PRINJHA, R. K. & GREENSMITH, L. 2014. Treatment with an antibody directed against Nogo-A delays disease progression in the SOD1G93A mouse model of Amyotrophic lateral sclerosis. *Hum Mol Genet,* 23**,** 4187-200.

BRUNETEAU, G., BAUCHE, S., GONZALEZ DE AGUILAR, J. L., BROCHIER, G., MANDJEE, N., TANGUY, M. L., HUSSAIN, G., BEHIN, A., KHIAMI, F., SARIALI, E., HELL-REMY, C.,

SALACHAS, F., PRADAT, P. F., LACOMBLEZ, L., NICOLE, S., FONTAINE, B., FARDEAU, M., LOEFFLER, J. P., MEININGER, V., FOURNIER, E., KOENIG, J. & HANTAI, D. 2015. Endplate denervation correlates with Nogo-A muscle expression in amyotrophic lateral sclerosis patients. *Ann Clin Transl Neurol,* 2**,** 362-72.

BRYSON, J. B., HOBBS, C., PARSONS, M. J., BOSCH, K. D., PANDRAUD, A., WALSH, F. S., DOHERTY, P. & GREENSMITH, L. 2012. Amyloid precursor protein (APP) contributes to pathology in the SOD1(G93A) mouse model of amyotrophic lateral sclerosis. *Hum Mol Genet,* 21**,** 3871-82.

BUTLER, R., LEIGH, P. N., MCPHAUL, M. J. & GALLO, J. M. 1998. Truncated forms of the androgen receptor are associated with polyglutamine expansion in X-linked spinal and bulbar muscular atrophy. *Hum Mol Genet,* 7**,** 121-7.

CENTENERA, M. M., HARRIS, J. M., TILLEY, W. D. & BUTLER, L. M. 2008. The contribution of different androgen receptor domains to receptor dimerization and signaling. *Mol Endocrinol,* 22**,** 2373-82.

CHANG, D. W., XING, Z., PAN, Y., ALGECIRAS-SCHIMNICH, A., BARNHART, B. C., YAISH-OHAD, S., PETER, M. E. & YANG, X. 2002. c-FLIP(L) is a dual function regulator for caspase-8 activation and CD95-mediated apoptosis. *EMBO J,* 21**,** 3704-14.

CHEVALIER-LARSEN, E. S. & MERRY, D. E. 2012. Testosterone treatment fails to accelerate disease in a transgenic mouse model of spinal and bulbar muscular atrophy. *Dis Model Mech,* 5**,** 141-5.

CHEVALIER-LARSEN, E. S., O'BRIEN, C. J., WANG, H., JENKINS, S. C., HOLDER, L., LIEBERMAN, A. P. & MERRY, D. E. 2004. Castration restores function and neurofilament alterations of aged symptomatic males in a transgenic mouse model of spinal and bulbar muscular atrophy. *J Neurosci,* 24**,** 4778-86.

CHOMCZYNSKI, P. & SACCHI, N. 1987. Single-step method of RNA isolation by acid guanidinium thiocyanate-phenol-chloroform extraction. *Anal Biochem,* 162**,** 156-9.

CIECHANOVER, A. & KWON, Y. T. 2015. Degradation of misfolded proteins in neurodegenerative diseases: therapeutic targets and strategies. *Exp Mol Med,* 47**,** e147.

COFFEY, K. & ROBSON, C. N. 2012. Regulation of the androgen receptor by post-translational modifications. *J Endocrinol,* 215**,** 221-37.

COHEN, S., NATHAN, J. A. & GOLDBERG, A. L. 2015. Muscle wasting in disease: molecular mechanisms and promising therapies. *Nat Rev Drug Discov,* 14**,** 58-74.

CORTES, C. J. & LA SPADA, A. R. 2015. Autophagy in polyglutamine disease: Imposing order on disorder or contributing to the chaos? *Mol Cell Neurosci,* 66**,** 53-61.

CORTES, C. J., LING, S. C., GUO, L. T., HUNG, G., TSUNEMI, T., LY, L., TOKUNAGA, S., LOPEZ, E., SOPHER, B. L., BENNETT, C. F., SHELTON, G. D., CLEVELAND, D. W. & LA SPADA, A. R. 2014a. Muscle expression of mutant androgen receptor accounts for systemic and motor neuron disease phenotypes in spinal and bulbar muscular atrophy. *Neuron,* 82**,** 295-307.

CORTES, C. J., MIRANDA, H. C., FRANKOWSKI, H., BATLEVI, Y., YOUNG, J. E., LE, A., IVANOV, N., SOPHER, B. L., CARROMEU, C., MUOTRI, A. R., GARDEN, G. A. & LA SPADA, A. R. 2014b. Polyglutamine-expanded androgen receptor interferes with TFEB to elicit autophagy defects in SBMA. *Nat Neurosci,* 17**,** 1180-9.

DADON-NACHUM, M., MELAMED, E. & OFFEN, D. 2011. The "dying-back" phenomenon of motor neurons in ALS. *J Mol Neurosci,* 43**,** 470-7.

DE BRUYN, M., WIERSMA, V. R., HELFRICH, W., EGGLETON, P. & BREMER, E. 2015. The ever-expanding immunomodulatory role of calreticulin in cancer immunity. *Front Oncol,* 5**,** 35.

DEDHAR, S., RENNIE, P. S., SHAGO, M., HAGESTEIJN, C. Y., YANG, H., FILMUS, J., HAWLEY, R. G., BRUCHOVSKY, N., CHENG, H., MATUSIK, R. J. & ET AL. 1994. Inhibition of nuclear hormone receptor activity by calreticulin. *Nature,* 367**,** 480-3.

DING, H., HONG, C., WANG, Y., LIU, J., ZHANG, N., SHEN, C., WEI, W. & ZHENG, F. 2014. Calreticulin promotes angiogenesis via activating nitric oxide signalling pathway in rheumatoid arthritis. *Clin Exp Immunol,* 178**,** 236-44.

DING, Y., ADACHI, H., KATSUNO, M., HUANG, Z., JIANG, Y. M., KONDO, N., IIDA, M., TOHNAI, G., NAKATSUJI, H., FUNAKOSHI, H., NAKAMURA, T. & SOBUE, G. 2015. Overexpression of hepatocyte growth factor in SBMA model mice has an additive effect on combination therapy with castration. *Biochem Biophys Res Commun*.

DOYLE, K. M., KENNEDY, D., GORMAN, A. M., GUPTA, S., HEALY, S. J. & SAMALI, A. 2011. Unfolded proteins and endoplasmic reticulum stress in neurodegenerative disorders. *J Cell Mol Med,* 15**,** 2025-39.

DUBOWITZ, V. 1985. *Muscle Biopsy: A practical Approach,* London, Bailliere Tindall.

DUENNWALD, M. L. & LINDQUIST, S. 2008. Impaired ERAD and ER stress are early and specific events in polyglutamine toxicity. *Genes Dev,* 22**,** 3308-19.

DUFF, J., DAVIES, P., WATT, K. & MCEWAN, I. J. 2006. Structural dynamics of the human androgen receptor: implications for prostate cancer and neurodegenerative disease. *Biochem Soc Trans,* 34**,** 1098-102.

DUPLAN, L., BERNARD, N., CASSERON, W., DUDLEY, K., THOUVENOT, E., HONNORAT, J., ROGEMOND, V., DE BOVIS, B., AEBISCHER, P., MARIN, P., RAOUL, C., HENDERSON, C. E. & PETTMANN, B. 2010. Collapsin response mediator protein 4a (CRMP4a) is upregulated in motoneurons of mutant SOD1 mice and can trigger motoneuron axonal degeneration and cell death. *J Neurosci,* 30**,** 785-96.

ENDRES, K. & REINHARDT, S. 2013. ER-stress in Alzheimer's disease: turning the scale? *Am J Neurodegener Dis,* 2**,** 247-65.

ESTEVEZ, A. G., CROW, J. P., SAMPSON, J. B., REITER, C., ZHUANG, Y., RICHARDSON, G. J., TARPEY, M. M., BARBEITO, L. & BECKMAN, J. S. 1999a. Induction of nitric oxide-dependent apoptosis in motor neurons by zinc-deficient superoxide dismutase. *Science,* 286**,** 2498-500.

ESTEVEZ, A. G., SPEAR, N., PELLUFFO, H., KAMAID, A., BARBEITO, L. & BECKMAN, J. S. 1999b. Examining apoptosis in cultured cells after exposure to nitric oxide and peroxynitrite. *Methods Enzymol,* 301**,** 393-402.

FARGO, K. N., GALBIATI, M., FOECKING, E. M., POLETTI, A. & JONES, K. J. 2008. Androgen regulation of axon growth and neurite extension in motoneurons. *Horm Behav,* 53**,** 716-28.

FERNANDES, H. B., BAIMBRIDGE, K. G., CHURCH, J., HAYDEN, M. R. & RAYMOND, L. A. 2007. Mitochondrial sensitivity and altered calcium handling underlie enhanced NMDA-induced apoptosis in YAC128 model of Huntington's disease. *J Neurosci,* 27**,** 13614-23.

FERNANDEZ-RHODES, L. E., KOKKINIS, A. D., WHITE, M. J., WATTS, C. A., AUH, S., JEFFRIES, N. O., SHRADER, J. A., LEHKY, T. J., LI, L., RYDER, J. E., LEVY, E. W., SOLOMON, B. I., HARRIS-LOVE, M. O., LA PEAN, A., SCHINDLER, A. B., CHEN, C., DI PROSPERO, N. A. & FISCHBECK, K. H. 2011. Efficacy and safety of dutasteride in patients with spinal and bulbar muscular atrophy: a randomised placebo-controlled trial. *Lancet Neurol,* 10**,** 140-7.

FINSTERER, J., MISHRA, A., WAKIL, S., PENNUTO, M. & SORARU, G. 2015. Mitochondrial implications in bulbospinal muscular atrophy (Kennedy disease). *Amyotroph Lateral Scler Frontotemporal Degener***,** 1-7.

FINSTERER, J. & SORARU, G. 2015. Onset Manifestations of Spinal and Bulbar Muscular Atrophy (Kennedy's Disease). *J Mol Neurosci*.

FISCHER, L. R., CULVER, D. G., TENNANT, P., DAVIS, A. A., WANG, M., CASTELLANO-SANCHEZ, A., KHAN, J., POLAK, M. A. & GLASS, J. D. 2004. Amyotrophic lateral sclerosis is a distal axonopathy: evidence in mice and man. *Exp Neurol,* 185**,** 232-40.

FLIEGEL, L., BURNS, K., MACLENNAN, D. H., REITHMEIER, R. A. & MICHALAK, M. 1989. Molecular cloning of the high affinity calcium-binding protein (calreticulin) of skeletal muscle sarcoplasmic reticulum. *J Biol Chem,* 264**,** 21522-8.

FRATTA, P., COLLINS, T., PEMBLE, S., NETHISINGHE, S., DEVOY, A., GIUNTI, P., SWEENEY, M. G., HANNA, M. G. & FISHER, E. M. 2014a. Sequencing analysis of the spinal bulbar muscular atrophy CAG expansion reveals absence of repeat interruptions. *Neurobiol Aging,* 35**,** 443 e1-3.

FRATTA, P., NIRMALANANTHAN, N., MASSET, L., SKORUPINSKA, I., COLLINS, T., CORTESE, A., PEMBLE, S., MALASPINA, A., FISHER, E. M., GREENSMITH, L. & HANNA, M. G. 2014b. Correlation of clinical and molecular features in spinal bulbar muscular atrophy. *Neurology,* 82**,** 2077-84.

FUENTEALBA, R. A., UDAN, M., BELL, S., WEGORZEWSKA, I., SHAO, J., DIAMOND, M. I., WEIHL, C. C. & BALOH, R. H. 2010. Interaction with polyglutamine aggregates reveals a Q/N-rich domain in TDP-43. *J Biol Chem,* 285**,** 26304-14.

GALBIATI, M., ONESTO, E., ZITO, A., CRIPPA, V., RUSMINI, P., MARIOTTI, R., BENTIVOGLIO, M., BENDOTTI, C. & POLETTI, A. 2012. The anabolic/androgenic steroid nandrolone exacerbates gene expression modifications induced by mutant SOD1 in muscles of mice models of amyotrophic lateral sclerosis. *Pharmacol Res,* 65**,** 221-30.

GIORGETTI, E. & LIEBERMAN, A. P. 2016. Polyglutamine androgen receptor-mediated neuromuscular disease. *Cell Mol Life Sci*.

GOLD, L. I., EGGLETON, P., SWEETWYNE, M. T., VAN DUYN, L. B., GREIVES, M. R., NAYLOR, S. M., MICHALAK, M. & MURPHY-ULLRICH, J. E. 2010. Calreticulin: non-endoplasmic reticulum functions in physiology and disease. *FASEB J,* 24**,** 665-83.

GOLD, L. I., RAHMAN, M., BLECHMAN, K. M., GREIVES, M. R., CHURGIN, S., MICHAELS, J., CALLAGHAN, M. J., CARDWELL, N. L., POLLINS, A. C., MICHALAK, M., SIEBERT, J. W., LEVINE, J. P., GURTNER, G. C., NANNEY, L. B., GALIANO, R. D. & CADACIO, C. L. 2006. Overview of the role for calreticulin in the enhancement of wound healing through multiple biological effects. *J Investig Dermatol Symp Proc,* 11**,** 57-65.

GOLDENBERG, J. N. & BRADLEY, W. G. 1996. Testosterone therapy and the pathogenesis of Kennedy's disease (X-linked bulbospinal muscular atrophy). *J Neurol Sci,* 135**,** 158-61.

GRUNSEICH, C., KATS, I. R., BOTT, L. C., RINALDI, C., KOKKINIS, A., FOX, D., CHEN, K. L., SCHINDLER, A. B., MANKODI, A. K., SHRADER, J. A., SCHWARTZ, D. P., LEHKY, T. J., LIU, C. Y. & FISCHBECK, K. H. 2014a. Early onset and novel features in a spinal and bulbar muscular atrophy patient with a 68 CAG repeat. *Neuromuscul Disord,* 24**,** 978-81.

GRUNSEICH, C., ZUKOSKY, K., KATS, I. R., GHOSH, L., HARMISON, G. G., BOTT, L. C., RINALDI, C., CHEN, K. L., CHEN, G., BOEHM, M. & FISCHBECK, K. H. 2014b. Stem cell-derived motor neurons from spinal and bulbar muscular atrophy patients. *Neurobiol Dis,* 70**,** 12-20.

HALIEVSKI, K., HENLEY, C. L., DOMINO, L., POORT, J. E., FU, M., KATSUNO, M., ADACHI, H., SOBUE, G., BREEDLOVE, S. M. & JORDAN, C. L. 2015a. Androgen-dependent loss of muscle BDNF mRNA in two mouse models of SBMA. *Exp Neurol*.

HALIEVSKI, K., MO, K., WESTWOOD, J. T. & MONKS, D. A. 2015b. Transcriptional profile of muscle following acute induction of symptoms in a mouse model of Kennedy's disease/spinobulbar muscular atrophy. *PLoS One,* 10**,** e0118120.

HARDING, A. E., THOMAS, P. K., BARAITSER, M., BRADBURY, P. G., MORGAN-HUGHES, J. A. & PONSFORD, J. R. 1982. X-linked recessive bulbospinal neuronopathy: a report of ten cases. *J Neurol Neurosurg Psychiatry,* 45**,** 1012-9.

HASHIZUME, A., KATSUNO, M., SUZUKI, K., BANNO, H., SUGA, N., MANO, T., ARAKI, A., HIJIKATA, Y., GRUNSEICH, C., KOKKINIS, A., HIRAKAWA, A., WATANABE, H., YAMAMOTO, M., FISCHBECK, K. H. & SOBUE, G. 2015. A functional scale for spinal

and bulbar muscular atrophy: Cross-sectional and longitudinal study. *Neuromuscul Disord*.

HAZE, K., YOSHIDA, H., YANAGI, H., YURA, T. & MORI, K. 1999. Mammalian transcription factor ATF6 is synthesized as a transmembrane protein and activated by proteolysis in response to endoplasmic reticulum stress. *Mol Biol Cell,* 10**,** 3787-99.

HEINE, E. M., BERGER, T. R., PLUCIENNIK, A., ORR, C. R., ZBORAY, L. & MERRY, D. E. 2015. Proteasome-mediated proteolysis of the polyglutamine-expanded androgen receptor is a late event in spinal and bulbar muscular atrophy (SBMA) pathogenesis. *J Biol Chem,* 290**,** 12572-84.

HEINLEIN, C. A. & CHANG, C. 2002. The roles of androgen receptors and androgen-binding proteins in nongenomic androgen actions. *Mol Endocrinol,* 16**,** 2181-7.

HETZ, C. 2012. The unfolded protein response: controlling cell fate decisions under ER stress and beyond. *Nat Rev Mol Cell Biol,* 13**,** 89-102.

HETZ, C. & MOLLEREAU, B. 2014. Disturbance of endoplasmic reticulum proteostasis in neurodegenerative diseases. *Nat Rev Neurosci,* 15**,** 233-49.

HOLASKA, J. M., BLACK, B. E., LOVE, D. C., HANOVER, J. A., LESZYK, J. & PASCHAL, B. M. 2001. Calreticulin Is a receptor for nuclear export. *J Cell Biol,* 152**,** 127-40.

HOLASKA, J. M., BLACK, B. E., RASTINEJAD, F. & PASCHAL, B. M. 2002. Ca2+-dependent nuclear export mediated by calreticulin. *Mol Cell Biol,* 22**,** 6286-97.

HONG, M., LUO, S., BAUMEISTER, P., HUANG, J. M., GOGIA, R. K., LI, M. & LEE, A. S. 2004. Underglycosylation of ATF6 as a novel sensing mechanism for activation of the unfolded protein response. *J Biol Chem,* 279**,** 11354-63.

HUANG DA, W., SHERMAN, B. T. & LEMPICKI, R. A. 2009a. Bioinformatics enrichment tools: paths toward the comprehensive functional analysis of large gene lists. *Nucleic Acids Res,* 37**,** 1-13.

HUANG DA, W., SHERMAN, B. T. & LEMPICKI, R. A. 2009b. Systematic and integrative analysis of large gene lists using DAVID bioinformatics resources. *Nat Protoc,* 4**,** 44-57.

HUEN, N. Y., WONG, S. L. & CHAN, H. Y. 2007. Transcriptional malfunctioning of heat shock protein gene expression in spinocerebellar ataxias. *Cerebellum,* 6**,** 111-7.

HUGUENARD, A. L., FERNANDO, S. M., MONKS, D. A. & SENGELAUB, D. R. 2011. Overexpression of androgen receptors in target musculature confers androgen sensitivity to motoneuron dendrites. *Endocrinology,* 152**,** 639-50.

IIDA, M., KATSUNO, M., NAKATSUJI, H., ADACHI, H., KONDO, N., MIYAZAKI, Y., TOHNAI, G., IKENAKA, K., WATANABE, H., YAMAMOTO, M., KISHIDA, K. & SOBUE, G. 2014. Pioglitazone suppresses neuronal and muscular degeneration caused by polyglutamine-expanded androgen receptors. *Hum Mol Genet*.

JIANG, Y., DEY, S. & MATSUNAMI, H. 2014. Calreticulin: roles in cell-surface protein expression. *Membranes (Basel),* 4**,** 630-41.

JOHANSEN, J. A., YU, Z., MO, K., MONKS, D. A., LIEBERMAN, A. P., BREEDLOVE, S. M. & JORDAN, C. L. 2009. Recovery of function in a myogenic mouse model of spinal bulbar muscular atrophy. *Neurobiol Dis,* 34**,** 113-20.

JOHN, L. M., LECHLEITER, J. D. & CAMACHO, P. 1998. Differential modulation of SERCA2 isoforms by calreticulin. *J Cell Biol,* 142**,** 963-73.

JOHNSON, R. J., PYUN, H. Y., LYTTON, J. & FINE, R. E. 1993. Differences in the subcellular localization of calreticulin and organellar Ca(2+)-ATPase in neurons. *Brain Res Mol Brain Res,* 17**,** 9-16.

JOKIC, N., GONZALEZ DE AGUILAR, J. L., DIMOU, L., LIN, S., FERGANI, A., RUEGG, M. A., SCHWAB, M. E., DUPUIS, L. & LOEFFLER, J. P. 2006. The neurite outgrowth inhibitor Nogo-A promotes denervation in an amyotrophic lateral sclerosis model. *EMBO Rep,* 7**,** 1162-7.

JORDAN, C. L. & LIEBERMAN, A. P. 2008. Spinal and bulbar muscular atrophy: a motoneuron or muscle disease? *Curr Opin Pharmacol,* 8**,** 752-8.

KALMAR, B. & GREENSMITH, L. 2009. Activation of the heat shock response in a primary cellular model of motoneuron neurodegeneration-evidence for neuroprotective and neurotoxic effects. *Cell Mol Biol Lett,* 14**,** 319-35.

KATSUNO, M., ADACHI, H., DOYU, M., MINAMIYAMA, M., SANG, C., KOBAYASHI, Y., INUKAI, A. & SOBUE, G. 2003. Leuprorelin rescues polyglutamine-dependent phenotypes in a transgenic mouse model of spinal and bulbar muscular atrophy. *Nat Med,* 9**,** 768-73.

KATSUNO, M., ADACHI, H., KUME, A., LI, M., NAKAGOMI, Y., NIWA, H., SANG, C., KOBAYASHI, Y., DOYU, M. & SOBUE, G. 2002. Testosterone reduction prevents phenotypic expression in a transgenic mouse model of spinal and bulbar muscular atrophy. *Neuron,* 35**,** 843-54.

KATSUNO, M., ADACHI, H., MINAMIYAMA, M., WAZA, M., TOKUI, K., BANNO, H., SUZUKI, K., ONODA, Y., TANAKA, F., DOYU, M. & SOBUE, G. 2006a. Reversible disruption of dynactin 1-mediated retrograde axonal transport in polyglutamine-induced motor neuron degeneration. *J Neurosci,* 26**,** 12106-17.

KATSUNO, M., ADACHI, H., WAZA, M., BANNO, H., SUZUKI, K., TANAKA, F., DOYU, M. & SOBUE, G. 2006b. Pathogenesis, animal models and therapeutics in spinal and bulbar muscular atrophy (SBMA). *Exp Neurol,* 200**,** 8-18.

KATSUNO, M., SANG, C., ADACHI, H., MINAMIYAMA, M., WAZA, M., TANAKA, F., DOYU, M. & SOBUE, G. 2005. Pharmacological induction of heat-shock proteins alleviates polyglutamine-mediated motor neuron disease. *Proc Natl Acad Sci U S A,* 102**,** 16801-6.

KEMP, M. Q., POORT, J. L., BAQRI, R. M., LIEBERMAN, A. P., BREEDLOVE, S. M., MILLER, K. E. & JORDAN, C. L. 2011. Impaired motoneuronal retrograde transport in two models of SBMA implicates two sites of androgen action. *Hum Mol Genet,* 20**,** 4475-90.

KENNEDY, W. R., ALTER, M. & SUNG, J. H. 1968. Progressive proximal spinal and bulbar muscular atrophy of late onset. A sex-linked recessive trait. *Neurology,* 18**,** 671-80.

KIERAN, D., HAFEZPARAST, M., BOHNERT, S., DICK, J. R., MARTIN, J., SCHIAVO, G., FISHER, E. M. & GREENSMITH, L. 2005. A mutation in dynein rescues axonal transport defects and extends the life span of ALS mice. *J Cell Biol,* 169**,** 561-7.

KINIRONS, P. & ROULEAU, G. A. 2008. Administration of testosterone results in reversible deterioration in Kennedy's disease. *J Neurol Neurosurg Psychiatry,* 79**,** 106-7.

KOBAYASHI, Y., KUME, A., LI, M., DOYU, M., HATA, M., OHTSUKA, K. & SOBUE, G. 2000. Chaperones Hsp70 and Hsp40 suppress aggregate formation and apoptosis in cultured neuronal cells expressing truncated androgen receptor protein with expanded polyglutamine tract. *J Biol Chem,* 275**,** 8772-8.

KONDO, N., KATSUNO, M., ADACHI, H., MINAMIYAMA, M., DOI, H., MATSUMOTO, S., MIYAZAKI, Y., IIDA, M., TOHNAI, G., NAKATSUJI, H., ISHIGAKI, S., FUJIOKA, Y., WATANABE, H., TANAKA, F., NAKAI, A. & SOBUE, G. 2013. Heat shock factor-1 influences pathological lesion distribution of polyglutamine-induced neurodegeneration. *Nat Commun,* 4**,** 1405.

KOUROKU, Y., FUJITA, E., JIMBO, A., KIKUCHI, T., YAMAGATA, T., MOMOI, M. Y., KOMINAMI, E., KUIDA, K., SAKAMAKI, K., YONEHARA, S. & MOMOI, T. 2002. Polyglutamine aggregates stimulate ER stress signals and caspase-12 activation. *Hum Mol Genet,* 11**,** 1505-15.

KOUROKU, Y., FUJITA, E., TANIDA, I., UENO, T., ISOAI, A., KUMAGAI, H., OGAWA, S., KAUFMAN, R. J., KOMINAMI, E. & MOMOI, T. 2007. ER stress (PERK/eIF2alpha phosphorylation) mediates the polyglutamine-induced LC3 conversion, an essential step for autophagy formation. *Cell Death Differ,* 14**,** 230-9.

LA SPADA, A. R., PETERSON, K. R., MEADOWS, S. A., MCCLAIN, M. E., JENG, G., CHMELAR, R. S., HAUGEN, H. A., CHEN, K., SINGER, M. J., MOORE, D., TRASK, B. J., FISCHBECK, K. H., CLEGG, C. H. & MCKNIGHT, G. S. 1998. Androgen receptor YAC transgenic mice carrying CAG 45 alleles show trinucleotide repeat instability. *Hum Mol Genet,* 7**,** 959-67.

LA SPADA, A. R. & TAYLOR, J. P. 2010. Repeat expansion disease: progress and puzzles in disease pathogenesis. *Nat Rev Genet,* 11**,** 247-58.

LA SPADA, A. R., WILSON, E. M., LUBAHN, D. B., HARDING, A. E. & FISCHBECK, K. H. 1991. Androgen receptor gene mutations in X-linked spinal and bulbar muscular atrophy. *Nature,* 352**,** 77-9.

LI, M., CHEVALIER-LARSEN, E. S., MERRY, D. E. & DIAMOND, M. I. 2007. Soluble androgen receptor oligomers underlie pathology in a mouse model of spinobulbar muscular atrophy. *J Biol Chem,* 282**,** 3157-64.

LI, M., MIWA, S., KOBAYASHI, Y., MERRY, D. E., YAMAMOTO, M., TANAKA, F., DOYU, M., HASHIZUME, Y., FISCHBECK, K. H. & SOBUE, G. 1998a. Nuclear inclusions of the androgen receptor protein in spinal and bulbar muscular atrophy. *Ann Neurol,* 44**,** 249-54.

LI, M., NAKAGOMI, Y., KOBAYASHI, Y., MERRY, D. E., TANAKA, F., DOYU, M., MITSUMA, T., HASHIZUME, Y., FISCHBECK, K. H. & SOBUE, G. 1998b. Nonneural nuclear inclusions of androgen receptor protein in spinal and bulbar muscular atrophy. *Am J Pathol,* 153**,** 695-701.

LIEBERMAN, A. P., YU, Z., MURRAY, S., PERALTA, R., LOW, A., GUO, S., YU, X. X., CORTES, C. J., BENNETT, C. F., MONIA, B. P., LA SPADA, A. R. & HUNG, G. 2014. Peripheral androgen receptor gene suppression rescues disease in mouse models of spinal and bulbar muscular atrophy. *Cell Rep,* 7**,** 774-84.

LIN, Q., CAO, Y. & GAO, J. 2014. Serum calreticulin is a negative biomarker in patients with Alzheimer's disease. *Int J Mol Sci,* 15**,** 21740-53.

LU, J., VAN DER STEEN, T. & TINDALL, D. J. 2015a. Are androgen receptor variants a substitute for the full-length receptor? *Nat Rev Urol,* 12**,** 137-44.

LU, Y. C., WENG, W. C. & LEE, H. 2015b. Functional Roles of Calreticulin in Cancer Biology. *Biomed Res Int,* 2015**,** 526524.

LYNCH, J. M., CHILIBECK, K., QUI, Y. & MICHALAK, M. 2006. Assembling pieces of the cardiac puzzle; calreticulin and calcium-dependent pathways in cardiac development, health, and disease. *Trends Cardiovasc Med,* 16**,** 65-9.

MACHADO, P. M., AHMED, M., BRADY, S., GANG, Q., HEALY, E., MORROW, J. M., WALLACE, A. C., DEWAR, L., RAMDHARRY, G., PARTON, M., HOLTON, J. L., HOULDEN, H., GREENSMITH, L. & HANNA, M. G. 2014. Ongoing developments in sporadic inclusion body myositis. *Curr Rheumatol Rep,* 16**,** 477.

MACPHERSON, P. C., WANG, X. & GOLDMAN, D. 2011. Myogenin regulates denervation-dependent muscle atrophy in mouse soleus muscle. *J Cell Biochem,* 112**,** 2149-59.

MALENA, A., PENNUTO, M., TEZZE, C., QUERIN, G., D'ASCENZO, C., SILANI, V., CENACCHI, G., SCARAMOZZA, A., ROMITO, S., MORANDI, L., PEGORARO, E., RUSSELL, A. P., SORARU, G. & VERGANI, L. 2013. Androgen-dependent impairment of myogenesis in spinal and bulbar muscular atrophy. *Acta Neuropathol,* 126**,** 109-21.

MALIK, B., NIRMALANANTHAN, N., BILSLAND, L. G., LA SPADA, A. R., HANNA, M. G., SCHIAVO, G., GALLO, J. M. & GREENSMITH, L. 2011. Absence of disturbed axonal transport in spinal and bulbar muscular atrophy. *Hum Mol Genet,* 20**,** 1776-86.

MALIK, B., NIRMALANANTHAN, N., GRAY, A. L., LA SPADA, A. R., HANNA, M. G. & GREENSMITH, L. 2013. Co-induction of the heat shock response ameliorates disease progression in a mouse model of human spinal and bulbar muscular atrophy: implications for therapy. *Brain,* 136**,** 926-43.

MARRON, T. U., GUERINI, V., RUSMINI, P., SAU, D., BREVINI, T. A., MARTINI, L. & POLETTI, A. 2005. Androgen-induced neurite outgrowth is mediated by neuritin in motor neurones. *J Neurochem,* 92**,** 10-20.

MARTINEZ, J. A., ZHANG, Z., SVETLOV, S. I., HAYES, R. L., WANG, K. K. & LARNER, S. F. 2010. Calpain and caspase processing of caspase-12 contribute to the ER stress-induced cell death pathway in differentiated PC12 cells. *Apoptosis,* 15**,** 1480-93.

MEININGER, V., PRADAT, P. F., CORSE, A., AL-SARRAJ, S., RIX BROOKS, B., CARESS, J. B., CUDKOWICZ, M., KOLB, S. J., LANGE, D., LEIGH, P. N., MEYER, T., MILLERI, S., MORRISON, K. E., ORRELL, R. W., PETERS, G., ROTHSTEIN, J. D., SHEFNER, J., LAVROV, A., WILLIAMS, N., OVEREND, P., PRICE, J., BATES, S., BULLMAN, J., KRULL, D., BERGES, A., ABILA, B., MENO-TETANG, G. & WURTHNER, J. 2014. Safety, pharmacokinetic, and functional effects of the nogo-a monoclonal antibody in amyotrophic lateral sclerosis: a randomized, first-in-human clinical trial. *PLoS One,* 9**,** e97803.

MENZIES, F. M., FLEMING, A. & RUBINSZTEIN, D. C. 2015. Compromised autophagy and neurodegenerative diseases. *Nat Rev Neurosci,* 16**,** 345-57.

MERRY, D. E., KOBAYASHI, Y., BAILEY, C. K., TAYE, A. A. & FISCHBECK, K. H. 1998. Cleavage, aggregation and toxicity of the expanded androgen receptor in spinal and bulbar muscular atrophy. *Hum Mol Genet,* 7**,** 693-701.

MICHALAK, M., CORBETT, E. F., MESAELI, N., NAKAMURA, K. & OPAS, M. 1999. Calreticulin: one protein, one gene, many functions. *Biochem J,* 344 Pt 2**,** 281-92.

MICHALAK, M., GROENENDYK, J., SZABO, E., GOLD, L. I. & OPAS, M. 2009. Calreticulin, a multi-process calcium-buffering chaperone of the endoplasmic reticulum. *Biochem J,* 417**,** 651-66.

MICHALIK, A. & VAN BROECKHOVEN, C. 2003. Pathogenesis of polyglutamine disorders: aggregation revisited. *Hum Mol Genet,* 12 Spec No 2**,** R173-86.

MIELCAREK, M., TOCZEK, M., SMEETS, C. J., FRANKLIN, S. A., BONDULICH, M. K., JOLINON, N., MULLER, T., AHMED, M., DICK, J. R., PIOTROWSKA, I., GREENSMITH, L., SMOLENSKI, R. T. & BATES, G. P. 2015. HDAC4-myogenin axis as an important marker of HD-related skeletal muscle atrophy. *PLoS Genet,* 11**,** e1005021.

MINAMIYAMA, M., KATSUNO, M., ADACHI, H., WAZA, M., SANG, C., KOBAYASHI, Y., TANAKA, F., DOYU, M., INUKAI, A. & SOBUE, G. 2004. Sodium butyrate ameliorates phenotypic expression in a transgenic mouse model of spinal and bulbar muscular atrophy. *Hum Mol Genet,* 13**,** 1183-92.

MO, K., RAZAK, Z., RAO, P., YU, Z., ADACHI, H., KATSUNO, M., SOBUE, G., LIEBERMAN, A. P., WESTWOOD, J. T. & MONKS, D. A. 2010. Microarray analysis of gene expression by skeletal muscle of three mouse models of Kennedy disease/spinal bulbar muscular atrophy. *PLoS One,* 5**,** e12922.

MOLINARI, M., ERIKSSON, K. K., CALANCA, V., GALLI, C., CRESSWELL, P., MICHALAK, M. & HELENIUS, A. 2004. Contrasting functions of calreticulin and calnexin in glycoprotein folding and ER quality control. *Mol Cell,* 13**,** 125-35.

MONKS, D. A., JOHANSEN, J. A., MO, K., RAO, P., EAGLESON, B., YU, Z., LIEBERMAN, A. P., BREEDLOVE, S. M. & JORDAN, C. L. 2007. Overexpression of wild-type androgen receptor in muscle recapitulates polyglutamine disease. *Proc Natl Acad Sci U S A,* 104**,** 18259-64.

MONTAGUE, K., MALIK, B., GRAY, A. L., LA SPADA, A. R., HANNA, M. G., SZABADKAI, G. & GREENSMITH, L. 2014. Endoplasmic reticulum stress in spinal and bulbar muscular atrophy: a potential target for therapy. *Brain,* 137**,** 1894-906.

MORENO, J. A., HALLIDAY, M., MOLLOY, C., RADFORD, H., VERITY, N., AXTEN, J. M., ORTORI, C. A., WILLIS, A. E., FISCHER, P. M., BARRETT, D. A. & MALLUCCI, G. R. 2013. Oral treatment targeting the unfolded protein response prevents neurodegeneration and clinical disease in prion-infected mice. *Sci Transl Med,* 5**,** 206ra138.

MORENO, J. A., RADFORD, H., PERETTI, D., STEINERT, J. R., VERITY, N., MARTIN, M. G., HALLIDAY, M., MORGAN, J., DINSDALE, D., ORTORI, C. A., BARRETT, D. A., TSAYTLER, P., BERTOLOTTI, A., WILLIS, A. E., BUSHELL, M. & MALLUCCI, G. R. 2012. Sustained translational repression by eIF2alpha-P mediates prion neurodegeneration. *Nature,* 485**,** 507-11.

MULLER, D., CHERUKURI, P., HENNINGFELD, K., POH, C. H., WITTLER, L., GROTE, P., SCHLUTER, O., SCHMIDT, J., LABORDA, J., BAUER, S. R., BROWNSTONE, R. M. & MARQUARDT, T. 2014. Dlk1 promotes a fast motor neuron biophysical signature required for peak force execution. *Science,* 343**,** 1264-6.

MUSARO, A., MCCULLAGH, K., PAUL, A., HOUGHTON, L., DOBROWOLNY, G., MOLINARO, M., BARTON, E. R., SWEENEY, H. L. & ROSENTHAL, N. 2001. Localized Igf-1 transgene expression sustains hypertrophy and regeneration in senescent skeletal muscle. *Nat Genet,* 27**,** 195-200.

NAKAGAWA, T. & YUAN, J. 2000. Cross-talk between two cysteine protease families. Activation of caspase-12 by calpain in apoptosis. *J Cell Biol,* 150**,** 887-94.

NAKAGAWA, T., ZHU, H., MORISHIMA, N., LI, E., XU, J., YANKNER, B. A. & YUAN, J. 2000. Caspase-12 mediates endoplasmic-reticulum-specific apoptosis and cytotoxicity by amyloid-beta. *Nature,* 403**,** 98-103.

NAKAMURA, K., BOSSY-WETZEL, E., BURNS, K., FADEL, M. P., LOZYK, M., GOPING, I. S., OPAS, M., BLEACKLEY, R. C., GREEN, D. R. & MICHALAK, M. 2000. Changes in endoplasmic reticulum luminal environment affect cell sensitivity to apoptosis. *J Cell Biol,* 150**,** 731-40.

NGUYEN, M. M., DINCER, Z., WADE, J. R., ALUR, M., MICHALAK, M., DEFRANCO, D. B. & WANG, Z. 2009. Cytoplasmic localization of the androgen receptor is independent of calreticulin. *Mol Cell Endocrinol,* 302**,** 65-72.

NIHEI, Y., ITO, D., OKADA, Y., AKAMATSU, W., YAGI, T., YOSHIZAKI, T., OKANO, H. & SUZUKI, N. 2013. Enhanced aggregation of androgen receptor in induced pluripotent stem cell-derived neurons from spinal and bulbar muscular atrophy. *J Biol Chem,* 288**,** 8043-52.

NISHITOH, H., MATSUZAWA, A., TOBIUME, K., SAEGUSA, K., TAKEDA, K., INOUE, K., HORI, S., KAKIZUKA, A. & ICHIJO, H. 2002. ASK1 is essential for endoplasmic reticulum stress-induced neuronal cell death triggered by expanded polyglutamine repeats. *Genes Dev,* 16**,** 1345-55.

OKI, K., HALIEVSKI, K., VICENTE, L., XU, Y., ZEOLLA, D., POORT, J., KATSUNO, M., ADACHI, H., SOBUE, G., WISEMAN, R. W., BREEDLOVE, S. M. & JORDAN, C. L. 2015. Contractile dysfunction in muscle may underlie androgen-dependent motor dysfunction in SBMA. *J Appl Physiol (1985)***,** jap 00886 2014.

OKI, K., WISEMAN, R. W., BREEDLOVE, S. M. & JORDAN, C. L. 2013. Androgen receptors in muscle fibers induce rapid loss of force but not mass: implications for spinal bulbar muscular atrophy. *Muscle Nerve,* 47**,** 823-34.

OSTWALD, T. J. & MACLENNAN, D. H. 1974. Isolation of a high affinity calcium-binding protein from sarcoplasmic reticulum. *J Biol Chem,* 249**,** 974-9.

PALAZZOLO, I., BURNETT, B. G., YOUNG, J. E., BRENNE, P. L., LA SPADA, A. R., FISCHBECK, K. H., HOWELL, B. W. & PENNUTO, M. 2007. Akt blocks ligand binding and protects against expanded polyglutamine androgen receptor toxicity. *Hum Mol Genet,* 16**,** 1593-603.

PALAZZOLO, I., GLIOZZI, A., RUSMINI, P., SAU, D., CRIPPA, V., SIMONINI, F., ONESTO, E., BOLZONI, E. & POLETTI, A. 2008. The role of the polyglutamine tract in androgen receptor. *J Steroid Biochem Mol Biol,* 108**,** 245-53.

PALAZZOLO, I., STACK, C., KONG, L., MUSARO, A., ADACHI, H., KATSUNO, M., SOBUE, G., TAYLOR, J. P., SUMNER, C. J., FISCHBECK, K. H. & PENNUTO, M. 2009.

Overexpression of IGF-1 in muscle attenuates disease in a mouse model of spinal and bulbar muscular atrophy. *Neuron,* 63**,** 316-28.

PARBOOSINGH, J. S., FIGLEWICZ, D. A., KRIZUS, A., MEININGER, V., AZAD, N. A., NEWMAN, D. S. & ROULEAU, G. A. 1997. Spinobulbar muscular atrophy can mimic ALS: the importance of genetic testing in male patients with atypical ALS. *Neurology,* 49**,** 568-72.

PARK, K. H., FRANCIOSI, S. & LEAVITT, B. R. 2013. Postnatal muscle modification by myogenic factors modulates neuropathology and survival in an ALS mouse model. *Nat Commun,* 4**,** 2906.

PARODI, S. & PENNUTO, M. 2011. Neurotoxic effects of androgens in spinal and bulbar muscular atrophy. *Front Neuroendocrinol,* 32**,** 416-25.

PENNUTO, M. & BASSO, M. 2016. In Vitro and In Vivo Modeling of Spinal and Bulbar Muscular Atrophy. *J Mol Neurosci,* 58**,** 365-73.

PERUTZ, M. F., JOHNSON, T., SUZUKI, M. & FINCH, J. T. 1994. Glutamine repeats as polar zippers: their possible role in inherited neurodegenerative diseases. *Proc Natl Acad Sci U S A,* 91**,** 5355-8.

PICCIONI, F., PINTON, P., SIMEONI, S., POZZI, P., FASCIO, U., VISMARA, G., MARTINI, L., RIZZUTO, R. & POLETTI, A. 2002. Androgen receptor with elongated polyglutamine tract forms aggregates that alter axonal trafficking and mitochondrial distribution in motor neuronal processes. *FASEB J,* 16**,** 1418-20.

POLO, A., TEATINI, F., D'ANNA, S., MANGANOTTI, P., SALVIATI, A., DALLAPICCOLA, B., ZANETTE, G. & RIZZUTO, N. 1996. Sensory involvement in X-linked spino-bulbar muscular atrophy (Kennedy's syndrome): an electrophysiological study. *J Neurol,* 243**,** 388-92.

POORT, J. E., RHEUBEN, M. B., BREEDLOVE, S. M. & JORDAN, C. L. 2016. Neuromuscular junctions are pathological but not denervated in two mouse models of spinal bulbar muscular atrophy. *Hum Mol Genet*.

QIANG, Q., ADACHI, H., HUANG, Z., JIANG, Y. M., KATSUNO, M., MINAMIYAMA, M., DOI, H., MATSUMOTO, S., KONDO, N., MIYAZAKI, Y., IIDA, M., TOHNAI, G. & SOBUE, G. 2013. Genistein, a natural product derived from soybeans, ameliorates polyglutamine-mediated motor neuron disease. *J Neurochem,* 126**,** 122-30.

RAMZAN, F., MCPHAIL, M., RAO, P., MO, K., HALIEVSKI, K., SWIFT-GALLANT, A., MENDOZA-VIVEROS, L., CHENG, H. Y. & MONKS, D. A. 2015. Distinct Etiological Roles for Myocytes and Motor Neurons in a Mouse Model of Kennedy's Disease/Spinobulbar Muscular Atrophy. *J Neurosci,* 35**,** 6444-51.

RANGANATHAN, S., HARMISON, G. G., MEYERTHOLEN, K., PENNUTO, M., BURNETT, B. G. & FISCHBECK, K. H. 2009. Mitochondrial abnormalities in spinal and bulbar muscular atrophy. *Hum Mol Genet,* 18**,** 27-42.

RAOUL, C., BUHLER, E., SADEGHI, C., JACQUIER, A., AEBISCHER, P., PETTMANN, B., HENDERSON, C. E. & HAASE, G. 2006. Chronic activation in presymptomatic amyotrophic lateral sclerosis (ALS) mice of a feedback loop involving Fas, Daxx, and FasL. *Proc Natl Acad Sci U S A,* 103**,** 6007-12.

RAOUL, C., ESTEVEZ, A. G., NISHIMUNE, H., CLEVELAND, D. W., DELAPEYRIERE, O., HENDERSON, C. E., HAASE, G. & PETTMANN, B. 2002. Motoneuron death triggered by a specific pathway downstream of Fas. potentiation by ALS-linked SOD1 mutations. *Neuron,* 35**,** 1067-83.

RAOUL, C., HENDERSON, C. E. & PETTMANN, B. 1999. Programmed cell death of embryonic motoneurons triggered through the Fas death receptor. *J Cell Biol,* 147**,** 1049-62.

RAOUL, C., PETTMANN, B. & HENDERSON, C. E. 2000. Active killing of neurons during development and following stress: a role for p75(NTR) and Fas? *Curr Opin Neurobiol,* 10**,** 111-7.

RAUCH, F., PRUD'HOMME, J., ARABIAN, A., DEDHAR, S. & ST-ARNAUD, R. 2000. Heart, brain, and body wall defects in mice lacking calreticulin. *Exp Cell Res,* 256**,** 105-11.

REIJONEN, S., PUTKONEN, N., NORREMOLLE, A., LINDHOLM, D. & KORHONEN, L. 2008. Inhibition of endoplasmic reticulum stress counteracts neuronal cell death and protein aggregation caused by N-terminal mutant huntingtin proteins. *Exp Cell Res,* 314**,** 950-60.

RENIER, K. J., TROXELL-SMITH, S. M., JOHANSEN, J. A., KATSUNO, M., ADACHI, H., SOBUE, G., CHUA, J. P., SUN KIM, H., LIEBERMAN, A. P., BREEDLOVE, S. M. & JORDAN, C. L. 2014. Antiandrogen flutamide protects male mice from androgen-dependent toxicity in three models of spinal bulbar muscular atrophy. *Endocrinology,* 155**,** 2624-34.

RINALDI, C., BOTT, L. C., CHEN, K. L., HARMISON, G. G., KATSUNO, M., SOBUE, G., PENNUTO, M. & FISCHBECK, K. H. 2012. Insulinlike growth factor (IGF)-1 administration ameliorates disease manifestations in a mouse model of spinal and bulbar muscular atrophy. *Mol Med,* 18**,** 1261-8.

RINALDI, C., BOTT, L. C. & FISCHBECK, K. H. 2014. Muscle matters in Kennedy's disease. *Neuron,* 82**,** 251-3.

RINGEL, S. P., LAVA, N. S., TREIHAFT, M. M., LUBS, M. L. & LUBS, H. A. 1978. Late-onset X-linked recessive spinal and bulbar muscular atrophy. *Muscle Nerve,* 1**,** 297-307.

RUSMINI, P., CRIPPA, V., CRISTOFANI, R., RINALDI, C., CICARDI, M. E., GALBIATI, M., CARRA, S., MALIK, B., GREENSMITH, L. & POLETTI, A. 2015a. The Role of the Protein Quality Control System in SBMA. *J Mol Neurosci*.

RUSMINI, P., POLANCO, M. J., CRISTOFANI, R., CICARDI, M. E., MERONI, M., GALBIATI, M., PICCOLELLA, M., MESSI, E., GIORGETTI, E., LIEBERMAN, A. P., MILIOTO, C., ROCCHI, A., AGGARWAL, T., PENNUTO, M., CRIPPA, V. & POLETTI, A. 2015b. Aberrant Autophagic Response in The Muscle of A Knock-in Mouse Model of Spinal and Bulbar Muscular Atrophy. *Sci Rep,* 5**,** 15174.

SAHASHI, K., KATSUNO, M., HUNG, G., ADACHI, H., KONDO, N., NAKATSUJI, H., TOHNAI, G., IIDA, M., BENNETT, C. F. & SOBUE, G. 2015. Silencing neuronal mutant androgen receptor in a mouse model of spinal and bulbar muscular atrophy. *Hum Mol Genet*.

SAXENA, S., CABUY, E. & CARONI, P. 2009. A role for motoneuron subtype-selective ER stress in disease manifestations of FALS mice. *Nat Neurosci,* 12**,** 627-36.

SCHIAFFINO, S. & MAMMUCARI, C. 2011. Regulation of skeletal muscle growth by the IGF1-Akt/PKB pathway: insights from genetic models. *Skelet Muscle,* 1**,** 4.

SCHINDLER, M., FABRE, C., DE WEILLE, J., CARREAU, S., MERSEL, M. & BAKALARA, N. 2012. Disruption of nongenomic testosterone signaling in a model of spinal and bulbar muscular atrophy. *Mol Endocrinol,* 26**,** 1102-16.

SCHMIDT, B. J., GREENBERG, C. R., ALLINGHAM-HAWKINS, D. J. & SPRIGGS, E. L. 2002. Expression of X-linked bulbospinal muscular atrophy (Kennedy disease) in two homozygous women. *Neurology,* 59**,** 770-2.

SEIDMAN, R. J. 2013. *Skeletal Muscle Pathology* [Online]. Medscape. Available: http://emedicine.medscape.com/article/1869808-overview#a1 [Accessed 02/11/2015 2015].

SIMEONI, S., MANCINI, M. A., STENOIEN, D. L., MARCELLI, M., WEIGEL, N. L., ZANISI, M., MARTINI, L. & POLETTI, A. 2000. Motoneuronal cell death is not correlated with aggregate formation of androgen receptors containing an elongated polyglutamine tract. *Hum Mol Genet,* 9**,** 133-44.

SIMON, N. G., TURNER, M. R., VUCIC, S., AL-CHALABI, A., SHEFNER, J., LOMEN-HOERTH, C. & KIERNAN, M. C. 2014. Quantifying disease progression in amyotrophic lateral sclerosis. *Ann Neurol,* 76**,** 643-57.

SOKKA, A. L., PUTKONEN, N., MUDO, G., PRYAZHNIKOV, E., REIJONEN, S., KHIROUG, L., BELLUARDO, N., LINDHOLM, D. & KORHONEN, L. 2007. Endoplasmic reticulum

stress inhibition protects against excitotoxic neuronal injury in the rat brain. *J Neurosci,* 27**,** 901-8.

SOPHER, B. L., THOMAS, P. S., JR., LAFEVRE-BERNT, M. A., HOLM, I. E., WILKE, S. A., WARE, C. B., JIN, L. W., LIBBY, R. T., ELLERBY, L. M. & LA SPADA, A. R. 2004. Androgen receptor YAC transgenic mice recapitulate SBMA motor neuronopathy and implicate VEGF164 in the motor neuron degeneration. *Neuron,* 41**,** 687-99.

SORARU, G., D'ASCENZO, C., POLO, A., PALMIERI, A., BAGGIO, L., VERGANI, L., GELLERA, C., MORETTO, G., PEGORARO, E. & ANGELINI, C. 2008. Spinal and bulbar muscular atrophy: skeletal muscle pathology in male patients and heterozygous females. *J Neurol Sci,* 264**,** 100-5.

STENOIEN, D. L., CUMMINGS, C. J., ADAMS, H. P., MANCINI, M. G., PATEL, K., DEMARTINO, G. N., MARCELLI, M., WEIGEL, N. L. & MANCINI, M. A. 1999. Polyglutamine-expanded androgen receptors form aggregates that sequester heat shock proteins, proteasome components and SRC-1, and are suppressed by the HDJ-2 chaperone. *Hum Mol Genet,* 8**,** 731-41.

SUVARNA, S. K., LAYTON, C. & BANCROFT, J. D. 2013. *Bancroft's theory and practice of histological techniques*, Churchill Livingstone.

SZABO, E., QIU, Y., BAKSH, S., MICHALAK, M. & OPAS, M. 2008. Calreticulin inhibits commitment to adipocyte differentiation. *J Cell Biol,* 182**,** 103-16.

SZKLARCZYK, D., FRANCESCHINI, A., WYDER, S., FORSLUND, K., HELLER, D., HUERTA-CEPAS, J., SIMONOVIC, M., ROTH, A., SANTOS, A., TSAFOU, K. P., KUHN, M., BORK, P., JENSEN, L. J. & VON MERING, C. 2015. STRING v10: protein-protein interaction networks, integrated over the tree of life. *Nucleic Acids Res,* 43**,** D447-52.

TADIC, V., PRELL, T., LAUTENSCHLAEGER, J. & GROSSKREUTZ, J. 2014. The ER mitochondria calcium cycle and ER stress response as therapeutic targets in amyotrophic lateral sclerosis. *Front Cell Neurosci,* 8**,** 147.

TAKAHASHI, T., KATADA, S. & ONODERA, O. 2010. Polyglutamine diseases: where does toxicity come from? what is toxicity? where are we going? *J Mol Cell Biol,* 2**,** 180-91.

TAKAHASHI, T., KIKUCHI, S., KATADA, S., NAGAI, Y., NISHIZAWA, M. & ONODERA, O. 2008. Soluble polyglutamine oligomers formed prior to inclusion body formation are cytotoxic. *Hum Mol Genet,* 17**,** 345-56.

THOMAS, M., HARRELL, J. M., MORISHIMA, Y., PENG, H. M., PRATT, W. B. & LIEBERMAN, A. P. 2006a. Pharmacologic and genetic inhibition of hsp90-dependent trafficking reduces aggregation and promotes degradation of the expanded glutamine androgen receptor without stress protein induction. *Hum Mol Genet,* 15**,** 1876-83.

THOMAS, M., YU, Z., DADGAR, N., VARAMBALLY, S., YU, J., CHINNAIYAN, A. M. & LIEBERMAN, A. P. 2005. The unfolded protein response modulates toxicity of the expanded glutamine androgen receptor. *J Biol Chem,* 280**,** 21264-71.

THOMAS, P. S., JR., FRALEY, G. S., DAMIAN, V., WOODKE, L. B., ZAPATA, F., SOPHER, B. L., PLYMATE, S. R. & LA SPADA, A. R. 2006b. Loss of endogenous androgen receptor protein accelerates motor neuron degeneration and accentuates androgen insensitivity in a mouse model of X-linked spinal and bulbar muscular atrophy. *Hum Mol Genet,* 15**,** 2225-38.

TOKUI, K., ADACHI, H., WAZA, M., KATSUNO, M., MINAMIYAMA, M., DOI, H., TANAKA, K., HAMAZAKI, J., MURATA, S., TANAKA, F. & SOBUE, G. 2009. 17-DMAG ameliorates polyglutamine-mediated motor neuron degeneration through well-preserved proteasome function in an SBMA model mouse. *Hum Mol Genet,* 18**,** 898-910.

TOYOSHIMA, Y. & TAKAHASHI, H. 2014. TDP-43 pathology in polyglutamine diseases: with reference to amyotrphic lateral sclerosis. *Neuropathology,* 34**,** 77-82.

TRUANT, R., RAYMOND, L. A., XIA, J., PINCHEV, D., BURTNIK, A. & ATWAL, R. S. 2006. Canadian Association of Neurosciences Review: polyglutamine expansion neurodegenerative diseases. *Can J Neurol Sci,* 33**,** 278-91.

TSUKAGOSHI, H., SHOJI, H. & FURUKAWA, T. 1970. Proximal neurogenic muscular atrophy in adolescence and adulthood with X-linked recessive inheritance. Kugelberg-Welander disease and its variant of late onset in one pedigree. *Neurology,* 20**,** 1188-93.

TUFI, R., PANARETAKIS, T., BIANCHI, K., CRIOLLO, A., FAZI, B., DI SANO, F., TESNIERE, A., KEPP, O., PATERLINI-BRECHOT, P., ZITVOGEL, L., PIACENTINI, M., SZABADKAI, G. & KROEMER, G. 2008. Reduction of endoplasmic reticulum Ca2+ levels favors plasma membrane surface exposure of calreticulin. *Cell Death Differ,* 15**,** 274-82.

UEDA, M., LI, S., ITOH, M., HAYAKAWA-YANO, Y., WANG, M. X., HAYAKAWA, M., HASEBE-MATSUBARA, R., OHTA, K., OHTA, E., MIZUNO, A., HIDA, Y., MATSUMOTO, M., CHEN, H. & NAKAGAWA, T. 2014. Polyglutamine expansion disturbs the endoplasmic reticulum formation, leading to caspase-7 activation through Bax. *Biochem Biophys Res Commun,* 443**,** 1232-8.

VAN DE LOO, S., EICH, F., NONIS, D., AUBURGER, G. & NOWOCK, J. 2009. Ataxin-2 associates with rough endoplasmic reticulum. *Exp Neurol,* 215**,** 110-8.

VAN DEN BOSCH, L., VANDENBERGHE, W., KLAASSEN, H., VAN HOUTTE, E. & ROBBERECHT, W. 2000. Ca2+-permeable AMPA receptors and selective vulnerability of motor neurons. *Journal of the Neurological Sciences,* 180**,** 29-34.

VILLAGOMEZ, M., SZABO, E., PODCHEKO, A., FENG, T., PAPP, S. & OPAS, M. 2009. Calreticulin and focal-contact-dependent adhesion. *Biochem Cell Biol,* 87**,** 545-56.

VLADUTIU, G. D. & IDICULLA, S. 1997. Association between internalized nuclei and mitochondrial enzyme defects in muscle. *Muscle Nerve,* 20**,** 760-3.

WAISMAN, D. M., SALIMATH, B. P. & ANDERSON, M. J. 1985. Isolation and characterization of CAB-63, a novel calcium-binding protein. *J Biol Chem,* 260**,** 1652-60.

WALTHER, R. F., LAMPRECHT, C., RIDSDALE, A., GROULX, I., LEE, S., LEFEBVRE, Y. A. & HACHE, R. J. 2003. Nuclear export of the glucocorticoid receptor is accelerated by cell fusion-dependent release of calreticulin. *J Biol Chem,* 278**,** 37858-64.

WANG, J., DUNCAN, D., SHI, Z. & ZHANG, B. 2013. WEB-based GEne SeT AnaLysis Toolkit (WebGestalt): update 2013. *Nucleic Acids Res,* 41**,** W77-83.

WANG, W. A., GROENENDYK, J. & MICHALAK, M. 2012. Calreticulin signaling in health and disease. *Int J Biochem Cell Biol,* 44**,** 842-6.

WAZA, M., ADACHI, H., KATSUNO, M., MINAMIYAMA, M., SANG, C., TANAKA, F., INUKAI, A., DOYU, M. & SOBUE, G. 2005. 17-AAG, an Hsp90 inhibitor, ameliorates polyglutamine-mediated motor neuron degeneration. *Nat Med,* 11**,** 1088-95.

WENG, W. C., LIN, K. H., WU, P. Y., LU, Y. C., WENG, Y. C., WANG, B. J., LIAO, Y. F., HSU, W. M., LEE, W. T. & LEE, H. 2014. Calreticulin Regulates VEGF-A in Neuroblastoma Cells. *Mol Neurobiol*.

XU, Y., HALIEVSKI, K., HENLEY, C., ATCHISON, W. D., KATSUNO, M., ADACHI, H., SOBUE, G., BREEDLOVE, S. M. & JORDAN, C. L. 2016. Defects in Neuromuscular Transmission May Underlie Motor Dysfunction in Spinal and Bulbar Muscular Atrophy. *J Neurosci,* 36**,** 5094-106.

YAMAMOTO, T., YOKOTA, K., AMAO, R., MAENO, T., HAGA, N., TAGURI, M., OHTSU, H., ICHIKAWA, Y., GOTO, J. & TSUJI, S. 2013. An open trial of long-term testosterone suppression in spinal and bulbar muscular atrophy. *Muscle Nerve,* 47**,** 816-22.

YANG, Y. C., FU, H. C., HSIAO, B. L., SOBUE, G., ADACHI, H., HUANG, F. J., HSUUW, Y. D., WEI, K. T., CHANG, C., HUANG, K. E. & KANG, H. Y. 2013. Androgen receptor inclusions acquire GRP78/BiP to ameliorate androgen-induced protein misfolding stress in embryonic stem cells. *Cell Death Dis,* 4**,** e607.

YANG, Z., CHANG, Y. J., YU, I. C., YEH, S., WU, C. C., MIYAMOTO, H., MERRY, D. E., SOBUE, G., CHEN, L. M., CHANG, S. S. & CHANG, C. 2007. ASC-J9 ameliorates spinal and bulbar muscular atrophy phenotype via degradation of androgen receptor. *Nat Med,* 13**,** 348-53.

YU, Z., DADGAR, N., ALBERTELLI, M., GRUIS, K., JORDAN, C., ROBINS, D. M. & LIEBERMAN, A. P. 2006. Androgen-dependent pathology demonstrates myopathic contribution to the Kennedy disease phenotype in a mouse knock-in model. *J Clin Invest,* 116**,** 2663-72.

YU, Z., WANG, A. M., ADACHI, H., KATSUNO, M., SOBUE, G., YUE, Z., ROBINS, D. M. & LIEBERMAN, A. P. 2011. Macroautophagy is regulated by the UPR-mediator CHOP and accentuates the phenotype of SBMA mice. *PLoS Genet,* 7**,** e1002321.

YU, Z., WANG, A. M., ROBINS, D. M. & LIEBERMAN, A. P. 2009. Altered RNA splicing contributes to skeletal muscle pathology in Kennedy disease knock-in mice. *Dis Model Mech,* 2**,** 500-7.

ZBORAY, L., PLUCIENNIK, A., CURTIS, D., LIU, Y., BERMAN-BOOTY, L. D., ORR, C., KESLER, C. T., BERGER, T., GIOELI, D., PASCHAL, B. M. & MERRY, D. E. 2015. Preventing the Androgen Receptor N/C Interaction Delays Disease Onset in a Mouse Model of SBMA. *Cell Rep,* 13**,** 2312-23.

ZHANG, B., KIROV, S. & SNODDY, J. 2005. WebGestalt: an integrated system for exploring gene sets in various biological contexts. *Nucleic Acids Res,* 33**,** W741-8.

ZIELONKA, D., PIOTROWSKA, I., MARCINKOWSKI, J. T. & MIELCAREK, M. 2014. Skeletal muscle pathology in Huntington's disease. *Front Physiol,* 5**,** 380.